Volume 18, Number 4

April, 1965

SOVIET ATOMIC ENERGY

АТОМНАЯ ЭНЕРГИЯ
(ATOMNAYA ÉNERGIYA)

TRANSLATED FROM RUSSIAN

CONSULTANTS BUREAU

ATOMNAYA ÉNERGIYA

SOVIET ATOMIC ENERGY

A translation of **ATOMNAYA ÉNERGIYA,** *a publication of the Academy of Sciences of the USSR*

Vol. 18, No. 4 April, 1965

CONTENTS

Annual Subscription: $95 **Single Issue: $30** **Single Article: $15**

CONTENTS (continued)

The Russian press date (podpisano k pechati) of this issue was 4/14/1965. Publication therefore did not occur prior to this date, but must be assumed to have taken place reasonably soon thereafter.

Publisher

INTERACTION OF MODULATED HEAVY-CURRENT ELECTRON-PULSE BEAMS WITH PLASMA IN A LONGITUDINAL MAGNETIC FIELD

(UDC 533.9)

A. K. Berezin, G. P. Berezina, L. I. Bolotin,
Yu. M. Lyapkalo, and Ya. B. Fainberg

Translated from Atomnaya Énergiya, Vol. 18, No. 4,
pp. 315-322, April, 1965
Original article submitted July 1, 1964

Results of experiments on the interaction of modulated heavy-current electron-pulse beams with plasma in a longitudinal magnetic field are presented. The plasma is formed by the beam itself. It is shown that under certain conditions the modulated electron beam interacts much more strongly with the plasma than an unmodulated beam. Longitudinal waves with a considerably greater electric field strength (some seven times) than in the absence of initial modulation are excited in the beam and the plasma. An explanation of the results is offered.

As was shown theoretically in [1, 2] and experimentally in [3-5], one of the causes of the effective interaction of an initially unmodulated electron beam with plasma is automodulation, leading to coherent interaction of the beam with the plasma. The depth of modulation is determined by the field strength of the excited oscillations, and the field strength depends substantially on the initial perturbation amplitude, which for originally unmodulated beams is determined by comparatively small fluctuation fields. Hence automodulation becomes appreciable only at the end of the interaction region, where the field strengths become considerable owing to exponential growth.

Thus we may expect that, if the beams pass through a region of modulating field at the entrance into the interaction region, the effectiveness of the interaction between electron beam and plasma will rise considerably [2, 6-8]. This arises from several causes. Firstly, the amplitude of the initial field intensities rises considerably as compared with the fluctuation fields, and, secondly, under certain conditions, when the beam passes through an external region of hf field, particle bunching develops, reinforcing the effects of coherence.

It must be noted that, for a very large depth of modulation, in the long run, oscillations increasing neither in time nor space are established in the beam-plasma system.

The interaction of modulated charged-particle beams with plasma may be used for heating the plasma, capturing particles in traps, developing new methods of accelerating charged particles, and amplifying and regenerating hf oscillations [2].

The exponential growth of instability is caused, as we know, by the fact that the fields arising on instability increase the degree of bunching of the particles, and this in turn amplifies the field. Deep modulation at a given frequency leads to a situation where the degree of bunching no longer changes with further increase of field strength, and the growth of the field ceases. Preliminary modulation disrupts the bunching of particles at frequencies differing from the modulation frequency, and leads to the collapse of the whole instability spectrum. Here we must watch that the coherency conditions $a < \lambda_{pl}$, where a = length of particle bunch, $\lambda_{pl} = 2\pi v_f/\omega_0$ (v_f is the phase velocity of the wave, ω_0 is the electronic Langmuir plasma frequency) for the excitation of characteristic plasma frequencies are not satisfied. For this it is sufficient that the wavelength of the modulation $\lambda_m = a/2$. It should be noted that, in removing the ordinary instabilities by modulating the beam, there may arise other instabilities engendered by parametric resonances, but, since the breadth of parametric resonances is small, the considerable inhomogeneities and collisions in an actual plasma lead to the collapse of these instabilities.

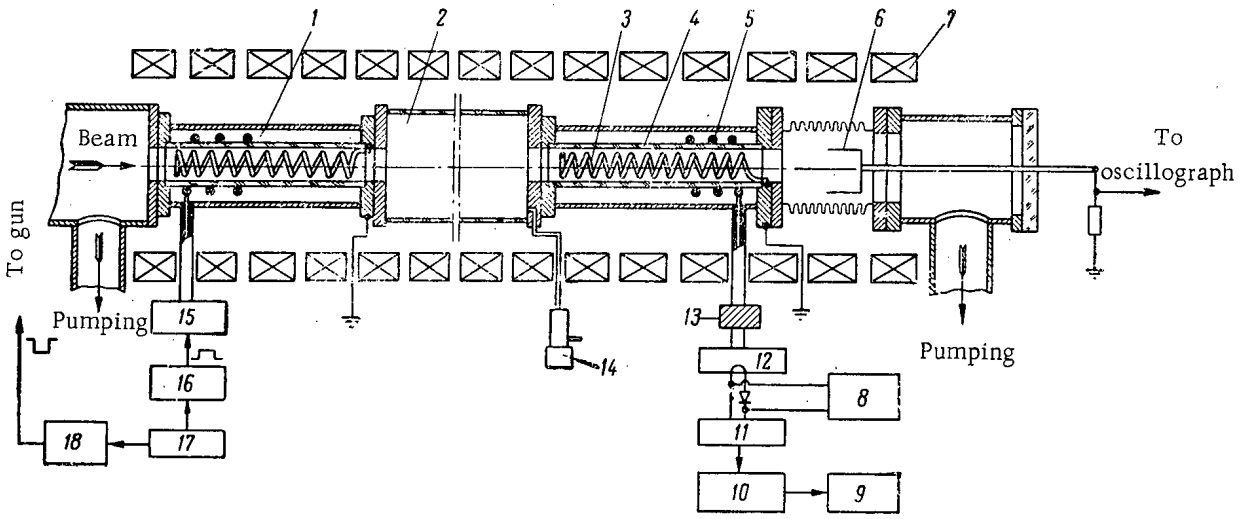

Fig. 1. Block diagram of apparatus for studying the interaction of modulated electron beams with plasma in a longitudinal magnetic field: 1) first spiral transit section; 2) plasma chamber; 3) inner spiral of second spiral transit section; 4) glass tube; 5) outer spiral; 6) current collector; 7) solenoid for longitudinal magnetic field; 8) oscillograph; 9) ÉPP-09M1; 10) integrating circuit; 11)ShU-10; 12) wavemeter; 13) attenuator; 14) mechanical leak; 15) generator; 16) modulator; 17) start-up system; 18) modulator for gun start-up.

The effectiveness of the interaction between the modulated beam and the plasma depends substantially on the method of modulation. Thus, for example, in the klystron method of modulation, particle bunching is effected by means of velocity differences; hence in some cases this may weaken or even cut off the development of instability owing to the large velocity spread thus engendered in the beam.

In our experiments, the initial modulation was effected by means of a short spiral ($L_{sp} < L_{int.\,sp}$, where L_{sp} = length of spiral and $L_{int.\,sp}$ = length of interaction space). In this case, depending on the length of the spiral, we may have either the klystron or the phase mechanism of bunching. Since there is so far no full theoretical treatment of the interaction of a beam initially so modulated with plasma, we shall only estimate the possibilities of increasing the efficiency of interaction with initial modulation of the beam.

When an inorganic plasma interacts with a modulated electron beam in which the alternating-current density j varies as

$$j = \delta j_0 \exp[i(\omega t - k_3 z)], \tag{1}$$

the maximum strength of the electric fields excited in the system [8] is

$$E_z^0 = \frac{2\pi\delta j_0}{\nu}, \tag{2}$$

where δ is the modulation depth of the electron beam, j_0 is the current density, ν the collision frequency. This relation is obtained for the case in which the beam temperature and the feed-back effect of the field on the beam can be neglected. For values $j_0 = 5$ A/cm^2, $\delta \approx 0.1$ and $\nu = 10^8$ sec^{-1} we obtain

$$E_z^0 \approx 30 \text{ kg/cm}.$$

The question of interaction between the plasma and an electron beam modulated by means of a pair of grids was considered in [7]. It follows from this that the field strength in the beam-plasma system is connected with the modulating intensity by the relation

$$E = V_0 \frac{\omega_0^2 e^{\gamma_{sp} z}}{8\pi v_0 \left(1 - \frac{\omega_0^2}{\omega^2}\right)\omega} \tag{3}$$

in the approximation $(1-(\omega_0^2/\omega^2)) \approx \gamma/\omega_0$ and $\gamma \approx (n_1/n_0)^{1/3}\omega_0$, where V_0 is the modulating intensity, ω_0 the plasma frequency, ω the modulation frequency, v_0 the beam velocity, γ_{sp} the spatial increment, γ the beam-instability increment, n_1 the beam density, n_0 the plasma density.

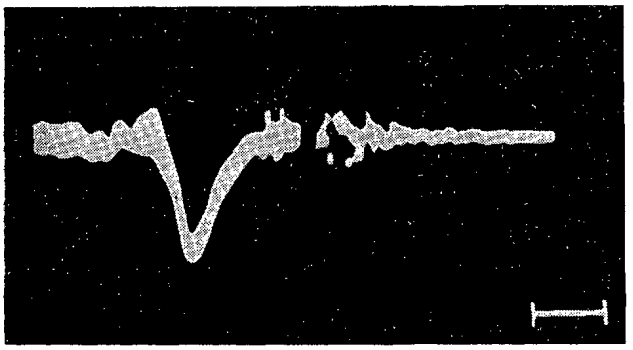

Fig. 2. Oscillogram showing the variation in the oscillation power with time, taken at the output of the beam-plasma system. Beam current 5 A, energy 21 keV; longitudinal magnetic field strength 1300 Oe; modulation frequency 835 Mc/sec; scale marker 1 μsec.

For a current of 5 A, modulating-field amplitude 10 V/cm, interaction length 32 cm, $v_0 = 8 \cdot 10^9$ cm/sec, and $n_0 = 2 \cdot 10^{10}$ cm^{-3}, the intensity at the end of the system, according to this formula, should be 8 kV/cm. These figures serve as estimates only, since in our case modulation was effected by means of a short spiral.

The experimental study of interaction between plasma and modulated electron beams with relatively small currents forms the subject of [9-12]. The present paper sets out the results of an experimental study of interaction between modulated heavy-current electron-pulse beams and plasma in a longitudinal magnetic field.

Description of Apparatus

The block diagram of the experimental apparatus is indicated in Fig. 1. The electron source is the electron gun described earlier [13]. The electron beam, of diameter 10 to 11 mm, current up to 5 A, energy ~20 keV, and pulse width 4.5 μsec (50 pulses per sec), passed through a modulating-spiral transit section, the plasma chamber, and a demodulating spiral, and then fell on a collector. High-frequency oscillations of definite frequency and given power were supplied through a coaxial feeder from a special generator to the modulating-spiral transit section, which effected the initial modulation of the electron beam at the entrance into the plasma chamber. This spiral transit section also served to create a pressure drop from 10^{-5} to $2 \cdot 10^{-3}$ torr between the electron gun and plasma chambers. It constituted a system of two coaxial spirals set inside and outside a glass tube of internal diameter 13 mm and wound in opposite directions (radius of inner spiral ~0.6 cm, radius of shorter outer spiral ~1.2 cm). The parameters of the spirals were chosen so that the phase velocity of the wave propagating in the spiral should be approximately equal to that of the electron beam, and hence also the phase velocity of the wave propagating in the plasma. The glass tube was vacuum-sealed at both ends.

The outer spiral was connected to a coaxial cable, the wave resistance of which was 75 Ω. The inner spiral was connected to an electrode at zero potential ("grounded"). The ends of the glass tube were covered with a layer of aquadag. Thus the electrons falling on the ends of the glass tube and the inner spiral were taken to ground. The length of the spiral transit section was around 12 cm. The voltage standing-wave coefficient (VSWC) at the input of this spiral transit section did not exceed 2.0 in the frequency range 650 to 5000 Mc/sec. The initial modulation was effected at frequencies 835 and 900 Mc/sec, for which the VSWC ≤ 1.4. These measurements were carried out in systems without an electron beam. On passing the electron beam through the spiral, the VSWC varied very little.

Passing through the plasma chamber, the electron beam ionized the gas therein (air), formed a plasma, and interacted with it. The plasma density was measured by a method based on the properties of plasma waveguides [4]. For the optimum case of interaction at pressure $2 \cdot 10^{-4}$ torr, the density was $2 \cdot 10^{10}$ cm^{-3} without initial modulation. The beam current was 5 A, the electron energy 21 keV, and the magnetic-field intensity 1300 Oe. For initial modulation at frequency ~835 Mc/sec with 600-W power, the plasma density was $2.5 \cdot 10^{10}$ cm^{-3}.

Passing through the plasma chamber, the beam fell into a demodulating-spiral transit section, and then on to the collector. The hf power was collected from the beam by the demodulating-spiral section. The construction and characteristics of the modulating- and demodulating-spiral sections are analogous. The length of the second transit section is 15 cm. In view of possible beam broadening, the aperture for the beam in the second transit section was 15 mm as compared with 10.5 mm in the first. Some 75 to 80% of the total beam current passed through this system and interacted with the plasma.

The oscillations taken off by means of the demodulating-spiral transit section from the electron beam at the exit from the interaction space passed through a coaxial feeder with wave resistance 27 Ω and a fixed attenuator into a resonance wavemeter. After passing the crystal detector at the wavemeter output, the signal was passed to the vertical input of a cathode-ray oscillograph. A sample oscillogram taken for current 5 A and frequency 835 Mc/sec appears in Fig. 2.

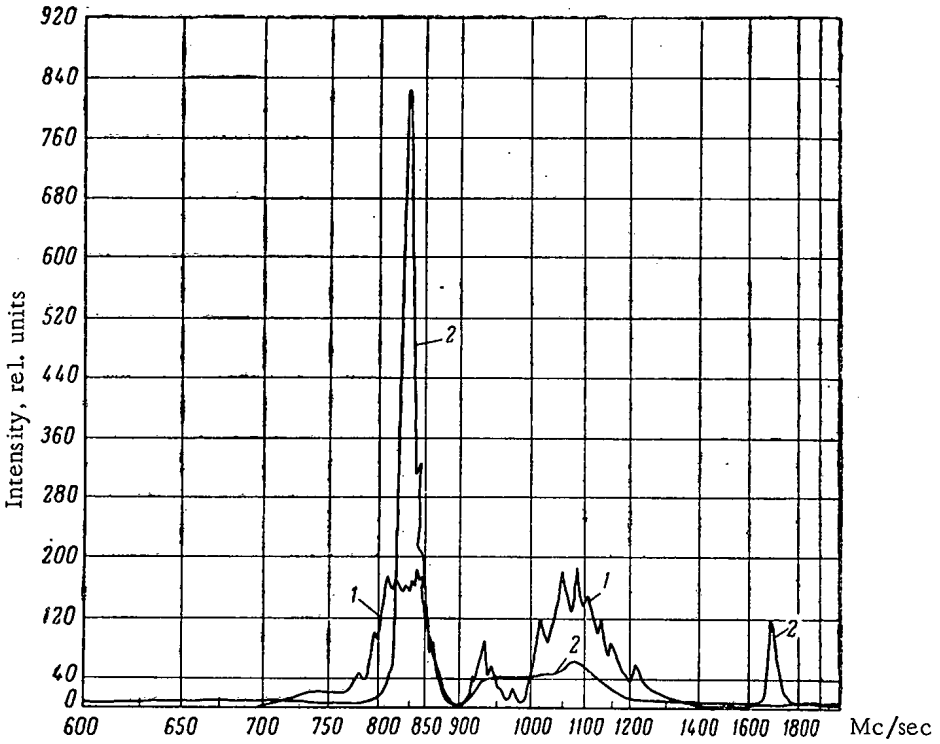

Fig. 3. Spectra of oscillations excited in initially-unmodulated (curve 1) and modulated (curve 2) electron beams. Beam current 5 A, energy 21 keV, longitudinal magnetic-field intensity 1320 Oe, pressure $2 \cdot 10^{-3}$ torr, modulation frequency 835 Mc/sec.

The maximum power of the hf oscillations was determined by means of fixed attenuators and a calibrated wavemeter with band half-width 1.5 Mc/sec. The waveguide, incorporating a crystal detector, was first calibrated with respect to a standard-signal generator. To the output of the wavemeter were connected in parallel an oscillograph and a wide-band amplifier, which was connected through a cathode follower to an integrating unit with an electronic potentiometer ÉPP-09. On adjusting the wavemeter with respect to frequency, the electronic potentiometer described the frequency spectra of the oscillations excited in the electron beam (intensity versus frequency).

Results of the Measurements

The method described was used to obtain the frequency spectra of the oscillations obtained when the plasma interacted with both modulated and unmodulated electron beams carrying 5, 3.8, and 2.3 A. The current reaching the collector was 4, 3, and 2 A, respectively. The beam energy remained at 21 keV, and the longitudinal magnetic-field strength ~1300 Oe. The beam was modulated at 835 Mc/sec. The master generator operated in the range 700 to 950 Mc/sec with output power 1 to 16 W in the continuous condition and 3 to 600 W in the pulsed condition (pulse width 10 μsec).

In the pulse condition the generator was started by a special start-up device synchronized with that of the pulse line feeding the electron gun.

The most intense oscillations were excited for an air pressure of $\sim 2 \cdot 10^{-4}$ torr in the plasma chamber. The spectrum of the oscillations excited in the initially unmodulated electron beam carrying 5 A of current at the end of the interaction region appears in Fig. 3 (curve 1). As seen from the graph, the most intense oscillations are excited at frequencies 800 to 840 Mc/sec (half-width 50 to 70 Mc/sec) and 1000 to 1150 Mc/sec. There are no oscillations at 900 Mc/sec in the spectrum. The maximum power of the excited oscillations for current 5 A is 120 to 150 W. For currents 2.3 and 3.8 A, the maximum power is respectively 19 and 70 W.

For initial modulation at 835 Mc/sec, the beam-plasma system operates as an amplifier, and amplified signals of considerable intensity (band halfwidth 8 to 10 Mc/sec) are recorded at the output. The frequency spectrum of the oscillations excited in the beam modulated at 835 Mc/sec and carrying 5 A of current appears in Fig. 3, curve 2.

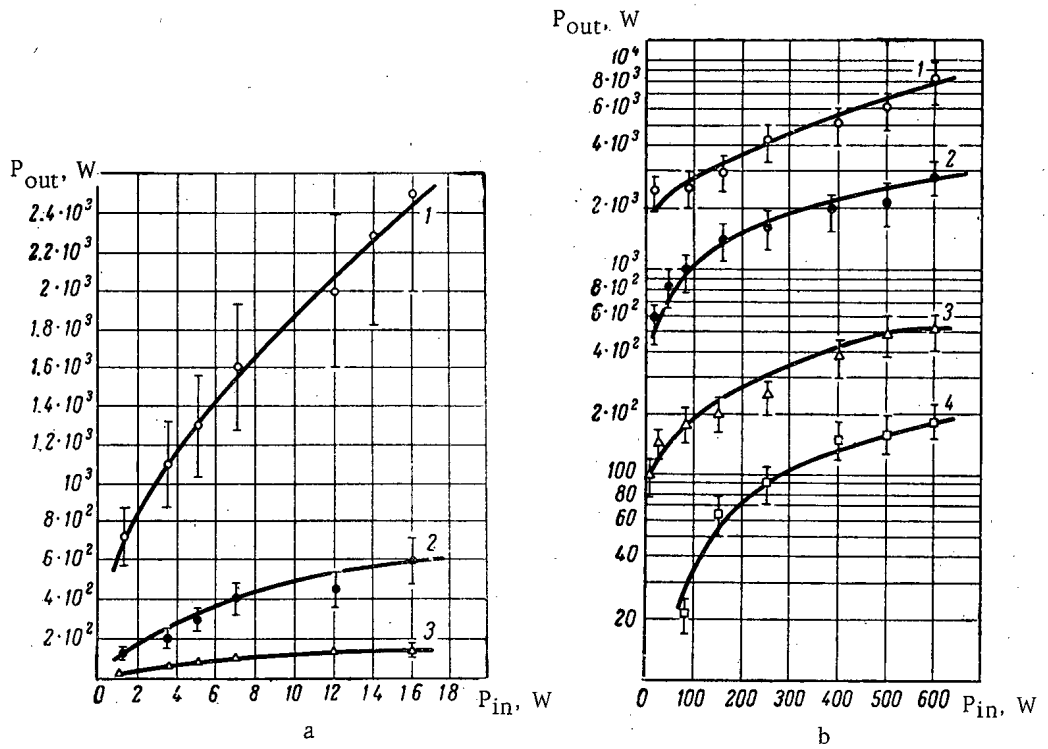

Fig. 4. Hf-oscillation power at the output of the plasma-beam system as a function of modulation power for various currents [a: 1) 5 A; 2) 3.8 A; 3) 2.3 A; b: 1) to 3) as before; 4) second harmonic (1670 Mc/sec for 5 A current].

TABLE 1. Power in Higher Harmonics of the Modulating Frequency

Number of harmonic	Oscillation frequency, Mc/sec	Maximum power of the oscillations, W
1	835	$8 \cdot 10^3$
2	1670	180
3	2505	7
4	3340	0.2
5	4175	10^{-3}
6	5010	10^{-4}

Comparing the spectra of the oscillations excited on interaction of the modulated and initially unmodulated electron beams with the plasma, we note that initial modulation (600 W) leads to the suppression of oscillations for the whole band of frequencies differing from the modulation band (power reduced 16 times). The power of the oscillations generated at modulation frequency 835 Mc/sec, however, rises substantially (from 120 to 150 W without initial modulation to 8 kW for modulation at 600 W).

Figures 4a and b show the variation of the maximum output power of the amplified oscillations with the initial modulation power (1 to 600 W) at frequency 835 Mc/sec and currents of 5, 3.8, and 2.3 A. It must be noted that identical data were obtained on operating the master generator in the continuous and pulsed conditions, all experimental points falling neatly on the same curves. It follows that the operating conditions of the master generator do not affect the results obtained.

As seen from the graphs presented, the amplification factor of the beam-plasma system increases with rising beam current. By amplification factor in this case we mean the ratio of the hf-oscillation power at the output of the system to the modulating-signal power. The amplification factors for a system 40-cm long are 12, 19, and 26 dB for currents 2.3, 3.8, and 5 A, respectively (modulation power several W). With increasing modulation power, the amplification factor of the system falls. Thus, whereas for small levels of modulating signal (several W) it is 26 dB for current 5 A, for 600 W power it is 11 dB in the same interaction distance. For a current of 2.3 A at small levels of modulating signal, the amplification factor is 12 dB, and then it reaches saturation for signal powers of 500 to 600 W.

At the end of the interaction region, the electric-field intensities of the oscillations excited in the beam as a result of interaction with the plasma were determined.

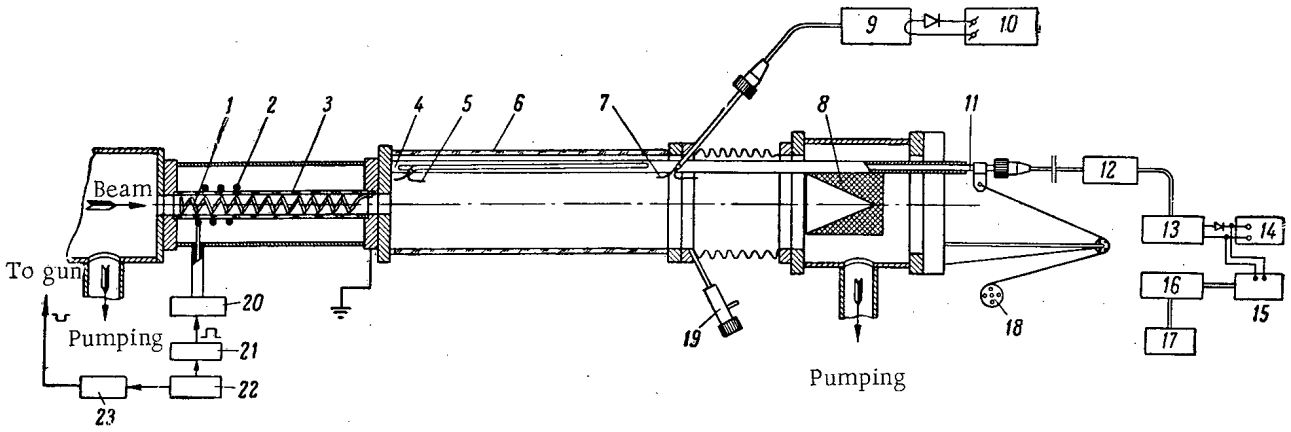

Fig. 5. Block diagram of apparatus for measuring the distribution of the E_z component of hf field in the plasma along the axis of the system: 1) inner spiral; 2) outer spiral; 3) glass tube; 4) guide; 5) half-wave dipole; 6) plasma chamber; 7) receiver antenna (immovable); 8) adiabatic load (current collector); 9) resonance wavemeter; 10), 14) cathode-ray oscillographs; 11) coaxial cable; 12) attenuator; 13) wavemeter; 15) amplifier; 16) integrating system; 17) ÉPP-09; 18) RD-09 motor; 19) mechanical leak; 20) generator; 21) modulator; 22) starting device; 23) modulator for starting gun.

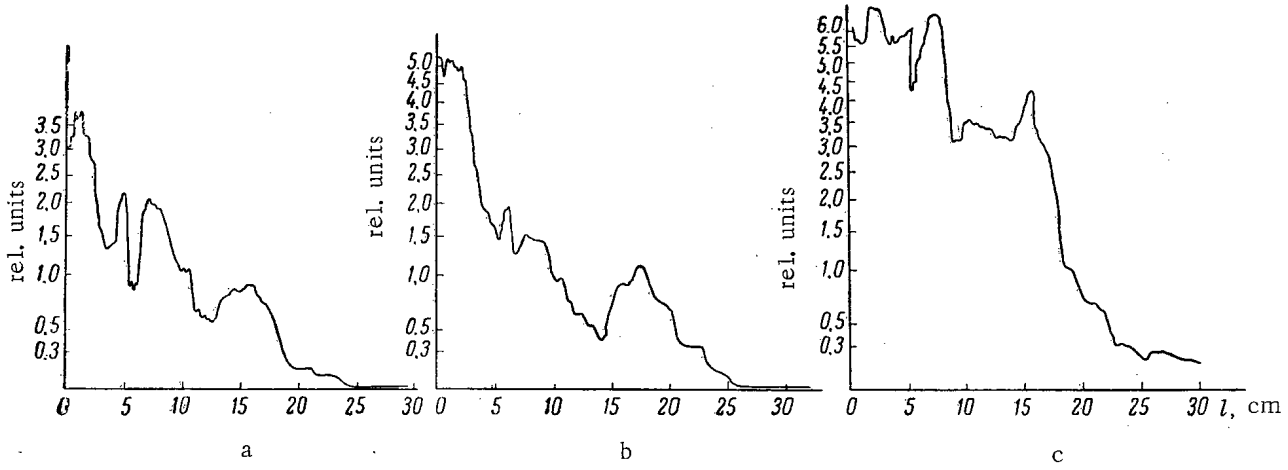

Fig. 6. Distribution of E_z component of hf field in the plasma along the axis of the system for various values of modulation power (a: 50 W; b: 80 W; c: 350 W) for constant beam current 5 A.

Estimates show that the electric-field strengths of the longitudinal charge-density oscillations at the end of the interaction space equal approximately 0.45 kV/cm for initially unmodulated electron beams and 3.2 kV/cm for a modulated electron beam with initial-modulation power 600 W (beam current 5 A).

Thus by means of the initial modulation of the electron beam the electric-field strength of the longitudinal charge-density oscillations can be increased some seven times.

As we see from the graph of Fig. 3 (curve 2), on initial modulation at 835 Mc/sec, apart from the fundamental frequency, higher harmonics of the modulating frequency are also found, these not being in the frequency spectra of the modulated beam. Figure 4b clearly shows the second harmonic at frequency 1670 Mc/sec. The second-harmonic power depends on the power of the modulating generator and increases together with this. It follows from the graph that, for a modulating-generator power of 600 W, the second-harmonic power at the end of the electron beam-plasma interaction space is 180 W.

In all we were able to record six harmonics experimentally. Table 1 shows the powers of the first six harmonics for a 5 A beam with initial-modulation power 600 W.

As seen from Table 1, the amplitudes of the harmonics fall with increasing harmonic number.

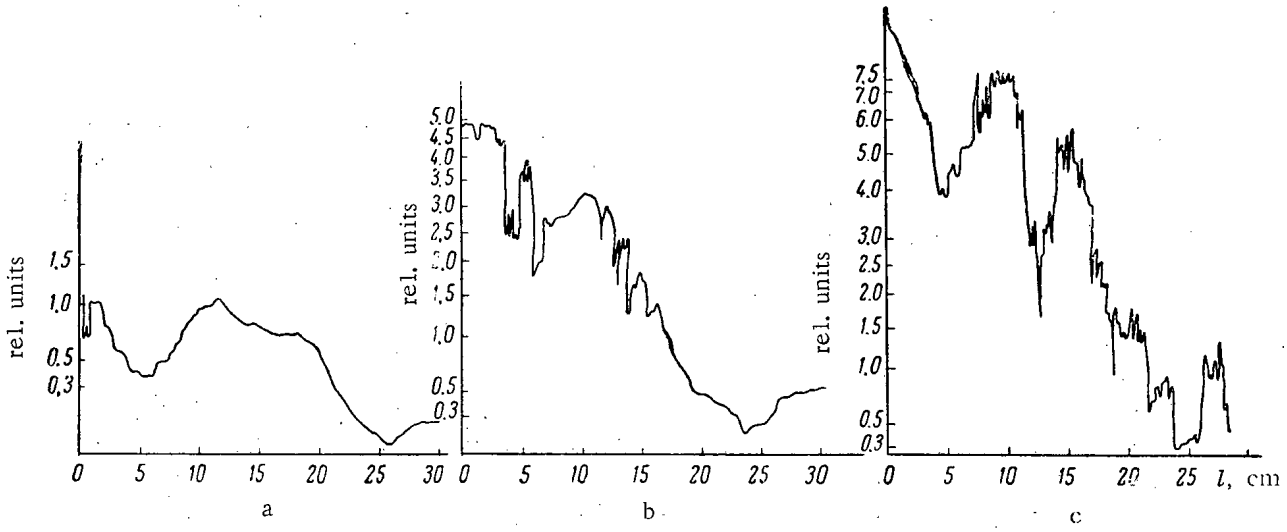

Fig. 7. Distribution of E_z component of hf field in the plasma along the axis of the system for various currents (a: 2.3 A; b: 3.8 A; c: 5 A) for modulation power 600 W (coordinate reckoned from right to left on the graphs).

The distribution of the E_z component of the hf field in the plasma was measured along the axis of the system. The block diagram of the apparatus is shown in Fig. 5. In order to remove reflections, a graphite cone was placed at the end of the plasma chamber, this serving as an adiabatic load for the waves propagating in the plasma and also as a current collector. Along the axis of the system moved a coaxial cable with a half-wave dipole oriented to measure the E_z-component of the hf field.

Graphs giving the distribution of the E_z-component of hf field along the axis of the system for various initial-modulation powers (50, 80, and 350 W) at constant beam current (5 A) appear in Fig. 6a, b, c, and for various beam currents (2.3, 3.8, and 5 A) at constant initial-modulation power (600 W) in Fig. 7a, b, and c.

From these graphs we may calculate the spatial increments γ_{sp} for various beam currents and initial-modulation powers. The value of γ_{sp} is found from the relation

$$\gamma_{sp} \approx \frac{1}{(z_2 - z_1)} \ln \frac{E_2}{E_1} = \frac{1}{2(z_2 - z_1)} \ln \frac{W_2}{W_1}, \quad (4)$$

where E_1, E_2, W_1, and W_2 are the field strengths and powers of the propagating waves at points z_1 and z_2.

Thus, whereas for an initial-modulation power of 50 W the spatial increment is 0.8 cm^{-1}, for an initial-modulation power of 600 W it equals 0.13 cm^{-1} (current 5 A).

For currents of 5, 3.8, and 2.3 A and initial-modulation power 600 W, the increments respectively equal 0.13, 0.09, and 0.06 cm^{-1}.

Thus it follows from the graphs that, as the beam current and the hf power of the initial modulation increase, the spatial increments rise sharply. The apparent contradiction between the relationships for the amplification factor and spatial increment as functions of the modulating-signal power is due to the fact that the power of the oscillations excited by the beam falls at the beginning of the interaction space and then rises monotonically (Fig. 7). The value of γ_{sp} is determined from relation (4) on the rising part of the curve, and the amplification factor from the ratio of the signals on the falling and rising parts of the curve. We may suppose that the fall in the signal on the descending part of the curve is connected with the expenditure of power going into the beam modulation.

Experiments show that the modulated electron beam should interact more strongly with the plasma than the unmodulated, or, in other words, the former should lose more energy in passing through the plasma than the latter. In order to confirm this, we used a sensitive calorimeter to measure the mean energy of an electron beam with current 5 A and energy 21 keV after passing through the demodulating-spiral transit section, both in the presence of initial modulation at 835 Mc/sec and 600-W power and also without initial modulation. From these measurements we determined the change in the electron-beam energy as a function of initial modulation.

The block diagram of the apparatus is fully described in [14]. The precision of measuring the mean electron-beam energy by means of the calorimeter was ±1 to 1.5%. The calorimeter was placed at the end of the interaction region.

As a result of the measurements it was shown that, thanks to the initial modulation, the electron beam lost an extra 7 ± 3% of its original energy as compared with the losses of the unmodulated electron beam under otherwise-equal conditions (beam current 5 A, energy 21 keV, longitudinal magnetic-field intensity 1300 Oe). Thus the calorimetric measurements agree closely with those made earlier.

LITERATURE CITED

1. A. I. Akhiezer and Ya. B. Fainberg, "Dokl. AN SSSR," 69, 555 (1949); ZhÉTF, 21, 1262 (1951).
2. Ya. B. Fainberg, "Atomnaya énergiya," 11, 313 (1961).
3. I. F. Kharchenko et al., ZhÉTF, 38, 685 (1960); A. K. Berezin et al., "Atomnaya énergiya," 11, 493 (1961).
4. A. K. Berezin et al., Collection "Plasma Physics and Problems of Controlled Nuclear Synthesis" [in Russian], 3, Kiev, Izd. AN UkrSSR (1963), p. 125.
5. A. K. Berezin et al., "Atomnaya énergiya," 14, 249 (1963).
6. Ya. B. Fainberg, Collection "Plasma Physics and Problems of Controlled Nuclear Synthesis" [in Russian], 1, Kiev, Izd. AN UkrSSR (1962), p. 20.
7. Ya. B. Fainberg and N. A. Khizhnyak, Collection "Plasma Physics and Problems of Controlled Nuclear Synthesis" [in Russian], 1, Kiev, Izd. AN UkrSSR (1962), p. 71.
8. N. A. Kondratenko, "Ukr. fiz. zh.," 7, 371 (1962); Collection "Plasma Physics and Problems of Controlled Nuclear Synthesis" [in Russian], 2, Kiev, Izd. AN UkrSSR (1963), p. 176.
9. I. F. Kharchenko et al., Collection "Plasma Physics and Problems of Controlled Nuclear Synthesis" [in Russian], 2, Kiev. Izd. AN UkrSSR (1963), p.118.
10. G. Boyd, L. Field, and R. Gould, Phys. Rev., 109, 1393 (1958).
11. E. V. Bogdanov, V. Ya. Kislov, and Z. S. Chernov, "Radiotekhnika i élektronika," 5, 229 (1960).
12. V. Ya. Kislov and E. V. Bogdanov, Ibid., p. 1974.
13. A. K. Berezin et al., "Pribory i tekhnika éksperimenta," No. 2, 136 (1962).
14. A. K. Berezin et al., "Atomnaya énergiya," 18, 271 (1965).

All abbreviations of periodicals in the above bibliography are letter-by-letter transliterations of the abbreviations as given in the original Russian journal. *Some or all of this periodical literature may well be available in English translation.* A complete list of the cover-to-cover English translations appears at the back of this issue.

INTERACTION OF A STRAIGHT PLASMA PINCH WITH A VARYING MAGNETIC FIELD OF QUADRUPOLE CONFIGURATION

(UDC 533.9.07)

D. V. Orlinskii

Translated from Atomnaya Énergiya, Vol. 18, No. 4,
pp. 323-329, April, 1965
Original article submitted May 22, 1964

The interaction of a straight plasma pinch (current up to 4 kA) with a high-frequency (~1.3 Mc/sec) quadrupolar magnetic field (~100 Oe) is studied by very simple methods.

Long-wave perturbations of a straight or toroidal self-constricted discharge may be stabilized, as first shown by S. M. Osovets [1] (see also [2]), by means of a high-frequency transverse magnetic field. This field may be created by a system of currents flowing through two, four, or more straight rods, and may thus have a dipole, quadrupole, or more complex configuration. The action of such a field on a plasma pinch held in a compressed state by the field of a current flowing through it is to a certain extent analogous to that of a magnetic field with a fall-off index varying in space on a beam of particles in a strong-focusing accelerator.

The aim of the present paper is a qualitative explanation of the main features in the flow of a straight discharge in a hf magnetic field of quadrupolar configuration. For this we used the simplest diagnostic means, photographing the discharge, measuring the magnetic field, and recording the longitudinal magnetic flux.

A pulse discharge in deuterium was created in a glass tube 8 cm in diameter and 80 cm in length. The distance between the cylindrical molybdenum electrodes of diameter 1.4 cm was 60 cm. The discharge was fed from an artificial line giving a rectangular current pulse 120 μsec long with a growth time of 4 μsec through the gas. The return conductor was made in the form of six rods situated symmetrically around the axis of the discharge chamber. Thus the discharge tube remained open for photography. The majority of the experiments were made for an initial voltage of $U_0 = 10$ to 30 kV between the electrodes (the current through the gas being 1.2 to 3.6 kA) and initial deuterium pressure $p_0 = 0.02$ to 0.15 mm Hg.

For the creation of the hf field we used a system consisting of four rods connected into an oscillatory circuit in such a way that at any moment of time the current in diametrically opposite rods was in the same direction. Together with series capacitors and connecting elements, the system formed a circuit with a resonance frequency of 1465 kc/sec and selectivity $Q = 200$. The circuit formed part of the resonance system of a pushpull autogenerator operating at 1278 kc/sec. With development of the hf discharge in the discharge chamber, the frequency rose to 1292 kc/sec and the selectivity fell to $Q = 50$ to 70. The pulse power fed into the circuit at $p_0 = 0.06$ mm Hg was 200 kW.

The configuration of the magnetic field created by the system of four rods in principle facilitates the stabilization of the plasma pinch on the discharge-tube axis. The conditions for the stabilization of the harmonic component of perturbation with wavelength λ in this case have the form [1]:

$$\omega > \frac{2I_0}{c} \cdot \frac{2\pi}{\lambda} \sqrt{\frac{\ln \frac{\lambda}{\pi r_0}}{2MN}}, \tag{1'}$$

$$\frac{\partial \tilde{H}}{\partial r} > \frac{2I_0}{c} \left(\frac{2\pi}{\lambda}\right)^2 \ln \frac{\lambda}{\pi r_0}, \tag{1''}$$

where M is the mass of an ion, N the number of ions in the pinch cross section per unit length, r_0 the radius of the plasma pinch, $\tilde{H}$ the hf-field strength, and I_0 the current through the gas.

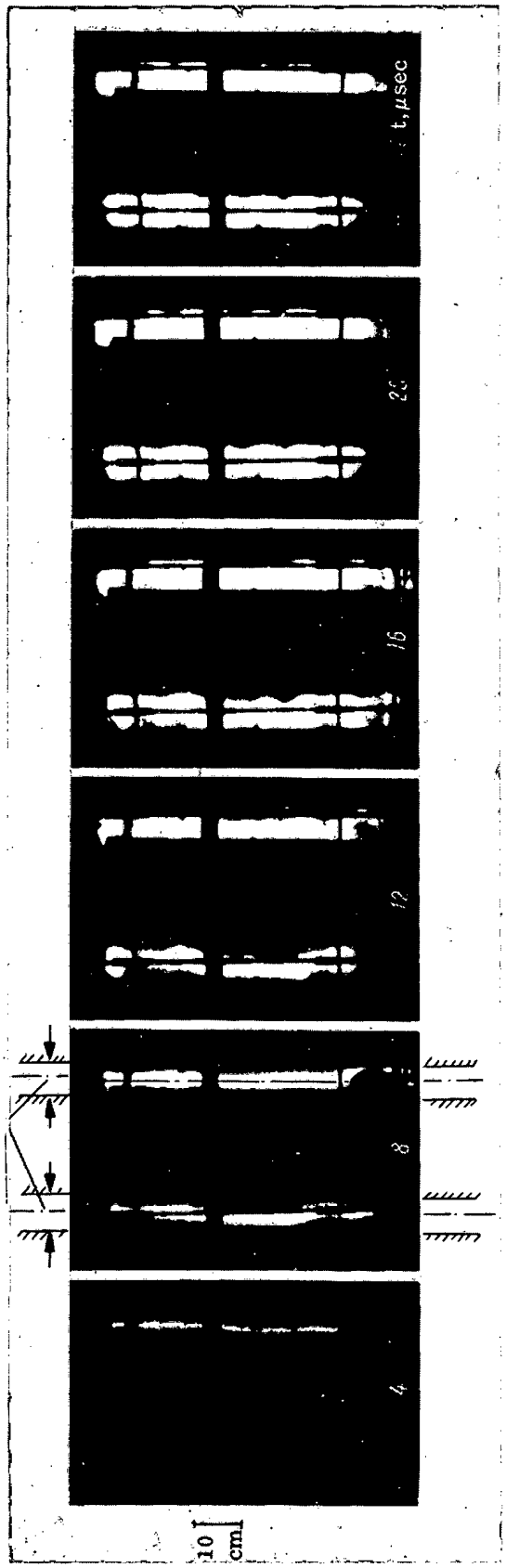

Fig. 1. Photograph of discharge without hf field for $p_0 = 0.07$ mm Hg, $U_0 = 15$ kV ($I_{0\,max} = 1.6$ kA).

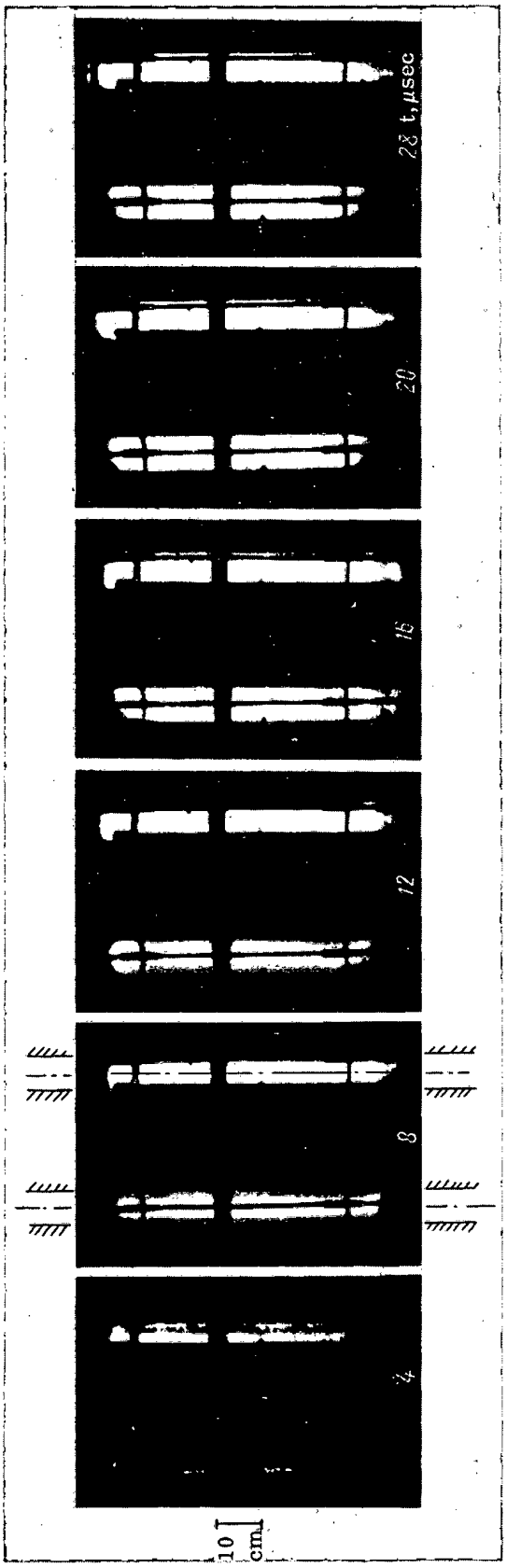

Fig. 2. Photograph of discharge. High-frequency breakdown takes place simultaneously with start of current pulse through gas: $p_0 = 0.07$ mm Hg, $U_0 = 15$ kV ($I_{0\,max} = 1.6$ kA).

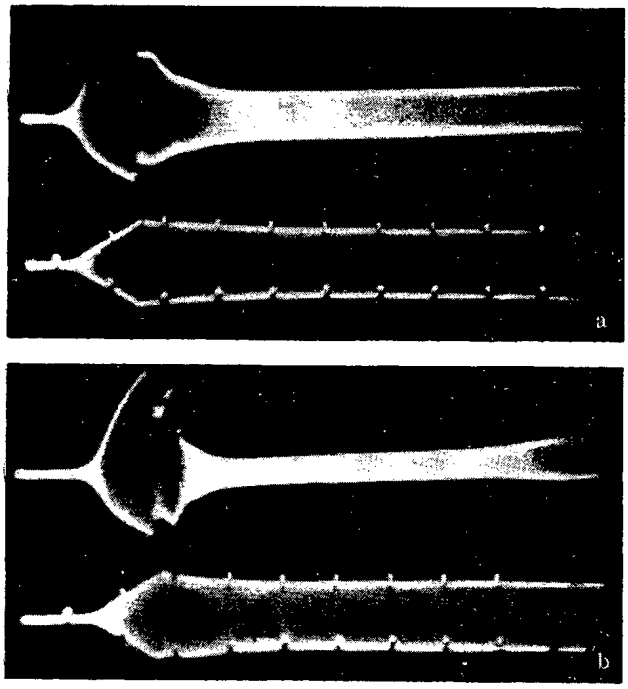

Fig. 3. Oscillograms of current through the rods (lower beam) and magnetic field $\tilde{H}_z$ (upper beam); time markers every 20 μsec: a) $U_0 = 0$; b) $U_0 = 12$ kV ($I_{0\,max} = 1.4$ kA).

Experiments were made for constant operating conditions of the hf generator. The current through each rod was $\tilde{J} \approx 800$ A, and $\partial\tilde{H}/\partial r \approx 25$ Oe/cm. Thus condition (1') was satisfied for any values of λ. In order to satisfy condition (1"), we must have $I_0 < I_{0\,cr}$. The values of $I_{0\,cr}$ for various λ with $r_0 = 1$ cm are:

λ, cm	120	60	30	15	7.5
$I_{0\,cr}$, kA . . .	13	4	1.3	0.5	0.2

The discharge was photographed with a time magnifier (streak photography) with a 4 μsec interval between frames. As shown by repeated checks with the aid of a photomultiplier placed behind the film under exposure, the first frame in the photograph corresponds to the start of the discharge. The discharge was photographed simultaneously on both sides by means of a mirror placed around the discharge chamber. The currents through the rods and through the gas were measured by Rogowski coils.

If the discharge between the electrodes takes place without the hf field, then the plasma pinch developing after the breakdown on the axis of the tube at once begins to twist itself into a spiral (Fig. 1). The pitch of the spiral, at first approximately equal to the distance between the electrodes, rapidly diminishes to the order of the tube diameter, and in 20 to 50 μsec the pinch collapses.[1]

The discharge presents a different picture in the case when breakdown between the electrodes is effected with simultaneous superimposition of the hf field (Fig. 2).

The plasma pinch, as in the case $\tilde{J} = 0$, appears on the chamber axis, but, instead of coiling up, gradually broadens and fills the whole cross section of the tube. If the hf discharge begins somewhat before (by 10 to 20 μsec) the potential is applied to the electrodes, then the pinch on the axis is not observed, the discharge filling the tube cross section from the very beginning.

The course of the discharge may also be judged from the change in the distribution of the hf field along the tube radius.

The hf-field strength was measured by magnetic probes introduced into a glass tube of external diameter 3 mm. The radial field component $\tilde{H}_r$ and the azimuthal component $\tilde{H}_\varphi$ were measured separately in two directions: near the rod (where $\tilde{H}_\varphi \gg \tilde{H}_r$) and between the rods (where $\tilde{H}_r \gg \tilde{H}_\varphi$).

The hf-field distribution along the diameter of the discharge tube was taken by measuring the field in turn at various distances from the axis of the chamber. The interval between neighboring positions of the probe was 0.5 cm. In this way the distribution curve was averaged over approximately 20 discharges.

Figure 3 shows two characteristic oscillograms of $\tilde{H}_r$ obtained for $p_0 = 0.06$ mm Hg. The distance from the probe to the axis equals ~1.5 cm. One oscillogram (see Fig. 3a) was obtained for $U_0 = 0$ and the other (see Fig. 3b) for $U_0 = 12$ kV ($I_{0\,max} = 1.4$ kA). In the first case, after the hf breakdown the field remains steady for some time (~6 μsec), and then falls to a certain level at which it remains for the whole hf pulse. The fall in the field is explained by the rise in plasma conductivity and hence the displacement of the field from the central region of the discharge. In the second case, almost immediately after the hf breakdown, a longitudinal current begins to flow along the tube axis. The magnetic probe is near the boundary of the plasma. Around the boundary of the pinch,

[1]Here by "collapse" of the pinch we mean that the whole chamber is filled with almost uniform luminescence, on the background of which the pinch becomes indistinguishable.

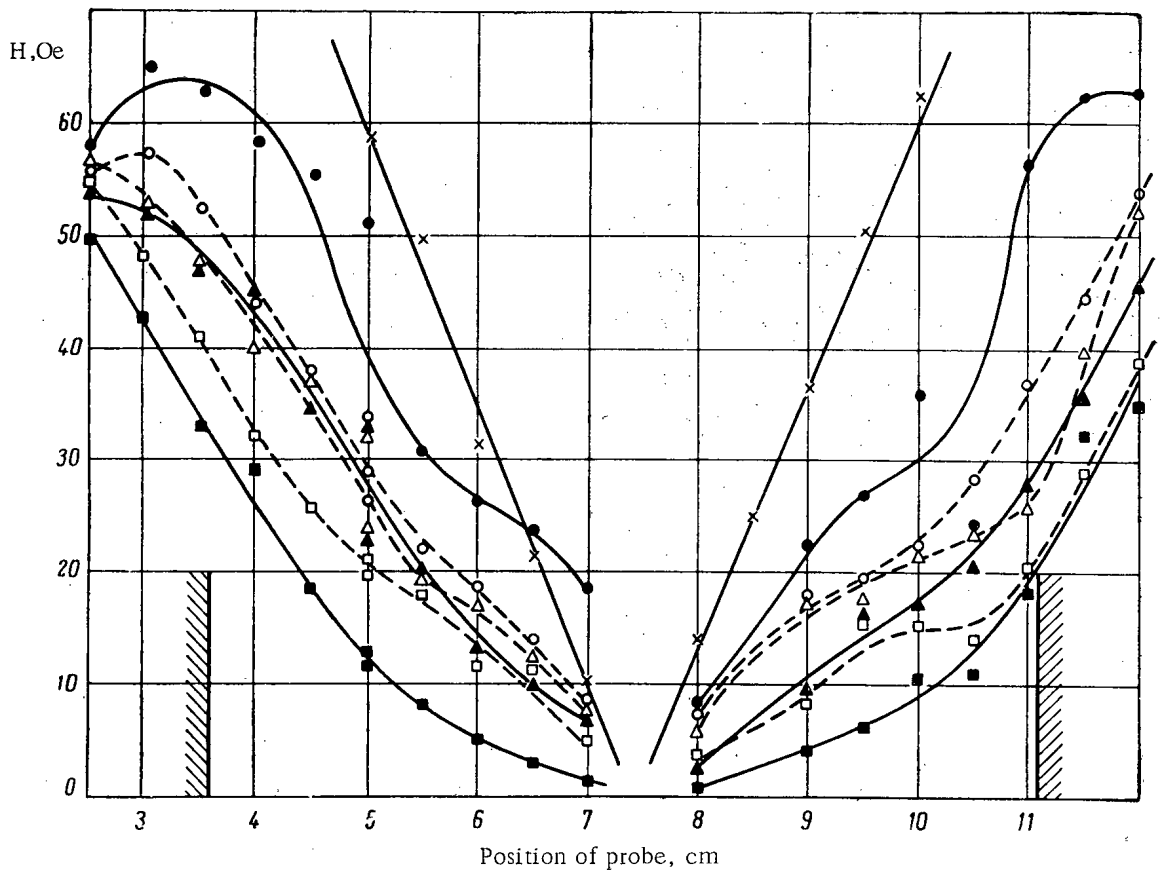

Fig. 4. Distribution of $\tilde{H}_r(r)$ at various moments of time after the onset of the discharge (between the rods, where $\tilde{H}_r \gg \tilde{H}_\varphi$) for $I_0 = 1400$ A: for $p_0 = 0.06$ mm Hg: ○, ●) for $U_0 = 0$ and 12 kV respectively, $t_1 = 5\,\mu$sec; △, ▲) for $U_0 = 0$ and 12 kV respectively, $t_2 = 10\,\mu$sec; □, ■) for $U_0 = 0$ and 12 kV respectively, $t_3 = 50\,\mu$sec; ×) $p_0 = 2 \cdot 10^{-6}$ mm Hg.

the hf field is larger (on account of the field of induction currents) than when the pinch is absent, and hence the signal from the probe increases. When, however, as a result of the spreading of the plasma, the probe falls inside the pinch, the signal sharply diminishes.

Typical distribution curves for the hf field along the tube radius are shown in Fig. 4 ($\tilde{H}_r$ between the rods). For convenience of comparison, all the curves are referred to the same value of current through the rod ($\tilde{J} = 830$ A). Soon after the appearance of the plasma pinch ($t_1 = 5\,\mu$sec), the field in the central part of the tube becomes considerably larger than in the case when $I_0 = 0$ (broken curve). At the following instant ($t_2 = 10\,\mu$sec), however, owing to the redistribution of the "collapsing" plasma, the difference between the distribution curves for $U_0 = 0$ and 12 kV diminishes; subsequently (e.g., at $t_3 = 50\,\mu$sec) the magnetic field for $U_0 = 12$ kV passes out of the plasma to a greater extent than for $U_0 = 0$. This is apparently because the longitudinal current through the plasma causes an increase in both the degree of ionization and the temperature. A similar type of variation in field distribution occurs for other discharge conditions as well. The plasma conductivity σ estimated from the thickness of the skin layer (as seen in Fig. 4, the skin layer is about 1 cm thick) is approximately $2 \cdot 10^{13}$ cgs. If we consider that collisions of electrons with neutral atoms predominate, then for $\sigma = 2 \cdot 10^{13}$ the electron concentration $n_e \approx 2 \cdot 10^{13}$ cm^{-3} and the degree of ionization is $\eta < 1\%$.

The distribution of the magnetic field H_{φ_0} of the longitudinal current I_0 along the tube radius was measured by a magnetic probe differing from that used in measuring the hf field only by the larger number of turns in the measuring coil. The probe sensitivity was ~2.5 kOe/V.

From the measured distribution of $H_{\varphi_0}(r)$, the distribution of current through the gas over the tube cross section, $j_0(r)$, was calculated. Here it was assumed that the axial symmetry of the discharge-current distribution was preserved while the $H_{\varphi_0}(t)$ oscillograms remained satisfactorily reproducible. Figure 5 shows curves of the relative distribution of $j_0(r)$ for various instants of time from the onset of the current pulse through the gas. As seen from the

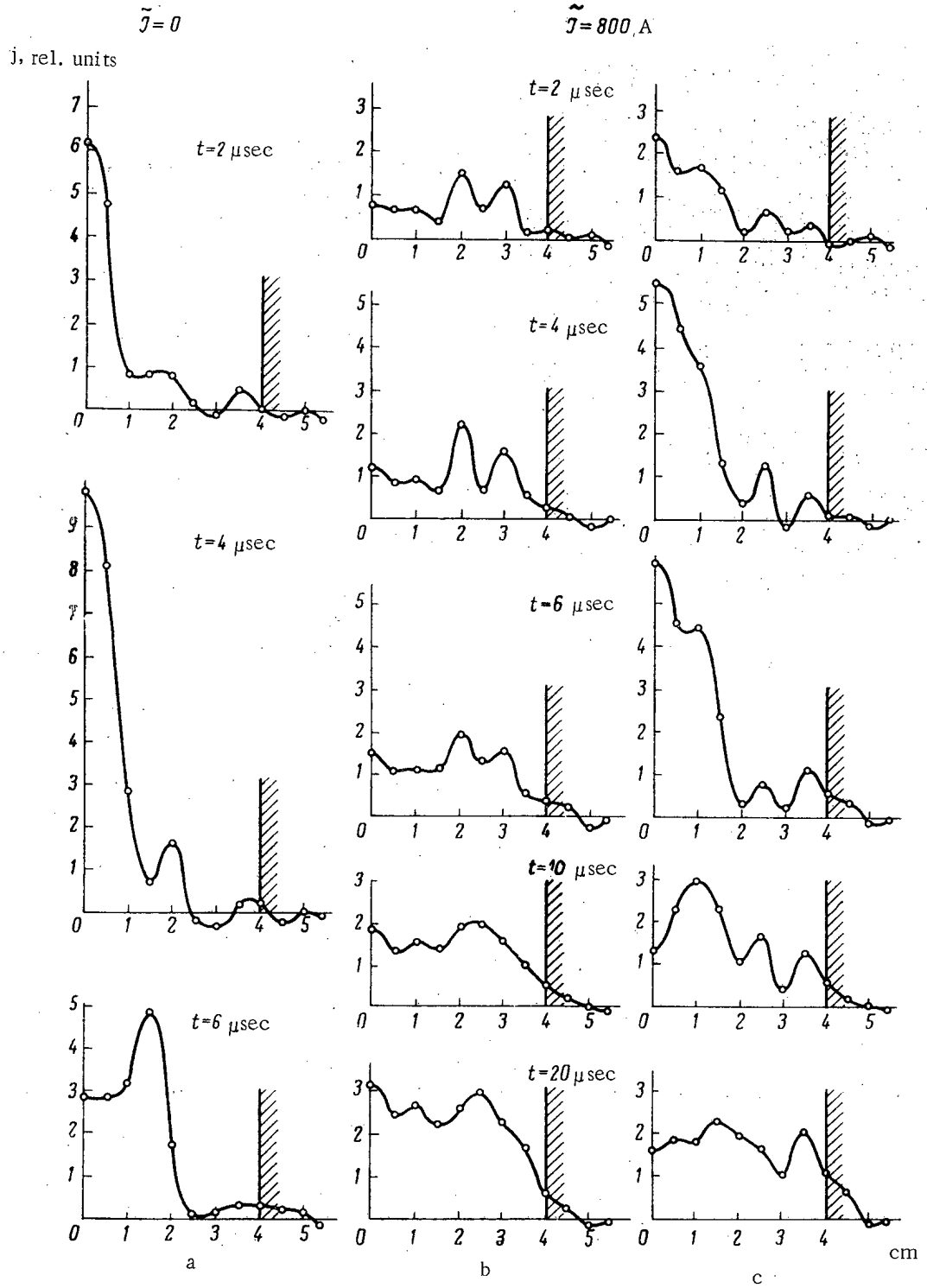

Fig. 5. Distribution curves of direct-current density $j_0(r)$ through the gas at various instants of time from the onset of the current: a) hf field absent, $\tilde{J}=0$, for $t>6$ μsec the symmetry of the discharge is disrupted; b) discharge between electrodes begins after ignition of hf discharge, current flows the whole time around the walls, the pinch is absent; c) hf field applied to formed pinch 0 to 6 μsec after onset of direct discharge; current undergoes redistribution out of the central part of the discharge tube into the peripheral region.

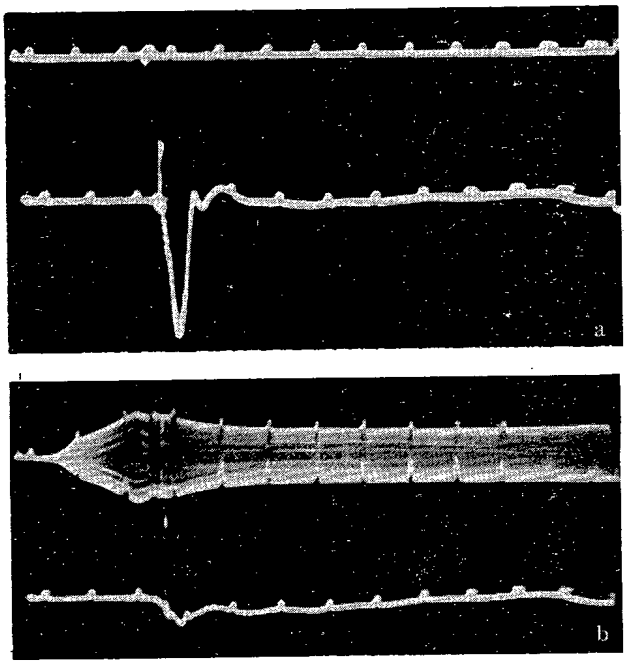

Fig. 6. Oscillograms of longitudinal flux Φ_z for p_0 = 0.05 mm Hg, U_0 = 15 kV ($I_{0\,max}$ = 1.6 kA), time markers every 20 μsec. Scale 1000 Mx/cm: a) $\tilde{J} = 0$; b) $\tilde{J} \neq 0$.

$j_0(r)$ curves of Fig. 5a, for $\tilde{J} = 0$ the breakdown takes place on the chamber axis, after which the pinch gradually broadens. Some 6 μsec after the beginning of the discharge, the symmetry of $j_0(r)$ is broken. If the breakdown occurs after the hf discharge is ignited, the current appears at once at the walls of the chamber (see Fig. 5b) and, growing, continues there the whole time. Finally, when the hf field is switched on after the breakdown (see Fig. 5c), the symmetry of the $j_0(r)$ distribution relative to the axis is preserved, but the current is gradually redistributed. The proportion of current flowing along the axis diminishes, and that near the tube walls increases. Thus the curves show, first, that the rate of current increase ($dI_0/dt \approx 10^8$ A/sec) is insufficient to displace the discharge at the initial stage to the periphery of the tube with subsequent constriction and skimming of the neutral gas to the axis (thickness of the skin layer, determined by the derivative dI_0/dt, exceeds tube radius) [3]; and, secondly, that the value of current I_0 bounded by the stability condition (1"), i.e., by the value of $\tilde{J}$, is insufficient for constriction in the case when the straightforward discharge begins after the high-frequency one and the current I_0 flows around the tube walls. Unfortunately, an increase in tube diameter leads to a fall in $\partial\tilde{H}/\partial r$, and an increase in I_0 demands a simultaneous increase in $\tilde{J}$, i.e., in the hf-generator power.[2]

In the bending of the compressed plasma pinch, the magnetic field of the current flowing through it is distorted, and a longitudinal component appears. From the change in the size of this component we may also judge the stabilizing effect of the hf field.

In order to record the flux of the longitudinal magnetic field, a 20-turn coil was wound on the discharge tube. The signal from the coil was integrated in its self-inductance and shunting resistance (time constant ~0.1 msec). In the oscillograms of Fig. 6 we see that, on applying the hf field, the signal from the coil sharply diminishes. The maximum flux recorded by the coil without the hf field was ~250 Mx, which for a 4-cm diameter of the plasma-pinch spiral corresponds to $\bar{H}_z$ = 20 Oe. However, despite the small value of the magnetic flux, the oscillograms indicate the suitability of this method of recording the instability of the plasma pinch in such experiments.

The results of our preliminary study of the interaction between a straight, self-constricted discharge and a hf magnetic field of quadrupole configuration indicate the stabilizing effect of the hf field (see Fig. 1, 2, and 6), although there remain some doubts connected with the fact that the hf field itself (independently of its configuration) may affect the course of the straight discharge. It is more expedient, however, to check this for large currents I_0 and correspondingly large $\tilde{J}$.

We see from the photographs of the discharge that, when the hf field is absent, the plasma pinch coils into a spiral gradually. In order to stabilize the perturbation with the minimum observable wavelength ($\lambda \approx 7.5$ cm), the current through the gas must not exceed 200 A. In our experiments, a stable, though not long-lasting, torn-off plasma pinch existed for $I_0 \leq 3000$ A, while, according to the stability condition, perturbations could only be suppressed for $\lambda \geq 60$ cm. This gives rise to the idea that, on stabilization of the long-wave perturbations, the development of

[2]For p_0 = 0.02 mm Hg and electron temperature T = 15 eV, the current I_0 necessary for constriction of the plasma must exceed $\sqrt{4c^2NkT} \approx 25$ kA, which corresponds (according to the stability criterion for λ = 60 cm) to current $\tilde{J} \approx 5$ kA. To obtain this current, we must raise the generator power some 40 times. Special measures taken to match the generator with the low-Q "plasma" load raised the power absorbed by the plasma to 2 MW and the current through the rods to $\tilde{J}$ = 2.5 kA. It was not possible, however, to achieve the desired change in the processes taking place. For a proportionate increase in I_0, the qualitative picture of the discharge remained as before.

short-wave perturbations is also hindered. In the case of the stabilization of a plasma pinch by a steady magnetic field, this effect cannot be detected, since, on satisfying the stabilization condition for large wavelengths, that for the stabilization of short-wave perturbations is automatically satisfied.

Both the photographs of the discharge and the current density distribution curves $j_0(r)$ along the radius of the discharge tube indicate the brief duration of the stable pinch. For a more prolonged containment of the plasma, it is (in our view) necessary to raise the current through the gas, and hence also that through the rods, substantially.

The author considers it his duty to express thanks to S. M. Osovets and Yu. F. Nasedkin for advice and discussion of the results, and also V. M. Atamanov, G. M. Balkov, V. P. Mokshantsev, V. G. Nikolaevskii, and A. Ya. Chermoshentsev for assistance in the work.

LITERATURE CITED

1. S. M. Osovets, ZhÉTF, 39, 311 (1960).
2. M. L. Levin and M. S. Rabinovich, ZhTF, 33, 164 (1963).
3. N. A. Borzunov, D. V. Orlinskii, and S. M. Osovets, "Atomnaya énergiya," 4, 149 (1958).

All abbreviations of periodicals in the above bibliography are letter-by-letter transliterations of the abbreviations as given in the original Russian journal. *Some or all of this periodical literature may well be available in English translation.* A complete list of the cover-to-cover English translations appears at the back of this issue.

EXPERIMENTAL STUDY OF PLASMA INJECTION INTO A PROGRAMMED MAGNETIC FIELD

(UDC 533.9)

O. I. Fedyanin

Translated from Atomnaya Énergiya, Vol. 18, No. 4,
pp. 329-335, April, 1965
Original article submitted April 22, 1964; revision submitted December 21, 1964

The authors give experimental results on the capture of an injected plasma by a rising magnetic field. It is shown that a long-lived plasma pinch is formed, localized at a distance from the wall of the vacuum chamber: the plasma density is $\sim 10^{12}$ cm^{-3}.

In the study of high-temperature plasmas, one of the main problems is how to fill magnetic traps with plasma. Most work on plasma injection into traps is connected with plasma–plasma and plasma–magnetic field interaction and with interaction between beam and plasma in the magnetic field, etc. [1-4]. In this paper we discuss the possibility of using irreversible processes in a plasma compressed by a rapidly rising magnetic field to secure injection into the magnetic trap.

Experimental Method

The principal purpose of this experiment was to study the possibility of lateral injection into a programmed magnetic field.

Figure 1 shows the topography of the magnetic field at various times. The field is uniform and quasistationary and has "wells" in time and space. The plasma is injected when the field on the axis is zero (see Fig. 1a). The field is then rapidly increased so that the lines of force become parallel and the plasma is compressed (see Fig. 1b and c).

In Fig. 2 the magnetic field is plotted against time in the center of the system. The maximum intensity is $\sim$4000 Oe, the duration of zero field is $\sim 20\ \mu$sec, and the rate of increase of the field $(dH/dt)_{max} \approx 1.7 \cdot 10^9$ Oe/sec; the field is increased according to the relation $H = H_0(1-e^{-t/\tau})$, where $\tau \approx (2.5\text{-}3) \cdot 10^{-6}$ sec.

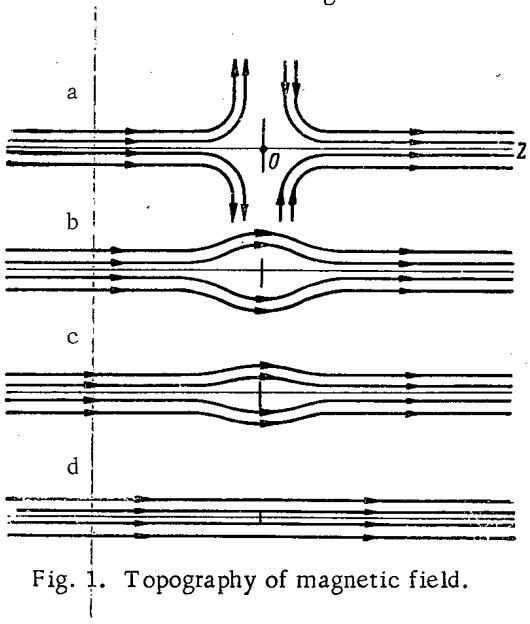

Fig. 1. Topography of magnetic field.

The magnetic system contains two parts: a solenoid giving a quasistationary field (half-period 4 msec) and two compensating coils which modulate the field in time and space in the injection region. The plasma is injected from two diametrically arranged injectors at time t_3 (see Fig. 2). The plasma sources were electrode injectors with the discharge on the surface of a plastic dielectric. The vacuum chamber (positioned within the solenoid) is a glass tube of diameter 12 cm, length 220 cm. The central part has two ground joints for the injector assembly. The system is evacuated to $5 \cdot 10^{-6}$-10^{-5} torr.

In studying the injection, we used the following measuring devices: a local electrically shielded probe, a luminescent screen [5], hf probes (frequencies 3000 and 10000 Mc) [6], and annular electric and magnetic probes for measuring the current and plasma discharge. In some experiments, where detailed localization of the measurements was not needed, the local probe (giving the plasma current density at a point) was replaced by a flat probe

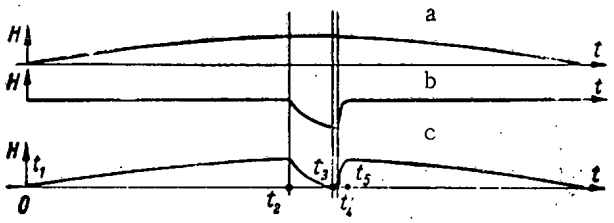

Fig. 2. Time dependence of field. a) Quasistationary field; b) compensating field; c) total programmed field in injection region.

composed of seven concentric collector rings (ring probes). The other methods used were the standard ones employed in laboratory studies of plasma physics.

The plasma-current configuration escaping from the magnetic trap created by the programmed field was investigated mainly by means of the luminescent probe. Figure 3a gives screen figures showing the electron image of the stable plasma-pinch configuration. It is seen that the plasma pinch, which is isolated from the walls of the vacuum chamber, lasts for a long time ($t \approx 10^{-4}$ sec); its width is 4-6 cm.

These results were obtained by a long series of measurements, intended to determine the effect of physical conditions on the formation of a plasma pinch. The criterion of optimum conditions was the presence of a localized plasma current on the axis. The following conditions were found to be necessary for a stable pinch:

1. The amplitude of the compensating field (see Fig. 2) must be equal, at least on the axis, to the axial field; the allowable deviation is 5-10%.
2. The working conditions may be either periodic or aperiodic; for the first current half-wave μ must be parallel to H (where H is the direction of the axial uniform magnetic field, μ the magnetic moment of the injector current).
3. The two sources must work identically (injecting the same number of particles).
4. The interval between the moment of injection and the beginning of increase in the magnetic field ($t_4 - t_3$) must be 3-6 μsec.

If these conditions are satisfied, the configuration obtained resembles that shown in Fig. 3a. Although a localized pinch is observed when the conditions are broken, the screen figures are then nonrepeating (see Fig. 3b), showing that there is no stable plasma configuration.

Local measurements of the plasma densities in two cross sections were made by means of screened electric probes. Figure 4 plots the current density distribution at distances z = 25 and 60 cm from the injector axis. The curves show that there is a plasma pinch which lasts for 80-100 μsec.

From probe measurements it was also established that, if the plasma injectors work aperiodically ($\Delta t \approx 10^{-6}$ sec), the plasma stream obtained by compressing the increasing field has a double structure: a rapid low-density leader is first formed ($v \approx 10^7$ cm/sec, $n \approx 10^{11}$ cm^{-3}), followed by movement of the main plasma body ($v = 5 \cdot 10^6$ cm/sec, $n \approx 10^{12}$ cm^{-3}). When the sources are changed to periodic working [$\Delta t \approx (5\text{-}6) \cdot 10^{-6}$ sec], the plasma has a different structure.

To measure the total number of trapped particles and obtain additional information on the radial plasma distribution, we investigated the pinch parameters by means of ring-shaped electric probes. The data given here refer to stable imaging of the localized pinch on the luminescent screen. The probe was 44 cm from the axis of the injectors. Figure 5 shows oscillograms for a ring-shaped probe. From similar oscillograms, we can plot the plasma-current distribution on the ring at various times (Fig. 6a) and, assuming axial symmetry of the plasma pinch, the density distribution, by converting nv to the plasma density (see Fig. 6b).

From the measurements with ring-shaped probes we can conclude that:

1. It is possible to make a differential measurement of the plasma current with separate rings, as the arithmetical sum of the signals from the separate rings agrees with the electrical sum, i.e., with the total current on all the rings connected together.
2. The total number of particles trapped by injection into the programmed magnetic field is $N \approx (3\text{-}5) \cdot 10^{15}$.
3. For $n = 10^{11}$ cm^{-3} the rate of density expansion is $v = 8 \cdot 10^6$ cm/sec; for $n = 10^{12}$ cm^{-3}, $v \approx 2.5 \cdot 10^6$ cm/sec.
4. A satisfactorily localized plasma pinch is obtained: when the radius is altered to 2.5 cm, the density decreases about tenfold.

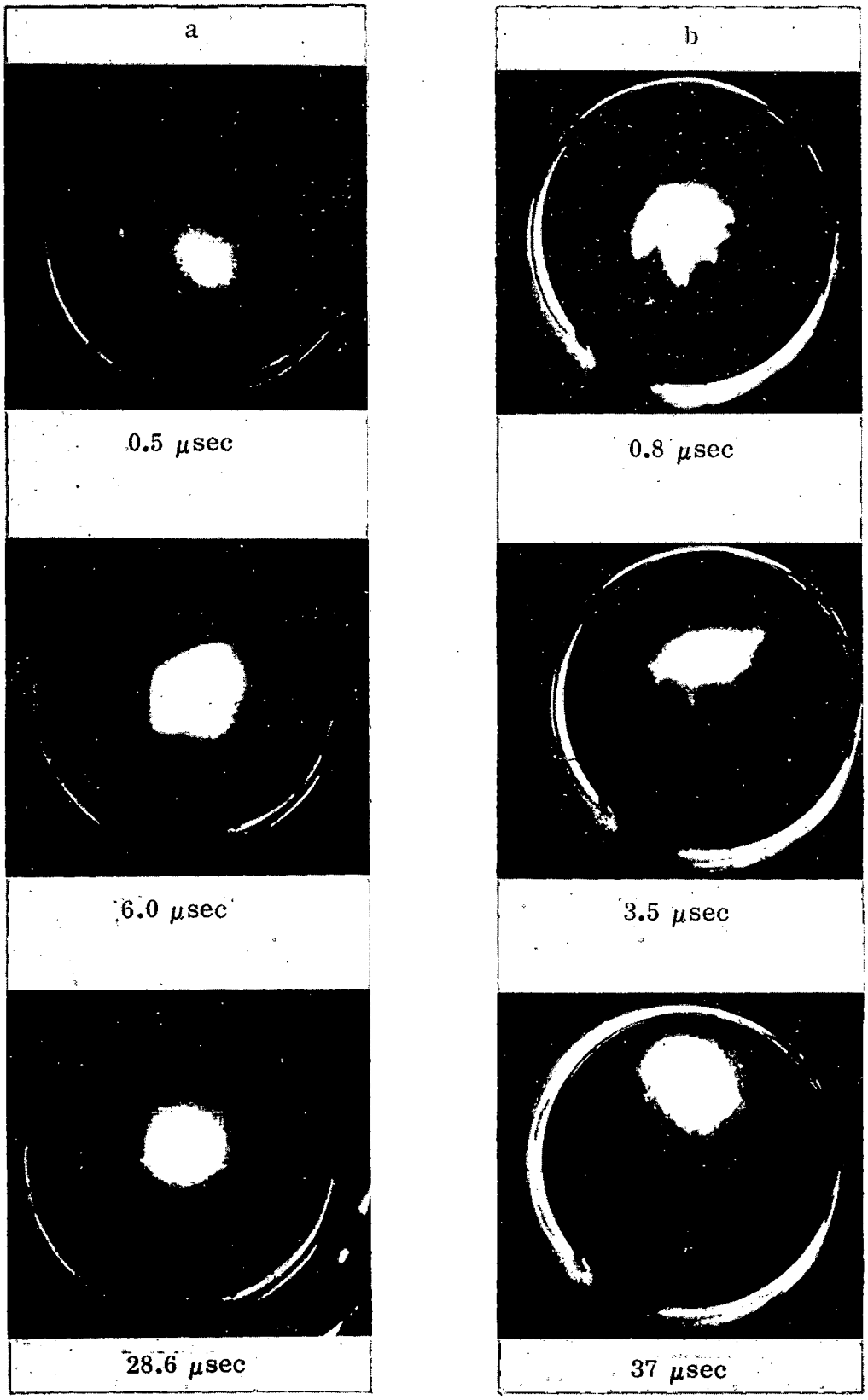

Fig. 3. Screen figures of plasma pinch (H = 2000 Oe, H_{comp} = 1400 Oe): a and b are plasma configurations, respectively; the times shown are measured from the beginning of the rise of the compressing magnetic field.

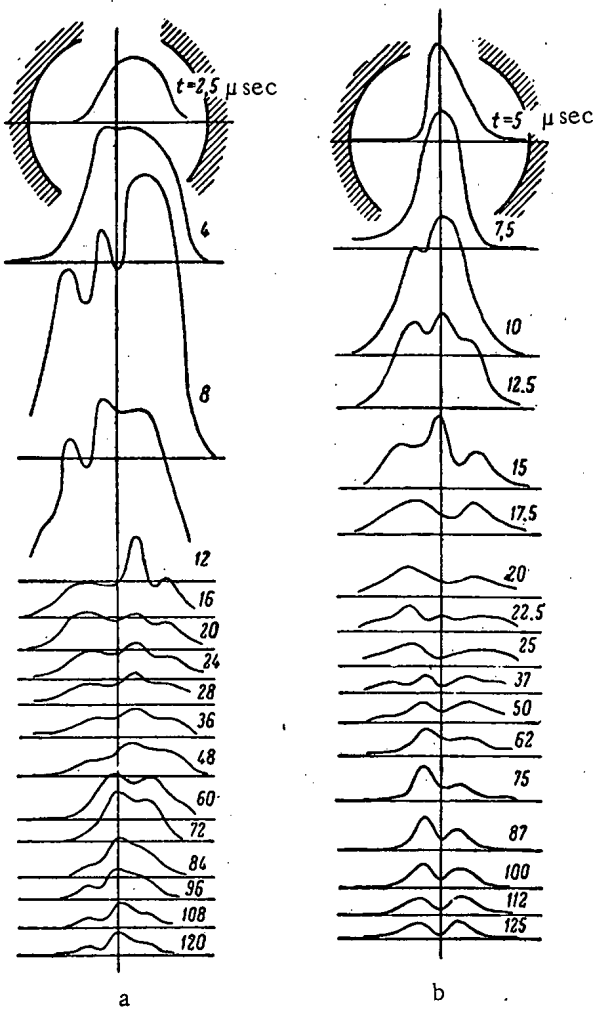

Fig. 4. Relative distributions of plasma-current densities at 25 (a) and 60 cm (b) from the injector axis, at various times.

5. The plasma caught in the magnetic field is distributed practically without loss along the lines of force. Measurements of the total current, made at various distances from the injection site, give a constant value within the region of existence of the magnetic field.

A high-frequency probe was used to afford an additional method, not associated with measurement of the plasma current, for measuring the resonance density of the plasma.

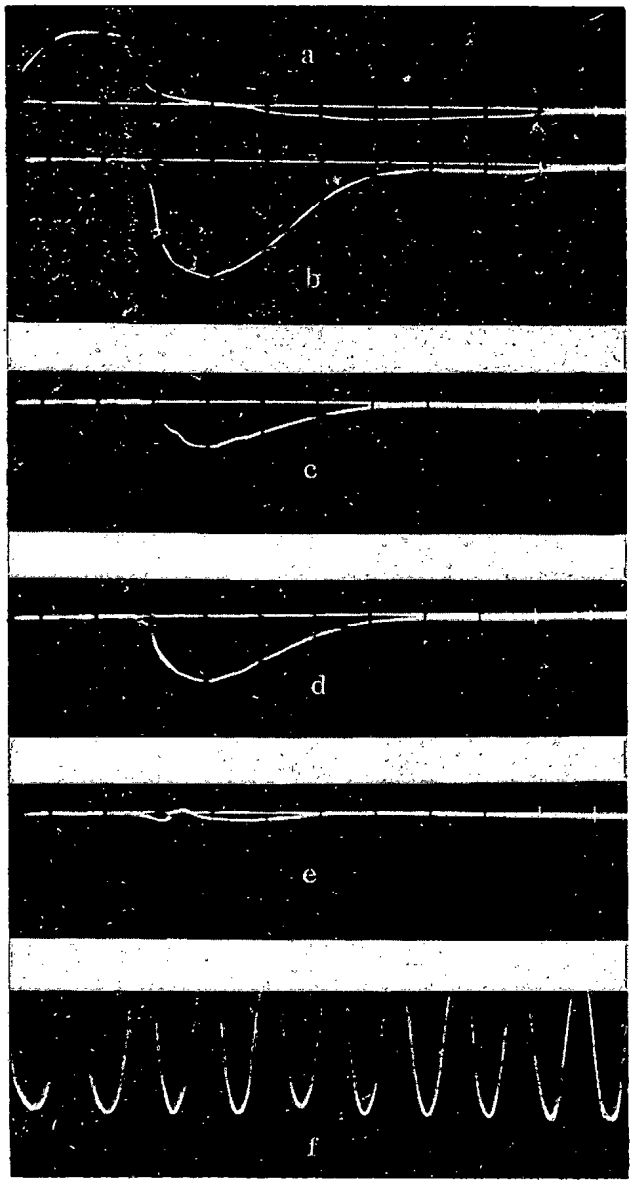

Fig. 5. Oscillograms of probe current to ring-shaped probe: a) compensating field; b) total signal for all rings; c) signal to first ring (diameter 1.1 cm, area 1 cm^2); d) signal to third ring (mean diameter 2.7 cm, area 3 cm^2, amplification factor 2.8); e) signal to seventh ring (mean diameter 9 cm, area 40 cm^2, amplification factor 7.6); f) calibration signal, $f = 100$ kc.

The hf probe was placed 60 cm from the injector axis. Figure 7 gives oscillograms with the probe working at wavelengths $\lambda = 10$ cm ($n_0 = 10^{11}$ cm^{-3}) and $\lambda = 3$ cm ($n_0 \approx 10^{12}$ cm^{-3}). In the region $R \leq 4$ cm, the density is $n = 10^{11}$ cm^{-3}, and in the region $R \leq 2.5$ cm, $n \approx 10^{12}$ cm^{-3}; the plasma with density 10^{11} cm^{-3} lasts much longer ($\sim 10^{-4}$ sec).

These results satisfactorily confirm the idea of localization of the plasma pinch.

To study the influence of electrodynamic forces on the mechanism of capture of the plasma by a rapidly increasing magnetic field, we made measurements of the induction current (magnitude < 0.1 kA). The compressed plasma was found to have little disturbing effect on the outer magnetic field.

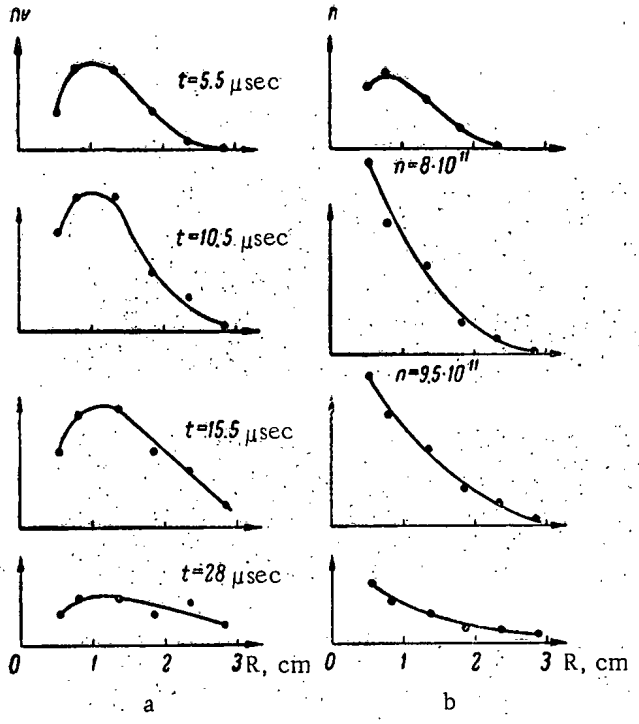

Fig. 6. Plasma-current distribution over chamber radius at various times. a) Current distribution; b) mean plasma-current density distribution (the characteristic densities are given below the curves).

Discussion of Results

It has been shown that lateral plasma injection is possible into a programmed magnetic field. So far we have obtained a plasma pinch of diameter 5-6 cm, isolated from the walls of the vacuum chamber for 80 μsec. With quasistationary field strength $H \approx 2$-2.5 kOe the maximum plasma density is $3 \cdot 10^{12}$ cm^{-3}. Preliminary measurements of the capture coefficient showed that this injection method gives adequate efficiency. The sources inject $\sim(0.7\text{-}1) \cdot 10^{16}$ particles, while the percentage of these captured is ~20-50%.

The plasma current travels 100 cm along the magnetic field with practically no losses.

The mechanism of plasma capture can be qualitatively represented as follows. The injected plasma fills the magnetic trap, the configuration of which is given in Fig. 1, and partly begins to flow along the lines of force. For slow compression, with $dH/dt \ll 8 \cdot 10^8$ Oe/sec, the capture efficiency (i.e., the number of captured particles) is 15-20 times less. After the trap is filled, compression begins. The compressed plasma forms a pinch, which spreads symmetrically along the axis away from the injection region.

The initial distribution of the plasma density within the trap is of great importance in the mechanism of capture. The presence of a residual non-compensated magnetic field in the region of distribution of the plasma sources leads to interaction between the injected plasma and these fields, and this may disturb the uniformity of filling. If the zero-field region is not symmetrically filled, the plasma pinch becomes unstable.

The compression of the plasma by the increasing magnetic field can be explained either by means of an MHD model or by considering the motion of individual particles in the drift approximation.

Using an idealized conception of the motion of a cylindrical layer of plasma under the action of a linearly increasing outer field [7], we can estimate the order of magnitude of the characteristic compression time. The plasma layer reaches the axis after a time

$$t = \sqrt[4]{48\pi \frac{r_0^2 \rho_0 \tau^2}{2H\Delta H}},$$

where r_0 is the initial radius of the plasma, ρ_0 the initial density, H the maximum field; $dH/dt = H/\tau$; $\Delta H = H_{ze} - H_{zi} = 4\pi j$ is the drop in the magnetic field at the plasma-vacuum boundary. For our apparatus, the compression time, estimated from the above formula, was $t \approx 2 \cdot 10^{-6}$ sec. Thus, even at relatively low plasma currents ($j < 100$ A), this very approximate model gives quite acceptable values for the duration of the motion.

Owing to unequal filling of the sources, lack of synchronization at the moment of action, or residual fields in the injection region, the trap may be nonuniformly filled with plasma: the pinch is then formed at a distance from the axis and later moves to the wall of the vacuum chamber. As the field in the injection region increases with distance from the trap axis, the force acting on the plasma is $\mathbf{F} = \text{grad}(\mu H)$, where μ is the magnetic moment of the plasma-current vortex; the presence of this force is a possible reason for the ejection of the plasma to the wall.

The compression of the plasma by the increasing magnetic field can also be explained by considering the motion of individual particles. The plasma, finding itself within the force tube (which in our case has the shape of a concentric funnel), becomes deformed as the dimensions of this tube alter. The displacement of the plasma pinch is due to drift of the plasma in the curvilinear field, which is completely removed when the force tube is symmetrically filled.

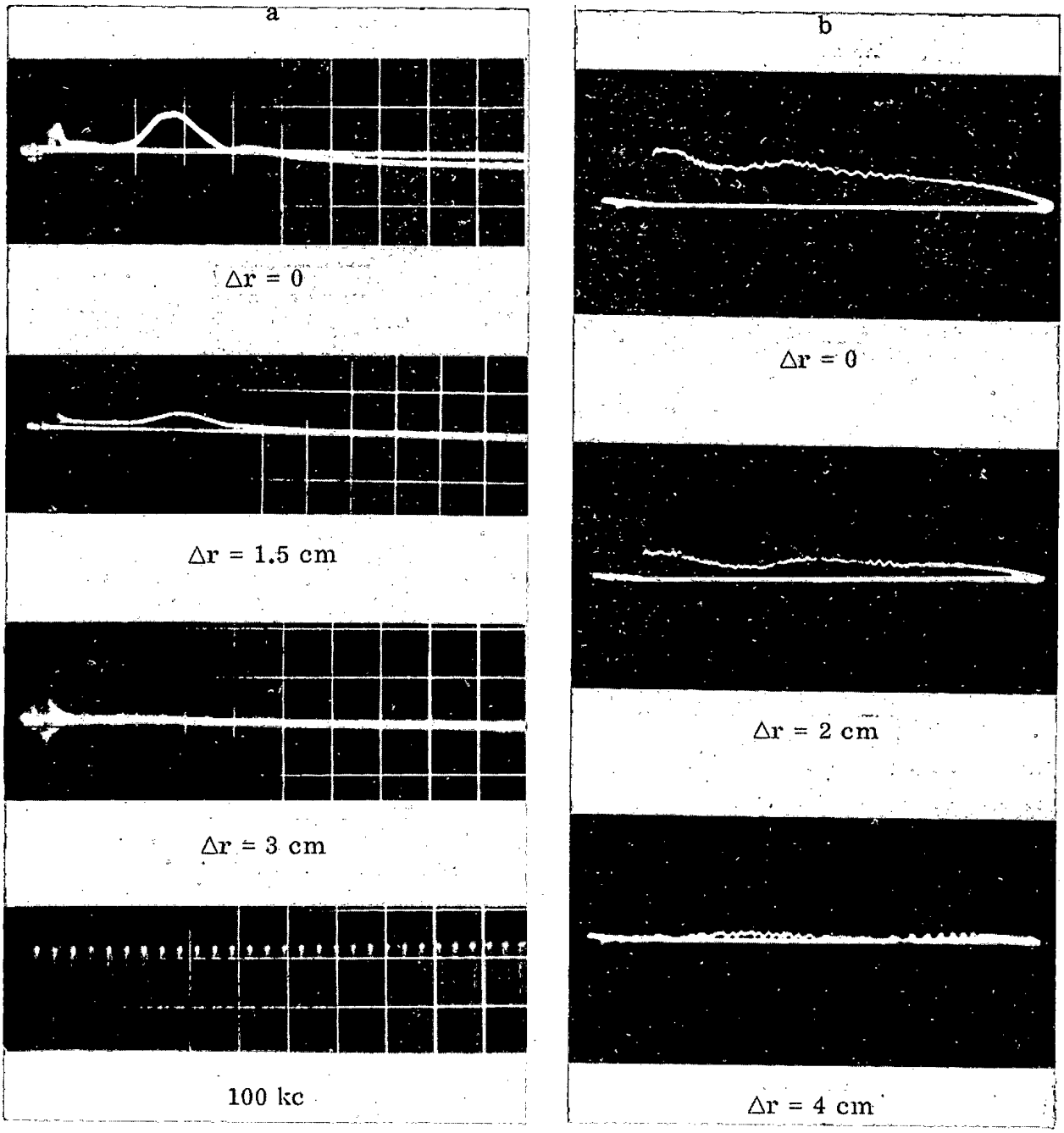

Fig. 7. Oscillograms of potential of high-frequency probe. a) Wavelength $\lambda = 3$ cm, $n_0 = 10^{12}$ cm^{-3}; b) wavelength $\lambda = 10$ cm, $n_0 = 10^{11}$ cm^{-3}; Δr is the distance between the probe and the chamber center.

The author wishes to thank M. S. Rabinovich and I. S. Shpigel' for valuable advice and useful discussion of the results, V. F. Pis'menko and E. N. Sobolev for help in the investigations, and N. V. Perov and the mechanics' collective under the leadership of V. P. Solov'ev for help in building the apparatus.

LITERATURE CITED

1. J. Tuck, Phys. Rev. Lett., 3, 313 (1959).
2. S. Yu. Luk'yanov, I. M. Podgornyi, and V. N. Sumarokov, ZhÉTF, 40, 448 (1961).
3. Eubank and Wilkerson, Phys. Fluids, 4, 1407 (1961).
4. M. A. Ivanovskii and G. M. Batanov, ZhTF, 35, 66 (1965).
5. M. A. Ivanovskii et al., In collection: "Plasma Diagnostics" [in Russian], Gosatomizdat, Moscow (1963), p. 263.
6. B. P. Kononov, A. A. Rukhadze, and G. V. Solodukhov, ZhTF, 31, 565 (1961).
7. L. A. Artsimovich, Controlled Thermonuclear Reactions [in Russian], Fizmatgiz, Moscow (1961).

A PULSED NEUTRON GENERATOR

(UDC 621.373.2:539.172.84)

G. E. Murguliya and A. A. Plyutto

Translated from Atomnaya Énergiya, Vol. 18, No. 4,
pp. 336-342, April, 1965
Original article submitted February 8, 1964

The authors give the results of physical investigations on a neutron generator with spark-ion source, yielding pulsed-neutron fluxes from the reactions D+D and D+T, with mean yields $\sim 7 \cdot 10^6$ and $\sim 10^9$ per pulse respectively. The total pulse length is ~100-250 μsec and the potential across the accelerator gap is ~110 kV.

A number of models of pulsed-neutron generators with spark ion sources have recently been developed [1, 2]. These are used in nuclear physics and its applications. However, they have not so far been subjected to detailed physical investigation. The working characteristics of a neutron generator are, of course, determined by the parameters of the ion beam (composition, current strength and time characteristics), the magnitude and stability of the accelerating voltage, and the target properties. We have studied the influence of these factors on the working of one type of neutron generator.

Description of Apparatus and Experimental Method

We first developed a suitable method and apparatus for the problem in hand.

The construction principles of the neutron generator (Fig. 1a) are similar to those of the model described in [3]. It differs from the latter in that a grid 3 is positioned in the selection and accelerator gap, and is connected to a capacitative potential divider (C_1 and C_2) and screen 7. This grid forms an intermediate electrode; when the generator is working it acquires a floating potential and prevents electrical breakdown. Screen 7 retains secondary electrons emitted from the target and protects the sides of porcelain chamber 4 from the deposition of a conducting layer, thus avoiding breakdown along the chamber sides. These modifications made it possible to increase the diameter of hole 2 in the limiting electrode to 16 mm, raising the ion current three or four times and increasing the accelerating potential to $V_G = 100$-110 kV.

By introducing a large inductance, L = 300-600 μH, into the spark circuit, it was possible to stabilize the evaporation of the working substance and increase the neutron yield. The working substance was evaporated from combined-electrode 9 and burnt out at a depth of ~5 mm, preserving the metal walls of the electrode channel. The secondary electron beam burns the working substance in the spark gap, which is situated on the axis of the spark source; for this reason, we used only the auxiliary gaps of the standard source.

To study the ion-beam composition and energy scatter, we used a mass spectrograph and the method of parabolae [4] (see Fig. 1b). The narrow ion beam was passed through a 1-mm-diameter hole in the target 6 and two collimating diaphragms 13, and then traversed a region of electrical and magnetic fields 15, where it was analyzed; it finally fell on a photographic plate 14, fluorescent screen, or Type II scintillation counter. By photography with MP plates, we studied the ion-beam composition averaged over ~100 pulses. The photographs were subjected to photometry (making a correction for the blackening produced by ions of different masses), and this enabled us to form some idea of the quantitative beam composition. When necessary, visual observations were made on the screen for qualitative control of the beam composition in each individual pulse. The time characteristics of the analyzed beam were studied by means of a Type II scintillation counter [CsJ(Ti), FÉU-29].

At the same time we investigated the neutron yield. The mean yield for neutrons from the D+D reaction was measured by the silver-activation method (see Fig. 1b). The apparatus was calibrated with standard Ra+Be and Po+Be

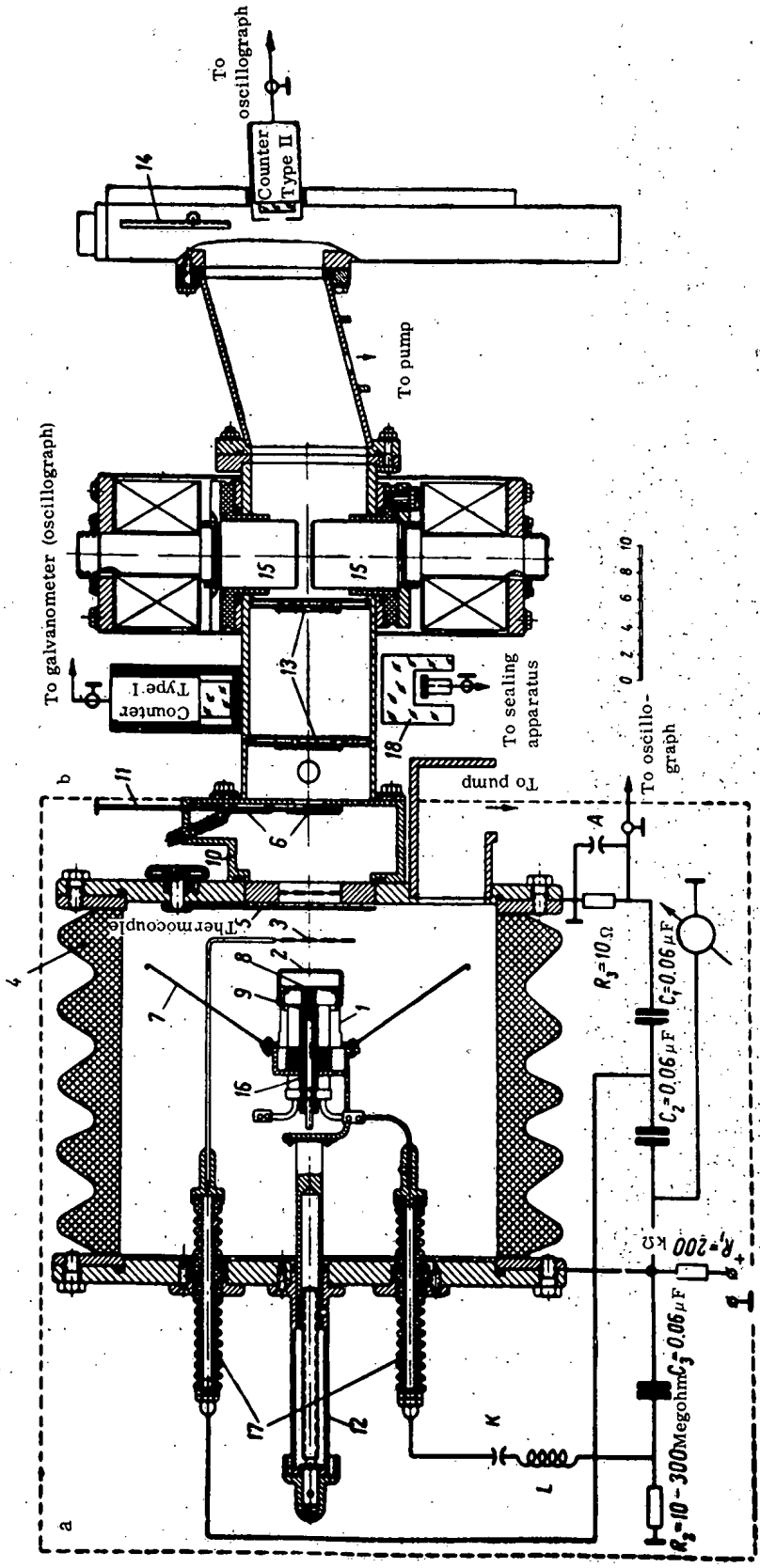

Fig. 1. Schematic cross section of apparatus. a) Neutron generator; b) mass spectrograph and other diagnostic devices. 1) Spark source; 2) selection grid; 3) intermediate electrode (grid); 4) porcelain chamber; 5) diaphragm; 6) targets; 7) screen; 8) LiD insert; 9) combined electrode; 10) cassette for targets; 11) rod for adjusting targets; 12) handle for adjusting ion source; 13) diaphragms; 14) photographic plate; 15) magnet pole; 16) porcelain tube; 17) insulators for leads; K, A) spark gaps; L, C_3) inductance and capacitance in spark circuit; C_1, C_2) capacitances in selector circuit; R_1, R_2) discharge resistances; R_3) current monitor in selector circuit; 18) apparatus for activation registration of neutrons; I, II) scintillators for recording neutrons and ions, respectively.

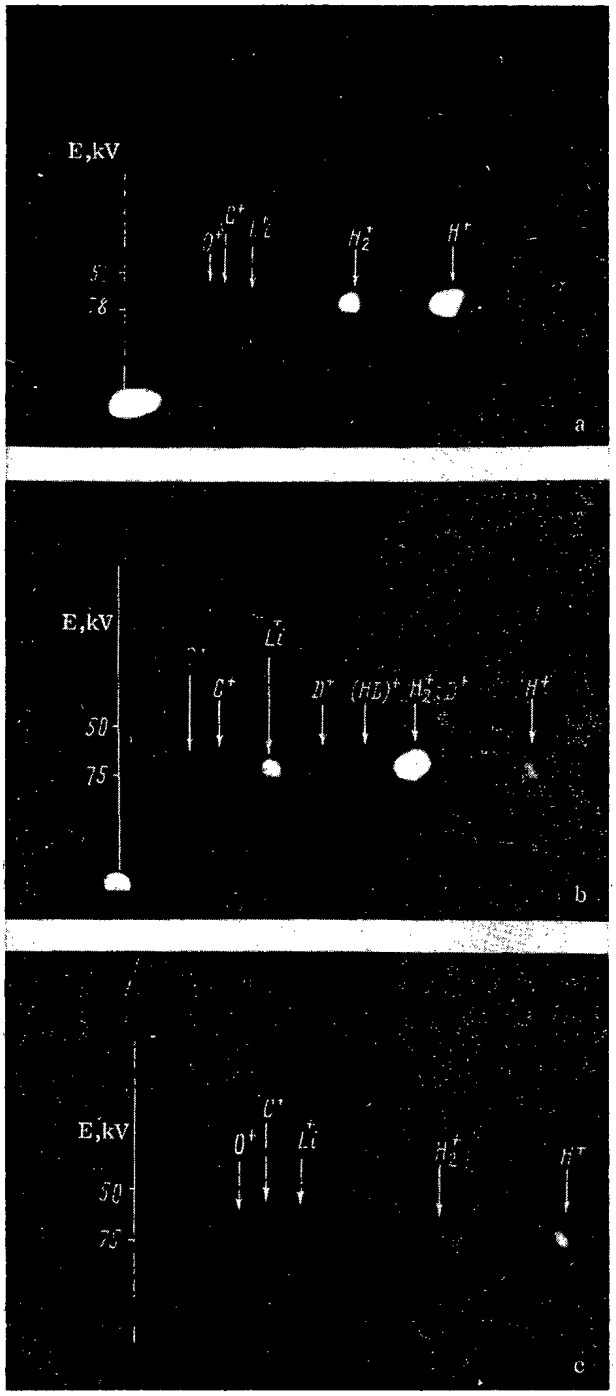

Fig. 2. Mass spectrograms of beam composition (E = ion energy, kV). a) Initial working stage of spark gap; b) optimum stage; c) beam composition after $3 \cdot 10^5$ pulses.

neutron sources. The neutron yield from the D+T reaction was measured by the copper-activation method. The time characteristics of the pulse were studied with a Type I counter, consisting of a plastic scintillator and an FÉU-24 [photocell]. The absolute number of neutrons in each separate pulse was determined by analyzing the tracks on the oscillograms [5]. A Type I counter was used to study the stability of the neutron yield from one pulse to another.

The total ion-induced current in the selector circuit was registered by measuring the potential across $R_3 = 10\,\Omega$. Spark gap A protects the measuring circuit from high-tension leakages occasioned by flashovers. The mean ion current to the target was determined by the thermal method, corrections being made for cooling. The D^+-ion current to the target was determined from the neutron yield.

Experimental Results

Ion-Beam Composition and Its Influence on the Neutron Yield. Mass-spectroscopic investigations showed that the neutron yield depends markedly on the ion-beam composition. The ion beam suffers definite changes owing to the working of the ion source and the heating up of the working substance. This is illustrated by the mass spectrograms shown in Figs. 2a, b and c. The H_2^+ and D^+ lines are superimposed, and their separate values are calculated from the lines of the molecular ions $(HD)^+$ and D_2^+.

During the first thousand or so pulses, the working substance is usually evaporated inefficiently. H^+, H_2^+, C^+ and O^+ ions predominate in the beam and there are few Li^+ ions (Fig. 2a). After aging—about 10^3-10^4 pulses—the source enters its optimum working state and the working substance is evaporated intensively. D^+ ions then predominate, sometimes reaching 80% of the beam (see Fig. 2b). Impurity ions (Li^+, C^+, O^+) and molecular ions [D_2^+, $(HD)^+$, H_2^+] are found only in small quantities. Li^+ ions adhere chemically to the source, as they react with elements in the porcelain. After about $5 \cdot 10^5$ pulses, this leads to destruction of the porcelain tube. The D^+ content of the ion beam remains stable at above 50% for about 10^5 pulses. After this, the number of impurity ions (H^+, H_2^+, Li^+, C^+ and O^+) then rises, and finally, after about $2\text{-}3 \cdot 10^5$ pulses, these ions become predominant (see Fig. 2c).

As the beam composition changes, so does the neutron yield. This is clearly seen from Fig. 3, which plots the relative intensity of D^+ and Li^+ ions, $\Delta S_{D^+}/\Delta S_{Li^+}$ (I), and the relative neutron yield, N (II), versus the number of pulses, n (i.e., the degree of burn-out of the working substance). The values during the optimum period are taken as unity. Curve I was obtained by photometry of a number of photographs like those in Fig. 2. In measuring curve II, it was necessary to eliminate the effect of target fatigue. For this purpose, the beam was directed on to the target for the short time necessary for the measurements, and the target was then covered with the diaphragm.

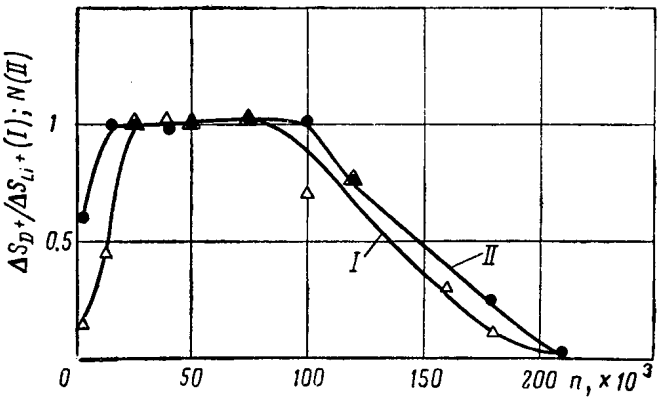

Fig. 3. $\Delta S_{D^+}/\Delta S_{Li^+}$, the relative D^+ content, and N, the neutron yield, versus n, the number of pulses. During the optimum period, $\Delta S_{D^+}/\Delta S_{Li^+}$ and N are normalized to unity.

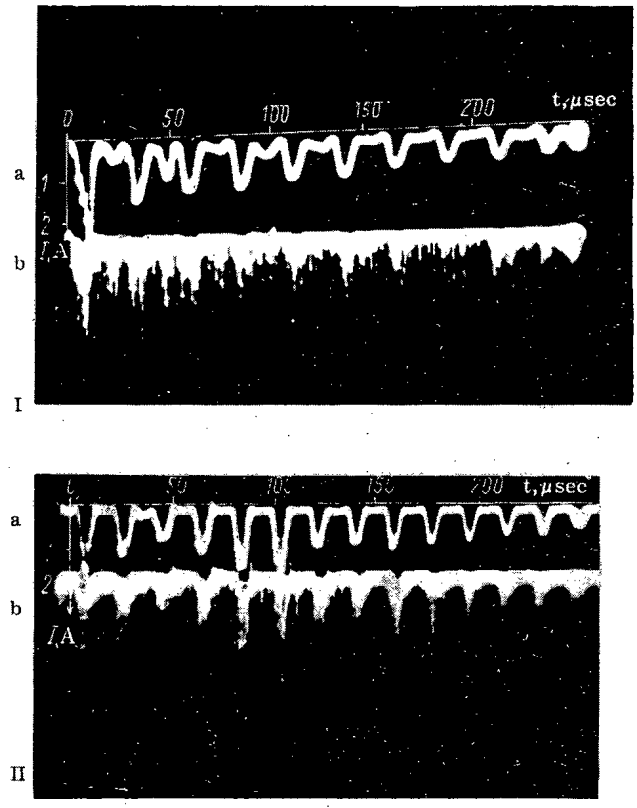

Fig. 4. Oscillograms of ion-electron current in accelerating gap (a) and neutron pulse (b) for reactions D+D (I) and D+T (II). t = duration of ion-current pulse, μsec.

By means of similar experiments, it was found that the number of pulses over which the neutron yield decreases by a factor of two (by comparison to the optimum yield) is about $1.5 \cdot 10^5$, whatever the spark gap. The over-all lifetime for the production model [6] is about 10^6 pulses.

The working substance can be a volatile organic compound (e.g., hydrocarbon) based on deuterium. This should preferably have a high deuterium content and not contain chemically active substances. By this means the source lifetime can be considerably increased.

Total Ion Current and Its Influence on the Neutron Yield. The mean ion current per pulse to the target, measured by a thermal method, increases proportionally to the spark power and reaches 0.5-1 A when the potential across the spark condenser is $V_S = 70$ kV and the mean pulse duration is ~100 μsec.

The time characteristics of the ion current were determined from oscillograms of the total ion current and the secondary-electron current in the selector circuit. The ion current was corrected for the coefficient of secondary emission, which in these experiments was 3.5-4 and did not vary appreciably in the accelerating voltage range $V_G = 60$-100 kV.

Figure 4a shows oscillograms of the total ion current: this oscillates with the natural frequency of the spark circuit and decreases proportionally to the oscillating current in the spark. Ion-current pulses are observed when the cathode spots fall on the combined electrode 9 (see Fig. 1).

In general, the neutron yields from the D+D and D+T reactions (see Fig. 4b) are strongly correlated in time with the ion current. The total ion current, determined from the neutron yield (taking account of the relative D^+ content [7]) at $V_G = 80$-100 kV, does not differ appreciably from the value determined by the thermal method.

At constant V_G, the neutron yield per pulse from the D+D reaction increases with the power of the spark discharge (Fig. 5). The spark power was increased by increasing the initial potential V_S across the spark capacitance C_3; the gap K was also widened. The pulse repetition frequency was kept constant by varying R_2 (see Fig. 1a). The rapid rise of the neutron yield for small V_S is due to increase of the D^+ current at target 6 (see Fig. 1a). The bend in the curve of Fig. 5 is due to the fact that the ion beam begins to fall outside the edges of the target. The absence of saturation is here caused by growth of the spark-plasma density, and consequently of the ion current, with increasing V_S.

At $V_G = 110$ kV and $V_S = 70$ kV, the maximum neutron yields from the D+D and D+T reactions per pulse of length ~250 μsec were $\sim 7 \cdot 10^6$ and $\sim 10^9$ respectively.

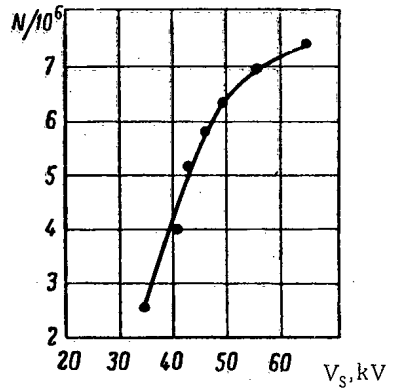

Fig. 5. Neutron yield per pulse versus spark power at $V_G = 106$ kV (V_S = initial potential across spark condenser C_3, N = number of neutrons per pulse).

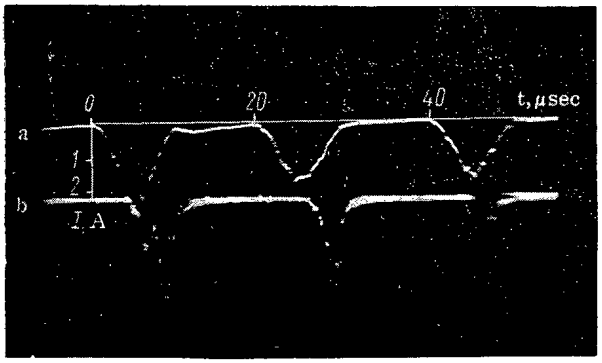

Fig. 6. Oscillograms of ion-electron current in accelerator gap (a) and D^+ current in analyzer (b).

Energy Scatter of Ions in the Beam and Its Influence on the Neutron Yield. The mass spectrograms (Fig. 2a, b, c) reveal that the ions have an energy scatter of up to −15 kV, due to decrease in the accelerating voltage at large pulse currents. By increasing C_1 and C_2, this falling-off in voltage can be reduced, but there is then an increase in gas evolution during flashover, and this hinders the operation of the generator. These adverse effects are especially noticeable at low accelerating voltages. At voltages $\gtrsim 100$ kV, voltage fluctuations reduce the neutron yield only by 10-15%.

In most cases, the sections of the mass-spectrogram parabolas (Fig. 2a, b, c) have a layer structure. This is due to current oscillations in the analyzer. Figure 6 illustrates this effect with oscillograms of the total ion-electron current in the selector circuit (a) and the D^+-ion current (b) in the analyzer. The beam usually enters the analyzer only during the decreasing stage of each oscillation of the total ion current. Between successive entries of the beam into the analyzer, the accelerating voltage falls off and the beam departs from the parabola, imparting a layer structure to the blackening. In some cases the analyzer current vanishes altogether, or does not at all correspond in amplitude and duration to the total ion current. These deviations in the analyzer current are apparently due to fluctuations in the emitting surface of the plasma; these cause changes in the conditions for transmission of the relevant beam component through the narrow opening in the target. The lack of correspondence between the analyzer current and the total ion current might cause errors in determining the beam composition: to ensure reliable analysis, we therefore averaged over a large number of pulses.

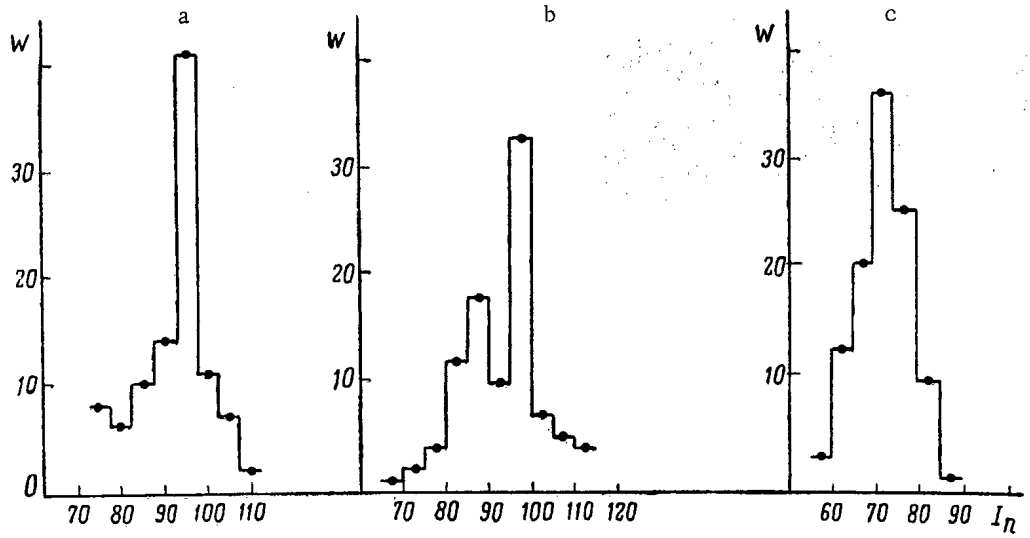

Fig. 7. Histograms showing stability of neutron yield, constructed from separate consecutive series of measurements taken over $\sim 10^4$ pulses. I_n = amplitude of neutron pulse, arbitrary units; W = number of pulses. a) $V_G = 96$ kV; b) $V_G = 90$ kV; c) $V_G = 87$ kV.

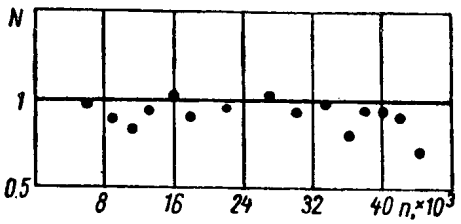

Fig. 8. Fatigue of T_iT target versus number of pulses, n. N = relative neutron yield, normalized to unity at $n = 5 \cdot 10^3$ pulses.

Stability of Neutron Yield

Target Fatigue. The stability of the neutron yield depends on the working of the ion source and on target fatigue. These two factors were studied separately.

The neutron yield was measured, with the generator working in the optimum state, for each of 100-150 pulses. The target was then covered with the diaphragm and a further series of measurements made over $\sim 10^4$ pulses, and so on. Similar measurements were made for all six spark gaps in the production-model ion source. On passing from one gap to another, the total neutron yield can change by a factor of two or three. For an individual gap, the neutron yield varied by about ±5-10%. In the conditions of our experiments, the vacuum spark thus developed with adequate stability. Figure 7 gives typical histograms of the neutron yield.

Fatigue of the target might be caused either by the formation of an organic film on its surface (oil from the diffusion pump) or by sputtering from the beam.

The fatigue of T_iT targets was investigated experimentally by the following method. The generator was brought into its optimum working stage, and the relative neutron yield from the D+T reaction was measured, keeping the accelerating voltage constant at $V_G = 90$ kV. Measurements were made over ~100 pulses out of each $\sim 3 \cdot 10^3$ pulses. The yield was measured by a monitor based on the short-lived induced activity of lead ($T_{1/2} = 0.8$ sec) [8]. A special electronic circuit ensured registration of the activity belonging to Pb^{207m}, formed mainly by the reaction $Pb^{208}(n, 2n)Pb^{207m}$. Fatigue of the T_iT target scarcely reduces the neutron yield during $\sim 4 \cdot 10^4$ pulses (Fig. 8).

Our investigations of this neutron generator with spark-ion source have thus enabled us to make considerable improvements in the working parameters of the first model [3]. The simple construction of the generator and associated electrical circuit make this a convenient device for laboratory investigations in nuclear physics and its applications. In particular, it has been used to study short-lived isotopes and isomers ($T_{1/2} \geq 1$ msec) formed in (n, 2n) reactions with various nuclei.

The authors would like to thank I. P. Selinov and I. M. Rozman for their interest and valuable advice.

LITERATURE CITED

1. J. Gow and H. Pollock, Rev. Scient. Instrum., 31, 3, 235 (1960).
2. B. Carr, Nucleonics, 18, 75 (1960).
3. G. E. Murguliya and A. A. Plyutto, Pribory i tekhnika éksperimenta, 5, 28 (1961).
4. A. Dempster, Rev. Scient. Instrum., 7, 46 (1936).
5. G. E. Murguliya, A. A. Plyutto, and I. M. Rozman, Pribory i tekhnika éksperimenta, 1, 54 (1962).
6. A. A. Plyutto, K. N. Kervalidze, and I. F. Kvartskhava, Atomnaya Énergiya, 8, 153 (1957).
7. É.-G. V. Aleksandrovich and V. A. Sokovishin, Pribory i tekhnika éksperimenta, 5, 7 (1961).
8. L. Ruby and J. Rechen, Nucl. Instrum. Methods, 15, 74 (1962).

FEASIBILITY OF USING THORIUM IN FAST POWER REACTORS

(UDC 621.039.526)

A. I. Leipunskii, O. D. Kazachkovskii,
S. B. Shikhov, and V. M. Murogov

Translated from Atomnaya Énergiya, Vol. 18, No. 4,
pp. 342-350, April, 1965
Original article submitted July 9, 1964

This paper gives data on the feasibility of using U^{233} and thorium in a breeding-reactor system. From the viewpoint of doubling time, the most promising method is the simultaneous use of U^{233}-Th and Pu^{239}-U^{238} in a mixed-fuel cycle in fast reactors; the thorium being distributed in the screens and the U^{233}, Pu^{239} and U^{238} in the cores. Consumption and breeding of U^{233} and Pu^{239} is arranged so that their amounts remain in constant ratio. The doubling time of a fast-reactor system working with a mixed-fuel cycle is considerably less than that of reactors using only U^{233} or thorium. The main raw material is thorium. A method is indicated for obtaining isotopically pure U^{233} containing $\sim 10^{-4}\%$ U^{232}.

The use of thorium for U^{233} breeding encounters substantial difficulties, which make this system uneconomical as compared, for example, with fast breeder reactors using plutonium.

These difficulties, which impede the use of U^{233} for nuclear power production, are as follows:

1. The low breeding rate in the U^{233}-Th thorium fuel cycle.

2. U^{233} has a higher activity than U^{235} or Pu^{239}, owing to accumulation of U^{232} and its daughter isotopes.

The available data on the nuclear constants of U^{233} and Th^{232} [1] indicate that the U^{233}-Th cycle can in principle be used to breed U^{233} from thermal or fast neutrons.

In the optimum case, taking account of all losses, the breeding ratio of thermal thorium reactors is up to ~1.1, while for fast reactors it is about 1.3. The minimum doubling time for such systems, allowing for the practical factors involved in nuclear power production, is 15-20 years [2]. For intermediate neutron energies (1 eV to 1 keV), ν_{eff}, the number of fission neutrons per absorbed neutron, is less than two for U^{233}: breeding is thus impossible under these conditions.

Fast plutonium-breeder reactors, in which the breeding ratio is ~1.5-2.0 and the doubling time can be much less than 15 years, and much more efficient than reactors employing U^{233} and Th.

However, it is found that the so-called mixed-fuel cycle, used with fast neutrons, can substantially improve the characteristics of fast reactors using thorium; a system can be devised with a doubling period nearly equal to that obtained with a pure plutonium fuel cycle. In addition, the activity of the U^{233} produced can be considerably reduced.

Breeding in Fast Reactors With a Mixed-Fuel Cycle

A "mixed-fuel cycle" is a breeding-reactor system using two fissionable isotopes simultaneously as nuclear fuels: these are Pu^{239} and U^{233}, and the raw materials from which they are bred are U^{238} and Th^{232}.

For a fast reactor working in such a cycle, the neutron balance is much better than that for the thermal thorium cycle, owing to the additional contribution from U^{238} fission and the high ν_{eff} of Pu^{239}.

A mixed-fuel cycle can be realized in either of two ways:

1. The nuclear fuel is placed in two reactors working in parallel. Thorium is placed in the breeding zone of both reactors. In the core of one reactor (which we shall provisionally call "Type 9"), the main fissionable isotope

is Pu^{239}, while the breeder raw material is U^{238}. In the core of the other (which we shall call "Type 3"), the main fissionable isotope is U^{233} and the raw material is again U^{238}. U^{233} is formed in the thorium used in the screens of both reactor types, and after chemical separation part of it is used to compensate for its consumption in the Type-3 reactor and the rest to construct new cores for reactors of the same type. Part of the secondary Pu^{239}, formed in the U^{238} of the Type-3 and -9 cores, is used to compensate for consumption in the Type-9 reactor, and the remainder is extracted in the chemical plant and used to construct new cores for reactors of the same type.

2. The fissionable isotopes—Pu^{239} and U^{233}—are regarded as a single-composite nuclear fuel, employed in the core of a single reactor, with some fixed isotopic ratio of U^{233} to Pu^{239}.

The plutonium and U^{233} can be either homogeneously mixed in the core, or placed separately in the inner and outer sections, or in separate cassettes. The breeding blanket of such a reactor contains thorium. The U^{233} formed in this is extracted in the chemical plant, and part of it is used to compensate for consumption of the mixed fuel.

Part of the secondary Pu^{239}, formed in the U^{238} of the core, is used to compensate for depletion. As excess of Pu^{239} and U^{233} is extracted from the thorium, new mixed fuel is available for the construction of new cores.

The dynamics of mixed cycles can conveniently be analyzed by means of Usachev's theory of the evolution of breeder-reactor systems [2].

Let us assume that all the excess fuel (U^{233} and Pu^{239}) produced by the mixed-fuel cycle is used in the construction of new reactors of Types 3 and 9. The appropriate non-stationary equations, allowing for the effect of delay, are:

$$\frac{dN_9}{dt} = i_9(t) - i_9(t - T_{a9}), \tag{1}$$

$$\frac{dN_3}{dt} = i_3(t) - i_3(t - T_{a3}), \tag{2}$$

$$i_9(t) = i_9(t - T_{a9} - T_{p.c9})[1 - \Delta_9(1 - \text{BRC}_9)]\varepsilon_9 + \frac{M_3}{M_9}\Delta_3\,\text{BRC}_3 i_3(t - T_{a3} - T_{p.c3})\,\varepsilon_9, \tag{3}$$

$$i_3(t) = i_3(t - T_{a3} - T_{p.c3})(1 - \Delta_3)\,\varepsilon_3 + \Delta_3 \frac{\text{BRS}_3^s}{T_{a3}} N_3(t - T_{sc3}^s - T_{p.sc}^s)\,\varepsilon_3$$

$$+ i_3(t - T_{a3} - T_{p.sc}^e)\,\Delta_3\,\text{BRS}_3^e\varepsilon_3 + \frac{M_9}{M_3} i_9(t - T_{a9} - T_{p.sc}^e)\,\Delta_9\,\text{BRS}_9^e\varepsilon_3 + \frac{M_9}{M_3}\cdot\frac{\Delta_9\,\text{BRS}_9^s}{T_{a9}} N_9(t - T_{sc9}^s - T_{p.sc}^s)\,\varepsilon_3. \tag{4}$$

In these equations the history of each fissionable isotope is traced through time. The indices 3 and 9 refer to parameters associated with U^{233} and Pu^{239} respectively.

$i_3(t)$ and $i_9(t)$ are the over-all rates of introduction of new cassettes in the cores of the working and newly-constructed reactors of Type 3 and 9 at time t. A convenient unit for i(t) is the number of cassettes in a core. In this case i(t) can be taken as the rate at which a given type of core passes through the reactor.

M_3 and M_9 are the initial charges of the corresponding fissionable isotopes in a core. Thus $M_3 i_3$ and $M_9 i_9$ are the rates at which the corresponding isotopes enter the cores, expressed in kg/year.

$N_3(t)$ and $N_9(t)$ are the numbers of reactors of each type working at time t. Then (1) and (2) represent the rate of change of the number of reactors of each type, and this is equal to the rate of introduction of cassettes (in core units) from the processing plant to the reactor installation at time t, minus the rate at which cores leave the reactor for the processing plant at time t, which is equal to their rate of introduction to the reactor at time $t-T_a$, where T_a is the run period of a reactor, i.e., the mean time during which the cassettes are kept in the core.

Equations (3) and (4) indicate which elements contribute to the rates of entry into the cores of the fissionable isotopes Pu^{239} and U^{233}.

Δ_3 and Δ_9 are the amounts of fissionable isotopes burnt up, relative to their initial loadings.

The breeding ratios are broken down into two components. These are BRC (the breeding ratio of a core, also called the inner breeding ratio) and BRS (the breeding ratios of the screens): $\text{BRS} = \text{BRS}^s + \text{BRS}^e$, where the indices s and e refer to side and end screens, and each component of the breeding ratio can have the index 3 or 9 according to the reactor type. Thus BRC_3 and BRC_9 are the rates of formation of Pu^{239}, relative to the rates of burn-up of

TABLE 1. Main Initial Characteristics of Systems

Fuel type	Oxide fuel			Metallic fuel		
Fuel cycles	Plutonium	Mixed	Thorium	Plutonium	Mixed	Thorium
Fuel composition	PuO_2-UO_2	$PuO_2-U^{233}O_2-U^{238}O_2$	$U^{233}O_2-ThO_2$	Pu–U	$Pu-U^{233}-U^{238}$	$U^{233}-Th$
% Porosity of fuel in core	27.0	27.0	27.0	28.5	28.5	25.0
Maximum allowable temperature at center of fuel element, °C	2400	2400	2400	700	700	950
Maximum allowable burn-up, kg fragments per 1 t fuel	100	100	100	50	50	50
Heat-transfer agent	Sodium					
Mean rise in temperature of heat-transfer agent, °C	230					
Temperature of heat-transfer agent on entering reactor, °C	300					
Maximum velocity of heat-transfer agent, m/sec	10					
Thickness of fuel-element jacket, mm	0.4					
Flattening of core (D/H)	1.4					
Screen material	UO_2	Th	Th	UO_2	Th	Th
Fuel density in screen, g/cm^3	10	11	11	10	11	11
Construction material	Stainless steel					

Note. The composition and dimensions of the side screen were the same for all the systems: $\varepsilon_{fuel} = 0.60$; $\varepsilon_{Na} = 0.25$; $\varepsilon_{st} = 0.15$. The screen thickness is 60 cm.

U^{233} and Pu^{239} respectively, in cassettes or core of a Type 3 or Type 9 reactor; BRS_3 and BRS_9 are the rates of formation of U^{233} in the thorium screen of a Type 3 or 9 reactor, relative to the rates of burn-up of U^{233} and Pu^{239}, respectively.

The losses of fissionable isotopes U^{233} and Pu^{239} in the processing plant are represented respectively by ε_3 and ε_9; $(1-\varepsilon_3)$ and $(1-\varepsilon_9)$ are the amounts of irreversible loss during processing, relative to the total amount of a given isotope entering the plant.

T^s_{sc} is the lifetime of U^{233} in a thorium side screen.

The thorium end screen is discharged at the same time as the core; this is reflected in the third and fourth terms of (4).

$T_{p.c}$ and $T_{p.sc}$ are the processing times of cores and screens respectively; $T_{p.c}$ can be different in different types of reactor ($T_{p.c3}$ and $T_{p.c9}$). $T_{p.sc}$ for a side screen can be different for $T_{p.sc}$ for an end screen ($T^s_{p.sc}$ and $T^e_{p.sc}$). However, reactors of Types 3 and 9 have the same $T_{p.sc}$, as the same raw material is used in both cases for the screens.

The asymptotic solution of (1)-(4) is:

$$N_9(t) = e^{\omega t}, \quad N_3(t) = ce^{\omega t},$$
$$i_9(t) = ae^{\omega t}, \quad i_3(t) = be^{\omega t}. \tag{5}$$

A system of simultaneously operating reactors, in which the secondary fuel is expended only on the construction of new reactors, ultimately takes the form of (5), irrespective of the initial values of $N_9(t)$ and $N_3(t)$. The ratio of these quantities must finally attain a constant value, $c = N_3(t)/N_9(t)$, which is derived below. This means that, given all the initial reactor characteristics, the presence of U^{238} in the cores and Th^{232} in the screens unambiguously determines the rate of production of secondary fuel (Pu^{239} and U^{233}), and also their corresponding rates of expenditure in the construction of new reactors, which also ultimately satisfy the asymptotic relations (5).

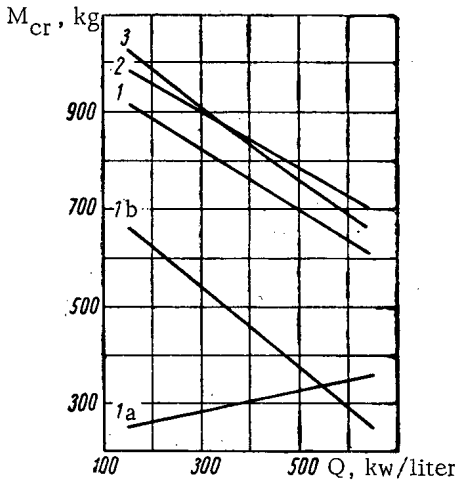

Fig. 1. Critical mass of reactors working with mixed plutonium and thorium oxide fuel, core volume 2000 liter, plotted versus mean power intensity $\bar{Q}$. 1) Reactor with mixed fuel; (1a, b) quantities of U^{233} and Pu^{239}, respectively, in critical mass of reactor with mixed fuel; 2) plutonium reactor; 3) thorium reactor.

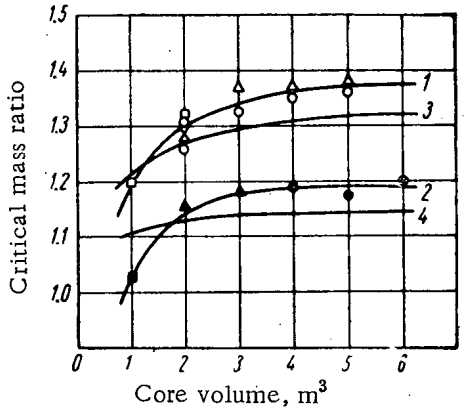

Fig. 2. Critical mass ratio, M_{cr}, and $(\bar{\nu}-1-\bar{\alpha})\bar{\sigma}_f$, for Type 3 and 9 reactors, plotted versus core volumes for various mean power intensities $\bar{Q}$, kW/liter: ○) 300; △) 400; □) 500; ▽) 600; 1, 2) M_{cr3}/M_{cr9} for oxide and metallic fuel, respectively; 3, 4) $\frac{(\bar{\nu}-1-\bar{\alpha})\sigma f_{U^{233}}}{(\bar{\nu}-1-\bar{\alpha})\bar{\sigma}_f Pu^{239}}$ in reactors with oxide and metallic fuel, respectively.

Substituting from (5) in (1)-(4) and eliminating the three unknowns, a, b, and c from the four equations obtained, we find the following characteristic equation (when $\varepsilon = \varepsilon_3 = \varepsilon_9$):

$$\frac{1}{\varepsilon}-e^{-\omega(T_{a3}+T_{p.c3})}(1-\Delta_3)\ -\frac{1-e^{-\omega T_{a3}}}{\omega T_{a3}}e^{-\omega(T^s_{sc3}+T^s_{p.sc})}\ \Delta_3\ BRS^s_3-\Delta_3\ BRS^e_3 e^{-\omega(T_{a3}+T^e_{p.sc})}$$

$$=\frac{\Delta_3 BRC_3 e^{-\omega(T_{a3}+T_{p.c3})}}{\frac{1}{\varepsilon}-e^{-\omega(T_{a9}+T_{p.c9})}[1-\Delta_9(1-\ BRC_9)]}\ [e^{-\omega(T_{a9}+T_{p.c.9})}\ \Delta_9\ BRS^e_9+\frac{1-e^{-\omega T_{a9}}}{\omega T_{a9}}\Delta_9\ BRS^s_9 e^{-\omega(T^s_{sc.9}+T^s_{p.sc})}, \quad (6)$$

from which we can calculate ω. The quantity $T_2 = \ln 2/\omega$ clearly has the physical meaning of the doubling time in a system of reactors working on a mixed-fuel cycle.

We obtain the following expressions for the coefficients a, b, and c:

$$\left.\begin{aligned} a&=\frac{\omega}{1-e^{-\omega T_{a9}}},\quad b=\frac{c\omega}{1-e^{-\omega T_{a3}}},\\ c&=\frac{M_9}{M_3}\cdot\frac{1-e^{-\omega T_{a3}}}{1-e^{-\omega T_{a9}}}\ \frac{\frac{1}{\varepsilon}-e^{-\omega(T_{a9}+T_{p.c9})}[1-\Delta_9(1-\ BRC_9)]}{\Delta_3\ BRC_3 e^{-\omega(T_{a3}+T_{p.c3})}}. \end{aligned}\right\} \quad (7)$$

It must be emphasized that T_2 is the doubling time for Pu^{239} and U^{233} simultaneously. From (5) and (7) it follows that, in a mixed reactor system, the ratio of the numbers of reactors of Types 3 and 9 remains constant:

$$\frac{N_3(t)}{N_9(t)}=c=\frac{b}{a}=\frac{i_3(t)}{i_9(t)}. \quad (8)$$

If we now consider a system of reactors with cores containing mixed fuel and U^{238} and screens containing thorium, (1)-(4) and (6) retain their form, provided that the core consists of a mixture of two types of cassette, i.e., Type 3, containing U^{238} enriched with U^{233}, and Type 9, containing U^{238} enriched with Pu^{239}. The definitions given above then retain their meanings and (8) shows that, in reactors with mixed fuel, the number of Type 3 and 9 cassettes remains constant.

For a system of reactors working with a mixed-fuel cycle, we can introduce the idea of a combined breeding ratio,

$$BR = \frac{\dot{N}_9 + \dot{N}_3}{\dot{Q}_9 + \dot{Q}_3}, \tag{9}$$

where $\dot{N}_9$ and $\dot{N}_3$ are the breeding rates of secondary plutonium in U^{238} and secondary U^{233} in thorium, and $\dot{Q}_9$ and $\dot{Q}_3$ are the rates of burn-up of Pu and U^{233} in the corresponding cassettes.

As the breeding ratio can always be split into an inner term BRC and an outer term BRS,

$$BR = BRC + BRS, \tag{10}$$

where

$$BRC = \frac{\dot{N}_9}{\dot{Q}_9 + \dot{Q}_3}, \tag{11}$$

$$BRS = \frac{\dot{N}_3}{\dot{Q}_9 + \dot{Q}_3}. \tag{12}$$

As Pu^{239} is produced in cassettes of Types 3 and 9,

$$\dot{N}_9 = Q_3 BRC_3 + \dot{Q}_9 BRC_9,$$

whence

$$BRC = \frac{BRC_9 + \beta\, BRC_3}{1 + \beta}, \tag{13}$$

where $\beta = \dot{Q}_3/\dot{Q}_9$. In the thorium screens U^{233} is formed by burning of U^{233} and Pu^{239} in Type 3 and Type 9 cassettes respectively. Therefore

$$\dot{N}_3 = \dot{Q}_3 BRS_3 + \dot{Q}_9 BRS_9,$$

where

$$BRS = BRS^s + BRS^e.$$

Consequently,

$$BRS = \frac{BRS_9 + \beta\, BRS_3}{1 + \beta}. \tag{14}$$

Numerical Results

As an example, we give comparative characteristics of fast power reactors working in plutonium, thorium and mixed-fuel cycles. The comparison is made for reactors with oxide and metallic fuel, with core volumes V_c of 1000, 3000, and 5000 liter, working at optimum power intensity, i.e., that corresponding to minimum doubling time.

The main parameters of the systems considered are given in Table 1 and are typical for planned fast power reactors [2]. The table also gives some characteristics of fuel materials used in the systems studied.

Let us consider the second method of realizing a mixed cycle, i.e., a fast reactor with mixed fuel.

The calculations were based on a 26-group system of constants [1], and were carried out with the aid of computers.

The results are given in Table 2 and Figs. 1-4.

The reactor characteristics were determined for mean isotopic composition of the core fuel, corresponding to a given depth of burn-up and taking account of accumulation of fission products and transuranic and transplutonic elements.

As seen from Table 2 and Fig. 1, the critical mass M_{cr} in reactors with mixed fuel is about 10% less than that of plutonium reactors, because $(\bar{\nu} - 1 - \bar{\alpha})\bar{\sigma}_f$ for U^{233} is higher than for Pu^{239} (see Fig. 2). At the same time,

TABLE 2. Physical Characteristics of Systems with Oxide and Metallic Fuels

Characteristic	Plutonium reactor PuO_2-UO_2			Reactor with mixed fuel $PuO_2-U^{233}O_2-U^{238}O_2$			Thorium reactor $U^{233}O_2-ThO_2$		
Oxide fuel									
V_{core}, liter	1000	3000	5000	1000	3000	5000	1000	3000	5000
$\bar{Q}_{core}$, kW/liter	500	400	300	500	400	300	500	400	300
ε_{fuel}	0.439	0.389	0.425	0.439	0.389	0.425	0.429	0.380	0.419
ε_{Na}	0.360	0.425	0.397	0.360	0.425	0.397	0.368	0.430	0.403
ε_{steel}	0.201	0.186	0.178	0.201	0.186	0.178	0.203	0.190	0.178
M_{cr_9}, kg	515	1140	1790	215	645	1200	–	–	–
M_{cr_3}, kg	–	–	–	250	365	430	520	1100	1740
$\bar{\sigma}f\ Pu^{239}$, barn	1.94	2.01	2.02	1.90	1.96	1.98	–	–	–
$\bar{\sigma}f\ U^{233}$, barn	–	–	–	2.85	3.12	3.20	2.70	2.88	2.92
$\bar{\sigma}f\ U^{238}$, barn	0.050	0.044	0.044	0.054	0.045	0.043	–	–	–
$\bar{\sigma}f\ Th^{232}$, barn	–	–	–	0.0030*	0.0028*	0.0027*	0.0116	0.0097	0.0092
$\nu_{eff}\ Pu^{239}$	2.42	2.36	2.40	2.46	2.39	2.38	–	–	–
$\nu_{eff}\ U^{233}$	–	–	–	2.26	2.21	2.20	2.28	2.26	2.23
Contribution to BR: U^{238}	0.24	0.23	0.19	0.18	0.19	0.18	–	–	–
Contribution to BR: Th^{232}	–	–	–	0.010	0.006	0.005	0.034	0.030	0.027
BR	1.57	1.50	1.55	1.33	1.35	1.40	1.22	1.17	1.19
BRC	0.51	0.69	0.87	0.44	0.65	0.81	0.40	0.56	0.69
T_2, years	7.1	6.9	7.4	12.4	10.6	10.8	19.9	19.7	21.0
Metallic fuel									
V_{core}, liter	1000	3000	5000	1000	3000	5000	1000	3000	5000
$\bar{Q}_{core}$, kW/liter	500	400	300	500	400	300	500	400	300
ε_{fuel}	0.379	0.351	0.414	0.379	0.351	0.414	0.464	0.412	0.464
ε_{Na}	0.357	0.422	0.393	0.357	0.422	0.393	0.349	0.414	0.386
ε_{steel}	0.264	0.227	0.193	0.264	0.227	0.193	0.187	0.174	0.150
M^9_{cr}, kg	575	1320	2120	250	870	1640	–	–	–
M^3_{cr}, kg	–	–	–	255	375	400	640	1360	2150
$\bar{\sigma}f\ Pu^{239}$, barn	1.84	1.85	1.84	1.81	1.83	1.82	–	–	–
$\bar{\sigma}f\ U^{233}$, barn	–	–	–	2.50	2.61	2.58	2.36	2.46	2.45
$\bar{\sigma}f\ U^{238}$, barn	0.045	0.040	0.039	0.048	0.040	0.040	–	–	
$\bar{\sigma}f\ Th^{232}$, barn	–	–	–	0.0024*	0.0022*	0.0022	0.0124	0.0102	0.0096
$\nu_{eff}\ Pu^{239}$	2.54	2.50	2.51	2.57	2.52	2.53	–	–	
$\nu_{eff}\ U^{233}$	–	–	–	2.31	2.29	2.30	2.35	2.23	2.26
Contribution to BR: U^{238}	0.34	0.33	0.29	0.27	0.35	0.30	–		
Contribution to BR: Th^{232}	–	–	–	0.008	0.005	0.004	0.044	0.041	0.046
BR	1.83	1.85	2.05	1.58	1.67	1.87	1.33	1.30	1.34
BRC	0.78	1.05	1.38	0.69	0.98	1.28	0.45	0.63	0.78
T_2, years	6.0	5.0	5.0	8.1	7.3	7.0	17.5	14.7	14.3

*For neutron spectrum in breeding zone.

substitution of U^{238} for thorium in the core spectrum leads to some increase in reactivity, so that the critical mass of a mixed-fuel reactor is somewhat less than the critical mass of U^{233} in a thorium reactor.

As well as the relative efficiencies of U^{233} and Pu^{239}, Fig. 2 gives the critical mass ratios of Type 3 and 9 reactors with oxide and metallic fuel, other conditions being equal. It is seen that the critical mass of U^{233} reactors with oxide fuel is 1.4 times less, and with metallic fuel 1.2 times less than the critical masses of the corresponding plutonium reactors.

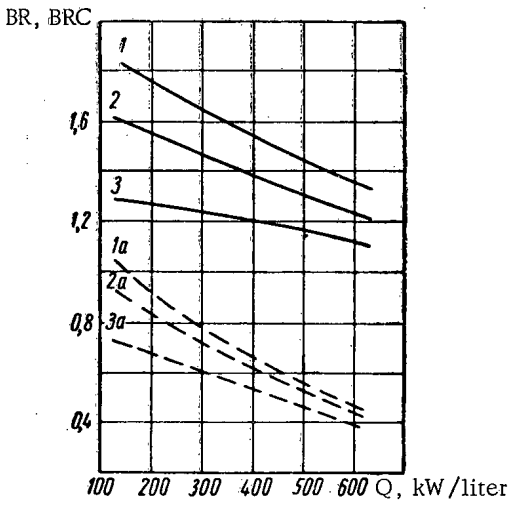

Fig. 3

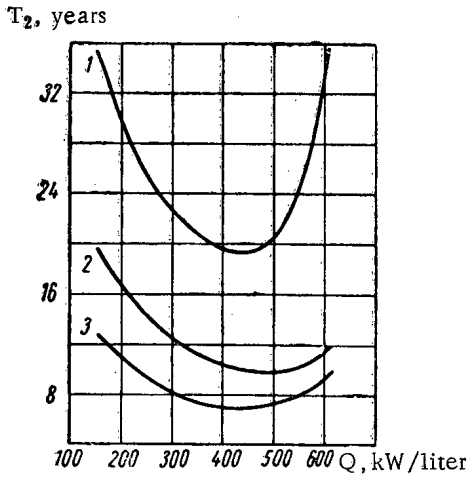

Fig. 4

Fig. 3. Total (———) and inner (– – – – –) breeding ratios of reactors with oxide fuel, working in various fuel cycles with core volume 2000 liter, plotted versus mean power intensity $\bar{Q}$: 1, 1a) plutonium reactors; 2, 2a) mixed-fuel reactors; 3, 3a) thorium reactors.

Fig. 4. Doubling times for reactors systems with oxide fuel, working in various fuel cycles with core volume 2000 liter, plotted versus mean power intensity $\bar{Q}$: 1) thorium reactors; 2) mixed-fuel reactors; 3) plutonium reactors.

In a mixed-fuel reactor (see Table 2 and Fig. 3), where Pu^{239}, U^{233} and U^{238} are located in the core, i.e., in the region with the hardest neutron spectrum, the combined breeding ratio is greater than the breeding ratio for a thorium reactor. This is explained, on the one hand, by the fact that the contribution to the BR from U^{238} fission is greater than that with thorium, thus increasing the BR by 0.2-0.3 for metallic fuel and 0.1-0.15 for the dioxide; on the other hand, the contribution of Pu^{239} is higher than that of U^{233} because of its greater ν_{eff}. It must be noted that, owing to the presence of thorium in the screens, there is little protactinium poisoning in mixed-fuel reactors. As a result, the breeding ratio is higher than that for a pure thorium cycle, by 0.1-0.2 for oxide fuel and by 0.25-0.5 for metallic fuel. At the same time, it is close to the value for a plutonium reactor.

In calculating the doubling times, the following characteristics of the fuel cycles were taken into account:

1. The period of operation was calculated for a given burn-up and reactor power (for a load coefficient of 0.85).

2. The time for processing in the chemical plant was taken as 0.5 years for all types of fuel and raw material, including the time required to prepare and transport new fuel elements. The processing losses were taken as 1.5% of the material processed.

3. T_{sc}, the delay time for production of secondary fuel from the screens, was determined on the assumption that the amount of secondary fuel accumulated was, in the limiting case and on average, 10 kg U^{233} per 1 t raw material.

The advantages of the mixed over the thorium fuel cycle are seen especially clearly when we consider the doubling times.

Table 2 and Fig. 4 show that the doubling time of a reactor system using thorium is much greater than T_2 for reactors working with mixed fuel. This is due to the differences in breeding ratio and critical mass. However, there is little difference in doubling time between a mixed-fuel cycle and pure plutonium: the difference is especially small for the variants where the greatest contribution to the breeding ratio and power comes from U^{238} fission.

Let us consider some quantities associated with the rates of Th and U^{238} consumption in an evolving system of fast breeder power reactors. In this case the breeding requirements are mainly determined by the rate of construction

of new reactors and are associated with the expenditure of thorium and uranium in the creation of new breeding blankets and cores, respectively. The thorium charge in the screen is about ten times greater than the U^{238} charge in the core; this also determines their relative rates of consumption.

In addition, the raw materials are expended by being burnt up, and their requirements for this purpose are small by comparison with those for constructing breeding blankets and cores.

In an isolated reactor, the requirements for breeding materials are determined only by the burnup rate and processing losses. If the latter amount to 1.5% of the total processed, the ratio of the rates of expenditure of thorium and uranium in the reactors under consideration varies from one to four.

In the general case, the relative total thorium requirements (by comparison with uranium) vary over a wide range—from 1 to 15—and depend markedly on the type of fuel and the construction and sizes of the various parts of the reactor.

As well as accelerating breeding, the distribution of thorium in the screen of a fast reactor somewhat reduces the difficulties linked with the use of secondary U^{233}. The U^{233} and thorium activity in the screen is much less than when thorium is used in a thermal reactor or in the core of a fast reactor. In the first place, there is a marked reduction in the cross section of the reaction $Th^{232}(n, 2n)Th^{231}$, which leads to formation of U^{232}, the ancestor of a number of high-activity elements [3]. Furthermore, in the screen of a fast reactor the absorption cross section $\sigma(n, \gamma)Pa^{231}$ (an intermediate reaction leading to the formation of U^{232}) is about a hundred times less than in thermal thorium reactors. Owing to these factors, the U^{233} activity obtained in the screen of a fast reactor may be about an order of magnitude lower than that obtained in thermal reactors and in the cores of fast reactors. In the second place, the separate disposition of U^{233} and thorium reduces the concentration of Th^{228} and Th^{232}, on account of systematic removal of U^{233} from the screen, and thus also of U^{232}, a source of accumulated Th^{228}.

Summary

The use of mixed-fuel cycles thus opens new opportunities for using thorium in the breeding of nuclear fuel, in conjunction with U^{238}. Mixed-fuel cycles have the following advantages:

1. A high combined breeding ratio is obtained, close to that for plutonium reactors, owing to the high contribution of U^{238} fission to the BR and to the high ν_{eff} of Pu^{239} in the neutron spectrum of a fast reactor.

2. The critical mass of a mixed-fuel reactor is somewhat less than that of a plutonium reactor.

3. As a result, the doubling time of a mixed system is close to that for a system of plutonium breeder reactors and is much less than for a system of thorium reactors.

4. Thorium is taken up by a mixed-type reactor system faster than uranium. In an isolated mixed-fuel reactor, the rate of consumption of thorium is comparable with that of uranium.

5. The use of thorium in the screen of a mixed-fuel reactor has the consequence that protoactinium poisoning is reduced to a negligible level.

6. The removal of thorium into the screen of the fast reactor makes it possible to reduce by an order of magnitude the activities of Th^{232} and the resultant U^{233}, in comparison with the usual methods of using thorium in thermal reactors or in fast reactor cores.

In conclusion, the authors wish to thank M. F. Troyanov and L. N. Usachev for helpful discussion of the results, and A. N. Shmelev for performing the computer work.

LITERATURE CITED

1. L. P. Abagyan et al., Group Constants for Reactor Calculations [in Russian], Gosatomizdat, Moscow (1964).
2. A. I. Leipunskii et al., Report No. 369, presented by the USSR to the Third International Conference on the Peaceful Uses of Atomic Energy, Geneva (1964).
3. M. Benedict and T. Pickford, Chemical Technology of Nuclear Materials [Russian translation], Atomizdat, Moscow (1960).

TRANSMISSION OF NEUTRON RADIATION FROM A REACTOR THROUGH HYDROGEN-FREE MEDIA

(UDC 621.039.538:539.171.4)

S. G. Tsypin, B. I. Sinitsyn, and V. K. Daruga

Translated from Atomnaya Énergiya, Vol. 18, No. 4,
pp. 350-357, April, 1965
Original article submitted April 28, 1964

The results of experimental and theoretical investigations into the transmission of neutrons through hydrogen-free, uniform materials and mixtures are discussed. The relaxation lengths obtained for neutrons of different energy groups are discussed. It is shown that under certain assumptions the magnitude of the flux attenuation for neutrons of the upper energy group ($E_n \geq 3$ MeV) in a hydrogen-free medium can be obtained from very simple empirical expressions by using well-known constants: the removal cross section σ_{rem}, the cross section obtained from the reciprocal of the relaxation length ($\sigma_{1/\lambda}$) and the asymptotic cross section σ_{as}. Values are derived for these constants.

A vast quantity of experimental and theoretical data have been accumulated concerning shielding from the neutron radiation from nuclear reactors and can be found in numerous papers by various authors (see [1-25]). As a consequence of this the necessity has arisen for generalizing and systematizing this information and for developing general laws and relationships which will facilitate the evaluation and planning of specific types of reactor shielding. These laws are obtained on the basis of experiments as well as on the basis of precise calculations. For this, all the existing data can be presented in the form of quite simple algorithms and approximations which will enable accurate solutions to be obtained for many problems without recourse to complex calculations.

In order to derive the simple relationships it is necessary, obviously, to reduce the number of parameters describing one or another of the processes in the shielding to a minimum. The significant successes in this direction are shown by the example of investigations into hydrogenous shielding (water, hydrocarbons, concrete, etc.), where it has been found possible on the basis of the numerous experimental data and various methods of calculation, to solve almost any problem concerning the construction of a specified reactor shielding by using a specified number of known parameters and simple empirical expressions [1-3]. However, hydrogenous materials, no matter how good they are from the point of view of neutron attenuation and simplicity of calculation, are not so versatile if more rigorous technological requirements are set: temperature stability, thermal conductivity, etc. In this respect, the investigations which have been carried out recently into hydrogen-free shielding materials are of great value. There are now adequate data of an experimental nature available concerning the transmission of reactor spectrum neutrons through uniform media (graphite, sodium, iron, lead) as well as through mixtures (iron-graphite, iron ore, boron carbide). For certain materials the calculations for the transmission of fission spectrum neutrons are well known. Calculations by the method of moments have been carried out for beryllium, beryllium oxide, carbon, and iron.

It should be noted that the calculation of hydrogen-free shielding is much more complex and less accurate than the calculation for hydrogenous shielding. The inaccuracy in the values of the elementary interaction cross sections of neutrons with the nuclei of the shielding material are displayed to a great extent in hydrogen-free media since in hydrogenous media the nature of the neutron attenuation function is determined mainly by hydrogen, whose cross section is known with high accuracy and the presence of other components is taken into account as a perturbation leading to some absorption. Nevertheless, in the case of hydrogen-free shielding, at least for neutron groups with energies in excess of 3 MeV, all the data obtained can also be interpreted by quite simple empirical relationships.

For this, in addition to the well-known constants used in calculations of hydrogenous shielding (for example, the removal cross section), the cross section $\sigma_{1/\lambda}$ or the asymptotic cross section are also used.

TABLE 1. Relaxation Lengths of Neutrons in Shielding with Minimum Hydrogen Content

Medium	Composition (wt. %) and density (g/cm^3)	Relaxation length λ, cm	
		$E_n>0.5$ MeV	$E_n<0.5$ MeV
Fe—H_2O [6]	$2.8H_2O$; $\varrho=6.6$	7.3	7.7
Concrete [3]	50 Fe; $30O_2$; $3H_2O$; $\varrho=3,6$	9.6	9
Fe—O—H_2O [17]	55Fe; $32O_2$; $\sim 3H_2O$; $\varrho=2,6$	12.5	11

In this paper a review is given of the principal experimental investigations and calculations of hydrogen-free shielding and the possibility is discussed of using simple empirical expressions which will enable the shielding properties of certain ideal materials, especially mixtures, to be evaluated. It is shown that the values obtained in this manner agree with the experimental data within the limits of 10-20% accuracy.

Review of Experimental and Calculated Data

The planning of shielding for nuclear reactors, as a result of their diversity, reduces to the solution of a defined circle of physical and technological problems. In the majority of practical cases it is required that the shielding materials should attenuate the flux of neutrons and γ-radiation emerging from the reactor by 9-10 orders of magnitude. However, materials which are good attenuators of the reactor radiation cannot always be used in a specified shielding, since they must satisfy the necessary technological requirements: they must have chemical and radiation stability, simplicity of stacking, operating capability in high-temperature regimes, minimum cost, etc. Failure of the special thermal shielding requires that the material should have good thermal conductivity.

The overwhelming majority of reactor shielding found in operation at present are different types of concrete, the basis of which consists of a water binding and heavy fillers (iron, barium, etc.). Detailed investigations of concretes and other hydrogenous materials (metal hydrides, hydrocarbons) are reported in numerous papers [1-5] and will not be discussed here. We shall dwell only on data which has been obtained for "transition" regions, when the hydrogen content in the shielding is a minimum.

The higher the hydrogen content of the shielding material, the more complex and expensive it is [3], but a reduction of the hydrogen content below a certain minimum sharply worsens the neutron attenuation, especially in the intermediate regions of energy of the reactor spectrum. Since for the medium and heavy elements defined it is precisely this region of neutron energies that is of interest, it is reasonable to determine the minimum of hydrogen at which hydrogenous shielding shows no further noticeable reduction of its qualities. The characteristics of this "minimized" shielding can serve as a criterion for hydrogen-free shielding. Experiments [6, 17] and calculations [2, 3], which are in good agreement, give about 0.3% hydrogen as the minimum. As a result of this, it is quite valid to use the removal cross section for calculating the dose attenuation of neutrons in a medium, i.e., the equation for the relaxation lengths of fast and thermal group neutrons (Table 1) remains valid. It was assumed previously that this minimum was 0.5-1% [4, 7]. From comparison of Tables 1 and 3 it can be seen that the addition of such a small quantity of hydrogen reduces considerably the relaxation length of neutrons with intermediate energies. This is associated with the fact that the cross section for hydrogen, which is considerable in this energy region, screens the minimal in the cross sections of other elements in the medium. It can be expected that by an appropriate choice of some other light component, different from hydrogen, the same effect could be achieved for higher technological characteristics of the medium. The number of such substitutes is quite limited: they are lithium, beryllium, boron, carbon, oxygen, and nitrogen.

The information available in the literature concerning the transmission of reactor-spectrum neutrons through substances different from hydrogen and their mixtures, is discussed briefly below.

Beryllium and Beryllium Oxide (BeO). Data on these substances are contained in [1, 2, 8]. The results of calculations (by the method of moments) of the transmission of fission-spectrum neutrons (for thicknesses up to 200 g/cm^2) through beryllium and beryllium oxide are given in [1, 2]; for beryllium the calculated spectrum is given in the energy region 0.33-18 MeV and for beryllium oxide only the dose-attenuation curve is given. In [8], the calculation data of [1] for beryllium are verified experimentally. The experimental results are in good agreement with the calculation. It is interesting to note for densities $\rho_{Be} = 1.84$ g/cm^3 and $\rho_{BeO} = 2.8$ g/cm^3 the relaxation lengths obtained from the dose curves agree closely (Table 2).

The use of beryllium and beryllium oxide as light components in shielding is limited because of their relatively high cost.

TABLE 2. Neutron Relaxation Lengths, λ, for Different Energy Groups in Hydrogen-Free Shielding, cm*

Detector	Effective threshold or energy range	Spectrum of neutron source	Be [8, 1]		BeO [2]	C [9, 11, 1]		B_4C [10]	Na [13, 14]		Fe[15, 11, 9]	Fe–C [9]	Fe–O [17]	Pb [11]
			λ_{exp}	λ_{calc}	λ_{calc}	λ_{exp}	λ_{calc}	λ_{exp}	λ_{exp}	λ_{calc}	λ_{exp}	λ_{exp}	λ_{exp}	λ_{exp}
Cu(n, γ); BF_3	All	Reactor spectrum	–	–	–	–	–	7.0	>40	>40	24	–	21	–
Cu(n, γ) in Cd	Epithermal		–	–	–	12.3‡ 13.0‡	–	–	–	–	24	10.8	20	–
In(n, γ) in Cd	1.44 eV		–	–	–	–	–	–	–	–	–	9.1	20	–
Recoil proton counter†	0.5 MeV		–	7.0	6.8	12.9	12.6	–	40	–	13.5	9.1	13.9	–
Th^{232}(n, f); U^{238}(n, f)	2 MeV		–	–	–	14.5	13.0	10.0	–	–	7.5; 7.6–7.1	11	–	–
P(n, p); S(n, p)	3 MeV		7.7	–	–	15.9	14.4	10.2	25	26	6.5	9.6	14.6	–
Al(n, p); Mg(n, p)	5 MeV	Fission spectrum	–	–	–	–	–	10.2	26	–	6.3	–	–	–
Al(n, α)	7 MeV		–	–	–	15.9	16.2	–	28	–	6.3	10.4	15.0	–
Scintillation spectrometer	3–11 MeV		–	–	–	14.0	–	–	–	–	6.4	–	–	9.8
	5–11 MeV		–	–	–	15.7	–	–	–	–	6.1	–	–	9.6
	7–11 MeV		–	–	–	17.8	–	–	–	–	6.1	–	–	9.7

* All relaxation lengths are obtained for shielding thicknesses greater than several mean free paths.
† Energy threshold 0.5 MeV.
‡ Data from the different authors.

Declassified and Approved For Release 2013/09/24 : CIA-RDP10-02196R000700010004-3

Carbon and Boron Carbide (B_4C). Table 2 shows the experimental[9] and calculated (by the method of moments) [1] relaxation lengths for reactor-spectrum neutrons from the BR-5 reactor [15] and fission-spectrum neutrons in carbon with a thickness of 100 cm. It follows from [15] that for neutrons with energy $E_n \geq 3$ MeV these spectra are identical. It can be seen from Table 2 that the calculated and experimental relaxation lengths of neutrons in carbon agree satisfactorily in the energy region $E_n > 3$ MeV. In the energy region $E_n > 0.5$ MeV the variation of the relaxation lengths is small (experimental values 12.9-15.9 cm, calculated values 12.6-16.2 cm). It should be noted that in carbon at distances greater than 100 cm all fast neutron groups follow after the most penetrating group with energy $E_n \geq 7$ MeV. This is confirmed by measurements with a proton recoil counter ($E_{thresh} = 0.5$ MeV) at distances greater than 90 cm, where the measured relaxation length is increased from 12.9 to 16 cm [9].

In [11], the spectral distribution of the neutrons was studied experimentally for various thicknesses of carbon. The interpretation of the data from this paper is made difficult because of some indeterminacy in the geometries of the source, detector, and medium. However, no significant disagreement between the results obtained in [11] and the data of other authors [1, 9] is observed.

At present, carbon is one of the best light components for the construction of shielding. The effective attenuation of neutrons in the intermediate energy range in carbon is combined with good thermal conductivity and stability at elevated temperatures. Moreover, it is relatively inexpensive.

Some better data concerning neutron attenuation have been obtained from boron carbide [10]. For equal densities (1.67 g/cm^3) the attenuation of reactor-spectrum neutrons with energy $E_n > 2$ MeV is somewhat higher (λ = 10.2 cm) than in carbon ($\lambda = 14.5$ cm), and the relaxation length, depending on the shielding thickness and on the neutron energies, varies only weakly. However, boron carbide is considerably more expensive than graphite and is less workable.

Sodium. An investigation of metallic sodium is of interest for calculating the deterioration of shielding with large capacities and conduits by sodium coolant. A study of the properties of sodium is of some value as being representative of average elements form the point of view of material systematics.

In [13], the transmission of fast neutrons from the BR-5 reactor in a sodium prism with a thickness of 150 cm was investigated. The relaxation length for neutrons in the energy region $E_n \geq 3$ MeV, where the spectrum of the BR-5 neutrons is identical with the spectrum of fission neutrons, is not strongly altered and is equal to 26 ± 3 cm, which agrees with the calculated length of $\lambda = 26$ cm obtained from the data in [14] (taking account of the geometry) for U^{238} chambers (effective threshold $E_{eff} = 2$ MeV). Measurements with a proton recoil counter ($E_{thresh} = 0.5$ MeV) give significantly increased relaxation lengths up to 40 cm. This can be explained in the following manner. A group of neutrons with energies below 1 MeV [14] (the cross section of sodium falls sharply in the region 0.5-0.7 MeV) is the controlling group in sodium, while the contribution in this region in the counter is equal to the contribution by energies of $E_n > 1$ MeV (BR-5 spectrum, [15]). Measurements with resonance indicators for manganese and sodium give $\lambda > 40$ cm [14] in the intermediate neutron energy region.

Inelastic interactions play the predominant role in fast neutron attenuation for the heavier elements (iron, nickel, etc.). The most penetrating group is the one with energy $E_n < 1$ MeV.

Iron. Iron is the most widely-used heavy component of shielding and attenuates γ-radiation as well as fast reactor neutrons. Adequate experimental data concerning this material are available [9-11, 15].

In the energy region above 3 MeV, the relaxation length of fission-spectrum neutrons is about 6.3 cm [15] and it varies weakly as a function of energy and thickness of the medium (see Table 2). With reduction of the detector threshold the neutron relaxation length in iron increases. Thus, for an effective threshold $E_{eff} = 2$ MeV, $\lambda = 7.5$ cm [10, 15]. For the proton recoil counter ($E_{thresh} = 0.5$ MeV) the relaxation length increases further by a factor of two [9] and almost by a factor of four for the intermediate neutron energy region [detector Cu(n, γ) screened with cadmium]. This is associated with the presence of gaps in the iron cross section in regions of neutron energies of ~1 MeV and 20 keV (for example, the removal cross section for iron varies by a factor of two as a result of varying E_n from 1 to 4 MeV [16]). The gap in the iron cross section in the 20-keV region also determines the relaxation length of intermediate neutrons as equal to 24 cm.

The cross section $\sigma_{1/\lambda}$ for iron, calculated according to data from all the papers mentioned, is almost identical with σ_{rem} (for an effective detector threshold $E_{eff} = 3$ MeV, see Table 4).

TABLE 3. Comparison of Neutron Attenuation in Iron-Containing Shielding for Identical Nuclear Density of the Iron Component

Detector	Effective threshold, MeV	Fe [15, 9]	Fe–C [9]	Fe–O [17]
		$\rho_{nuc} = 1.54 \cdot 10^{22}$ cm^{-3}	k* = 1 : 1.65	k = 1 : 2
		λ, cm†		
Al (n, α)	7	35	21	15
Proton recoil counter	~0.5	74	22	14
Cu (n, γ)	–	130	22	20

*k is the ratio of the nuclear densities of the elements constituting the mixture.
†The values of λ are rounded off within the limits of experimental error.

TABLE 4. Values of the Constants σ_{rem}, $\sigma_{1/\lambda}$ and σ_{as}, Used for Shielding Calculations, in Barn

Substance	σ_{rem} [22, 23]	$\sigma_{1/\lambda}$	σ_{as} (1.4–∞ MeV) [24, 25]
Li	1.01	1.07	1.03
Be	1.07	1.05 [8]	1.20
B	0.97	1.12 [10]	1.12
B_4C	4.70	–	–
C	0.81	0.75 [9]	0.95
O	0.99; 0.74 [1]	–	0.74*
B_2O_3	4.30	–	–
Na	1.26	1.50 [13]	1.36; 1.58
Mg	1.29	–	1.35
Al	1.30	–	1.42
K	1.57	–	1.54
Si	1.37	–	1.23
Ti	1.82	–	1.62
Cr	1.77	–	1.98
Fe	1.98	1.81 [15]	1.87
Ni	1.89	1.90 [16]	1.84
Cu	2.04	1.78 [16]	2.04
Zr	2.36	–	2.43
Nb	2.37	–	2.30
Mo	2.38	–	2.85
Ba	2.82	–	3.14
W	3.36	–	3.94
Pb	3.53; 3.3 [19]	3.15 [11]	2.63; 3.33†
Bi	3.49	–	2.62; 3.53†

*Taking into account self-screening of the oxygen cross section in water.
†Calculation for 2.5 to ∞ MeV groups.

TABLE 5. Comparison of Relaxation Lengths for Neutrons with $E_n > 3$ MeV, Calculated by Formula (4) and Obtained Experimentally

Medium	λ_{cm}, cm	
	experiment	calculated by formula (4)
Iron–carbon (=4 g/cm³) [9]	9.6	10.4
Iron–oxygen (=2.6 g/cm³) [17]	14.6	16

A calculation by the method of moments is given in [18] for the transmission of neutrons through iron. The divergence from experimental data [15] in determining the value of the relaxation length is about 15%.

Iron-Carbon Mixture. A heterogeneous mixture of iron with carbon (graphite) is for the time being one of the best hydrogen-free shielding materials and it has all the essential qualities for operating at elevated temperatures.

According to the data in [9], the optimum shielding concentration lies within the limits of 70-80 wt. % iron. The relaxation length of the BR-5 reactor-spectrum neutrons varies weakly as a function of energy and distance (for a thickness 60-90 cm). Carbon obviously closes the gap in iron in the region of $E_n \approx 1$ MeV and completely defines the relaxation length for neutrons of intermediate energy. According to measurements with an indium resonance indicator, a relaxation length $\lambda = 9.1$ cm is obtained. In the fast neutron region λ does not exceed 11 cm (for an iron-carbon mixture with a carbon content of 26 wt. %).

The calculated verification, on the basis of the conclusions in [16], was carried out according to the empirical formula (the additivity principle was used):

$$\frac{1}{\lambda_{cm}} = \frac{P_{Fe}}{\lambda_{Fe}} + \frac{P_C}{\lambda_C}, \quad (1)$$

where P_{Fe} and P_C are the volume concentrations of iron and carbon; λ_{Fe} and λ_C are the relaxation lengths in cm of neutrons with $E_n > 3$ MeV in iron and carbon respectively; λ_{cm} is the neutron relaxation length in cm in the mixture. The value of λ_{cm} calculated by formula (1), agrees within the limits of experimental error with the experimental value determined by measurements with a S(n, p) detector with an effective threshold $E_{eff} = 3$ MeV (see Table 5).

Iron-Oxygen Mixture. The investigation in [17] of neutron attenuation in an iron ore medium with an iron content of ~60 wt. % and oxygen ~30 wt. % is interesting. The content of other elements (Si, Mg, Ca etc.) is ~10% and can be considered as a certain perturbation in the medium which does not play a significant role. Thus, the question actually is one of a homogeneous mixture of iron and oxygen (essentially Fe_2O_3).

Comparison of the neutron attenuation in an iron-ore medium, iron and carbon mixtures (all the investigations were carried out with the BR-5 reactor neutron spectrum) indicates the significant role of oxygen in the over-all attenuation of the shielding for fast as well as for intermediate neutrons in particular.

The neutron relaxation lengths, calculated according to the data in [9, 15, 17] are given in Table 3 for a comparable nuclear density of iron of $1.54 \cdot 10^{22}$ cm^{-3}. It can be seen that oxygen also effectively screens the gaps in the iron cross section, just as in the case of carbon.

For the region $E_n > 3$ MeV, a calculated verification was carried out using the removal cross section according to the formula

$$\frac{1}{\lambda_{cm}} = \sigma_{rem(O)} \nu_{(O)} + \sigma_{rem(Fe)} \nu_{(Fe)} + \bar{\sigma}_{rem} \bar{\nu}, \quad (2)$$

where $\sigma_{rem(O, Fe)}$ and $\nu_{(O, Fe)}$ are the removal cross sections in barn (Table 4) and the nuclear densities in cm^{-3} for oxygen and iron in the mixtures respectively; $\bar{\sigma}_{rem}$ and $\bar{\nu}$ are the mean removal cross sections and nuclear density of the remaining elements. The value of λ_{cm} obtained from expression (2) was compared with the experimental data [S (n, p) detector with and effective threshold $E_{eff} = 3$ MeV]. The results agree within the limits of measurement error. For this, it was assumed in [17] that $\sigma_{rem(O)} = 0.74$ barn. The value of $\sigma_{rem(O)} = 0.79$ barn, obtained from data for B_2O_3 and boron, (see Table 4), has been used for calculating λ_{cm} in Table 5.

The prospects for utilizing iron-ore shielding are linked with the possibility of obtaining a higher density of the medium (~3-3.5 g/cm³) or the introduction of stable hydrogen-containing additives (CaH_2, serpentine-$3MgO \cdot SiO_2 \cdot 2H_2O$ [5]) into that portion of the iron-ore shielding which is external relative to the reactor core, where as a result of the good thermal conductivity of the inner portion the temperatures are quite low. Such a "two-layered"

shield would represent a combination of the qualities of an iron-carbon shield and an iron-water shield (see Table 1 and 2) with relatively inexpensive starting material and with a high thermal stability.

Lead. The attenuation of neutrons from a water-cooled, water-moderated reactor has been studied in [11] by means of a neutron scintillation counter. The spectrum of the neutron flux incident on a lead assembly is identical with the fission spectrum for neutron energies in excess of 2 MeV. It is shown that the relaxation length of fast neutrons is weakly dependent on the energy ($\lambda \approx 10$ cm for the energy region E_n from 3 to 11 MeV) and on the shielding thickness (λ varies by several percent as a result of doubling the thickness). The cross sections $\sigma_{1/\lambda}$, calculated according to these measurements for $E_n > 3$ MeV is close to the value of $\sigma_{rem} = 3.3$ barn [19] and σ_{as} for the group 2.5-∞ MeV (see Table 4).

General Laws of Neutron Attenuation in Hydrogen-Free Media.

Empirical Relationships and Parameters

The experimental and calculated data which have been discussed above, concerning the transmission of neutrons through hydrogen-free shielding enable the conclusion to be drawn that the nature of attenuation of neutrons with $E_n > 2$ to 3 MeV in the shielding material can be approximated with adequate accuracy to a function of the form

$$\Phi(x) \sim \exp(-qx). \tag{3}$$

Here q is some empirical parameter, which will be defined below. The range of applicability of expression (3) is included within the limits of variation of x from 2 to 15 mean free paths [1, 2, 8, 9, 10, 13, 14, 15, 17, 18] inside a thick shield.

It is essential to note that for very large shield thicknesses the neutron relaxation length, because of filtration by the medium, will be determined by the minimum neutron-interaction cross section in the energy range of the reactor spectrum.

The following quantities can be used as the parameter q [16]:

1) the macroscopic removal cross sections Σ_{rem}, if the neutron group with energy in excess of 3 MeV is considered;

2) the macroscopic cross sections $\Sigma_{1/\lambda}$, obtained from the reciprocal relaxation lengths for neutron groups with energies in excess of 3 MeV;

3) the asymptotic macroscopic cross sections, obtained from the solution of the one-velocity kinetic equation in transport approximation, using the system of group constants [24, 25] for the energy groups 1.4 to ∞ or 2.5 to ∞ MeV.

Data concerning the parameters mentioned, taken from various published papers, are presented in Table 4. It can be seen from the table that there is satisfactory agreement between the three stated parameters. The maximum deviation from the mean value for these quantities does not exceed 10%. This agreement can be explained qualitatively as resulting on the one hand from the determination of the stated parameters, and on the other hand from the physical significance of the processes which occur. It is well known that the minimum distance R_{min} in the hydrogenous material, in which the removal cross section is measured, depends on the energy threshold of the detector and decreases as the energy threshold is increased [16]. At the same time, the magnitude of the removal cross section depends weakly on the threshold of the detector up to an energy of 7-8 MeV [19-21]. In principle, there exists such a value for the detector threshold for which $R_{min} \to 0$ and, consequently the removal cross section must be identical with the reciprocal neutron-relaxation length measured in this medium by a detector with the same energy threshold. As mentioned above, this threshold is equal to $E_{eff} = 3$ MeV. The conformity of the asymptotic cross section and the cross section calculated from the reciprocal relaxation length, for neutron energies in excess of 3 MeV is a consequence of the fact that the neutron spectrum in the medium does not vary strongly (asymptotic approximation is valid) with distance (within the limits stated above) and the neutron absorption is not very great (transport approximation is valid).

The description of neutron attenuation in a shield by a function of the form of Eq. (3) is generally valid for homogeneous materials as well as for homogeneous and heterogeneous mixtures.

If the shielding consists of a mixture of several elements, then the parameter q in Eq. (3) can be determined

from the expression

$$q\,[1/\mathrm{cm}] = \sum_{i=1}^{n} \frac{\sigma_i P_i}{A_i} N_A \varrho \cdot \mathrm{cm} \qquad (4)$$

where σ_i is a constant for the i-th element in the mixture, taken from Table 4; N_A is Avogadro's number; P_i is the concentration by weight of the i-th element in the mixture; A_i is the atomic weight of the i-th element.

By way of example of the application of formula (4), the determination of λ for neutrons with energy $E_n >$ 3 MeV for the iron-carbon and iron-oxygen media described in this paper can be cited (see Table 5). It can be seen from Table 5 that within the limits of measurement error ($\Delta_\lambda = 10\%$) the calculated values agree with the experimental results and verify the validity of applicability of expressions (3) and (4) for calculating the transmission of neutrons in the upper energy group through hydrogen-free mixtures.

Thus, it can be seen from a review of the data concerning the investigation of the transmission of reactor spectrum neutrons through hydrogen-free media, that a considerable portion of the information is obtained from experimental projects. The experimental investigations in the majority of cases have been carried out for actual thickness of shielding under so-called infinite geometry conditions with a unidirectional source most convenient for comparison with the data from calculations.

Further experiments are desirable with the objective of elaborating the data obtained for narrower energy groups of neutrons in the materials already studied (beryllium, B_4C) and mixtures (iron-carbon, iron-oxygen). In addition, it is important to investigate experimentally certain materials for supplementing the data and verifying the general laws. These materials are lithium, nickel, molybdenum and tungsten. The almost total absence of data (experimental as well as theoretical) concerning the transmission of reactor-spectrum neutrons in the intermediate energy region should be particularly noted. It is obvious that this problem will be resolved after the development of special detectors (of the "intermediate" chamber type).

By comparison with experimental data there is considerably less calculated data concerning hydrogen-free shielding. It is extremely essential to have accurate calculations (for example, by the method of moments) on the transmission of neutrons in B_4C, sodium, iron, and lead. Even one precise calculation should be carried out for a mixture of the type iron-oxygen or iron-carbon especially as there are experimental data for practically infinite media.

The parameters used in hydrogen-free shielding calculations, which are given in Table 4, can be assumed to be completely satisfactory from the point of view of their accuracy (the deviation from the mean value is 10%). The exception is oxygen. For oxygen, the known values of the removal cross section fluctuate from 0.74 to 0.99. Obviously, "pure" experiment (for example, with liquid oxygen) will give the answer.

The authors render thanks to A. I. Leipunskii and I. I. Bondarenko for valuable comments and advice in the preparation of the present paper.

LITERATURE CITED

1. G. G. Gol'dshtein, Primary Reactor Shields [in Russian], Gosatomizdat, Moscow (1961).
2. R. Aronson and C. Klahr, Reactor Handbook. III. Part B, ch. 9. Ed. E. Blizard, New York (1962).
3. D. L. Broder et al., Atomnaya Énergiya, 16, 26 (1964).
4. B. Price, K. Horton, and K. Spiney, Protection from Nuclear Radiations [Russian translation], Izd-vo, IL, Moscow (1959).
5. I. A. Arshinov, In the collection "Problems in the Physics of Reactor Shielding" [in Russian], Edited by D. L. Broder et al., Gosatomizdat, Moscow (1963), p. 327.
6. V. P. Mashkovich et al., Atomnaya Énergiya, 17, 65 (1964).
7. D. Wood, Nucl. Sci. Engng., 5, 45 (1959).
8. J. Moteff, The Use of Threshold and Resonance Foils for Neutron-Spectrum Determinations, Caius College, Cambridge, England (August 16-29, 1958).
9. V. K. Daruga et al., Atomnaya Énergiya, 17, 60 (1964).
10. D. L. Broder et al., In the book "Proceedings of the Second International Conference on the Peaceful Uses of Atomic Energy" [in Russian], Report of Soviet Scientists, 2, Atomizdat, Moscow (1959), p. 674.
11. A. P. Veselkin et al., Atomnaya Énergiya, 16, 32 (1964).
12. S. G. Tsypin, Atomnaya Énergiya, 12, 300 (1962).

13. V. K. Daruga et al., Atomnaya Énergiya, 17, 145 (1964).
14. A. Kania et al., Long-Distance Propagation of Neutron Fluxes in Fast Reactors [in French], Seminar on Reactor Physics, 5, International Atomic Energy Agency, Vienna (1961).
15. V. P. Mashkovich and S. G. Tsypin, Atomnaya Énergiya, 11, 251 (1961).
16. B. I. Sinitsyn and S. G. Tsypin, Atomnaya Énergiya, 12, 306 (1962).
17. V. K. Daruga, I. I. Lazutkin, et al., Atomnaya Énergiya, 17, 63 (1964).
18. A. P. Suvorov et al., In the Collection "Problems in the Physics of Reactor Shielding" [in Russian], Edited by D. L. Broder et al., Gosatomizdat, Moscow (1963), p. 44.
19. J. Bourgeois et al., Report No. 1190 presented by France at the Second International Conference on the Peaceful Uses of Atomic Energy [Russian translation], Geneva (1958).
20. S. F. Degtyarev et al., In the Collection "Neutron Physics" [in Russian], Gosatomizdat, Moscow (1961).
21. V. I. Kukhtevich and B. I. Sinitsyn, Atomnaya Énergiya, 10, 511 (1961).
22. R. N. MacDonald and H. H. Baucom, Nucleonics, 20, 158 (1962).
23. G. Chapman and C. Storrs, Effective Neutron Removal Cross Sections for Shielding, Report AECO-3978 (1955).
24. I. V. Gordeev et al., Handbook of Nuclear Physics Constants for Reactor Calculations [in Russian], Atomizdat, Moscow (1960).
25. L. P. Abagyan et al., Group Constants for Nuclear Reactor Calculations [in Russian], Atomizdat, Moscow (1964).

INTERRELATION BETWEEN THE GRAIN ORIENTATION AND THE RADIATION GROWTH OF URANIUM RODS

(UDC 621.039.548)

V. E. Ivanov, V. F. Zelenskii, V. V. Kunchenko, N. M. Roenko, A. I. Stukalov, M. A. Vorob'ev, and A. V. Azarenko

Translated from Atomnaya Énergiya, Vol. 18, No. 4, pp. 357-361, April, 1965
Original article submitted May 4, 1964

The results obtained in radiation tests of β-heat-treated uranium rods at temperatures of 200-300; 450-470; 480°C are given. Dependences of the radiation-growth coefficients G_i on the growth index GI characterizing the grain orientation of the tested specimens were plotted. The elongation component resulting from the radiation growth due to grain orientation was determined. The dependence of the radiation-growth coefficient on the test temperature for weakly-pronounced grain orientations is given. It is shown that the mean values of the linear thermal-expansion coefficient α, measured in one direction only, do not provide information on the character and degree of the grain orientation if the latter is not uniaxial.

The grain orientation which appears in uranium as a result of its mechanical treatment is one of the main causes of irreversible changes in the shape of parts exposed to radiation. In [1], a quantitative relationship between the degree to which the grain orientation [010] is pronounced and the radiation growth coefficient was established, and it was shown that the latter tends to zero in a metal with a quasi-isotropic structure. It is known that such a structure can be obtained in uranium subjected to cooling in the β- or γ-phase. However, according to data supplied by various authors, the radiation-growth coefficient of such a metal is not equal to zero; it is equal to 15-30 [2-4]. This may be caused by at least two factors: 1) the presence of weakly pronounced grain orientations in hardened uranium, the existence of which was confirmed by many authors [5, 6]; 2) the conditions under which the fuel elements are tested, where the observed irreversible changes may be caused by factors unconnected with the grain orientation (swelling, creep, thermal oscillations, etc.).

The separate effect of each of these factors on the over-all change in the dimensions of fuel elements containing unalloyed hardened uranium is of great importance, since it provides the possibility of controlling the variation of the shape of fuel-element cores by controlling the degree of grain orientation in uranium and the test conditions.

In the present article, we shall analyze the grain orientations arising in uranium during its heat treatment, and we shall establish a quantitative relationship between the degree of grain orientation and the radiation-growth coefficient of uranium. This investigation was performed in connection with the development of rod fuel elements [7].

Material and the Investigation Method

For the investigations, we used uranium of 99.78-99.80% purity, where the percentage of each of the basic impurities (Fe, Al, Si, C) did not exceed 0.02%. The diameter of the specimens was 4 mm.

Grain orientations with different characteristics, marked in various degrees, were produced by regulating the parameters of the β-heat-treatment of uranium: the characteristics of heating to the temperatures at which the β-phase is present, the exposure time at these temperatures, and the cooling conditions [8].

The grain orientation of hardened uranium was investigated by using the x-ray structural and dilatometric analysis methods.

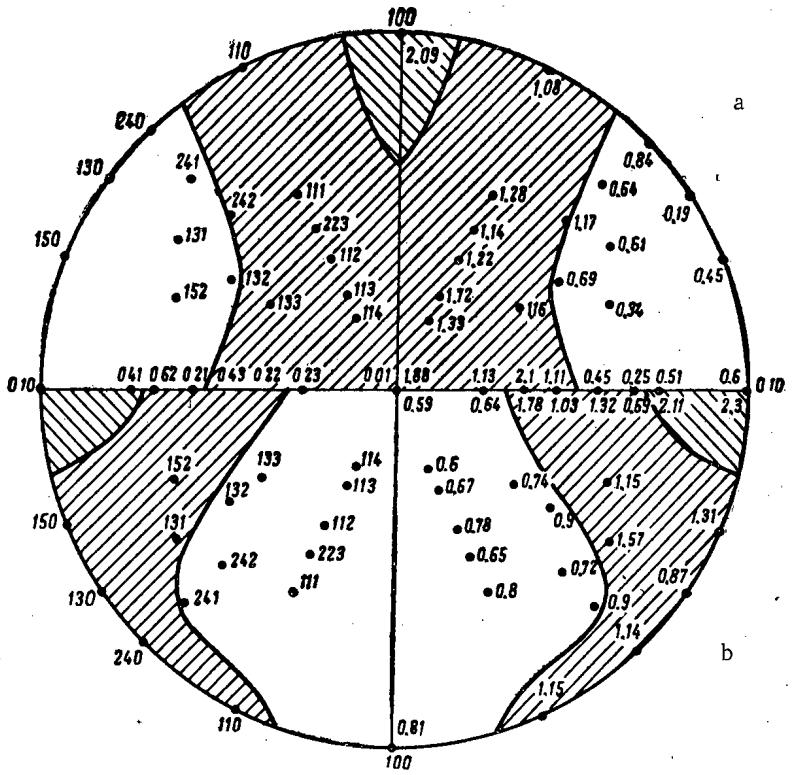

Fig. 1. Reverse pole figure for a uranium rod whose axial thermal expansion coefficient was $\alpha = 12.5 \cdot 10^{-6} °C^{-1}$. a) Longitudinal section; b) end-face section.

The "growth index" method, proposed by the authors of [9], was used for describing the grain orientation in connection with anisotropic radiation growth. The quantitative parameter—the growth index GI—was derived from x-ray measurements similar to those used earlier for plotting reverse pole figures [10]. The growth index is found by determining the product between the volume of grains with a certain orientation and the weighting function of the deformation tensor of anisotropic growth.

The choice of the tensor weighting function is based on the observed deformation of uranium (at constant volume), while it does not depend on the deformation mechanism. The expression for the growth index can be written in the following manner:

$$GI = \sum_i \{P_i - P_r\} (\cos^2 \beta_i - \cos^2 \alpha_i),$$

where $P_i = \dfrac{\mathcal{J}_i / \mathcal{J}_i^0}{\frac{1}{n} \sum_i \mathcal{J}_i / \mathcal{J}_i^0}$ is the density of poles, expressed in terms of the intensities $(\mathcal{J}_i)$, of the x-ray interferences

observed on the specimen under investigation and corresponding to the interference $(\mathcal{J}_i^0)$ of a standard specimen with disordered structure; the index i pertains to the (hk*l*) planes; $P_r = 1$ is the pole density of a specimen with an isotropic structure; β_i and α_i are the angles between the crystallographic planes (hk*l*) and the planes (010) and (100), respectively.

The growth index yields a single quantitatively defined value for the given grain orientation.

The coefficients of linear thermal expansion (α) along the rod axis were measured in the temperature range from 20 to 100°C by means of a dilatometer on specimens with a length of 100 mm. The measurement error was equal to ±1% [8].

The radiation tests were performed in experimental gas loops on enriched-uranium specimens at core temperatures of 200-480°C. The temperature was controlled by means of miniature thermocouples, which were placed inside the cores. On the average, the heat release density was 15 MW/t. In order to prevent the corrosion of uranium specimens in the gas stream, they were covered with magnesium-based alloys.

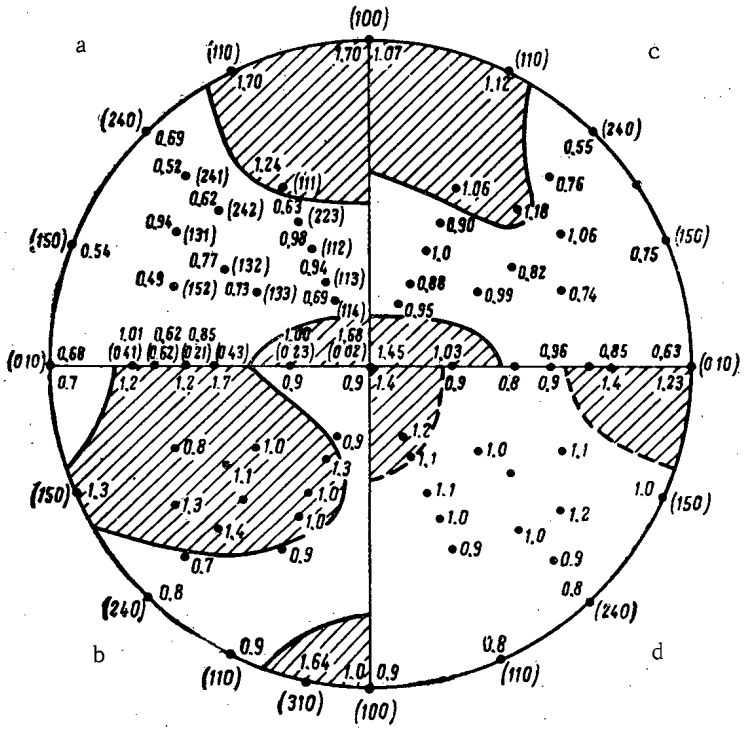

Fig. 2. Reverse pole figures for the end-face sections of β-heat-treated rods. a) and b) Specimens 3 and 4 with $\alpha = 15.3 \cdot 10^{-6}\,°C^{-1}$; c) and d) specimens 1 and 2 with $\alpha = 14.8 \cdot 10^{-6}\,°C^{-1}$.

Results, Their Discussion, and Conclusions

Comparing the results of x-ray studies of the grain orientation and of dilatometric measurements of the linear expansion coefficients of the same specimens, we found that the grain orientation [010] was formed along the specimen's axis in uranium wire that had not been subjected to heat treatment. The more pronounced the [010] grain orientation, the lower the values of the linear expansion coefficient.

In metal subjected to β-treatment, the degree of the [010] grain orientation is relatively low, although under certain treatment conditions (slow heating to a temperature of 740°C, exposure over a period of 20 min, and hardening in water), it can be considerable (Fig. 1). In correspondence with this, the coefficient of linear thermal expansion of the specimens was much smaller than the isotropic expansion coefficient; its value was in the $(12\text{-}13) \cdot 10^{-6}\,°C^{-1}$ range.

By varying the conditions of β-heat-treatment, the type and degree of grain orientation in hardened uranium can be varied in a wide range. In this case, there is no well-defined mutual correspondence between the degree of grain orientation and the linear expansion coefficient, since, as a rule, a double or a more complex grain orientation is observed in the direction of the rod axis (Fig. 2). Consequently, the mean linear expansion coefficient, measured in one direction (for instance, along the rod axis), may have the same value for grain orientations which are different with respect to their degree and character. Thus, this coefficient does not provide information on the character and degree of the grain orientation if the latter is not uniaxial. This, in turn, does not make it possible to use such dilatometric data for predicting the anisotropic radiation growth of uranium rods.

For a certain given type of fuel elements and the chosen irradiation conditions, it is possible to use the growth index method for predicting three-dimensional changes in the rods resulting from their anisotropic growth due to irradiation. We used this method for analyzing the results of radiation tests of several batches of specimens with the aim of determining the effect of the character and degree of grain orientation and of some other factors on the elongation of rods. By using the radiation test results and taking into account the grain orientation of "indicator rods," we plotted the dependences of the radiation-growth coefficients G_i on the growth index GI.

Figure 3 shows the dependence of G_i on GI for specimen batches 1, 2, and 3 with positive as well as negative growth index values, which were tested in the temperature range from 200 to 300°C. As a result of radiation tests,

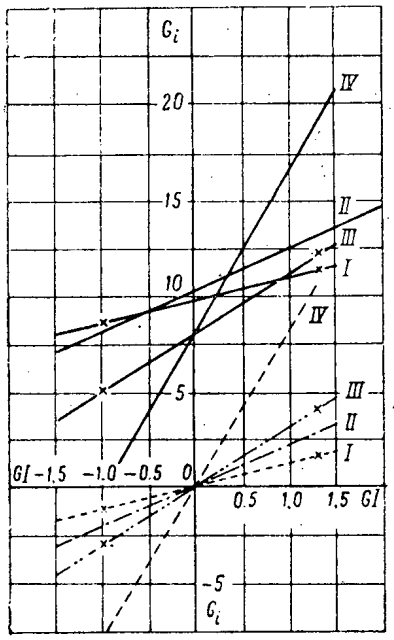

Fig. 3. Dependence of G_i on GI for specimens tested at different temperatures. I) Batch 6, temperature, 480°C; II) batch 4, temperature, 470°C; III) batch 5, temperature, 460-470°C; IV) batches 1-3, temperature, 200-300°C.

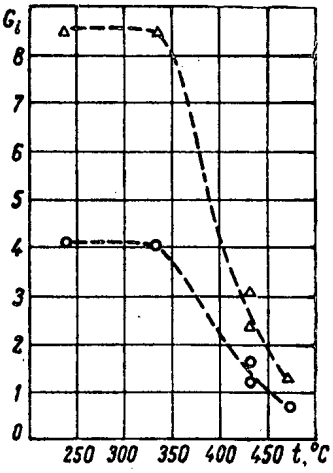

Fig. 4. Dependence of G_i on the test temperature. Δ) GI = 1.0; O) GI = 0.5.

elongation or contraction of the corresponding specimens should have been observed [9]. However, curve IV in Fig. 3 was shifted with respect to the axis by approximately eight G_i units. Consequently, the elongation of rods during the irradiation process was caused not only by radiation growth as a result of the grain orientation, but also by other factors. The elongation which is due only to radiation growth can be determined by means of the corresponding dashed curve IV, obtained by translation of the curves to the coordinate origin.

A similar dependence of G_i on GI was plotted for the fourth batch of specimens, which were tested at a nominal temperature of 470°C under a load of 0.25 kg/mm^2 to a depletion of 0.23%. In this case, during 10-15% of the over-all testing time, the specimens were at a lower temperature (as low as 300°C) as a result of reactor shut-downs and temperature fluctuations. The measured elongations were converted to the corresponding values of the radiation-growth coefficient, while the obtained curve II was also shifted along the axis by approximately 11 G_i units.

The contribution of radiation growth to the over-all elongation can also be estimated by means of the other dashed curve II passing through the coordinate origin. The solid curves in this figure show the corresponding dependences for batch 5, which was tested at a temperature of 460-470°C to 0.18% depletion (curve III), and for batch 6, which was tested at 480°C to 0.25% depletion (curve I).

The translation of the curves to the coordinate origin (dashed curves) makes it possible to estimate with respect to their slope the "pure" radiation growth for specimens with a certain given grain orientation. A dependence of the radiation growth on temperature, which agrees well with the general concepts, is observed. With an increase in the test temperature, radiation growth caused by the grain orientation diminishes; it almost vanishes at ~500°C.

The dependence of the radiation-growth coefficient on the test temperature for a certain given grain orientation (GI = const), which is shown in Fig. 4, indicates that the behavior of the dependence of G_i on the test temperature is roughly the same for weakly as well as strongly pronounced grain orientations [11].

The following conclusions were drawn from an analysis of the results obtained:

1. Factors unconnected with the initial grain orientation may exert a considerable influence on changes in the shape of uranium rods with a weakly pronounced grain orientation in radiation tests.

2. An increase in the testing temperature to 460-480°C leads to a comparatively small increase in elongation, which is probably due to swelling (curve I in Fig. 3).

3. A load of 0.25 kg/mm^2 applied axially to the specimens at a test temperature of 470°C causes a negligible increase in elongation (curve II in Fig. 3).

LITERATURE CITED

1. Buckley, Report submitted at the Spring Symposium on Uranium and Graphite at the Institute of Metals (London, March, 1962). Khar'kov, Institute of Physics and Technology, Academy of Sciences, USSR (1962).
2. Fut, In the book: Nuclear Power Engineering Metallurgy and the Effect of Radiation on Materials. Reports by foreign scientists at the International Conference on the Peaceful Uses of Atomic Energy (Geneva, 1955) [Russian translation], Metallurgizdat, Moscow (1956), p. 89.
3. Kittel and Paine, In the book: Transactions of the Second International Conference on the Peaceful Uses of Atomic Energy. Selected reports by foreign scientists [Russian translation], 6, Atomizdat, Moscow (1959), p. 310.
4. Metallography of Reactor Materials. Surveys of the Battle Institute [Russian translation], 1, Gosatomizdat, Moscow (1961).
5. J. Store, M. Englander, and M. Gotron, In the book: Transactions of the Second International Conference on the Peaceful Uses of Atomic Energy. Selected reports by foreign scientists [Russian translation], 6, Atomizdat, Moscow (1959), p. 515.
6. A. S. Zaimovskii, V. V. Kalashnikov, and I. S. Golovnin, Atomic Reactor Fuel Elements [in Russian], Gosatomizdat, Moscow (1962).
7. P. I. Khristenko et al., In the book: Transactions of the Second International Conference on the Peaceful Uses of Atomic Energy. Reports by Soviet scientists [in Russian], 3, Atomizdat, Moscow (1959), p. 655.
8. V. E. Ivanov et al., Atomnaya Énergiya, 16, 325 (1964).
9. E. Strurcken and W. McDonall, J. Nucl. Materials., 7, 85 (1962).
10. G. B. Harris, Phyilos, Mag., 43, 114 (1952).
11. G. Ya. Sergeev, V. V. Titova, and K. A. Borisov, Metallography of Uranium and Some Other Reactor Materials [in Russian], Atomizdat, Moscow (1960), p. 78.

IN MEMORIAM: ANDREI VLADIMIROVICH LEBEDINSKII

Translated from Atomnaya Énergiya, Vol. 18, No. 4,
2 page insert following p. 360, April, 1965

We are grieved to report the untimely death, on January 3, 1965, of Professor Andrei Vladimirovich Lebedinskii, Member of the Communist Party of the Soviet Union, Acting Member of the Academy of Medical Sciences of the USSR, a highly esteemed active scientist of the Russian Soviet Federated Socialist Republic, a Major General in the medical services, and Doctor of Medical Sciences, in the 63rd year of his life.

Soviet and world science has suffered the loss of an outstanding physiologist, scientist, and true continuator of the work of I. P. Pavlov and L. A. Orbel'.

During the four decades of his scientific and teaching activities, Andrei Vladimirovich had a lengthy and active career, his scope of activities ranging from medical practitioner to one of the most prominent scientists in Soviet physiological science. A. V. Lebedinskii belonged to that generation of physiologists whose scientific viewpoints were formed after the Great October Socialist Revolution, during the period of the creative fluourishing of ideas of the remarkable galaxy of Russian physiologists, such as: I. M. Sechenov, I. P. Pavlov, N. E. Vvedenskii, L. A. Orbel', A. A. Ukhtomskii.

Even while enrolled in course IV of the Military Medical Academy, A. V. Lebedinskii embarked on his career of scientific research activities on joining the staff of the laboratory supervised by L. A. Orbel'. After completing his studies at the Academy, he worked as neuropathologist from 1924 to 1928, combining his practical activities with scientific research at the psychophysiological laboratory of the Military Aviation Fleet. Thereafter his activities for the next 25 years were inseparably connected with the Military Medical Academy. During that period, A. V. Lebedinskii performed his duties in the physiology department of that institution, first as instructor, and later as its director. At the same time, A. V. Lebedinskii took upon his shoulders the management of the physiological sector of the psychophysiological laboratory of the GVF Leningrad Institute of Engineers, the physiology laboratory of the Leningrad Ophthalmological Institute, the physiological sector of the V. M. Bekhterev Brain Institute, and the theoretical sector of the Leningrad A. L. Polenov Neurosurgical Research Institute, occupying these several posts for a number of years.

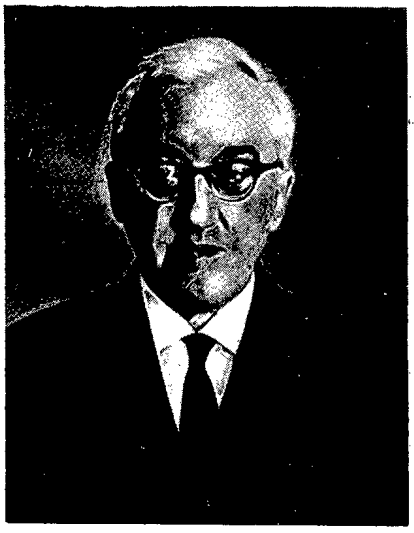

From his very first steps in scientific activities, A. V. Lebedinskii began to concern himself with the problems of nerve trophic activity, and particular its biophysical fundamentals. This problem was a determining factor in the entire range of his scientific activities.

Andrei Vladimirovich was one of the pioneers in the use of electronics as a research tool in studying trophic effects of the sympathetic nervous system and afferent pathways. The richest experimental materials and theoretical conclusions on that topic were generalized by A. V. Lebedinskii in 1945 in the form of the monograph "On mechanisms underlying neurogenic dystrophy."

A. V. Lebedinskii was the country's leading specialist in the field of physiological optics. The research findings he published in this field have received high recognition from ophthalmologists and have become incorporated into clinical practice. The scope of Andrei Vladimirovich's interests was amazingly broad. He did not limit himself to research solely in the field of the sight analyzer. The work done by A. V. Lebedinskii and his co-workers on the interaction of various afferent systems were awarded the 1936 I. P. Pavlov Medal by the Leningrad Society of Physiologists.

Over a span of many years, Andrei Vladimirovich Lebedinskii supervised specialized research in the field of radiation medicine. In 1953 he was appointed Director of the Institute of Biophysics under the Ministry of Public Health of the USSR, in which capacity he continued to expand and deepen investigations in the field of radiation physiology.

A. V. Lebedinskii was one of the founders of the Soviet school of radiobiology. Beginning in the Fifties, he proceeded to concentrate the brunt of his attention on the study of the response patterns of the organism to exposure to ionizing radiation. He was one of the first to advance the notion of the high sensitivity of the central nervous system to ionizing radiation. The research of Andrei Vladimirovich and his disciples in the field of studies of the response of the nervous system to radiation effects acquired particular importance. The major conclusion arrived at in these investigations was the postulation of a change in the functional state and the breakdown of the adaptability of all levels of nerve regulation from the cortex of the cerebral hemispheres to the post-ganglion neuron system.

In 1958, A. V. Lebedinskii expressed the hypothesis that the principal point of application of radiation effects on the nervous system is that of synaptic formations, where depolarization processes take place. This thought found confirmation in the research done by co-workers at A. V. Lebedinskii's laboratory.

A. V. Lebedinskii and his associates carried out some impressive work on the study of changes in endocrine regulation in an organism exposed to radiation, resulting in the inference that post-irradiation breakdown of the normal "hormone ensemble" ensues in the organism.

Focusing on the most crucial problems in radiobiology, Andrei Vladimirovich proceeded to solve some of them from an overall physiological vantage point. His laboratory unearthed data providing evidence of not only harmful action, but also stimulatory action by ionizing radiation. A. V. Lebedinskii was one of the first to turn particular attention to the problem of low-dosage effects of ionizing radiation on the organism.

One salient feature of the entire lifelong scientific activity of Andrei Vladimirovich was the striving to study the biophysical fundamentals of physiological processes. He is considered by right the leading scientist of the nation in various topics in biophysics, and physiological and pathological manifestations of metabolism.

The study of the fundamentals of shielding of the human organism and of animals from radiation effects occupied a special place in the creative efforts of A. V. Lebedinskii. Under his guidance, the staff of the laboratory participated in programs to develop a radiation safety system serving the world's first nuclear-powered icebreaker, the LENIN.

A. V. Lebedinskii devoted much attention to radiation safety problems in outer-space travel. But it is not only for that the name of A. V. Lebedinskii is indissolubly linked to the founding and development of this new branch of biological science: aviation and space biology and medicine. For he began his research in this direction as far back as the Twenties, returning to it in his later years. In collaboration with the leading physiologists of the nation, A. V. Lebedinskii developed the fundamentals of space physiology. Under this guidance, a large staff of assembled specialists pursued research on the mechanisms of extreme responses occurring under the conditions encountered in space flight. A. V. Lebedinskii is one of the founders of the Soviet school of space biology.

A. V. Lebedinskii was not only a great scientists but also a brilliant teacher. He devoted much time and effort to the training of the young generation of doctors and research scientists. Under his leadership, 7 doctoral and over 30 candidate theses were accepted. The textbook co-authored by A. V. Lebedinskii and A. D. Ginetsinskii is a splendid tool for students and a reference for a large number of doctors and research scientists.

Andrei Vladimirovich carried out intensive activities in the service of the scientific community. He was a member of the board of directors of the All-Union Society of Physiologists, a Vice-Chairman of the board of directors of the Moscow Society of Physiologists, chairman of the scientific councils of the USSR Academy of Sciences on the problems "Radiobiology" and "Specialized Physiology." A. V. Lebedinskii was assistant editor of the periodicals Radiobiologiya, Byulleten' éksperimental'noi biologii i meditsiny [Bulletin of Experimental Biology and Medicine], a member of the editorial staff of the "Radiobiology" section of the Great Medical Encyclopedia, a member of the editorial council of the Fiziologicheskii zhurnal SSSR, and a member of the editorial staff of Excerpta medica. Andrei Vladimirovich also acted over a protracted period as part of the editorial staff of our Atomnaya Énergiya.

From 1955 to 1958, A. V. Lebedinskii was the representative of Soviet radiology in the Scientific Committee on Atomic Radiation of the U. N. In his work in the U. N. he actively defended humanistic policies on behalf of our government and expended many efforts and energies in the cause of the struggle for cessation of nuclear-weapons testings and for the abolition of nuclear weaponry.

The socio-political and scientific activities of A. V. Lebedinskii were highly esteemed by the Soviet government. He was awarded two Orders of Lenin, the Order of the Red Flag, the Order of the Red Star, two Orders of the Labor Red Flag, and miscellaneous medals.

A. V. Lebedinskii was not only an outstanding thinker and scientist, and but also a highly principled splendid and charming individual, possessed of inexhaustible optimism and fervid energy.

A. V. Lebedinskii died in the flowering of his creative forces. The glorious memory of this outstanding Soviet scientist and Communist will always retain a warm place in the hearts of the Soviet people.

A Group of Comrades

RADIATION STABILITY OF VITRIFIED RADIOACTIVE PREPARATIONS

(UDC 539.12.04)

F. S. Dukhovich and V. V. Kulichenko

Translated from Atomnaya Énergiya, Vol. 18, No. 4,
pp. 361-367, April, 1965
Original article submitted March 12, 1964

Data are cited on the effect of ionizing radiations on the chemical stability of vitreous materials intended for radioactive waste disposal. It is shown that exposure in air leads to a change in the chemical composition of the surface of specimens as a result of heterogeneous radiation-chemical reactions involving the solid preparations and components of the air. Suggested reaction products are carbonates, hydroxides, and nitrates.

A good deal of research of singular importance for the solution of problems encountered in the safe disposal of radioactive wastes has been devoted to the production of fused vitrified preparations containing uranium fission products. Vitrified preparations are also in wide use as β-radiation sources. The excellent chemical and thermal stability of these materials provides grounds for considering them safe for use in waste disposal operations [1-6].

But the radiation stability of fused concentrates and the effect of ionizing radiation on the behavior of radioactive isotopes present in them have not received adequate study. It has been mentioned in some papers [7, 8] that irradiation of vitreous materials of this type with Co^{60} gammas does not result in any substantial modifications in the structure of the preparation irradiated, nor in its mechanical strength of chemical stability. No effect of β-radiation or γ-radiation on the chemical stability of conventional glasses has been discovered either [9]. Only in one paper [10] has any increased solubility of glass after irradiation been reported, this being a case of glass exposed to radon alphas.

With the object of studying the effect of irradiation on the properties of vitreous materials recommended for immobilizing radioactive wastes, preparations were made by fusing dessicated and calcined residues of solutions simulating radioactive wastes in composition with various fusing additives. Selected fusing additives for use in this context were silicon dioxide, soda, boric acid, fluorspar, etc. Some of the preparations contained uranium fission products and featured specific activities as high as 2.6 Ci/g. Preparations containing no radioactive isotopes were irradiated on a Co^{60} source at an absorbed dose rate of 10, 50, 100, and 200 rad/sec. Either fused materials previously pulverized to a specified fraction, or preparations coated in melt form on a substrate with a known surface, were subjected to irradiation. In contrast to other investigations [9], the specimens were not subjected to any additional post-irradiation machining or other mechanical treatment, and were not rinsed, prior to the solubility determination. The chemical stability with respect to distilled water was determined at 30°C by the method of measuring the electrical conductivity of the solution, and was expressed in terms of the damage depth δ (A) of the specimen by water in a specified time. The value of δ was found from a familiar formula [11].

The fused materials studied are vitrified bodies whose natural surfaces were homogeneous as a rule. Surfaces of the fused preparation obtained in reflected unpolarized light and magnified 550 times appear in Fig. 1. Beginning with an absorbed dose $\sim 5 \cdot 10^7$ rad, there appear on the external surface of preparations irradiated in air by Co^{60} gammas some small dark spots visible under the microscope, with size and concentration increasing with the absorbed dose. The internal layers of the preparation undergo no marked changes in the process. The corrosion products are fairly stable and do not change once the irradiation is terminated. However, they are weakly associated with the preparation and may be removed to an appreciable extent by simply using a soft cloth, or partially by playing water on the preparation (cf. Fig. 1). After rinsing the exposed preparations with water, we discovered the presence of nitrate ion in the solution, as well as a content of alkali and alkali earth metals greater than that found in an unexposed preparation. Preparations containing $Sr^{90} \rightarrow Y^{90}$ with specific activity of 20 mCi/g suffer similar changes when exposed to internal β-radiation (Fig. 2).

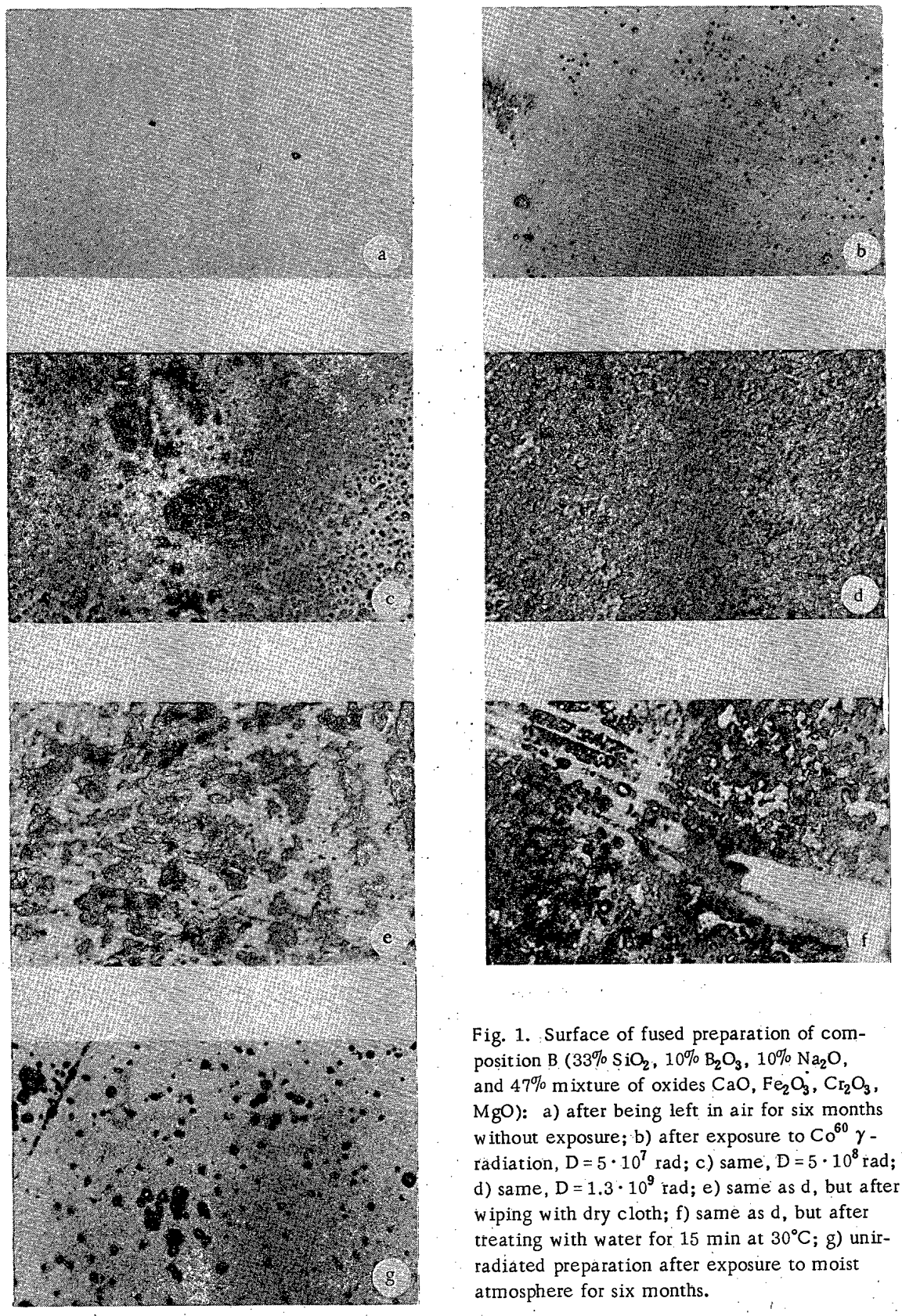

Fig. 1. Surface of fused preparation of composition B (33% SiO_2, 10% B_2O_3, 10% Na_2O, and 47% mixture of oxides CaO, Fe_2O_3, Cr_2O_3, MgO): a) after being left in air for six months without exposure; b) after exposure to Co^{60} γ-radiation, $D = 5 \cdot 10^7$ rad; c) same, $D = 5 \cdot 10^8$ rad; d) same, $D = 1.3 \cdot 10^9$ rad; e) same as d, but after wiping with dry cloth; f) same as d, but after treating with water for 15 min at 30°C; g) unirradiated preparation after exposure to moist atmosphere for six months.

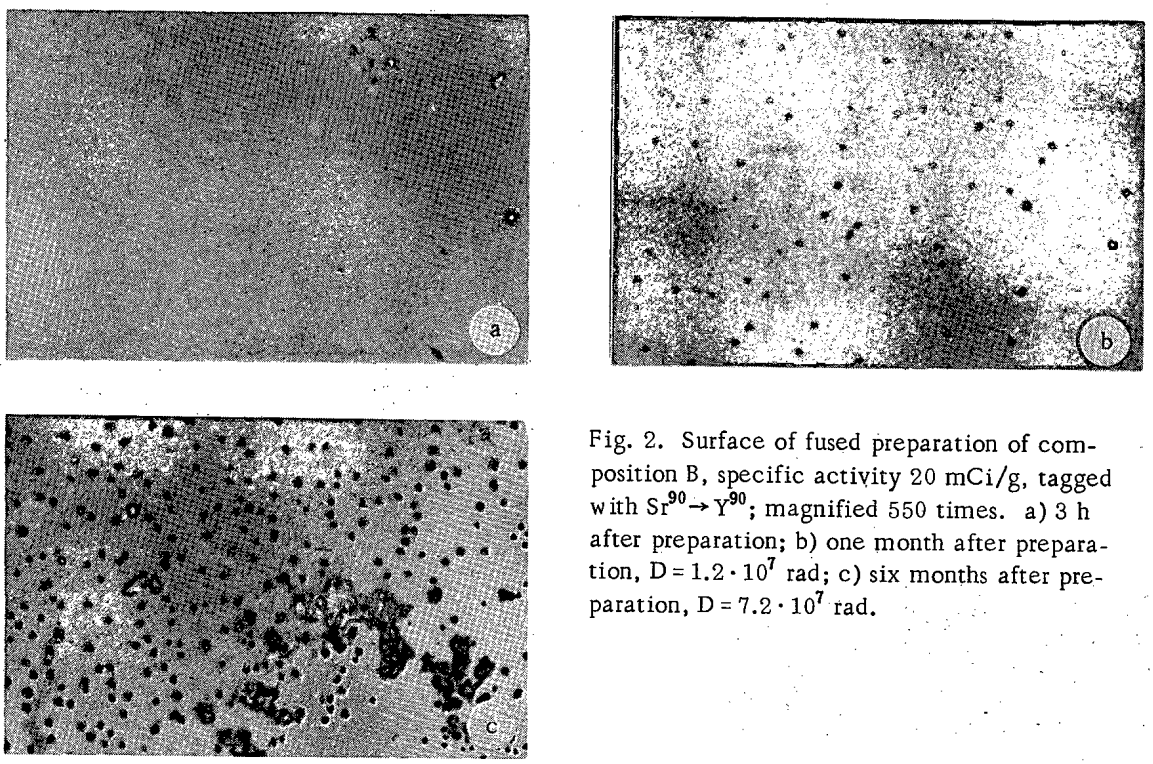

Fig. 2. Surface of fused preparation of composition B, specific activity 20 mCi/g, tagged with $Sr^{90} \rightarrow Y^{90}$; magnified 550 times. a) 3 h after preparation; b) one month after preparation, $D = 1.2 \cdot 10^7$ rad; c) six months after preparation, $D = 7.2 \cdot 10^7$ rad.

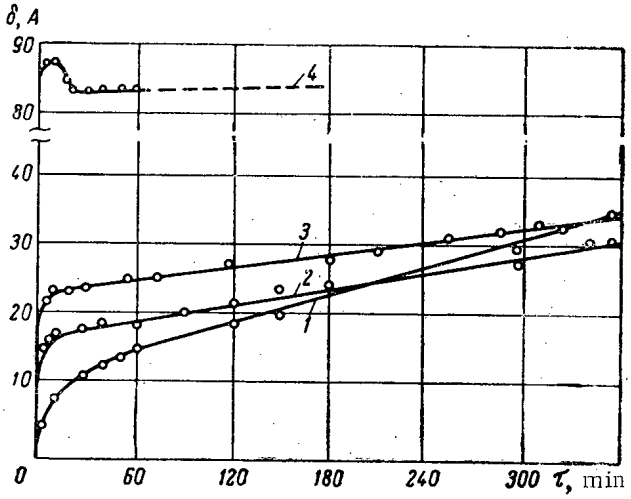

Fig. 3. Variation in chemical stability of preparation of composition B in response to exposure to Co^{60} gammas: 1) unirradiated; 2) $D = 4 \cdot 10^8$ rad; 3) $D = 7 \cdot 10^8$ rad; 4) $D = 1.3 \cdot 10^9$ rad.

The following patterns are typical of the dissolution of an irradiated preparation: a sharp increase in the rate of dissolution corresponding to increased absorbed dose for the first 5 to 10 min of contact with water, and a decrease in the rate of dissolution compared to that of unirradiated specimens in the subsequent period (Fig. 3).[1] The difference between the damage depth in irradiated and unirradiated specimens 5 min after dissolution commences is taken to be the magnitude of the radiation effect. This magnitude depends on the absorbed dose and is independent of dose rate in the 10 to 200 rad/sec range (Fig. 4).

The greatest degradation is that suffered by preparations containing a heightened amount (over 10-20%) of sodium oxide or boron oxide. Even at doses of $5 \cdot 10^8$ rad, specimens enriched with boron oxide are readily covered with a flaky crystalline scale (Fig. 5) whose thickness increases with increased absorbed dose. X-ray structural analysis has revealed the layer of radiation-induced degradation in a fused preparation with an enhanced content of boron oxide and sodium oxide to consist principally of H_3BO_3 and $NaNO_3$. The greatest stability is that exhibited by preparations containing no boron oxide or sodium components (or else containing these only in slight quantities); even at doses of 10^8 to 10^9 rad the change in the surfaces of such specimens is comparatively modest (Fig. 6).

No changes in the chemical stability of the preparations are induced by irradiation in vacuum, nor do any visible structural-damage effects appear in the surfaces of the preparations.

[1] In all the diagrams τ indicates the time required for the specimen to become dissolved.

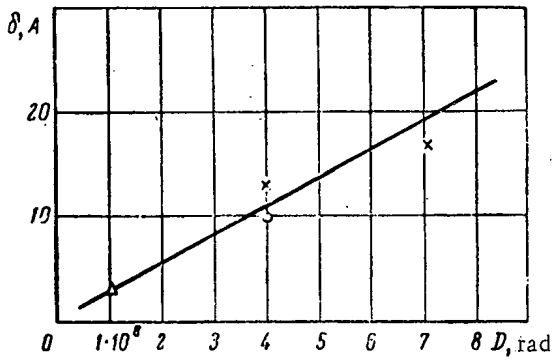

Fig. 4. Magnitude of radiation effect plotted vs absorbed dose at dose rate indicated in rad/sec: Δ) 10; O) 100; ×) 200.

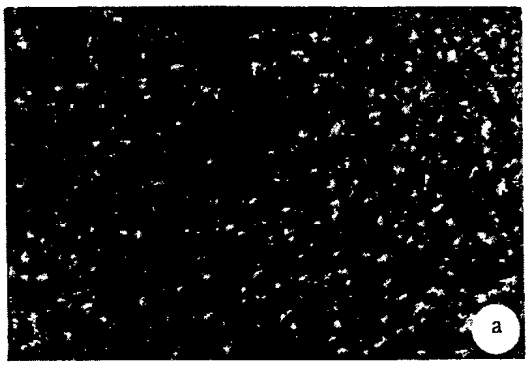

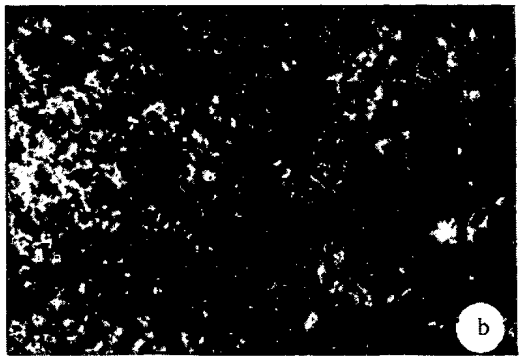

Fig. 6. Surface of fused preparation consisting of 35% SiO_2, 9% Al_2O_3, 4% TiO_2, 1% CaF_2, and 51% of a mixture of the oxides CaO, MgO, FeO, Fe_2O_3, Cr_2O_3 (550 times magnification): a) unirradiated; b) after exposure to Co^{60} gammas, $D = 5 \cdot 10^8$ rad.

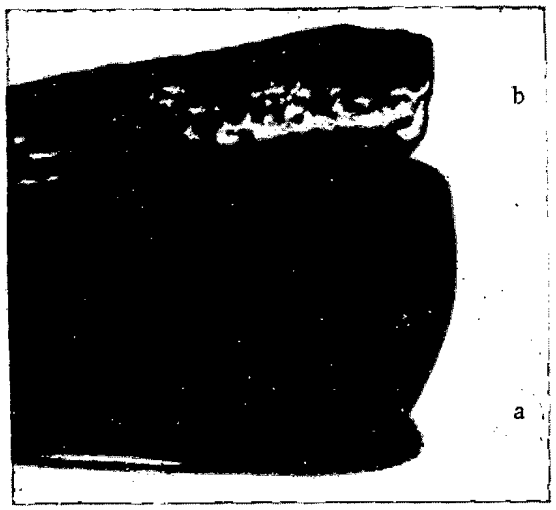

Fig. 5. External form (unmagnified) of fused preparation consisting of 20% CaO, 10% Na_2O, 10% SiO_2, 60% B_2O_3: a) prior to irradiation; b) after exposure to Co^{60} gammas; $D = 1.3 \cdot 10^9$ rad.

The external appearance of the corrosion products depends on the chemical composition of the specimen. Figure 7 shows a 550-times magnification of the surface of preparations enriched with strontium, borate, or sodium components, after irradiation at an absorbed energy dose of $6 \cdot 10^8$ rad. Various crystal formations stand out on the surface of the preparations, clearly as a result of the irradiation.

The investigations we conducted revealed that degradation of the surface of all the silicate materials investigated will be observed in irradiation in air. The absence of damage in the inner-lying layers of the specimens, as well as the absence of corrosion in irradiation in vacuum, militate in favor of the view that surface degradation is due to heterogeneous chemical reactions of the fused materials with air constituents. The process of atmospheric corrosion of glass takes place as a rule even in the absence of irradiation, but at a negligible reaction rate. The radiation-chemical reaction products decompose on the surface in the form of a layer only weakly bound to the basic structure. The thickness of the layer of degradation products depends on the chemical composition of the preparation. At identical values of absorbed dose, the degree of corrosion will increase with any increase in the content of alkali or alkali earth metals, as well as boron oxide. The special role of the oxides of the alkali metals and of the rare earths is confirmed by the increased content of these elements in water when the irradiated materials go into solution. The radiation instability of boron-containing compounds is confirmed by the presence of boric acid in the degradated layer.

Radiation effects may escape notice in an investigation of chemical stability if the preparations undergo granulation after the irradiation exposure. The fraction of the surface subjected to radiation damage may then become negligibly small (Fig. 8). Radiation effects may again escape notice if mineral acids in which the solubility of certain glasses rises steeply are used as solvents. These circumstances appear to account for the discrepancy in the results we obtained and the data reported elsewhere [8, 9].

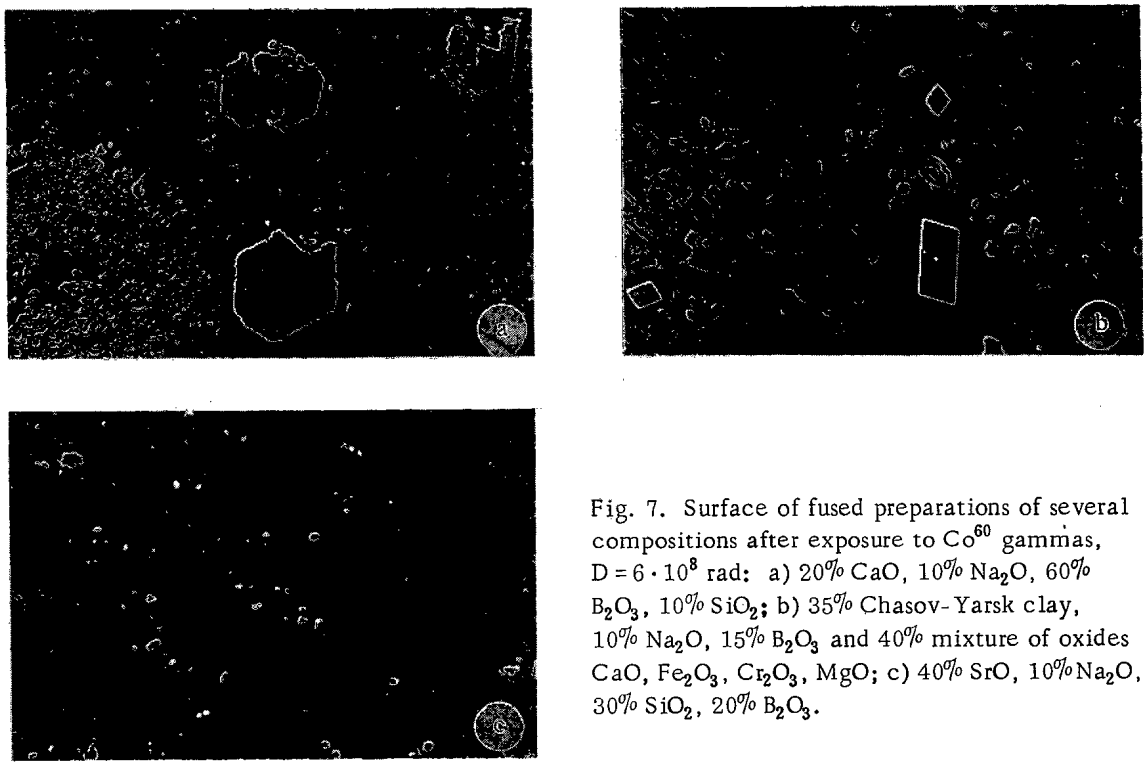

Fig. 7. Surface of fused preparations of several compositions after exposure to Co^{60} gammas, $D = 6 \cdot 10^8$ rad: a) 20% CaO, 10% Na_2O, 60% B_2O_3, 10% SiO_2; b) 35% Chasov-Yarsk clay, 10% Na_2O, 15% B_2O_3 and 40% mixture of oxides CaO, Fe_2O_3, Cr_2O_3, MgO; c) 40% SrO, 10% Na_2O, 30% SiO_2, 20% B_2O_3.

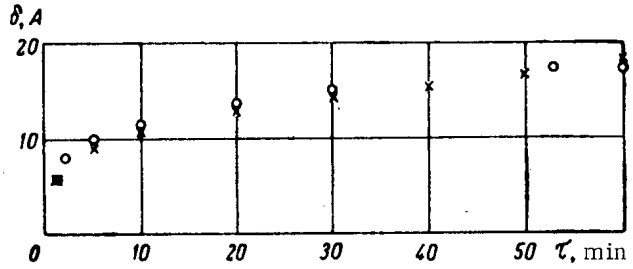

Fig. 8. Radiation-damage depth for water in a fused preparation of composition B: X) prior to irradiation; O) granulated after exposure to a Co^{60} source, $D = 1.3 \cdot 10^9$ rad.

On the basis of experimental findings, we may suggest the following mechanism to account for radiation-chemical destruction of vitreous preparations. Oxides of alkali and alkaline-earth metals are completely or partially bound to the silicate structures. Scission of old bonds and the formation of new bonds may occur in response to ionizing radiation through the excitation of the silicate molecule. The chemical effect of the irradiation is due to the formation of active centers in the solid and in the surrounding gaseous medium. The process may be schematized as

$$\overset{\beta,\ \gamma}{\rightsquigarrow} 3MeSiO_3 \xrightarrow{H_2O,\ CO_2,\ NO_2} Me(OH)_2 + MeCO_3 + Me(NO_3)_2 + 3SiO_2.^2$$

As a result of this reaction, the metal loses its linkage to the silicon-oxygen framework of the glass and forms a film in the form of a hydroxide, carbonate, or nitrate on the surface of the preparation. Corrosion products pass into the solution, thereby bringing about a pronounced increase in the rate of dissolution of the irradiated preparation (Fig. 9). The surface of the preparation becomes enriched with silica in the process, and that in turn results in a subsequent decline in the rate of dissolution of the irradiated specimen causing it to lag behind the rate of dissolution of the unirradiated counterpart (cf. Fig. 3). From the suggested mechanism we infer that: the higher the rate of dissolution of the irradiated preparation in the first period (5 to 10 min), the lower the value the rate will have to have later on, and this is confirmed experimentally. Oxides of metals present in the preparation in forms other than silicate compounds are also capable of participating in the radiation-chemical reactions, it is quite evident.

Radiation damage to the surface results in a greater rate of passage of radioactive isotopes into the solution. Figure 10 shows the variation in damage depth and leachability of fission products when a fused radioactive preparation is contacted with water and is left in air for different periods of time after being prepared. The preparation was made from process solutions; the specific activity of the preparation was 2.6 Ci/g.

[2]The nitrogen oxides form in air in response to the ionizing radiation [12].

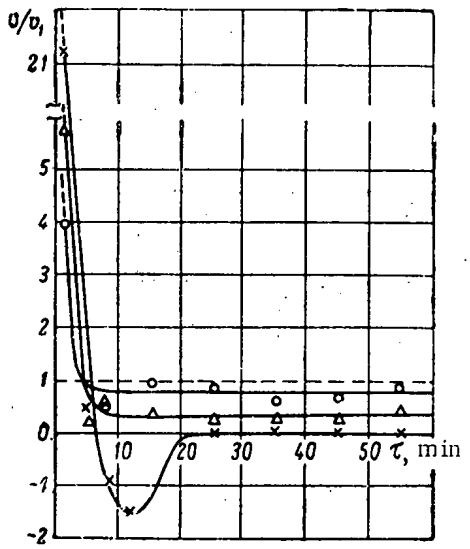

Fig. 9

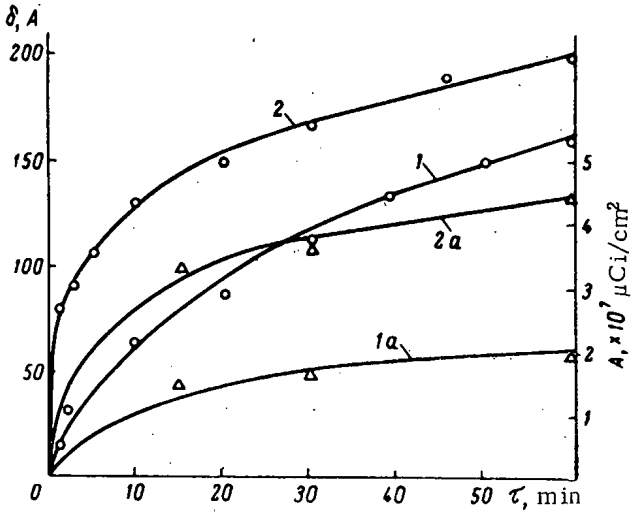

Fig. 10

Fig. 9. Ratio of rates of dissolution in water of irradiated (v) and unirradiated (v_1) fused preparation of composition B at absorbed doses: O) $4 \cdot 10^8$ rad; Δ) $7 \cdot 10^8$ rad; x) $1.3 \cdot 10^9$ rad.

Fig. 10. Effect of internal irradiation on chemical stability of fused preparation with specific radioactivity of 2.6 Ci/g, containing the sum of the uranium fission fragments (age of fragments: 300 days): 1) 30 min after preparation; 2) determination repeated 16 days after preparation, $D = 7 \cdot 10^8$ rad; 1a) elutability of radioactive isotopes A, expressed in mCi/cm^2 per 1 mCi of specific activity recorded in the first experiment; 2a) elutability of radioactive isotopes in repeated solubility determination 16 days later.

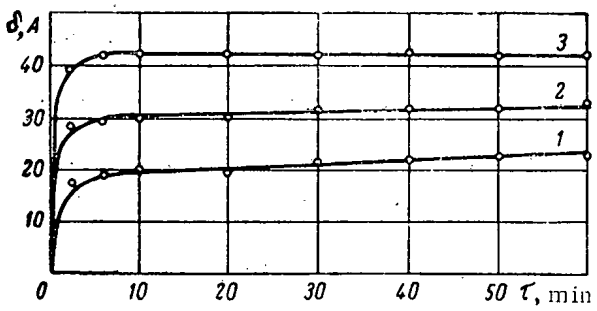

Fig. 11. Effect of Co^{60} γ-radiation on the chemical stability of "Druzhnaya gorka" glass: 1) prior to irradiation; 2) $D = 4 \cdot 10^8$ rad; 3) $D = 7 \cdot 10^8$ rad.

As a result of the surface character of the radiation-chemical reactions, only an insignificant fraction of the compounds included in the composition of the preparation and present on its surface will participate in those reactions. In the case of vitreous fragment concentrates, disposed of in waste burial in the form of metal-clad blocks, for which the surface to volume ratio is small and the contacting area with air is slight, radiation effects may be inconsequential. To minimize radiation effects, it is advisable to devise preparations containing no boron oxide and no oxides of the alkali metals, or at most containing them in only very slight quantities.

In the case where β-radiation sources are prepared in the form of an emamel, where the volume to surface ratio is low, and further an appreciable amount of boron and sodium components are introduced into the enamel in order to reduce viscosity, we may expect severe radiation damage to the preparation. A protective silicate glass film would hardly act to spare the source from radiation damage over a protracted span of time, since even chemically stable glasses fall victim to surface corrosion when bombarded by ionizing radiations (Fig. 11). The correct choice of radiation-stable compositions, as well as an effective solution to the problem of reliable hermetic sealing, is of paramount importance, then, in the design of safe sources of ionizing radiation.

LITERATURE CITED

1. Watson et al., "1958 Geneva Conference of the Peaceful Uses of Atomic Energy," Selected reports of foreign scientists, Vol.9, Atomizdat, Moscow (1959), p. 187.

2. P. V. Zimakov et al., "1958 Geneva Conference of the Peaceful Uses of Atomic Energy," Selected reports of Soviet scientists, 4, Atomizdat, Moscow (1959), p. 247.
3. P. V. Zimakov and V. V. Kulichenko, Disposal of radioactive wastes, IAEA, Vienna (1960), p. 431.
4. P. V. Zimakov and V. V. Kulichenko, Atomnaya énergiya, 10, 58 (1961).
5. C. Amphlett, Progr. in Nucl. Energy, III, Process Chemistry, 2, Pergamon Press (1958).
6. M. Goldman et al., Report No. 2004 presented by the U.S.A. at the Second International Conference on the Peaceful Use of Atomic Energy, Geneva (1958).
7. L. Watson, Glass Ind., 41, 264 (1960).
8. M. Elliot et al., Industr. Chemist, 37, 368 (1961).
9. T. Mike, B. Steierman, and E. Degering, J. Amer. Ceram. Soc., 43, 405 (1960).
10. I. Vistal', Steklo i keramika, No. 2, 30 (1937).
11. V. S. Molchanov, Zhur. prikladnoi khim., 13, 934 (1940).
12. S. Ya. Pshezhetskii, Mechanism of radiation-chemical reactions [in Russian], State chem. press, Moscow (1962), p. 148.

CONCENTRATION OF WATER SAMPLES FOR DETERMINING THE TRITIUM CONTENT

(UDC 621.039.332)

Ya. D. Zel'venskii, D. A. Nikolaev,
V. S. Tatarinskii, and V. A. Shalygin

Translated from Atomnaya Énergiya, Vol. 18, No. 4,
pp. 367-372, April, 1965
Original article submitted March 23, 1964

A method of concentrating the tritium in water samples by means of distillation under vacuum (~100 mm Hg) is suggested and experimentally verified. The degree of tritium enrichment is determined by the change in concentration of stable isotopes (oxygen or deuterium) on distillation of the sample. Two variations of the calculation are proposed: for the stationary state with the attainment of the maximum possible degree of fractionation and cessation of enrichment at the nonstationary state.

In order to determine the tritium content in natural waters, it is necessary to carry out a preliminary concentration of the sample by a factor of 100-1000 or more. It is obvious that the method of preliminary concentration of the sample should ensure not only sufficient enrichment of the sample in tritium but also the possibility of determining accurately the degree of enrichment.

For this purpose two methods can be used for concentrating the tritium: an electrolytic and a distillation method. Electrolytic enrichment takes place as a result of the electrolytic reduction of 250 ml of sample to a volume of less than 2.5 ml [1].

In [2], the degree of enrichment of the sample in tritium after distillation of the water in a packed column was determined relative to the volumes of liquid in the feed reservoir, in the vat and in the column packing on the basis of the tritium material balance equation. However, this method of determining the degree of enrichment is inaccurate and can be used only for low enrichment; moreover, the distillation process proceeds for a long time.

In this paper, the principal results of an investigation into the distillation of water, undertaken with the purpose of developing a more efficient method of concentrating samples in tritium, are discussed. The proposed method is based on the possibility of determining the degree of enrichment of a sample containing tritium according to analytical measurement taking place simultaneously with the change of concentration of the stable isotopes oxygen and deuterium. The experimental verification of this method of determining the degree of enrichment of water in tritium was taken into account in the investigation and also the explanation of the optimum conditions for distillation of the water.

Principle of the Method

Suppose we have a distillation column with an upper feed reservoir of sufficiently large volume, filled initially with water. As a result of the distillation process, the water in the lower section of the column will be enriched in tritium and other isotopes (deuterium and O^{18}), forming a less volatile species of water. The partition coefficients of the isotopes differ but little from unity, and the isotopic effects in the kinetics of mass exchange as a result of distillation are probably so insignificant that they can be neglected. Then, for given conditions of distillation

$$n_T = n_O = n_D, \tag{1}$$

where n_T, n_O, and n_D are the number of theoretical separation stages (or the number of transference units) with respect to tritium, oxygen and deuterium respectively. Hence it follows that enrichment of the water in the various

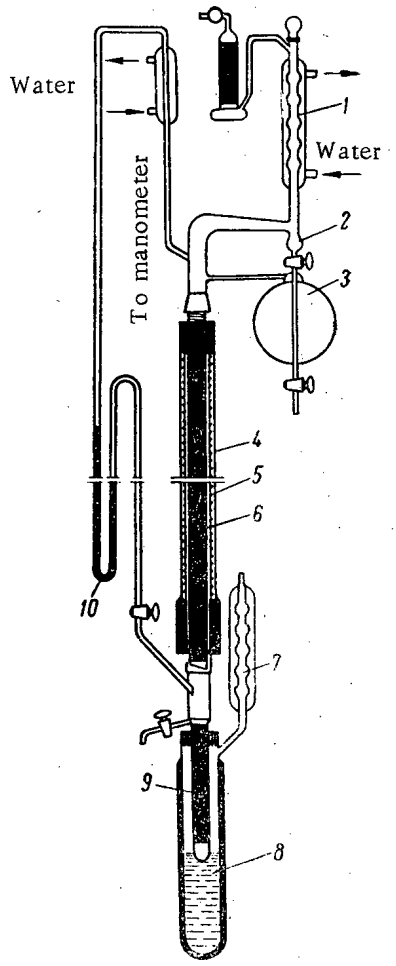

Fig. 1. Diagram of distillation apparatus: 1) condenser; 2) reflux gauge; 3) feed reservoir; 4) surrounding jacket; 5) heater coil; 6) distillation tube with packing; 7) cold trap; 8) coolant; 9) vat with packing; 10) differential manometer.

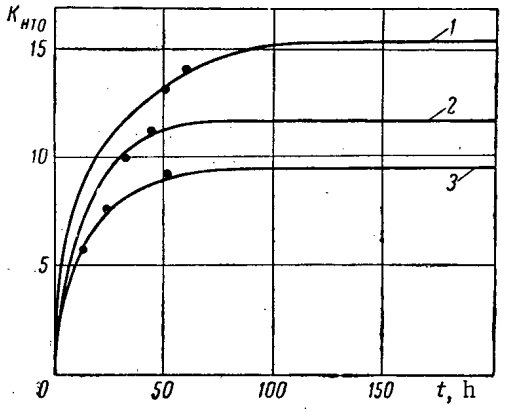

Fig. 2. Enrichment of water in tritium at atmospheric pressure and loading, kg/(m^2 · h): 1) 320; 2) 640; 3) 945.

isotopes (tritium, deuterium and O^{18}) should take place in a definite relationship with one another, determined by the value of the corresponding partition coefficients. For the stationary state, as a result of distillation with total reflux (without takeoff) on the basis of Eq. (1) we have by the well-known Fensk equation

$$\log K_T = \log K_O \frac{\log \alpha_T}{\log \alpha_O} = \log K_D \frac{\log \alpha_T}{\log \alpha_D}, \qquad (2)$$

where K_T, K_O and K_D are the degrees of fractionation (the ratio of the concentration in the upper and lower sections of the column); α_T, α_O, and α_D are the partition coefficients with respect to tritium, heavy oxygen and deuterium respectively. The values of α_T, α_O, and α_D are determined with high accuracy. Thus, if by means of the appropriate analytical procedures the degree of fractionation of the water is determined with respect to the heavy-oxygen isotope K_O or deuterium K_D, then Eq. (2) enables the degree of fractionation in the same sample of water to be found with respect to tritium (K_T) for stationary conditions.

If a high-efficiency column is used, then a specified sample enrichment can be obtained without reaching the stationary state, which permits a several-fold shortening of the duration of the distillation. According to the data from isotopic analyses on the content of deuterium or O^{18} in several samples taken off over known intervals of time, the number of theoretical degrees of fractionation n of the column can be determined by the equation for nonstationary distillation. Using the value found for n and the value for α_T corresponding to the distillation conditions, then by the same equation the required degree of fractionation of water with respect to tritium K_T can be calculated.

Experimental Procedure

Concentration of the water was carried out in a packed distillation column with a diameter of 25 mm; the height of the column packing layer was 1920 mm. Pieces of a spiral 2 × 1.5 mm noncorroding steel wire with a 0.2-mm diameter were used as the packing (a diagram of the apparatus is shown in Fig. 1). A weak solution of tritiated water, to which was added 1% heavy-oxygenated water H_2O^{18}, was distilled in order to increase the accuracy of the analytical control after varying the concentration of O^{18}.

The change of H_2O^{18} content at the ends of the column was controlled by a mass-spectrometric method. The samples of the solution for analysis were subjected to isotopic exchange with a known quantity of potassium carbonate K_2CO_3, which were decomposed by phosphoric acid; the carbon dioxide gas liberated was admitted to the inlet system of a mass-spectrometer. A Soviet-produced instrument of the type MI-1305 was used. The tritium concentrations at the ends of the column were measured by a scintillation method.

TABLE 1. Distillation of Water for Various Values of Pressure and Load

Pressure in upper section of column, mm Hg	Load (reflux density), kg/(m²·h)	Time elapsed from start of experiment, h	Activity due to content of HTO, imp/min		Concentration of H_2O^{18}, %	
			base of column	top of column	base of column	top of column
50	400	45	7501	181.0	1.5930	0.987
		59	8530	178.0	1.5941	0.983
50	212	17	5381	220.0	1.4515	1.021
		30	6562	203.0	1.5380	1.011
		48	7402	141.0	1.5989	0.999
		65	8023	133.0	1.6530	0.991
		80	8760	–	1.7259	–
		98	9840	127.0	1.7289	0.986
50	176	20	4440	181.3	1.2531	1.010
		33	6530	180.7	1.5002	0.996
100	575	16	2227	–	–	–
		17	2270	–	1.3574	–
		28	2685	120.9	–	–
		41	3063	120.0	1.4989	0.980
100	320	29	3700	128.0	1.6415	1.1089
		45	4539	109.0	1.8301	1.0763
		59	4977	98.0	1.6500	0.9953
		72	5947	90.6	1.8185	0.9942
100	176	6	660	–	1.2289	–
		19	2177	–	1.4699	–
		32	2795	–	1.8339	–
		50	4295	–	2.0293	–
		72	5423	91.0	2.0890	1.0193
300	960	13	2800	180.0	1.4500	1.016
		25	3611	179.0	1.4604	1.002
300	480	13	2500	171.0	1.4403	1.014
		25	3830	170.0	1.4802	1.011
300	192	39	4536	172.0	1.5070	1.011
		53	5980	168.0	1.5350	1.003
750	945	14	1030	180.8	1.2430	1.014
		23	1370	178.3	1.2461	1.014
750	640	33	1790	178.0	1.2630	1.012
		44	2005	176.8	1.3111	1.011
750	320	52	2318	176.0	1.349	1.008
		60	2480	175.0	1.372	1.006

TABLE 2. Efficiency of a Packed Column for Enriching Water in Tritium and the Heavy-Oxygen Isotope

Distillation conditions			Number of theoretical fractionation stages		EHTS, cm	Maximum degree of fractionation*		Degree of fractionation with respect to tritium calculated by Eq. (2)
pressure in uppersection of column, mm Hg	average temperature in column, °C	loading, kg/(m^2 · h)	with respect to O^{18}	with respect to tritium		with respect to oxygen isotope (K_O)	with respect to tritium (K_T)	
50	41.0	176	84	83	2.29	1.84	308	316
50	42.0	212	79	80	2.40	1.77	216	219
50	44.0	400	74	75	2.58	1.69	148	151
100	52.5	176	105	103	1.84	1.96	400	392
100	53.5	320	96	95	2.02	1.84	240	280
100	55.0	575	82	84	2.31	1.69	110	120
300	75.0	192	115	114	1.68	1.75	112	117
300	75.5	480	104	104	1.84	1.64	67.5	59.3
300	76.5	960	93	92	2.09	1.55	40.7	35.6
750	100.0	320	112	112	1.73	1.38	15.2	12.6
750	100.0	640	100	101	1.92	1.32	11.5	9.1
750	100.5	945	94	93	2.03	1.29	9.5	7.1

*Calculated by Fensk's equation for the mean value of α.

TABLE 3. Results of Verifying the Calculation of the Degree of Fractionation of Water Containing Tritium According to Data from the Nonstationary Enrichment of Water in O^{18}

Distillation conditions		Distillation, time, h	Degree of fractionation with respect to tritium	
pressure in upper section of column, mm Hg	loading, kg/(m^2 · h)		experiment	calculation
50	212	48	52.5	50
100	176	72	59.5	63
100	575	41	25.5	26
300	192	53	35.6	37
750	320	52	13.2	13.3

Experimental Data and Discussion

For the purposes of determining the optimum regime for enriching water in tritium and for experimental verification of the stated method under different conditions, experiments were carried out in the apparatus described for distilling water under a pressure of 50-750 mm Hg over the range of loads 176-960 kg/(m^2 · h). The experimental data obtained are given in Table 1.

It was assumed for the calculations that distillation of two binary mixtures takes place: $H_2O^{18}-H_2O^{16}$ and $HTO-H_2O$, since the presence in the water of small quantities of other isotopic species of water has practically no effect on its properties.

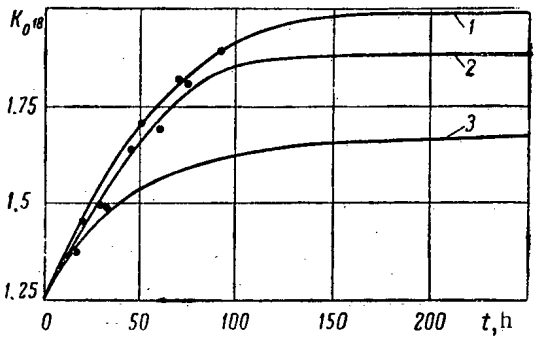

Fig. 3. Enrichment of water in the heavy-oxygen isotope O^{18} at a pressure of 100 mm Hg and a loading, kg/(m^2·h): 1) 176; 2) 320; 3) 575.

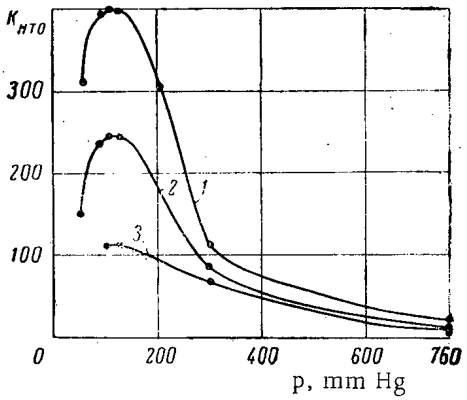

Fig. 4. Dependence of the maximum (stationary) degree of fractionation of water with respect to tritium on the pressure for a loading, kg/(m^2·h): 1) 176; 2) 320; 3) 575.

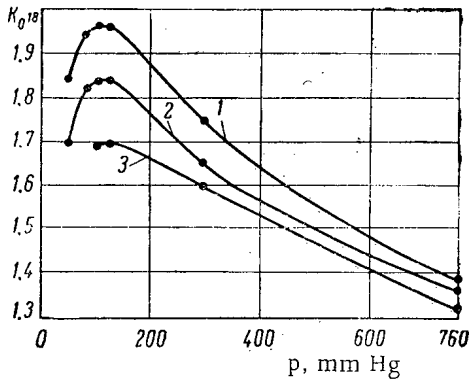

Fig. 5. Dependence of the stationary degree of fractionation of water in the oxygen isotope on the pressure for a loading, kg/(m^2·h): 1) 176; 2) 320; 3) 575.

Because the stationary state was not attained during the time of the experiment, the calculation was carried out according to the nonstationary distillation equation proposed by Berg and James [3]; a calculation according to the equations of S. I. Babkov and A. M. Rozen [4, 5] gives similar results.

The values for the partition coefficient α_O for the system $H_2O^{16}-H_2O^{18}$ were taken from [6]. According to data from our laboratory [7], the partition coefficient of the isotopes hydrogen-tritium for the distillation of water (system H_2O-HTO) over the temperature range 40-100°C is equal to

$$\log \alpha_T = \frac{38{,}80}{T} - 0.0935 \,. \qquad (3)$$

In order to calculate the column efficiency the mean value of α at the temperature of the upper and lower sections of the column was used.

The results of some of the experiments and calculations which were carried out are shown in Figs. 2 and 3; the experimental data are shown by points and the curves are drawn according to Berg and James' equation [3] for the values found for the number of theoretical degrees of fractionation of the column. It can be seen from the figures that the experimental data agree well with the calculated data. Similar graphs were obtained for other distillation conditions.

The equivalent height of a theoretical stage, EHTS, and the stationary degree of fractionation for operation without takeoff ($K = \alpha^n$) were calculated from the value found for n by the method described above. The results of the calculation are presented in Table 2. It can be seen from the table that the values for the number of theoretical degrees of fractionation, calculated by the change in concentration of tritium and O^{18}, agree amongst themselves, i.e., the experimental data confirm the validity of Eq. (1) and, consequently also, Eq. (2) which results from it.

A comparison of the degree of fractionation of water with respect to tritium, calculated by the proposed method, with the experimental values is presented in Table 3. It can be seen from the table that there is satisfactory agreement between the calculated and experimental data for stationary as well as for nonstationary distillation. It is obvious that similar results could be obtained if, for determining the degree of fractionation of water with respect to tritium, in place of the data concerning the change of concentration of the oxygen isotope the data from the isotopic analysis of the water with respect to deuterium are used.

If it is necessary to increase the concentration of O^{18} or deuterium in order to increase the accuracy of the isotopic analysis, then a known quantity of heavy-oxygenated water or deuterated water respectively can be added to the sample of water to be analyzed, prior to its distillation.

The results of the experiments which were carried out enable conclusions to be drawn also concerning the optimum distillation conditions. The relationship between the degree of fractionation of water with respect to the

TABLE 4. Characteristics for Enriching Water in Tritium by Distillation in a Packed Column at a Pressure of 100 mm Hg

Process parameters	Specified degree of fractionation of water with respect to tritium		
	100	500	1000
For stationary state of column:			
Number of theoretical degrees of fractionation	80	105	115
Height of packed portion of column, cm	185	242	265
Degree of fractionation of water with respect to O^{18}	1.64	1.93	2.04
Degree of fractionation of water with respect to deuterium	58	200	340
Operating time of apparatus, h*	500	600	650
For nonstationary distillation:			
Number of theoretical degrees of fractionation	100	130	150
Height of packed portion of column, cm†	190	247	285
Time during which a specified enrichment is achieved, h†	120	140	160
Degree of fractionation of water with respect to O^{18}	1.9	2.0	2.36
Degree of fractionation of water with respect to deuterium	30	200	650

*For column operation with a loading of 575 kg/(m^2 · h).
†For column operation with a loading of 180 kg/(m^2 · h).

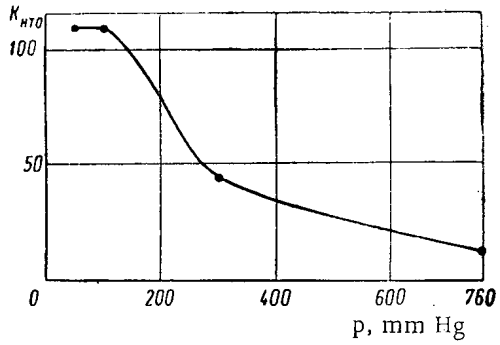

Fig. 6. Dependence of the degree of fractionation of water in tritium on the pressure, for nonstationary distillation and a loading of 176 kg/(m^2 · h).

heavy isotopes and the pressure for the stationary state of the column, operating with total reflux (when the maximum fractionation K is achieved) is given in Figs. 4 and 5. It can be seen from the figures that the maximum degree of fractionation of water for tritium as well as for the heavy-oxygen isotope at different loadings is observed at a pressure of 100-120 mm Hg, (upper section of column). The presence of an optimum pressure, corresponding to the maximum degree of fractionation, results from the nature of the dependence of α and the EHTS on the pressure (temperature) and it is typical for distillation in columns with efficient packing [8, 9]. The same interval of pressure can be assumed optimum in the case of nonstationary distillation also (Fig. 6). For identical duration of distillation, the maximum degree of fractionation of water with respect to tritium (and also with respect to the other isotopes) is achieved under a pressure of 100-120 mm Hg.

On the basis of the data obtained for enriching water in tritium, distillation under a pressure of 100-200 mm Hg (in the upper section of the column) can be recommended. The pressure used by Smith and Rawson [2], equal to 40 mm Hg, is not the optimum pressure.

It can be seen from the experimental data obtained that a significant relationship is observed between the degree of fractionation of water with respect to the different isotopes and the loading (reflux density or vapor rate) of the column. By decreasing the loading, as a consequence of the reduction of the EHTS (other conditions being equal) and increase in the enrichment is achieved. However, the stationary state is considerably more rapidly established at high loadings. Therefore, if enrichment is carried out under nonstationary conditions, it is advantageous to operate at small loadings, whereas for achieving a stationary state it is more advantageous to carry out the distillation at higher loadings. In the present project the reflux density amounted to 170-200 kg/($m^2 \cdot h$).

The parameters of the column necessary for achieving different degrees of fractionation of a sample with respect to tritium are shown in Table 4, and also the enrichment in the stable isotope O^{18} and deuterium obtained with it. Data are presented for two possible variants of the project: the stationary state with the attainment of the maximum possible degree of fractionation K and the cessation of enrichment at the nonstationary state. Table 4 is compiled for the following distillation conditions: the pressure in the upper section of the column is 100 mm Hg, the packing is of the same type as in this project, the loading of the column for operation up to the stationary state is 575 kg/($m^2 \cdot h$), and for nonstationary distillation it is 180 kg/($m^2 \cdot h$).

It follows from the data presented in Table 4 that if the attainment of the maximum possible enrichment for a given column (stationary state) is abandoned, then it is possible to considerably shorten the duration of the distillation by a small increase of the column height. However, as a result of this the calculation of the degree of fractionation is made more complex, since in place of the simple Eq. (2), the more complex relationships of nonstationary distillation must be used.

Conclusions

A method for enriching samples of water in tritium is proposed and proved experimentally by means of distillation under vacuum with the determination of the degree of fractionation on the basis of isotopic analysis of the distillate with respect to the heavy isotope of oxygen or deuterium.

It is shown that the maximum degree of fractionation is achieved by distillation under a pressure of 100 mm Hg.

LITERATURE CITED

1. H. Ostlund and E. Werner, Tritium in the Physical and Biological Sciences, 1, IAEA, Vienna (1962), p. 95.
2. D. Smith and D. Rawson, Tritium in the Physical and Biological Sciences, 1, IAEA, Vienna (1962), p. 105.
3. P. Berg and G. James, Chem. Engng. Progr., 44, 307 (1948).
4. S. I. Babkov, N. M. Zhavoronkov et al., Kernenergie, 5, 219 (1962).
5. A. M. Rozen, Theory of isotope separation in columns [in Russian], Atomizdat, Moscow (1960).
6. O. V. Uvarov, N. M. Sokolov, and N. M. Zhavoronkov, Kernenergie, 5, 323 (1962).
7. Ya. D. Zel'venskii et al., Atomnaya Énergiya, 18, 46 (1965).
8. Ya. D. Zel'venskii, A. A. Titov, and V. A. Shalygin, Khim. prom-st', No. 2, 116 (1963).
9. A. A. Efremov and Ya. D. Zel'venskii, Khim. prom-st', No. 3, 201 (1964).

URANIUM AND ARSENIC IN THE HYDROTHERMAL PROCESS

(UDC 549:533.495+553.497)

V. E. Boitsov and T. M. Kaikova

Translated from Atomnaya Énergiya Vol. 18, No. 4,
pp. 373-378, April, 1965
Original article submitted May 30, 1964

The authors give a brief description of the structural characteristics of hydrothermal uranium deposits, together with data on the mineral composition of their ores. The deposits are of the uranium sulfide type, mineral formation being a multistage process. The distinctive feature of the ore composition is extensive occurrence of native arsenic, which forms a paragenetic association with pitchblende. An analysis of the mineral composition of the ore and of the trends of paragenesis formation gives reason to suppose that there was a high arsenic concentration in the hydrothermal solutions, from which pitchblende was deposited at low temperatures and at shallow depths.

Industrial uranium deposits have a wide range of mineral associations. The distinctive feature of some deposits is extensive occurrence in quartz and carbonate, veins of arsenic-containing minerals associated with the main uranium minerals, i.e., pitchblende and coffinite.

The geochemical characteristics of uranium deposition from arsenic-containing hydrothermal solutions have mostly been based on studies of arsenide or five-mental deposits, in which pitchblende is present with nickel and cobalt diarsenides, or (far less frequently) sulfoarsenides.

Arsenic is a particularly useful element for a geochemical analysis of mineral associations because of its wide range of valence: $As^{2-}-As^{1-}-As^{0}-As^{2+}-As^{3+}-As^{5+}$. Arsenic may be present as anions (in reducing conditions, in which nickel and cobalt diarsenides, arsenopyrite, cobaltite and gersdorffite are deposited from the solutions), or as cations (in more oxidizing conditions, in which realgar, orpiment, arsenic-containing fahlerz and enargite are formed). Replacement of a (pitchblende-cobalt and nickel diarsenides) paragenetic association by a (pitchblende-sulfoarsenides) paragenetic association therefore indicates an increase in the solutions' redox potential. This increase is within the range corresponding to transition of As^{2-} to As^{1-} and does not impair uranium deposition from these solutions.

Present concepts of uranium and arsenic behavior in the hydrothermal process can be expanded by the new data obtained by the authors in a study of uranium sulfide deposits containing pitchblende and (presumably) coffinite in association with arsenic and arsenic-containing minerals. The characteristics of the geological structure of two deposits, and their mineralization, are summarized below.

Structural Characteristics of the Deposits

The region is composed mainly of Cambrian rocks contorted into a steep Caledonian anticline. Major tectonic zones controlling granite massifs are traced in the axial part of the anticline. The deposits are associated with rocks of a Cambrian effusive-sedimentary Cambrian complex and lie in the east and west exocontact zones of one of the massifs (composed primarily of granodiorite). This massif has breached and changed the Cambrian rocks and is overlain transgressively by Devonian red sandstone. The granite has been breached by alaskite granite stocks. In the region of the deposits the dike rocks are represented by aplite, pegmatite, alaskite granite, plagiaplite, dioritic and diabasic porphydrites. The latter occur very extensively around the western exocontact of the granodiorite massif, whereas aplite dikes are predominant around the eastern exocontact.

The region contains major tectonic zones oriented in a submeridional direction conformably with the eastern and western contacts of the granodiorite massif. The zones are up to 200-m thick and consist of several geosutures in echelon or virtually parallel.

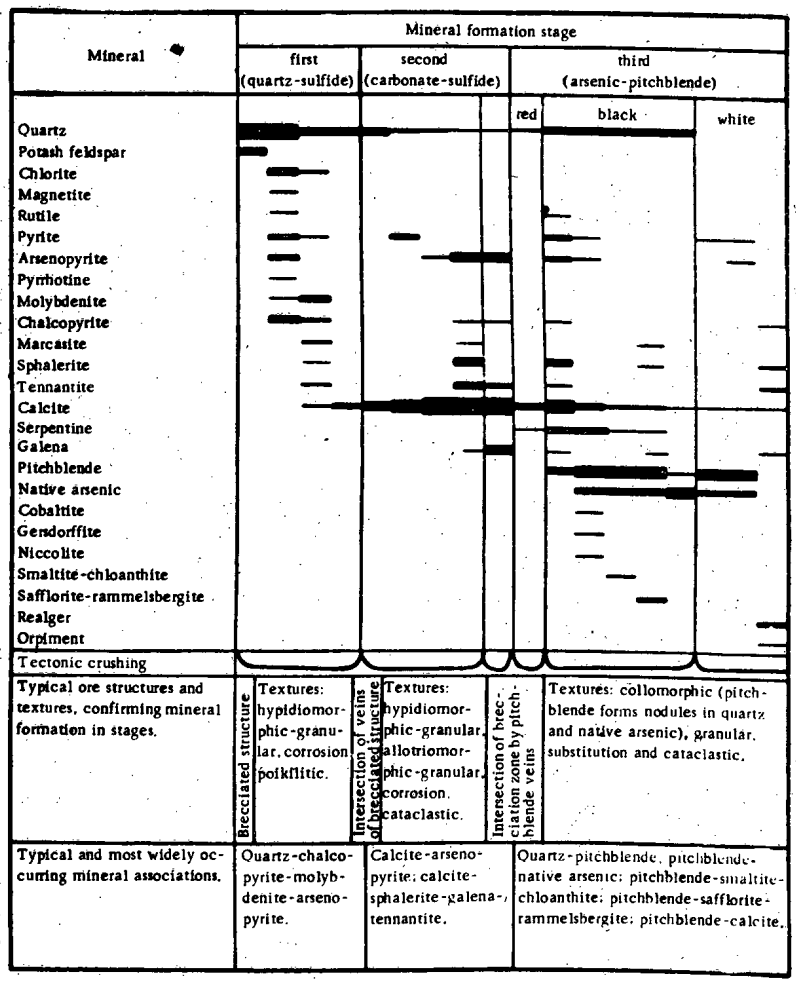

Fig. 1. Mineral formation sequence in the deposit in the western exocontact of the granodiorite massif. (Arsenic-containing minerals underlined.)

The tectonic zones are older and control the Caledonian granodiorite massifs. Subsequent tectonic movements overthrust the effusive-sedimentary rocks onto the Devonian sandstone.

Uranium mineralization is usually absent in the major faults of virtually meridional strike, being mainly concentrated in the feather faults.

Uranium mineralization in the deposit associated with the western exocontact of the granodiorite massif occurs in Cambrian limestone penetrated by diabasic porphyrite dikes, whereas in the eastern exocontact deposit it is present in the amphibolites at the edge of this massif.

Mineralization Stages and Mineral Segregation Sequence

Three hydrothermal veinlet types of different composition can be distinguished in the western contact deposit.

1. Sulfide-quartz veinlets. Their thickness is generally less than 1-1.5 cm; they contain quartz, potash feldspar, chlorite, calcite, magnetite, rutile, pyrite, arsenopyrite, pyyrhotine, molybdenite, chalcopyrite, marcasite, sphalerite and fahlerz. Pyrite, chalcopyrite and molybdenite occur most frequently in the ore minerals, and quartz in the vein minerals. The mineral contents vary widely both in the ore and vein minerals. One can therefore find the following facies varieties of quartz-sulfide veinlets: quartz, potash feldspathic-quartz and chlorite-quartz veinlets, containing ore minerals—mainly sulfides (the amount varying from 3 to 20%.

2. Sulfide-carbonate veinlets of thickness 2-3 mm to 20 cm. The calcite and (to a lesser extent) the quartz, which compose these veinlets and contain an impregnation of ore minerals, also serve as cement in the brecciation

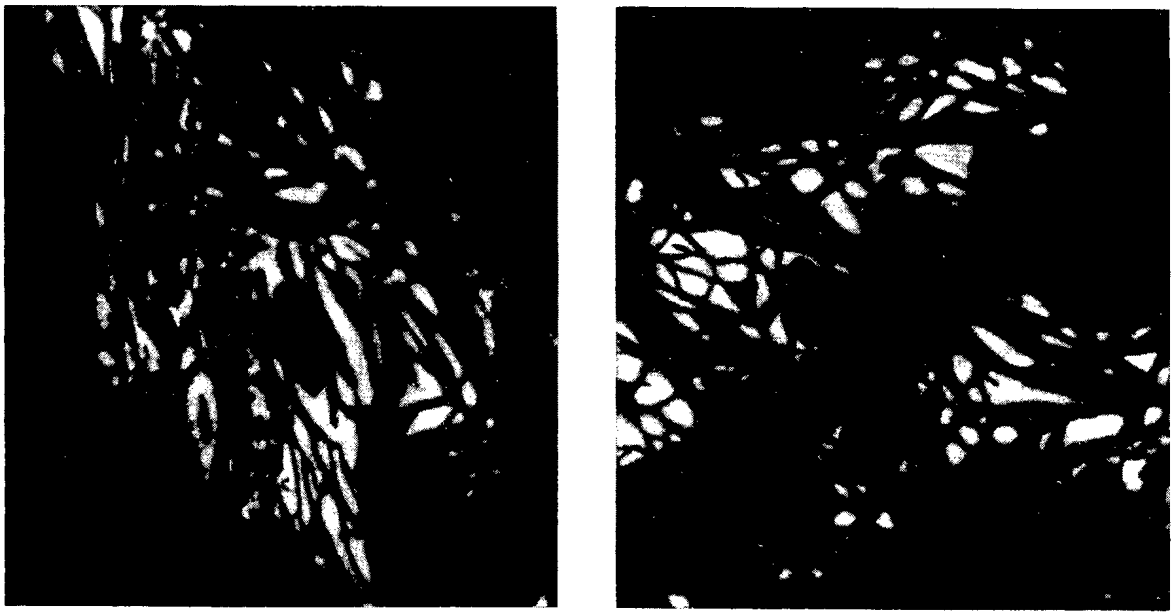

Fig. 2. Thread-like segregations of coffinite (?) (gray) in native arsenic (white) in quartz (dark) (× 1200).

zones (thickness 2.5 m). Ore minerals in these formations are represented by pyrite, arsenopyrite, sphalerite, galena, fahlerz and (less frequently) chalcopyrite and marcasite. The content of sulfides is usually less than 3-5% and that of sphalerite and galena reaches 10-15% only in a few veinlets.

3. Arsenic-quartz uranium-containing hydrothermal formations. These are usually fine veinlets of thickness up to 5-8 mm, single or contiguous at distances of a few meters. One sometimes observes zones (thickness up to 15-30 cm) of branching veinlets, passing over into brecciation zones at some points.

Individual veinlets of thickness up to 8-10 cm, and brecciation zones 1-1.5-m thick, are also found in the deposit.

The composition of the uranium-containing veinlets includes quartz, calcite and serpentine, pitchblende, coffinite (?), native arsenic and several arsenides and sulfides (Fig. 1). In most cases quartz and calcite are the only really important vein minerals in the ore veinlets. Serpentine is found near the contacts with the diabasic porphyrite dikes, from which magnesium was apparently acquired. The ore textures and age relationships of the different veinlet types indicate three mineralization stages in the deposit's formation. Formation of the sulfide-quartz veinlets to the second stage, and that of arsenic-quartz uranium-containing veinlets to the third one. In this deposit, as in the great majority of hydrothermal deposits of sulfide-uranium formation, the ore stage is also the final one. The diagram of mineral formation sequence (Fig. 1) highlights the extensive occurrence of arsenic-containing minerals in the deposit. Arsenopyrite and fahlerz (Chemical analysis confirmed this as tennantite) were formed in the first and second stages. In addition to these, native arsenic, cobaltite, gersdorffite, nicolite, realgar and orpiment were formed in the ore stage. Native arsenic is the most widely-occurring mineral; very small amounts of nickel and cobalt diarsenides are found (mostly near the diabasic porphyrite dikes).

A very characteristic feature of the ore veinlets is the presence of a constant spatial and paragenetic association of uranium minerals—pitchblende and coffinite (?)—and native arsenic which form co-segregations in fine-grained chalcedony-like quartz and (less frequently) calcite.

Pitchblende occurs most frequently in ore minerals of the third stage. X-ray analysis of three monomineralic specimens showed lattice parameters a_0 of 5.41, 5.42 and 5.43 A respectively. Pitchblende forms two segregation varieties, probably corresponding to different generations.[1]

Pitchblende of the first generation consists of segregations of various shape, dispersed in the quartz, the size varying from thousandths to tenths of a millimeter. In veinlets with the highest uranium contents, fine segregations

[1]In accordance with Betekhtin's definition [1], by "generations" we mean noncontemporary formations of a mineral in the same mineralization stage.

TABLE 1. Interplanar Spacings and Line Strengths of Native Arsenic

From the east-contact deposit		From the west contact deposit		Reference sample No. 32 [3]	
4	6.34	6	6.20	1	6.50
—	—	—	—	7	6.17
3	(3.50)	4	3.42	7	3.45
9	3.17	8	3.15	8	3.14
3	(3.10)	2	2.98	3	2.81
10	2.73	9	2.72	10	2.74
4	2.50	5	2.50	7	2.51
2	2.25	3	2.20	3	2.25
2	2.11	2	2.15	3	2.12
3	2.04	5	2.10	9	2.04
4	1.948	4	1.89	5	1.95
4	1.847	7	1.88	10	1.867
1	1.840	2	1.85	3	1.837
1	1.766	5	1.79	8	1.76
4	1.661	5	1.67	8	1.65
1	1.596	2	1.62	3	1.59
7	1.547	8	1.57	10	1.53
4	1.440	4	1.43	5	1.433
2	1.386	1	1.37	7	1.380
3	1.350	2	1.35	5	1.363
4	1.196	5	1.21	8	1.195

Note. Conditions as follows: BSV tube; unfiltered iron radiation; camera diameter 57.3 mm; diameter of cylindrical sample, 0.6 mm. The line strengths are based on a scale of 10.

TABLE 2. Ultimate Analyses of Organic Matter in Pitchblende

Wt. of sample mg	CO_2	H_2O	S	C	H	S	Ash content	
	mg			%			mg	%
10.350	0,335	0.941	—	0.83	0.87	—	9,570	92,46
10,895	0.302	0.978	—	0.76	0.80	—	10,205	93.66
11,230	0.290	0.882	—	0.71	0.88	—	10.480	93.32
72.88	—	—	0.36	—	—	0.49	—	—
79.01	—	—	0.41	—	—	0.52	—	—
75.94	—	—	0.38	—	—	0.50	—	—

of pitchblende, saturating the quartz, form—in conjuction with native arsenic (or sometimes with coffinite)—a dense impregnation, to which is attributable the black color of the ore quartz veinlets.

Second-generation pitchblende forms thread-like segregations or veinlets of thickness up to 2-2.5 mm, developed in or near the contacts in ore veins containing an impregnation of first generation pitchblende. Second generation pitchblende is also frequently associated with native arsenic. The ratios of these minerals vary over a wide range. Intimate concretions of their finest segregations, as well as individual nodules, are observed in native arsenic incrustations.

Microscopic investigation of specimens in native arsenic surrounded by quartz revealed branching thread-like segregations of a radioactive mineral differing from pitchblende by its lower reflectivity and the shape of the segregations (Fig. 2). The diagnostics of this mineral could not be established satisfactorily because these segregations

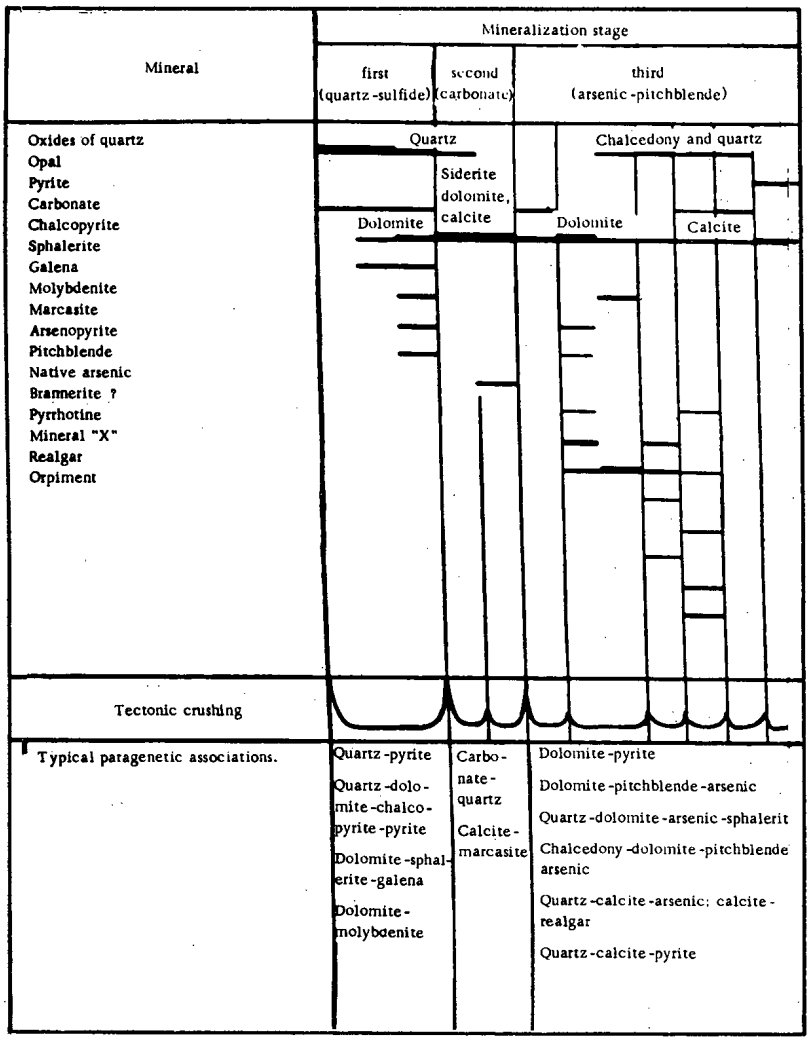

Fig. 3. Mineral formation sequence in the east-exocontact deposit.

were very small. However, from their optical and physical properties they may be attributed to coffinite. These thread-like segregations of coffinite (?) are very similar to those noted by Yu. M. Dymkov [2] in ore deposits of the Erzgebirge.

Like first-generation pitchblende, native arsenic forms very small segregations (frequently barely discernible under the microscope) in quartz, occupies the space between the nodular pitchblende segregations and coffinite (?) threads, and is itself nodular in some places; it forms vein-like segregations in the quartz and incrustation-fringes at the contact of the ore veinlets. Some of these fringes have complex structures: arsenic forms dendrites oriented perpendicular to the contact. In some cases the thickness of the lens-like segregations and veinlets reaches 3-4 mm. Finally, arsenic is also found in pitchblende itself, forming accumulations of nodules a few thousandths of a millimeter in size. Submicroscopic arsenic segregations very probably frequently "saturate" the pitchblende and quartz segregations.

The hardness and reflectivity of the large native arsenic segregations vary, most probably as a result of the different degrees of saturation of arsenic by the smallest pitchblende and coffinite segregations. The arsenic is frequently markedly anisotropic, which enables one to establish the fine-grained structure of its aggregates. Having a cryptocrystalline structure, it is sometimes isotropic.

The powder patterns of native arsenic show all the principal lines of this mineral (Table 1).

Formation of the deposit in amphibolites of the east exocontact zone also took place in three stages (Fig. 3). Sulfide-quartz veins distinguished by the presence of white or grayish-white mixed quartz and pyrite, were formed in

the first stage. The first-stage veins are intersected by carbonate and carbonate-quartz veinlets containing uranium minerals. Veinlets composed of carbonates, the composition of which varies from siderite to calcite, were formed in the second stage. Marcasite fringes are sometimes observed at the selvages of the calcite veinlets.

Veinlets formed in the second stage are associated with the same fractures, but those composed mainly of siderite are earlier formations and are intersected by calcite veinlets (these do not go beyond the siderite veinlets). Spectral analysis showed that siderite and calcite contain the same characteristic elements (admixtures)—arsenic and barium.

Ore veinlets consisting mainly of carbonate and quartz were formed in the third stage. Pitchblende and native arsenic are characteristic and widely occurring ore minerals in the third-stage veinlets, but carbonate-quartz veinlets with symmetrical-banded structure and without ore minerals also belong to this stage.

Third-stage veinlets have a more complex structure than the others, brought about by repeated intrastage movements in which minerals of the early generations were crushed and their fragments cemented by minerals of later generations. At the same time, some minerals were dissolved and redeposited.

Pitchblende is the deposit's principal uranium mineral of practical importance. X-ray analysis revealed a uraninite structure. Chemical analysis showed that its organic matter content is negligible (Table 2). It dissolves in hydrochloric acid, forming a silica gel.

Pitchblende sometimes forms very small segregations in the quartz veinlets. Quartz containing a dense impregnation of pitchblende becomes dark.

In addition to quartz, brown spar, native arsenic and occasionally galena, sphalerite and molybdenite are found in paragenetic association with pitchblende. In brown spar, as in quartz, pitchblende forms a fine dissemination; the ratios between them vary in a wide range. The uranium content in the carbonate veinlets reaches 2%.

Carbonate forms several generations. Late-generation carbonate is segregated together with native arsenic and corrodes the pitchblende. In some places, only relicts of pitchblende (0.01-0.03 mm) are retained in the carbonate veinlets.

Microscopic examination of native arsenic shows a fine-grained structure (sometimes fine polysynthetic twinning). Its diagnostic properties are the same as the reference specimens. Anisotropy is very weak in some segregations. X-ray analysis data of native arsenic are given in Table 1.

Native arsenic has an intimate spatial relationship with pitchblende. Early-generation arsenic is characterized by relatively large segregations; they are sometimes divided by veinlet-like segregations of pitchblende. Late-generation arsenic is segregated together with pitchblende, forming a paragenetic association, both of them being observed as very small modules or plates (some of which require more detailed examination because they resemble coffinite in their main diagnostic properties).

Together with quartz, native arsenic often corrodes fragments of early pyrite grains; reaction fringes of arsenopyrite or realgar, which one might expect to be present as a result of the action of arsenic-containing solutions on pyrite [1], are not observed at the contact of pyrite and native arsenic. It may therefore be supposed that the pyrite-native arsenic association is chemically in equilibrium.

Cleiophane and small amounts of pyrrhotine, chalcopyrite, arsenopyrite and molybdenite are also found in paragenetic assocation with native arsenic.

Our study of the ore composition of deposits, in whose formation uranium- and arsenic-enriched solutions participated, thus reveals the following characteristics.

1. Mineral formation took place in three stages. A study of the mineral complexes and their segregation sequence reveals common features between these deposits and uranium deposits belonging to the uranium sulfide formation.

2. The most important feature of these deposits is the extensive occurrence of a quartz-pitchblende-native arsenic association in the ore stage veinlets. This association may be accompanied by coffinite as well, particularly in ores of deposits located at the west exocontact.

3. The solutions from which pitchblende was deposited had initially a high sulfur concentration; somewhat later and before the end of pitchblende deposition they had a high concentration of sequentially oxidizable arsenic. This is confirmed by the fact that the As^{1-} (in arsenopyrite) arsenical minerals formed were subsequently replaced by As^{0} (in native arsenic) minerals, As^{3+} appearing (in realgar) after the end of pitchblende deposition.

The presence of arsenic-containing minerals like native arsenic and realgar is an indirect indication of the shallow depths at which the deposits were formed. It may therefore be concluded that these minerals and pitchblende were deposited from hydrothermal solutions at low temperatures.

LITERATURE CITED

1. A. G. Betekhtin, In the symp. "Fundamental Problems in the Study of Magmatogenic Ore Deposits" [in Russian], Moscow Izd-vo AN SSSR (1953).
2. Yu. M. Dymkov, Uranium Mineralization of the Erzgebirge [in Russian], Moscow, Atomizdat (1960).
3. V. I. Mikheev, X-Ray Identification of Minerals [in Russian], Moscow, Gosgeoltekhizdat (1957).

METHOD FOR CALCULATING THE RADIOACTIVE IMPURITY CONCENTRATION IN THE WATER AND THE BOTTOM LAYER OF STAGNANT RESERVOIRS

(UDC 621.039.7:628.515)

F. Ya. Rovinskii

Translated from Atomnaya Énergiya, Vol. 18, No. 4,
pp. 379-383, April, 1965
Original article submitted May 17, 1964

The present article is concerned with certain trends in the migration and redistribution of radioactive impurities in stagnant reservoirs after they have been contaminated only once. The capture of the dissolved impurities by the bottom layer occurs as a result of ion-exchange and molecular adsorption processes. On this basis, we derived equations describing the variation in the concentration of radioactive isotopes in dependence on the time of their presence in the water and the bottom layer. The derived equations make it possible to calculate the impurity percentages in the components of stagnant reservoirs.

It was shown in [1] that radioactive isotopes are distributed among the basic reservoir components (the water, the bottom deposits, and the biological mass) in such a manner that the amount of radioactive isotopes in the biological mass can be neglected. Consequently, a stagnant reservoir can be considered as a two-component system.

In order to predict the contamination levels of the water and the bottom deposits, we shall consider a reservoir where the water volume is V m^3, the surface area of the bottom layer is S m^2, while the average depth is small, not exceeding 4-5 m. Such a reservoir, which has the shape of a shallow basin, is characterized by intensive turbulent and convective mixing of the water mass, which leads to the interaction of the entire water mass with the bottom layer [2].

We shall assume that the radioactive impurity was introduced only once in an amount equivalent to A Ci, which initially entered only the water mass in the reservoir, so that this amount was instantaneously distributed throughout the entire volume V. We shall denote by Q(t) the amount (supply) of the radioactive impurity in the water and by P(t) the amount (supply) of the radioactive impurity absorbed by the bottom layer, which vary during the time t. Then, we can use the following initial conditions:

$$t=0, \quad Q_0=A, \quad P_0=0,$$

where Q_0 and P_0 are the initial impurity amounts in the water and the bottom layer, respectively. Since the impurity introduced in the reservoir will be subsequently redistributed only between water and the bottom layer, then, without considering for the moment radioactive decay, we obtain

$$A=Q(t)+P(t). \tag{1}$$

The capture of the dissolved impurity by bottom deposits occurs as a result of ion-exchange and molecular adsorption processes, and, therefore, in the general case, the change in the amount of impurity in the bottom layer (Fig. 1) can be described by the following equation:

$$\frac{dP(t)}{dt}=\mu_1 Q(t)-\mu_2 P(t), \tag{2}$$

where μ_1 and μ_2 are constants determining the sorption and desorption rates, respectively.

With a consideration of the initial conditions and Eq. (1), the solution of Eq. (2) is given by

$$P(t)=\frac{A}{1+\frac{\mu_2}{\mu_1}}\left(1-e^{-\mu_2\left(1+\frac{\mu_1}{\mu_2}\right)t}\right), \tag{3}$$

pes

$$Q(t)=\frac{A}{1+\frac{\mu_2}{\mu_1}}\left(\frac{\mu_2}{\mu_1}+e^{-\mu_2\left(1+\frac{\mu_1}{\mu_2}\right)t}\right). \tag{4}$$

t) and q(t) the mean values of the radioactive impurity's surface density in ration in water:

$$\frac{P(t)}{S}=\frac{A}{S}\cdot\frac{1}{1+\frac{\mu_2}{\mu_1}}\left(1-e^{-\mu_2\left(1+\frac{\mu_1}{\mu_2}\right)t}\right), \tag{5}$$

$$\frac{Q(t)}{V}=\frac{A}{V}\cdot\frac{1}{1+\frac{\mu_2}{\mu_1}}\left(\frac{\mu_2}{\mu_1}+e^{-\mu_2\left(1+\frac{\mu_1}{\mu_2}\right)t}\right). \tag{6}$$

these quantities for $t\to\infty$, we reach the conclusion that, in the course of urity is established between the water and the bottom layer in the reservoir:

$$\mu_1 V\bar{q}=\mu_2 S\bar{p}, \tag{7}$$

where $\bar{q}$ and $\bar{p}$ are the equilibrium concentrations in the water and the bottom layer, respectively.

By using Eqs. (1) and (7) and introducing a correction for the decay, we finally obtain:

$$p(t)=\bar{p}\left(1-e^{-\mu_2\frac{A}{A-p\bar{S}}t}\right)e^{-\lambda t}, \tag{8}$$

$$q(t)=\left(\bar{q}+\frac{A-\bar{q}V}{V}e^{-\mu_2\frac{A}{\bar{q}V}t}\right)e^{-\lambda t}. \tag{9}$$

Consequently, if the values of A, V, and S are known, the prediction of the impurity concentrations in the water and the bottom layer consists in determining $\bar{q}$, $\bar{p}$ and μ_2 (or μ_1).

We shall assume that we know q_1 and q_2—the results of measurements of the volume concentration at the instants of time t_1 and t_2. Then, after eliminating μ_2, we obtain

$$\frac{(q_2-\bar{q})V}{A-\bar{q}V}=\left(\frac{(q_1-\bar{q})V}{A-\bar{q}V}\right)^{t_2/t_1}. \tag{10}$$

TABLE 1. Hydrochemical Composition of the Lake Waters

Reservoir	Composition, mg/liter								
	Na^{+1}	K^{+1}	Mg^{+2}	Ca^{+2}	Cl^{-1}	HCO_3^{-1}	SO_4^{-2}	SiO_2	Total
First	105.3	9.3	56.4	25	57.1	354	125	4.7	759
Second	943	45.6	110.5	8.5	866	1282	127	3	3493

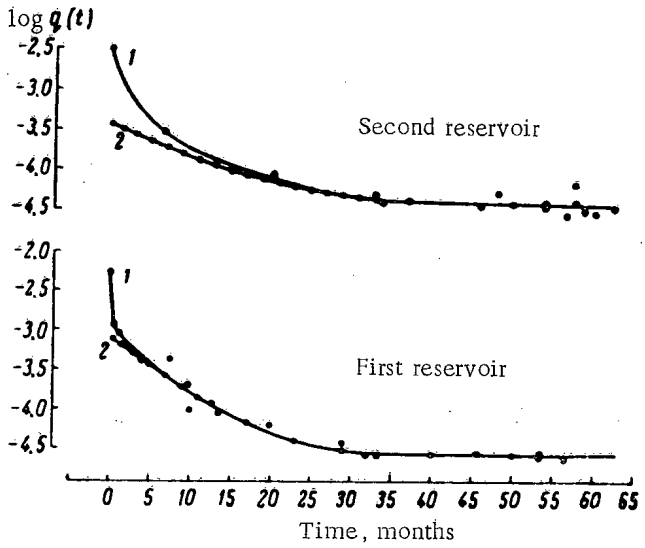

Fig. 2. Comparison between the actual (●) variation (1) of the concentration of isotopes in the water and the calculated (○) curve (2) of Sr^{90} concentration in the waters of the experimental reservoirs.

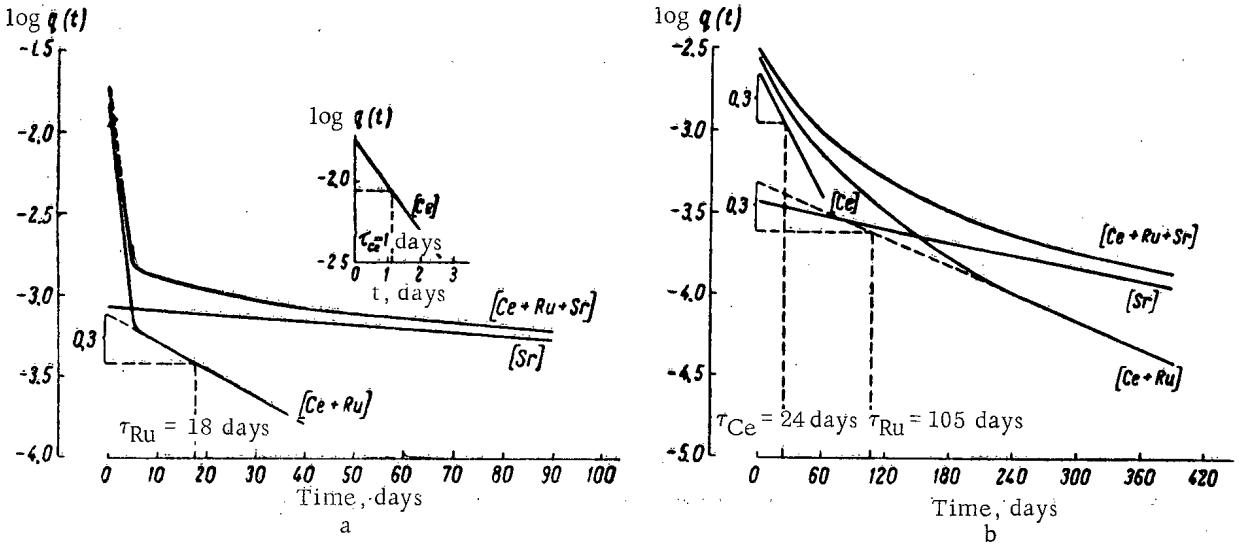

Fig. 3. Determination of the half-life of Ru^{106} and Ce^{144} in the first (a) and the second (b) reservoirs.

It is convenient to express q in explicit form if $\frac{t_2}{t_1} = 2$. In this case,

$$\bar{q} = \frac{Aq_2 - Vq_1^2}{A + Vq_2 - 2Vq_1}, \tag{11}$$

$$\mu_2 = \frac{V(Aq_2 - Vq_1^2)}{At_1(A + Vq_2 - 2Vq_1)} \ln \frac{A - \bar{q}V}{(q_1 - q_2)V}. \tag{12}$$

In practice, it is, of course, advisable to perform more than two measurements of q(t), while the times of measurement should be chosen in the form of terms of a geometric progression with a denominator equal to 2.

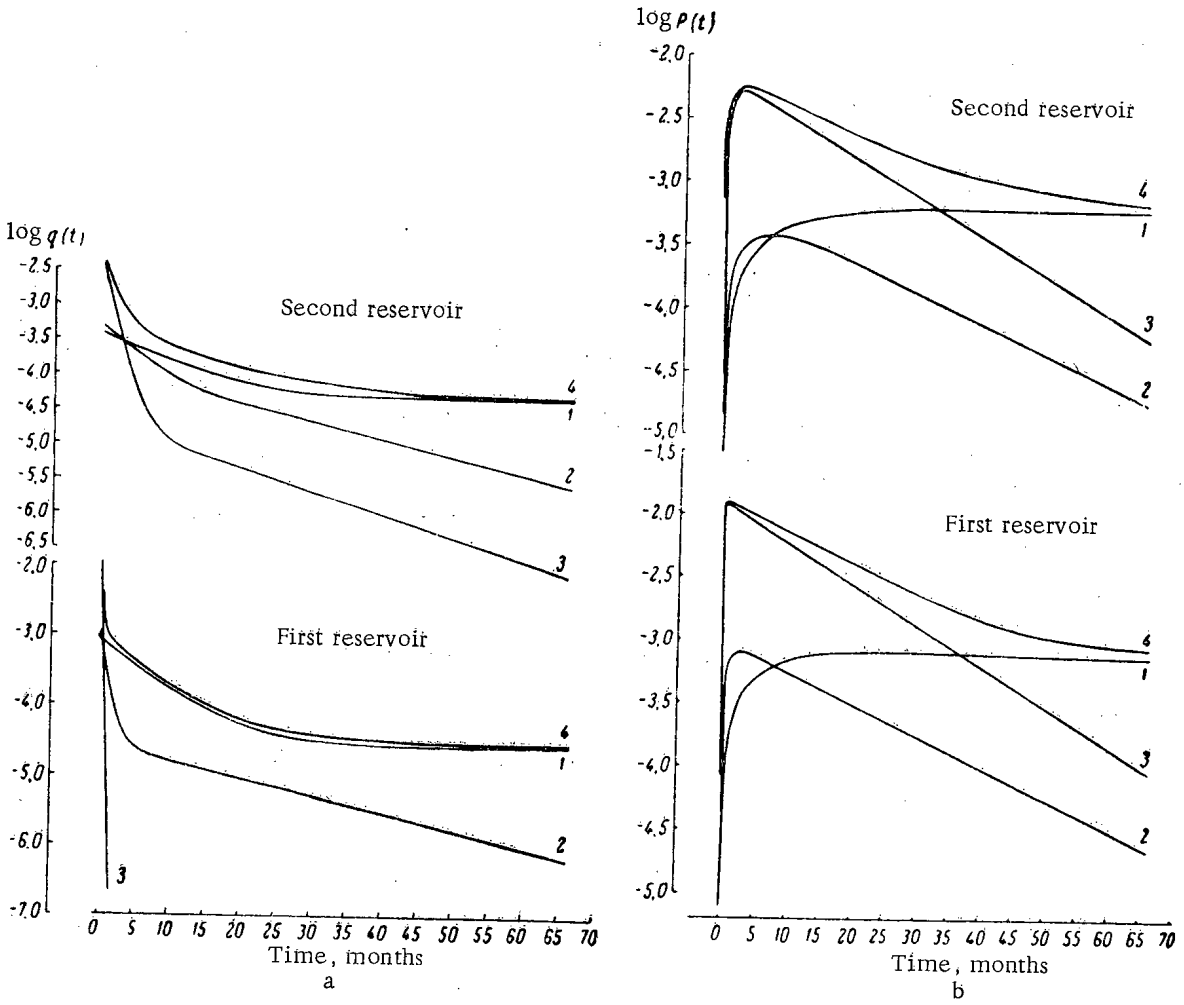

Fig. 4. Calculated concentration curves for radioactive isotopes in water (a) and in the bottom layer (b) of the experimental reservoirs. 1) Sr^{90}; 2) Ru^{106}; 3) Ce^{144}; 4) sum of three isotopes.

Thus, the above scheme of redistribution of the radioactive impurity in a stagnant reservoir makes it possible to calculate the percentages of the radioactive impurity in the reservoir components at any time after a single instance of contamination.

We shall apply the derived equations to the case of artificial contamination of two stagnant reservoirs by a mixture of Sr^{90}, Ru^{106} and Ce^{144} isotopes.

Eutrophic lakes, one with a surface area of 11.3 km^2 (the first reservoir) and the other with a surface area of 4.5 km^2 (the second reservoir), were used for the experiments. The lakes have shallow, saucershaped bottoms. They have large silt deposits, which have completely smoothed out the initial bottom relief. The shores are partially overgrown with reed; there is an abundance of submerged plants: milfoil (Myriophyllum), aquatic plant (Ceratophyllum demersum), and pond weed (Potamogeton). Good conditions for the development of the biological mass prevail in the lakes: the summer temperatures are high, there is a sufficient amount of oxygen and organic matter in the water, the water is well illuminated throughout its depth, etc. The hydrochemical composition of the lake waters is given in Table 1.

The results of the measurements of the concentration of isotopes in the water, which were performed over a period of five years after the isotopes were introduced in the lakes, were made available to us. The total activity of water samples was determined during the first three years, and radiochemical determinations of Sr^{90} were performed during the next two years. The results of these experimental observations are given in Fig. 2.

TABLE 2. Half-Life τ of Some Isotopes in Stagnant Water Reservoirs

Reservoir	Average depth m	τ, days			
		Y^{90}	Ce^{144}	Ru^{106}	Sr^{90}
First	1.0	1.1	1.0	18	116
Second.	1.9	10.9	24	105	180

Moreover, the constants A, V, S, $\bar{q}$, and $\bar{p}$ (besides μ_2) were found experimentally for calculation by means of the derived equations. The μ_2 constant for Sr^{90} was determined by means of Eq. (9), where the q(t) and t values found from curves 1 of Fig. 2 were substituted. It was assumed here that, beginning with the third year after the introduction of radioactive isotopes in the reservoirs, the contribution of Ru^{106} and Ce^{144} to the total activity of water was small in comparison with the contribution of Sr^{90} because of their radioactive decay and adsorption by the bottom layer. This assumption was confirmed by special analyses of the percentages of the above isotopes in the water.

The values of the μ_2 constant for Sr^{90} for the first and the second reservoir were equal to $1.9 \cdot 10^{-4}$ and $3.9 \cdot 10^{-4}$ day^{-1}, respectively.

Then, on the basis of the known constants, the Sr^{90} concentration for the entire period of time was calculated. A comparison between the actual variation of the isotope concentrations in the water and the calculated q(t) curves for Sr^{90} is given in Fig. 2.

The constant μ_2 for a certain isotope is connected with its half-life in water $(\tau)^1$ by the following simple relationship:

$$\mu_2 = 0.693 \frac{\bar{q}V}{A\tau} .$$

The value of τ for Ru^{106} and Ce^{144} for the first and the second reservoirs can be found by the well-known method of graphical analysis of a complex curve. The points on the curves for instants of times sufficiently close to t_0 represent the concentrations of three isotopes, i.e., [Ce + Ru + Sr]. If we subtract the calculated curves 2 from curves 1 (see Fig. 2), the thus obtained difference curves will correspond to the variation in the concentration of two components in the water [Ce + Ru] (Fig. 3a and b). The rectilinear section of the curves [Ce + Ru] corresponds to the variation of [Ru] in time due to migration (since a correction for the decay of Ru^{106} has been introduced here). The slope of this section of the curve can be used for determining the τ value for Ru^{106}.

Furthermore, if we subtract the [Ru] straight line from [Ce + Ru], we can separate the straight line corresponding to changes in the Ce^{144} concentration in water due to migration; the τ value for Ce^{144} can readily be found with respect to the slope of this straight line (see Fig. 3, a and b).

The half-life constitutes the quantitative characteristic of the migration of radioactive isotopes from the water to the bottom layer in stagnant reservoirs.

The Eq. (9) given above consists of two parts: a certain constant $\bar{q}$ and the variable

$$\frac{A-\bar{q}V}{V} e^{-\mu_2 \frac{A}{\bar{q}V} t} = \frac{A-\bar{q}V}{V} e^{-0.693 t/\tau}.$$

It is obvious that τ characterizes the rate at which q(t) tends to $\bar{q}$. The larger the τ value, the slower the rate at which equilibrium between water and the bottom layer is established in the reservoir, and, conversely, the smaller the τ value, the higher the rate at which the equilibrium state is established. Consequently, τ characterizes the equilibrium establishment time, but does not determine the equilibrium concentrations of isotopes in the reservoir.

[1] The term half-life of an isotope in the water of a stagnant reservoir denotes the time interval during which the isotope concentration in the water is reduced by one half solely as a result of isotope migration in the reservoir.

Table 2 provides the τ values for four isotopes, where the τ values for Ce^{144}, Ru^{106} and Sr^{90} were determined with respect to the experimental data given in Fig. 2, while the τ value for Y^{90} was found independently with respect to the shift of radioactive equilibrium between Sr^{90} and Y^{90} [3].

It is obvious from the table that the τ values for Y^{90} and Ce^{144} are close to each other for both reservoirs. This was to be expected, since the above isotopes are chemically similar, and the form of their state in a solution with pH = 7-9 is the same. Therefore, the processes of their absorption by the bottom layer must also be identical. Moreover, it should be mentioned that the τ values for all the radioactive isotopes were larger in the second reservoir than in the smaller first reservoir.

The found τ values make it possible to place the isotopes in order with respect to the rate at which equilibrium is established in the reservoir: rare earths, yttrium > ruthenium > strontium.

Thus, on the basis of the experimental data, we obtained the constants necessary for calculating q(t) and p(t) for Sr^{90}, Ru^{106} and Ce^{144} in two reservoirs by means of the equations derived by approximating a stagnant reservoir by a two-component system. The calculation results are shown in Fig. 4, a and b.

The variation of the total concentration of Sr^{90}, Ru^{106} and Ce^{144} in water (curves 4 in Fig. 4a) is in fairly good agreement with the actual behavior of the concentration of radioactive isotopes obtained by measuring the over-all β-activity of samples (see Fig. 2).

The p(t) curves (see Fig. 4b) have characteristic maximums, the existence of which can also be demonstrated analytically.

Thus, the results obtained in calculating the concentration of radioactive impurities in the water and the bottom layers of stagnant reservoirs are in fairly good agreement with the factual data available to us. The use of the equations derived also made it possible to determine some other characteristics of the behavior of Sr^{90}, Ru^{106} and Ce^{144} in stagnant reservoirs.

LITERATURE CITED

1. A. L. Agre and V. I. Karogodin, Med. Radiologiya, No. 1, 67 (1960).
2. B. B. Bogoslovskii, Limnology [in Russian], Moscow, Izd. MGU (1960), p. 84.
3. G. A. Sereda and F. Ya. Rovinskii, Atomnaya Énergiya, 14, 326 (1963).

RULES FOR DEPOSITING (STORING) ARTICLES

Translated from Atomnaya Énergiya, Vol. 18, No. 4,
p. 383, April, 1965

Articles of interest to a limited number of specialists are deposited either on the authors' request or in accordance with the decision of the Editorial Board of the journal.

Detailed abstracts of the deposited articles will be published in the journal, while the complete articles will be kept for five years at the editor's office and sent COD to readers on request. The volume of the abstracts to be published should not exceed 1/10 author's sheet (about two pages of typewritten text), while the maximum volume of the deposited text should not exceed 1 sheet. On the authors' request, diagrams, tables, the basic equations, etc, can be included in the abstract within the limits of its over-all volume.

An abstract will be published not later than three to four months after the article has been received at the editor's office (if the article is deposited on the authors' request) or after the authors have consented to deposit it (if this decision has been brought by the Editorial Board).

Deposited articles are regarded as scientific publications and are taken into consideration in the defense of dissertations.

The articles submitted for deposition must be suitable for photographic reproduction, and the text, equations, tables, etc., must be clear; the drawings must be made on tracing paper, included in the text and pasted on the paper, and provided with captions.

The price of a single copy of a deposited article is 40 k. In ordering copies of deposited articles, reference must be made to the registration number of the article given at the end of the abstract.

Orders should be mailed to the editorial office of the journal at the following address: 18 Kirov Street, Center, Moscow.

INTENSIVE MUON BEAMS IN THE OIYaI SYNCHROCYCLOTRON (No. 8/3155)

(UDC 621.384.611.1)

Yu. M. Grashin, B. A. Dolgoshein, V. G. Kirillov-Ugryumov,
A. A. Kropin, V. S. Roganov, A. V. Samoilov, and S. V. Somov

Translated from Atomnaya Énergiya, Vol. 18, No. 4,
p. 384, April, 1965
Original article submitted December 7, 1964; abstract submitted February 6, 1965

A strong-focusing channel for intensive muon beams with a low percentage of the pion admixture was put into operation at OIYaI by the end of 1963. The channel, whose aperture has a diameter of 20 cm, consists of 28 quadrupole magnetic lenses and a three-section analyzing magnet.

A negative muon flux of $3 \cdot 10^4$ sec^{-1} over an area of 80 cm^2 with a momentum of 130 $MeV \cdot c^{-1}$ polarization ($70 \pm 20\%$), and a pion admixture of less than 0.4% at the maximum of muon stoppings was obtained from the synchrocyclotron's internal target. Moreover, a negative muon flux of $3.5 \cdot 10^4$ sec^{-1} with a momentum of 280 $MeV \cdot c^{-1}$ was produced.

CONVERSION OF THE 1.5-m CYCLOTRON FOR THE ACCELERATION OF MULTICHARGE IONS (No. 9/3127)

(UDC 621.384.611)

V. V. Batyunya, Pai Fu-Wei, G. N. Vyalov,
B. A. Zager, and A. F. Linev

Translated from Atomnaya Énergiya, Vol. 18, No. 4,
p. 384, April, 1965
Original article submitted November 9, 1964; abstract submitted February 8, 1965

The 1.5-m cyclotron U-150 is designed for accelerating deuterons and α-particles to an energy of 12 MeV per nucleon for a magnetic field strength H = 14.1 kOe.

Investigations of nuclear reactions between complex nuclei constitute the main task of the Nuclear Reactions Laboratory at OIYaI. For the production of the multicharge ions required in experiments, the U-150 cyclotron was converted for operation under conditions where such ions are accelerated for an A/Z ratio equal to 2.6-3.2. Accelerated N_{14}^{+5}, C_{12}^{+4}, O_{16}^{+5}, etc., ions with a sufficiently high intensity at an energy of 6-7 MeV per nucleon were obtained at the terminal radius R = 66 cm as a result of this conversion.

In converting the cyclotron for use under the new operating conditions, it was necessary to increase the maximum wavelength of the hf oscillator from 34 to 40 m. New chamber lids, whereby the gap was reduced from 210 to 180 mm, were made for this purpose. The hf oscillator was modified accordingly.

The magnetic field was adjusted by shimming at a strength of 16.7 kOe. Radial coils were mounted in the external part of the magnet gap for ensuring the optimum field decay. The main effort was directed toward producing an internal beam of C_{12}^{+4} ions with a sufficiently high intensity and bringing it to the terminal radius with a relatively small intensity drop and a satisfactory orbit shape. An internal C_{12}^{+4} beam with a maximum intensity of up to 30 μA was obtained for an orbit center shift and a deviation from the median plane of ± 1 cm. The radial spread of ions on the target at the terminal radius was equal to 5-6 mm. The voltage between the dees was 200-220 kV.

After its formation at the terminal radius, the C_{12}^{+4} beam was extracted from the cyclotron chamber by means of an electrostatic deflector with a nonuniform field. Initially, the deflecting voltage was equal to 70-75 kV. It was then reduced to the minimum value of 35-40 kV by reducing the deflector's radial aperture, increasing the terminal radius by 10-15 mm, and using the optimum angle of ion entrance to the deflector. After subsequent adjustment, the operating deflecting voltage was in the 50-60 kV range. The intensity of the external beam of C_{12}^{+4} ions, focused to an area of 1.5 cm^2, attains 10 μA. The extraction coefficient is equal to 30-40%.

DECREASING THE ENERGY OF BEAMS OF MULTI-CHARGE IONS ON THE 1.5-m CYCLOTRON (No. 7/ 3156)

(UDC 621.384.611)

R. Ts. Oganesyan, G. Indreash, and B. A. Zager

Translated from Atomnaya Énergiya, Vol. 18, No. 4,
p. 385, April, 1965
Original article submitted December 7, 1964; abstract submitted February 3, 1965

The industrially manufactured V-150-1, 1.5-m cyclotron is designed for accelerating light ions (protons, deuterons, and α-particles). Readjustment of the cyclotron for acceleration of multi-charge ions made it possible to accelerate C_{12}^{+4} and N_{14}^{+5} ions to energies of 6 and 7 MeV per nucleon, respectively. The magnetic field was shaped by annular iron shims with H_0 = 16.7 kOe; the drop δH_f at the final radius amounted to 2.2%. The requirement of increased energy necessitated an increase of the magnetic field to H_0 = 17.5 kOe; the drop $\delta H_f'$ at the final radius amounted to 3.4%. It was proposed that the additional drop ($\delta H_f' - \delta H_f$ = 1.2%) be compensated by means of an external annular shim.

Magnetic measurements showed that it was possible by this method to adjust the magnetic field to 17.5 kOe, as required. No decrease in intensity was observed; the energy of the accelerated ions was increased by 10-14% and amounted to ~7 MeV per nucleon for C_{12}^{+4}.

INVESTIGATION OF HOW THE AGING OF Co^{60} RADIOACTIVE IMPURITIES ON St. 3 AFFECTS THE EFFICIENCY OF CHEMICAL AND ULTRASONIC DEACTIVATION METHODS (No. 11/2936)

(UDC 621.039.75)

S. M. Kochergin and S. K. Moiseenko

Translated from Atomnaya Énergiya, Vol. 18, No. 4,
pp. 385-386, April, 1965
Original article submitted May 14, 1964; abstract submitted February 20, 1965

In order to obtain repeatable results, we studied the effect of a number of factors on the degree of Co^{60} contamination of carefully cleaned and degreased specimens. As a measure of the degree of contamination of the materials, we used the coefficient of susceptibility (the ratio of the specific activity of the specimen to the specific activity of the solution, expressed as a percentage). After being contaminated under fixed conditions in solutions with specific activities of 0.2, 0.4, and 0.8 $\mu Ci/cm^3$, the specimens were washed with distilled water and then dried, after which the activity of each side was measured at least twice with a B-2 instrument. The results used were averages of at least four independent measurements.

It was found that the variation of the coefficient of susceptibility of St. 3 and duralumin as a function of the different factors was similar in nature. There is very little contamination of these metals in strongly acid media. The maximum deposit of Co^{60} is observed in almost neutral media, in which the coefficient of susceptibility of St. 3, after 3 h of exposure at 20°C, was 2-5 times as large as the coefficient of susceptibility of duralumin, depending on the specific activity of the solution used. In addition to the production of Co^{60} by an ion exchange mechanism, there was also deposition of Co^{60} in the radiocolloidal form. When the contact time was increased to three days, the repeatability became considerably poorer, owing to "aging" of the solutions and to corrosion processes. Raising the solution temperature to 60°C increased the coefficient of susceptibility by a factor of 1.5, but if repeatable results are desired, the contact time should not exceed 10 min.

Specimens of St. 3 contaminated at 20°C, with exposure times ranging up to 2 h inclusive, were subjected to deactivation at room temperature by an ultrasonic method in a cavitation field (power 1-1.5 W/cm^3, frequency 21-23 kc) and a chemical method (on a shaking apparatus). In individual cases the degree of contamination of the specimens was ten or more times as high as the maximum allowable contamination level of equipment before cleaning [1]. For our deactivation media we used the formulas found most effective [2] for the ultrasonic deactivation of duralumin: 10% H_2SO_4 + 15 g/liter $KMnO_4$; 10% HNO_3; 10% H_2SO_4 + 15 g/liter $K_2Cr_2O_7$. In these solutions a degree of deactivation (percentage of the activity removed) of more than 99.5% was reached after 2.5 min, 3 min, and 5 min, respectively, and the average weight loss in the specimens was 0.5%, 2.5%, and 1%, respectively. It was also shown [2] that when the duralumin contamination time was extended to four days, the ultrasonic treatment time required to attain the same degree of deactivation was 1.5-2 times as long; the weight losses of the specimens became about twice as large.

It was found that when St. 3 was deactivated in the same solutions by the ultrasonic method immediately after contamination, more than 96% of the Co^{60} was transferred to the solution in less than 15 sec. When the specimen was treated in the shaking apparatus, 90% of the Co^{60} was transferred into the solution in 1-1.5 min. In order to reach a degree of deactivation of the order of 99.5%, the total time consumed was 1.5-2 min in the ultrasonic method and 13-20 min in the chemical method, depending on the solutions used.

Aging the impurities on the specimens for four days led to an increase in the proportion of radioactive substances more strongly bound to the surface of the metal, which reduced the efficiency of both methods. In the case of ultrasonic deactivation, the time required was increased by a factor of 2-2.5, and the percentage weight loss of the specimens by a factor of 2.5; in the case of chemical deactivation, the time and the weight loss were increased

by a factor of 1.5-2; Under similar conditions, the time required for treatment on the shaking apparatus was 10 or more times as long as the time required for ultrasonic treatment. The weight losses in nitric acid solutions were 2-3 times as large as in sulfuric acid solutions containing potassium permanganate and potassium dichromate, but the nitric acid solutions compared favorably with the others with regard to their rate of deactivation in chemical treatment. On the basis of the experiments we conducted, we recommend the following as optimum compositions for the deactivation of St. 3 and duralumin: 10% H_2SO_4 + 15 g/liter $KMnO_4$ and 10% H_2SO_4 + 15 g/liter $K_2Cr_2O_7$ for the ultrasonic method; 10% HNO_3 for the chemical method.

LITERATURE CITED

1. Sanitary Rules for Work with Radioactive Substances and Sources of Ionizing Radiation [in Russian], Moscow, Gosatomizdat (1960), p. 68.
2. S. M. Kochergin and S. K. Moiseenko, Determination of effective compositions for the deactivation in an ultrasonic field of duralumin and St. 3 steel contaminated by Co^{60}. Zh. prikl. khim., 38, No. 5 (1965).

SPACE-ENERGY DISTRIBUTION OF NEUTRONS IN AN INFINITE ABSORBING MEDIUM (No. 12/2792)

(UDC 539.121.73:539.125.5)

I. A. Kozachok

Translated from Atomnaya Énergiya, Vol. 18, No. 4,
p. 386, April, 1965
Original article submitted January 4, 1964; abstract submitted March 5, 1965

The article discusses the stationary problem of decelerating the neutrons from a monochromatic point source in an infinite medium with an arbitrary variation of the effective absorption cross-sections as a function of energy. It is assumed that in the center-of-mass system the scattering of the neutrons is isotropic and that its cross section is independent of energy. In order to overcome the well-known difficulties involved in solving such a problem, the problem is formulated in the form of an integral equation whose kernel is the Green's function of the transport equation for neutrons in a medium where absorption is neglected.

The solution of the integral equation for the neutron collision density was found by the method of successive integration. The final results for an isotropic source are of the form

$$\Psi_0(r, u) = G_{00}(r, u)\, p(r, u),$$

$$p(r, u) = \left(1 + 1.5\frac{\beta u B}{R^2}\right)\exp\left[\alpha B\left(\frac{u\beta}{R} - 1\right) - \frac{1}{\xi} I(0, u)\right]$$

$$+ \left(1 - 2.5\frac{\beta u D}{R^2}\right)\frac{\alpha I(0, u)}{\xi(1-\mu)^2 R} \times \exp\left[\alpha D\left(1 - \frac{\beta u}{R}\right)\right] \times \left[1 - \frac{\alpha r^2}{3 l_s^2 R}\left(1 - \frac{\beta u D}{R^2}\right)\right],$$

$$I - (0, u) \equiv \int_0^u du' \frac{l(u')}{l_a(u')}, \quad R \equiv \sqrt{r^2 l_s^{-2} + \beta^2 u^2},$$

where G_{00} is the space-energy distribution of the neutrons in the medium without absorption; α, β, B, and D are parameters (the analytical expressions for these are given in the article); the other symbols are those of the generally accepted notation. By analogy with the well-known solution of the problem of the distribution of neutrons with respect to energy alone, the function p(r, u) may be regarded as the probability that a neutron will avoid capture when it has been decelerated to a lethargy of u at a distance r from the source.

Thus, in the general case, the absorption requires a change not only in the energy distribution of the neutrons, but also in their spatial distribution. The greater the anisotropy of the angular distribution of neutrons in an analogous medium without absorption, the more pronounced will be this redistribution in space.

From an analysis of the resulting formulas and of the numerical calculations performed by means of the formulas for dry silica and for a mixture of silica and water (20% by weight), it was found that p(r, u), the probability of avoiding resonance capture, decreased monotonically as r increased. Consequently, the effect of the decrease in neutron density daused by neutron absorption is more pronounced at large distances from the source than near the source. The dependence on r of the probability of avoiding resonance capture increases with increasing absorption intensity and also with increasing concentration of hydrogen nuclei in the medium (owing to the increased anisotropy of the angular distribution of neutrons). In a "dry" medium this dependence is smoother than in a hydrogenous medium (in the last case it was almost linear). If there is not much absorption, then the depence of p or r in such a medium is weak and may be neglected in a first approximation.

Thus, the solution found in this study differs in principle from the results yielded by the age theory. The main difference is manifested in the marked change of the spatial distribution of the neutrons, owing to neutron capture, which is not taken into account in the age-theory approximation. The age theory is found to be valid in a first approximation only for media with low nitrogen content and relatively weak absorption. The probability of avoiding resonance capture agrees with the known expressions obtained from the solution of problems dealing with the energy spectrum of neutrons integrated over the entire space.

Most chemical elements have the property of intensively absorbing slow neutrons, and this property is utilized in prospecting for certain minerals (for example, boron). The formulas found in this study are suitable for numerical calculations and may be useful in examining questions concerned with the theory of neutron prospecting methods.

REVIEWS OF GENEVA PAPERS

THERMOELECTRIC AND THERMOEMISSIVE CONVERTERS

N. N. Ponomarev-Stepnoi

Translated from Atomnaya Énergiya, Vol. 18, No. 4,
pp. 387-390, April, 1965

The physical principles of methods for the direct conversion of heat energy to electricity have been known for a long time. However, interest in this branch of physics and technology has been intensified only recently, in connection with the development of nuclear energy. This increased interest is due to the great similarity between nuclear heat sources and direct-conversion elements.

Thanks to the absence of moving parts in direct-conversion systems, we may anticipate the possibility of setting up reliable installations with long operating lifetimes; because the converters are compact, it will be possible to build energy-producing units with high power per unit weight and per unit volume, especially in the case where the heat sources are integrated with the conversion elements.

The properties of nuclear heat sources (high energy capacity and high specific power) can be advantageously combined with the properties of direct-conversion systems. The combination of these properties offers good prospects for the use of nuclear power units for the direct conversion of heat energy to electrical energy where there is a need for self-contained, reliable, and compact sources of electrical energy with long operating lifetimes.

Direct-conversion systems, especially those of the thermoemissive and magnetohydrodynamic types, are high-temperature systems, and this offers a possibility of increasing the efficiency of energy-producing units, especially when the direct-conversion elements used have the form of a high-temperature stage in combination with a mechanical converter. Nuclear sources can supply the high temperatures required for direct-conversion systems, offering good prospects for the future use of stationary nuclear installations with direct conversion.

At the Third Geneva Conference the questions of direct energy conversion were discussed at a special sectional meeting, at which the participants listened with great interest to papers[1] devoted to work done in the field of thermoelectric, thermoemissive, and magnetohydrodynamic converters.

THERMOELECTRIC SYSTEMS

(217, 218, 318, 873)[2]

The thermoelectric effect was regarded for a long time as unsuitable for energy production because of its low efficiency of converting heat energy to electrical energy, which was due to the low quality factor $Z = \frac{\alpha^2}{S\lambda}$ of metallic thermocouples (where α is the coefficient of thermoelectromotive force, S is the electrical conductivity, and λ is the thermal conductivity).

The development of semiconductor components, such as Bi_2Te_3, PbTe, SiGe, and others, made it possible to raise the quality factor of the equipment by a factor of several dozen, thus yielding acceptable values of conversion efficiency. Figures 1 and 2 (217) show how the dimensionless parameter ZT varies as a function of temperature for several semiconductor materials with n-type and p-type conductivity. Thermoelectric materials may be divided into three groups with regard to operating temperature: low-temperature materials based on Bi, Pb-based materials for the intermediate temperature range, and high-temperature materials such as the alloy SiGe. Material based on SiGe is promising as a thermoelectric material for high-temperature units, including outer-space systems (218), since it has an operating temperature of over 1000°C, a low vapor pressure at this temperature, and good mechanical properties and makes possible the electrical switching of thermoelements by metallurgical means.

[1] A list of the papers delivered by Soviet scientists was published in Atomnaya Énergiya, Vol. 17, No. 3, p. 235 (1964), and a list of the papers delivered by non-Soviet scientists appeared in Atomnaya Tekhnika Za Rubezhom, No. 9, p. 27 (1964).
[2] The numbers in parentheses are the numbers of the papers.

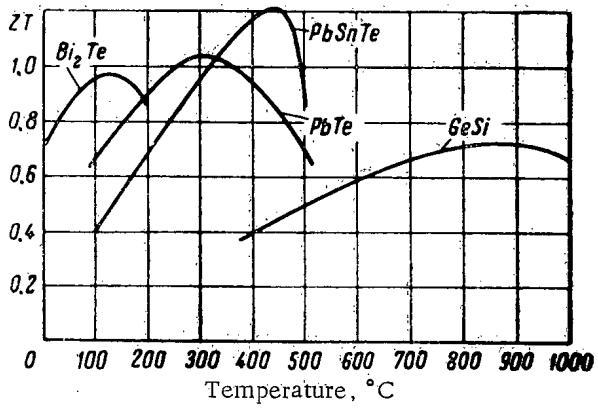

Fig. 1. Characteristics of n-type thermoelectric materials.

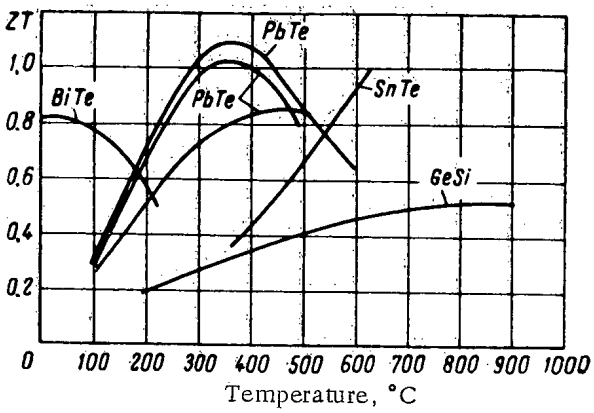

Fig. 2. Characteristics of p-type thermoelectric materials.

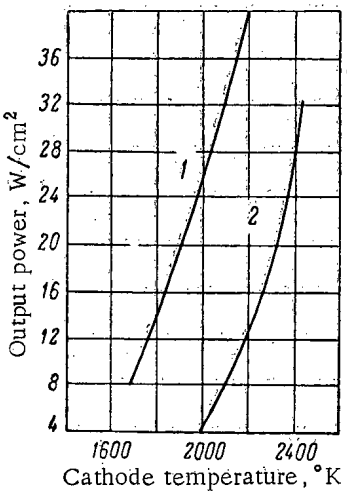

Fig. 3. Converter output power as a function of cathode temperature (for optimum values of cesium pressure and anode temperature): 1) tungsten cathode, nickel anode; 0.13 mm; 2) UC + ZrC cathode, 1.0 mm gap.

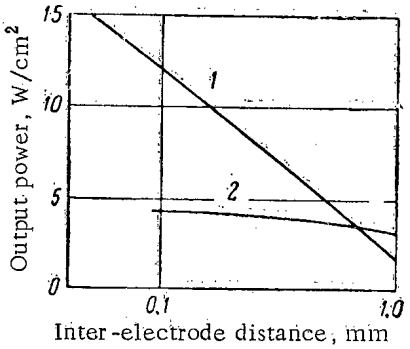

Fig. 4. Converter output power as a function of inter-electrode distance at a cathode temperature of 2100°K and optimum cesium-vapor pressure: 1) tungsten cathode; 2) uranium monocarbide cathode.

Isotopic Sources of Current. A number of electrical generators using thermoelectric converters with radioactive isotopes as their heat source have been developed and are operating at the present time. Soviet scientists reported (318) on two sources of this type. One of these sources uses Po^{210}; the heat source is a flat container (60 × 60 × 13 mm) with five Po^{210} capsules having activity values of 1000-2000 Ci and is surrounded by a battery of SiGe heat converters. The generator was successfully tested for several thousand hours. It had a power of ~ 6 W and an efficiency of ~ 2.4%. The temperature on the hot surface of the converter was 760°C, and the radiator temperature was 230°C. The second type of generator used Ce^{144}, which supplied electrical energy for an automatic radio weather station. It had an electrical power of ~ 5 W. The use of a special storage battery made it possible to increase the power to 150 W. Variations in thermal power were compensated by a special temperature-control system. The generator used solid solutions of $Bi_2Te_3 + Bi_2Se_3$ (n-type) and $Bi_2Te_3 + Sb_2Te_3$ (p-type) for its thermal elements.

Work on the development of isotopic energy sources with thermoelectric converters has been done in the United States (217). Units with electrical power values of 2 W to 60 W have been built and are in operation; the isotopes used are: Sr^{90} Pu^{238}; and Po^{210}. These units are designed to supply electrical energy to weather stations, navigational buoys, and satellites.

The testing of isotopic generators under operational conditions both in the Soviet Union and in the United States has shown that, thanks to their compactness, reliability, self-contained construction, and long operating lifetime, isotopic generators give great promise for use as low-power sources of electrical energy for inaccessible regions of the earth and for outer space.

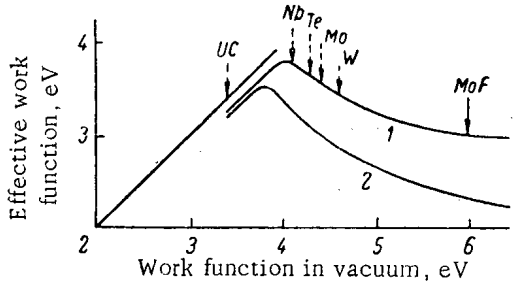

Fig. 5. Comparison of the effective work function in cesium vapor with the work function in a vacuum, at a cathode temperature of 1700°K: 1) cesium-vapor pressure $8 \cdot 10^{-2}$ mm Hg; 2) cesium-vapor pressure 0.8 mm Hg.

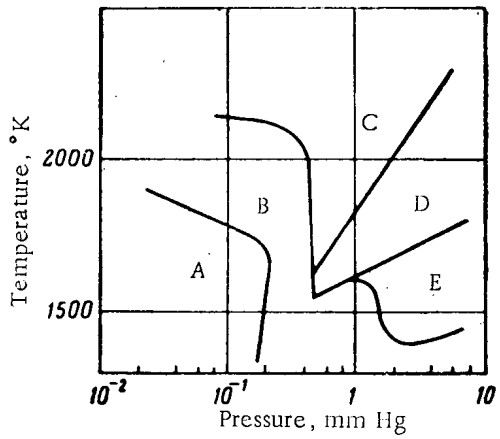

Fig. 6. Experimentally determined boundaries of operating modes of a converter with molybdenum cathode (gap 0.5 mm): A) quasi-vacuum mode; B) diffusion mode; C, D, E) arc modes.

Reactor Schemes. It is possible to obtain high electrical power values in units with thermoelectric generators if a nuclear reactor is used as the heat source. The first operating unit of this type is the Romashka high-temperature reactor-converter (873[3]), which began producing electric current on August 14, 1964. This unit is characterized by a complete absence of moving parts or mechanisms in the energy-conversion process. The heat generated by uranium dicarbide fuel elements is distributed by thermal conductivity and, passing through a beryllium reflector, is transmitted to a thermoelectric converter. A converter with silicon-germanium thermal elements is in contact with the external surface of a radial reflector. The heat in the converter elements is partly converted into electricity. The unutilized portion of the heat is removed by radiation into the environment.

A somewhat different principle of operation is used in the SNAP-10A thermoelectric-converter nuclear power unit, developed in the United States (218). This unit is now in the start-up and adjustment stage. The SNAP-10A unit uses a homogeneous thermal-neutron reactor. The moderator used is zirconium hydride, containing about 10% U^{235} by weight. The heat from the reactor is transmitted by means of a liquid-metal coolant (a eutectic NaK alloy) to the thermoelectric generator and is removed from the cold junctions of the thermoelements by radiation into the environment. Of the two possible materials, PbTe and SiGe, preference was given to SiGe, since it is capable of operating under high-vacuum conditions, while the use of PbTe requires special jacketing of the thermoelements in order to prevent sublimation.

The converter of this system, designed for 500 W, is divided into 120 modules. The heat from the reactor is transmitted by the coolant to the tubular part of the module. Twenty-four cylindrical thermoelements are arranged along each tube; these elements are electrically insulated from the tube by thin disks of aluminum oxide. On the hot side, the elements are connected to copper bus bars, and on the cold side, to aluminum radiation plates. All the interfaces between the tubes and the aluminum plates are metallurgically connected. The elements are designed with low thermal and electrical resistance, which makes it possible to prevent any parasitic heat flows. Each set of three successive modules in the converter is connected into a section. Forty sections are mounted on the surface of a cone frustum, forming parallel coolant loops between the input and output collectors. The 120 modules weigh 60 kg and have a radiating surface of 5.8 m^2. The sections of the converter are electrically connected in a series-parallel circuit, which improves the reliability of converter operation.

In addition to the main converter, the SNAP-10A unit has an auxiliary thermoelectric converter used for feeding a d-c electromagnetic pump. Two parallel PbTe thermocouples short-circuited across the operating part of the pump, supply 700 A of direct current. The heat reaches the thermocouples through the coolant tubing walls, and the unutilized heat is removed by radiation from aluminum radiation ribs. A 2400-gauss magnetic field is provided by a permanent magnet. The overall efficiency of the pump for the head so set up is 1%.

It is expected that when the development work has been completed, the SNAP-10A unit will be launched into outer space, where it will supply 500 W of power for about one year.

[3] This paper was published in Atomnaya Énergiya, Vol. 17, p. 329 (1964).

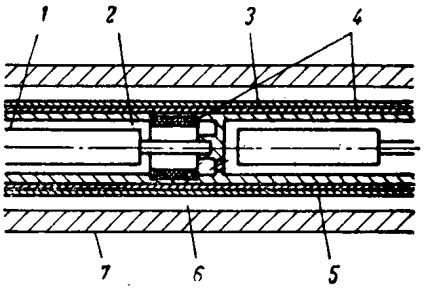

Fig. 7. Schematic diagram of the electricity-generating element of the reactor-converter: 1) heat-generating core with cathode; 2) cesium gap; 3) anode; 4) insulation; 5) niobium tubes; 6) coolant; 7) moderator.

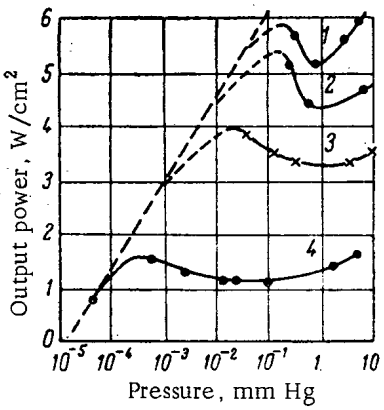

Fig. 8. Variation of the output power of a converter with a cathode made of a solid solution of uranium carbide and zirconium carbide as a function of cesium-vapor pressure, at the following temperatures: 1) 1600°C; 2) 1550°C; 3) 1500°C; 4) 1250°C.

THERMOEMISSIVE CONVERTERS

(44, 132, 219, 317)

The physical foundations of the thermionic emission process are determined by the high operating temperatures of thermoemissive converters. The output power of the converter increases sharply with temperature (Fig. 3) (219). Above 1500°K the specific power of the thermoemissive converter becomes more than 1 W/cm^2, which makes it very promising for use in conjunction with nuclear energy sources.

Earlier studies on thermionic emission were devoted to the investigation of vacuum operation of the converter. The use of this type of operation led to serious design and engineering difficulties, since in order to eliminate the space charge of electrons, the distance between the electrodes had to be reduced to 10 μ. Through the use of cesium vapor to compensate the space charge, it is possible to develop elements with a reasonable inter-electrode distance. Figure 4 (219) shows the variation of the converter output power as a function of the inter-electrode distance at a cathode temperature of 2100°K and optimum cesium vapor pressure.

The presence of cesium in the inter-electrode gap also manifests itself in a reduction of the work function at the cathode and the anode, thereby improving the characteristics of the converter. The effect of cesium on the work functions of various materials, determined theoretically and experimentally, is shown in Fig. 5, which graphically compares the effective work function in cesium vapor with the work function in a vacuum for a number of materials (219). The curves have been plotted for two values of cesium vapor pressure and a constant radiator temperature. A higher value of the work function in a vacuum means that the effective work function in cesium vapor will be lower. The quantitative data for specific materials may differ considerably because of the way these parameters are affected by surface structure, crystal orientation, presence of impurities in the cesium vapor, etc. Thus, for example, the work function of molybdenum in cesium vapor with an admixture of fluorine is 1.36 eV, whereas the value for pure cesium is 1.68 eV.

An analysis of the converter operating modes as a function of cesium vapor pressure yields a theoretical description of the diffusion mode (317). Figure 6 shows the boundaries of operating modes of a converter with a molybdenum cathode, as determined from experimental data.

The development of thermionic elements requires not only physical research but also the elimination of a number of technological difficulties. In particular, rigid requirements must be imposed on the insulating compounds, which must maintain a vacuum seal and a high dielectric strength (up to 1000 V/cm) at temperatures of up to 1000°K. Satisfactory properties were provided up to 900°K by aluminum oxide combined (by means of copper solder) with niobium. Higher temperatures of up to 1400°K require the use of vanadium-based solder or diffusion compounds (219). Figure 7 shows a schematic diagram of a thermoemissive converter (TEC) combined with a fuel element (the electricity-generating element of the reactor-converter). The reactor-converter consists of a cathode enclosing a heat-generating core (in some cases it is possible to use an unjacketed core, for example, a solid solution of uranium carbide and zirconium carbide). The cathode is surrounded by a cylindrical anode, and the gap between the electrodes is filled with cesium vapor. The individual components are connected in series, which increases the output voltage of the converter. The unconverted heat is removed by the coolant flowing past the metallic jacket which contains the series-connected components, separated from the jacket by a layer of electrical insulation.

The operating conditions of the TEC in the reactor aggravate the difficulties resulting from the high temperature of the TEC and create additional difficulties due to the presence of reactor radiation, the effect of fission fragments, and the distribution characteristics of the heat generation.

The accumulation of fission products at high burnout values for the heat-generating core material causes the core to expand. The diffusion of gaseous fission products in the cesium space affects the operating characteristics of the converter. Thus, the fission products whose condensation temperature is higher than the anode temperature will be deposited on the anode and will affect both its work function and its emissivity.

The strong temperature dependence of the electrical characteristics of the TEC makes it necessary to equalize the heat generation in the reactor-converter by redistributing the concentration of fuel or moderator.

Important results for the development of electricity-generating components of a reactor were obtained by investigating TEC specimens in a reactor (317). Tests were conducted on converters with cathodes constructed in various forms: as a rod made of a UC + ZrC solid solution with no jacket and as UO_2 rods in a molybdenum jacket with or without an outer coating of emissive material. Because of the uneven temperature distribution along the cathode, the experimental results were averaged over a range of temperatures. Figure 8 contains typical curves showing how the output power of a converter with a uranium-zirconium carbide solid-solution cathode varies as a function of cesium vapor pressure for different cathode temperatures. Tests conducted in a reactor showed that the TEC characteristics were fairly stable when the inter-electrode space was periodically pumped out. TEC operating lifetimes of several hundred hours were attained in the course of loop tests.

FAST REACTORS

O. D. Kazachkovskii

Translated from Atomnaya Énergiya, Vol. 18, No. 3,
pp. 390-395, April, 1965

One of the Conference sessions was devoted to the physics and technology of fast reactors and 17 reports were heard.[1] In addition, certain questions relating to the problem of fast reactors were discussed by other sections (nuclear fuel and its chemical processing, reactor kinetics, economics. Interesting data concerning the operation of fast reactors was presented by several countries at the scientific-technological exhibition (especially Great Britain, USSR and USA).

Physics of Fast Reactors

At the Conference, in contrast to the two previous ones, problems of measurement procedure (and also of theory) of nuclear-physical parameters used for calculating fast reactors were hardly considered. In certain papers (259 et al.)[2] the present-day level of knowledge of the nuclear-physical constants was assessed from the indications of the principal results obtained in recent years. It was found, in particular, that on the basis of precise experiments carried out the value of the fission cross section of U^{235} (σ_f^5) in the energy range from 50 keV to 1 MeV is given somewhat lower (by 5% in comparison with the values assumed earlier). This implies that other quantities also, for the measurement of which the value of σ_f^5 was used as the reference cross section and above all the fission cross section of other isotopes, should also be reduced correspondingly. The excellent agreement of the measurement results for the quantity $\nu(E)$, obtained in different laboratories and by different methods, testifies to the reliability and the high accuracy of the value of this parameter.

Great progress has been achieved in measurements of one of the most important quantities α, for determining the breeding ratio (the ratio of the radiative capture cross section to the fission cross section) for the principal fissile isotopes. The development of nanosecond techniques and the use of effective scintillation detectors has enabled the knowledge of the parameters of inelastic scattering and the radiative capture cross section σ_c for fast neutrons to be considerably improved. Progress in the range of measurement of σ_c for inactive isotopes is particularly significant, for which the experimental data were previously extremely meager. It should be noted, however, that in certain cases quite a large discrepancy is observed between the measurement data for σ_c in different laboratories; these data fall outside the limits of the prescribed accuracy of the results. The maximum discrepancy (approximately a factor of two) is observed in the region of neutron energies of order tens and hundreds of keV for Au, Ta, In.

Summary tables and graphs of the interaction parameters of neutrons with nuclei, including the most recent refinements, have been presented in several special publications [1-3], which were distributed at the Conference. At the same time, it was pointed out in public addresses that such a form of information storage is becoming cumbersome and obsolete. Increasingly more data are being accumulated everywhere (thousands of points for each isotope) and the use of all the data necessary for calculating reactors is in each case an extremely tedious and time-consuming manual operation. In certain laboratories methods have been developed for storing the appropriate data which are suitable for feeding the data directly into a machine (mainly on punched cards). The necessity was emphasized for creating on an international scale a single unified system for data storage, which would permit quite simple processing of the bulk of data, with adequate operability, and to introduce the incoming changes and refinements. The programs which have been developed enable a system of multigroup constants to be produced on computers, containing among them a very large number (several hundred) of groups. The latter are used for determining in simple geometry the detailed structure of the spectrum of fast reactors.

[1] The list of reports by Soviet scientists is published in Atomnaya Énergiya, 17, No. 3, 235 (1964), and a list of reports by foreign scientists in Atomnoi tekhnike za rubezhom, No. 9, 27 (1964).

[2] The numbers of the reports are shown in parentheses.

TABLE 1. Comparison of Theoretical and Experimental Values of Critical Masses

Index of assembly	Critical mass, kg U^{235}	
	experiment	theory
2 (Great Britain). . . .	416	414
3 (Great Britain). . . .	79.6	61.2
1A (USSR).	76.5	78.2
12 (USSR).	709.4	682
25 (USA)	661.0	581.6
36 (USA)	237.0	242.7

TABLE 2. Comparison of Theoretical and Experimental Values of the Breeding Ratio

Index of assembly	Breeding ratio	
	experiment	theory
1A	1.21 ± 0.15	1.27
6A	1.57	1.40
8	1.07 ± 0.08	1.00
12	1.13 ± 0.07	1.15

In some papers (18, 166, 259, 510) data are reported concerning the reference systems of multigroup constants which are used and which have been prepared by various authors. These systems, in comparison with those used previously, are characterized by an increase in the number of groups (up to 26-33) which occurred principally because of the introduction of additional lower groups. The reference systems provide for calculating the dependence of the group cross sections on the concentration of the corresponding isotope. This effect, which is associated with a homogeneous resonance blocking, appears for heavy nuclei at neutron energies below 25 keV.

Fast reactor calculations were carried out mainly in diffusion and S_n-approximations (166,259,368). Some results of critical mass calculations for large diluted systems and comparison with experiments carried out in critical assemblies are presented in Table 1.

In the majority of cases the calculation permits the critical mass to be predicted with an accuracy of ±5-6%. The neutron distribution density in the active zone and the relationships between the reaction intensities are calculated with approximately the same accuracy. However, the calculated lifetime of neutrons and correspondingly the effect of boron on the reactivity is found to be systematically too low in comparison with the experimental data (according to data from Report 265, by 30%). This indicates nonagreement between calculation and experiment in the very soft region of the neutron spectrum and shows the necessity for further improving the multigroup constants in the last groups. The value of the breeding ratio (more precisely, the conversion factor in the $U^{235}-U^{238}-Pu^{239}$ cycle) has been measured only in experiments carried out by Soviet authors (Table 2).

Relatively more consideration has been given to the calculation of quantities which are essential for studying the kinetics of fast reactors. The fast components of the reactivity power factor have the most important significance, among which the Doppler effect makes the primary contribution because of the presence of soft neutrons in the spectrum. The most progress has been achieved in calculating the Doppler coefficient; in almost all cases which are of interest this coefficient is negative and has a value of the order of $\sim 10^{-5}\Delta k/°C$. It is shown in (41) that by taking account of the partial screening of the U^{235} and Pu^{239} resonances by U^{238} (there is no inverse effect) this leads to intensification of the over-all negative Doppler effect.

Data are presented (41,259,539) concerning the calculation of the sodium reactivity coefficient. For this, the appearance of voids in the active zone is borne in mind, for example, because of effervescence of the sodium, etc. It should be noted that the contribution from thermal expansion of the sodium to the reactivity coefficient is almost negligible and amounts to $\sim 10^{-7}\Delta k/°C$. The effect of sodium loss on the reactivity is determined: a) by a decrease of neutron capture in the sodium itself (a positive but small effect); b) by an increase in the leakage of neutrons from the active zone (a negative effect, but the magnitude depends on the reactor dimensions); c) by an increase in the hardness of the spectrum (usually a positive effect for large reactors, it depends on the energy distribution of the neutron importance). It is shown in (41) that, because of self-blocking of the resonances in U^{238}, it leads to flattening of the importance distribution curve, which reduces considerably the positive component in the sodium coefficient. The calculated total sodium coefficient, even for very large reactors with an active zone volume of 5000 liters which have been studied, remains significantly negative. It is interesting to note that in the Enrico Fermi reactor (311), experimental investigations of the sodium coefficient were carried out in the startup period. For this, standard fuel element assemblies were loaded into the active zone with the sodium at various positions, in which, however, the sodium inlet and outlet ports were sealed hermetically. In accordance with calculation, it was found that the sodium coefficient, even for an assembly located at the center of the reactor, is negative. The data obtained relative to the power and sodium coefficient verify first and foremost the conclusions concerning the internal safety which is inherent with fast reactors and the possibility of ensuring controllable conditions in the event of trouble, even in the case of failure of the control rod and shielding system.

TABLE 3. Critical Test-Rigs

Name of assembly	Site location	Quantity of fissile material used, kg
VEPA	Aldermaston (Great Britain)	100
Qugga	Dounreay (Great Britain)	34
ZEBRA	Winfrith (Great Britain)	400
BFS	Obninsk (USSR)	700
ZPR-III	Idaho (USA)	600
ZPR-VI	Chicago (USA)	600
AETR	California (USA)	100

Estimates have been made of the possible magnitude of the hazard in the case of active zone melting and the formation of a supercritical system (41). It was shown as a result of this that in order to produce a dangerous energy excursion an improbably large rate of increase of reactivity is necessary.

Experiments are described in several papers (166, 265, and 368) on the physics of fast reactors carried out in critical test-rigs and numerous results are given. The operating test-rigs, about which reports were given at the Conference, are shown in Table 3.

Up to now, U^{235} has been used mainly as the fissile material. Table 3 includes only those assemblies which permit diluted active zones of large fast reactors to be simulated. As a rule, active zones with a volume of less than 1000 liters are simulated completely in the assemblies. Larger-scale reactors are studied by means of special inserts at the center of the critical assembly with the same concentration of materials as in the simulated active zone. In the peripheral parts of the assembly in order to achieve criticality, the concentration of fissile material is increased (in certain cases a moderator is introduced). For avoiding too large effects of heterogeneity, materials are used (in the form of small thin plates, etc.) in such a manner that the total number of elements used amounts to tens and hundreds of thousands of pieces. Consequently, the preparation of every assembly usually requires a long time, estimated at many days or weeks.

In addition to projects for determining the critical mass, for studying neutron distributions, etc., precision projects for studying experimentally the Doppler effect and the sodium coefficient effect are at present being carried out or are in the course of preparation on some assemblies.

In addition to the critical test-rigs which have been listed, there is yet another in Switzerland. However, no results of operations with it were presented. Three more new critical test-rigs are being constructed at present in the USA (specially for plutonium), France and the Federal German Republic.

Technology

Data were presented concerning operating trials with four sodium-cooled reactors: the British DFR (130), the Soviet BR-5 (312) and the American EBR-II and Enrico Fermi (207). The BR-5 reactor was started up in January 1959 and in July of the same year it attained its full design rating of 5 MW(th). A description of the operating experience with it has been given in [4].

The DFR was brought to 50% of its power in August 1962 and in July 1963 it attained full design rating of 60 MW(th). The electrical output is 14 MW. Sodium is used as the coolant, with the addition of 30% potassium. The difficulties which were encountered prior to 1962, associated with the entrance of inert gas from the cushions into the coolant and the presence in the loop of large quantities of oxides, were completely overcome. In the last two years all of the plant, including the reactor and the sodium loop equipment, has operated smoothly. The stability, the reliability of operation and the simplicity of maintenance are emphasized. The recharging system has functioned normally. During the whole time of operation the active zone charge has been replaced three times. Owing to the large magnitude of the neutron flux ($2.6 \cdot 10^{15}$ n/cm^2·sec), there are excellent opportunities for irradiation experiments in the reactor. Recently, the active zone was considerably reconstructed in order to provide facilities in it for a large number of samples and experimental fuel elements (for commercial fast reactors), mainly with ceramic fuel. The higher temperature conditions, corresponding to commercial reactors, are ensured by the installation of special cassettes with thermal insulation and by reducing the supply of coolant through them. A special

feature of the normal fuel elements used is the presence of pores in the can and the sodium flow directly "washing" the uranium. As a consequence of this, when operating at high power a large quantity of fission products enter the coolant from the fuel elements. In the nominal regime, the equilibrium activity of the coolant (due mainly to short-lived fission products) exceeds the activity of the Na^{24} by two orders of magnitude. It is shown that removal of fission products from the uranium takes place mainly by diffusion and not by the ejection of recoil nuclei. Owing to the very low pressure in the loop, it is easy to ensure complete containment and there are no traces of fission product activity beyond the bounds of the loop. The uranium itself is completely undissolved in the sodium. (It should be noted that similar results were obtained on the BR-5 reactor for fuel elements with an exposed surface of plutonium oxide.)

The increase in the rate of corrosion of niobium fuel element cans, which had been observed in the initial operation of the DFR, was soon reduced to a safe level. It is assumed that corrosion occurred because of the presence of a small quantity of extraneous impurities in the sodium (probably carbon). As a result of kinetic investigations, a change in magnitude of the reactivity coefficient during the operating period was observed, which was associated with heating up of the fuel. This effect (also observed in the BR-5 reactor) is explained by the change of contact conditions at the boundary between the fuel and the can (as a result of increased coupling) according to the extent of the burnup. Mention was made in the report of an interesting device in operation at Dounreay for observing the commencement of boiling of the sodium by the acoustic spectrum of the noise. This instrument can be useful in the case of a possible (but highly improbable) blocking of the channels carrying the sodium coolant to the various sections of the active zone.

The EBR-II reactor, with a nominal power of 60 MW and the Enrico Fermi reactor, estimated to have a thermal output of 200 MW as a result of operating on the first charge, were started up in mid-1963 and up to now they have operated at low power levels not exceeding hundreds of kW. Startup of both reactors was preceded by a large cycle of operations for eliminating defects which had been observed and which have been described previously.

In the reports presented at the Conference, a brief account of these operations is given. It is pointed out that in the Enrico Fermi reactor the recharging mechanism, which was withdrawn from service because of defective operations, is operating satisfactorily after reassembly. Measures were adopted which will enable recurrences of similar problems to be avoided in future. During the time of operation of the reactor, more than 250 cassettes were loaded into the active zone with the sodium and removed from it by means of the recharging mechanism. On the basis of the experience gained, a conclusion is drawn (207) concerning the advisability, in the future of using simpler equipment with the possibility of observing them visually during operation. The technology of operating with the large quantity of sodium in the loops of both reactors (hundreds of cubic meters) has been mastered quite well and has not given rise to difficulties. It is interesting to note that the sodium was delivered to the site in steel railroad tanks with a capacity of 30 m^3 and it was transferred from them directly into the loops or into overflow tanks. Sodium purification was carried out either by means of the normal equipment in the loops (in cold traps), or by means of successive heating in the loop and cooling (in the overflow tank). As a result of this, the content of oxides in the sodium charge was small. This is demonstrated, for example, by the fact that in the primary loops of the reactors, made from stainless steel, decontamination was accomplished quite rapidly. At the same time, in the secondary loops which were made of low-alloy chromo-molybdenum steel because of the presence of rust, considerably longer operation of the traps was necessary, as a consequence of which the trap was found to be completely blocked (in the EBR-II) and it had to be replaced.

The operating experience on the primary equipment of the sodium loops in the American reactors is generalized (228). The greater part of the equipment functioned successfully. For example, the centrifugal pumps in the Enrico Fermi reactor with a capacity of 2500 m^3/h operated successfully for more than 7000h, including two weeks at a temperature of 540°C. Certain difficulties arose in testing the steam generator of the reactor (at the operating temperature and with sodium circulation, but without power). Thus, in one of the three steam generators corrosion cracking of the tubes was observed at the bends (under stress). The corrosion was caused by inadequate purification from traces of washing solution. In another steam generator, because of the unfortunate mounting of the tubes, an increase of vibration was observed which ultimately led to rupture of one of the tubes. It is characteristic, however, that the entry of water and steam into the sodium which occurred did not lead to any dangerous consequences whatsoever in neither the one case nor the other. An increase in pressure was observed in the gas cushions of the sodium loop because of the release of hydrogen. Oxygen, as is well known, is firmly retained by sodium and there is no danger of creating a detonating mixture. The initial purification of the steam generators from traces of sodium prior to repair was accomplished by washing in alcohol with nitrogen bubbling to accelerate the reaction. The total quantity of sodium removed as a result of this amounted to about 100 kg.

It is pointed out that in welding operations for obtaining a sufficiently high-grade weld, thorough cleansing is necessary of the weld surrounds from traces of sodium, grease and dirt. The welding itself should be carried out in an inert atmosphere.

In further investigations on the American reactors, it is proposed also to emphasize the carrying out of experiments on the irradiation of fuel elements for future power-producing fast reactors.

In the American and British reactors, metallic uranium is used as fuel, alloyed with molybdenum or with a composition of components remaining in the regeneration of fuel by a pyrometallurgical method (Mo, Ru, Rh, Pd, Zr, Nb), i.e., with a fissium alloy. In the DFR reactor, a burnup of 1.8% of the total quantity of heavy atoms is attained in a recent fuel loading (uranium with 20 at.% of molybdenum). It is assumed that burnup towards the end of the run will reach 2.5%. The possibility of achieving high burnups in metallic uranium depends to a considerable degree on the temperature of the latter. In connection with this, for example, it is proposed to operate the Enrico Fermi reactor at a power of 100 MW on the first charge with uranium-molybdenum alloy, i.e., the power is reduced by a factor of two in comparison with the initially intended value. This reduction in power and the corresponding reduction in temperature of the uranium will lead, as it is stated, to an increase of the fuel burnup by a factor of two the operating period is increased by a factor of four, which is considerable according to economical considerations.

It is noted also that a metallic fuel of uranium–plutonium–fissium has better radiation stability than the uranium–fissium fuel. Thus, the outlook for this route is somewhat improved, since a mixture (or alloy) of uranium with plutonium might be used for normal operation of a fast reactor and uranium (enriched) without plutonium can be used only as a first charge. The most promising fuel, from the point of view of achieving deep fuel burnup (and also high operating temperatures) is–as acknowledged everywhere–a ceramic fuel, especially the one most studied –uranium oxide, plutonium oxide and their mixtures. The necessity was stressed in the foreign reports for converting to a fuel of this type at a subsequent stage. In the BR-5 reactor, a ceramic fuel is used (PuO_2) even in the first charge, and the burnup in this fuel up to the present has amounted to more than 6%.

Interesting data on the irradiation in thermal reactors of experimental fuel elements with ceramic fuel for fast reactors were presented at the "General Electric" exhibition. In addition to samples of normal fuel elements, fuel elements were used designed for discharging gaseous fission products into the coolant with a special hydrostatic seal preventing the entrance of sodium inside the fuel element. A burnup of order ~ 100,000 MW · day/t was confidently achieved in all the samples (for sealed as well as open to gas). The discharge of gaseous fission products into the sodium amounted to 45%, whilst the discharge of solid fission products was only a total of 10^{-4}%. In other experiments, fuel elements were used with openings in the can through which sodium was able to penetrate inside. These fuel elements withstood a repeated radiation cycling (with a steep front) without any indications of breakdown whatsoever.

Future Prospects

In the reports of France (41), USA (207), USSR (311), Belgium (516), Federal German Republic (539),and Switzerland (694), data were presented concerning the prospects of operating commercial nuclear power stations with fast reactors, and also the calculated reasons for selecting the type and power of the installations. Assessments of industrial power reactors are also presented in other reports (166, 363). A steady tendency is observed towards the construction of large unit power installations, which will ensure a high economical efficiency for the nuclear power station. For example, USSR, USA and France presented the characteristics of nuclear power stations being designed with a capacity of 1000 MW, whilst the USA reported on four different projects being undertaken by four different firms. In other cases, when there is no certainty that such a large capacity will conform with the conditions of the national power generation system, nuclear power stations with a capacity of 300-500 MW are being considered.

In the majority of cases sodium will be used as coolant in the reactors. The temperature of the sodium on exit from the reactor is 600-650°C, which will enable high efficiencies to be obtained and modern steam power plant to be used. However, in a report presented by the Federal German Republic, three variations are considered for the coolant: sodium, helium and steam. It is proposed to make the choice in 1967, after the appropriate investigations have been carried out. The possible advantage of reactors with gas and steam cooling, according to the opinion of the Federal German Republic, consists in the reduction of the number of loops in comparison with sodium reactors (in sodium reactors three consecutive circuits are specified: sodium, sodium and water). At the same time, it is not immediately clear yet how the difficulties associated with gas-cooling of fast reactors will be successfully overcome, and above all to guarantee their emergency cooling. In the Belgian project the removal of heat from the

reactor by means of steam is being considered (design with an external boiling zone) and in the Swiss project – by means of helium. It is proposed to use ceramic oxide and also carbide nuclear fuel. The power capacity of the active zone is 300-700 kW/liter in the case of using sodium and somewhat lower for gas. The breeding ratio for oxide fuel is 1.5 and for carbide fuel it is 1.6-1.7. The estimates of the economical efficiency of large nuclear power stations with sodium cooling which are given confirm the feasibility of achieving a value of $150/kW for the specific capital costs and a fuel component cost of electrical energy of 0.03-0.07 cent/kWh. The general conclusion points to the fact that fast reactors are attractive in their high efficiency index as well as in their ability to utilize completely all nuclear raw materials.

In the reports and statements presented at the Conference, the great value of power generation by fast reactors was stressed, and the fact that future programs for developing nuclear power generation should be based on these reactors. At the same time, in programs for developing nuclear power generation with fast reactors in the immediate future the situation is different in different countries [5]. Certain countries in which work on fast reactors is to be carried out or is contemplated in the near fugure, including Italy, Japan, Israel etc., have still not formulated their position with regards to this problem. Canada, alone of all countries, has declared its intention not to undertake work as yet on fast reactors.

Before installing types of nuclear power stations with fast reactors, it is proposed in certain countries to build prototype assemblies of intermediate power. Thus, for example, it is proposed to build power-generating fast reactors with a capacity of 200-300 MW(el) in this decade in the USA, in the Federal German Republic and, apparently in Great Britain and with a capacity of 80 MW(el) in France. In the Soviet Union, a nuclear power station with a capacity of 350 MW from a fast reactor is already under construction.

For the complex analysis of the engineering-technological problems, solutions of problems associated with the attainment of high fuel burnups, and for studying the kinetics of fast reactors under conditions of high (600-650°C) temperatures, large power capacities in the active zone (up to 1500 kW/liter), in addition to the various types of test-rigs, special research reactors are at present being constructed. In 1966-1968, it is proposed to bring into operation the following fast reactors: BR-60 with a capacity of 60 MW (USSR), FARRET with a capacity of 40 MW and SeFOR with a capacity of 20 MW (USA) and Rapsodie with a capacity of 20 MW (France). All these reactors will have sodium cooling.

LITERATURE CITED

1. Information Bulletin, Nuclear-physical constants [in Russian], (USSR 1964).
2. ANL-5800, (USA 1963).
3. Nuclear constants for reactor calculations, (Federal German Republic 1962).
4. A. I. Leipunskii et al., Atomnaya Énergiya, 17, 345 (1964).
5. B. B. Baturov and N. M. Sinev, Atomnaya Énergiya, 18, 157 (1965).

CONSTRUCTIONAL METALS AND ALLOYS FOR NUCLEAR REACTORS

A. S. Zaimovskii

Translated from Atomnaya Énergiya, Vol. 18, No. 4, pp. 395-400, April, 1965

The extremely large, if not decisive, influence of constructional materials in the technology of nuclear reactors was reflected in the work of the Conference. In the many papers of review and original content,[1] considerable attention was devoted to the most important materials of the active zone in power reactors: stainless steels, ferritic-pearlitic steels for the reactor body, zirconium and its alloys. Below we present an analysis of the work contributed and draw some conclusions regarding the contemporary state of the question.

Steels and Nickel Alloys

The embrittlement of ferritic-pearlitic and austenitic steels under the influence of neutron bombardment was considered earlier at the Second Geneva Conference. In the last six years, new very important theoretical and experimental data on the hardening and embrittlement of steel components of reactors have accumulated. These data formed the subject of a large number of papers read at the Third Geneva Conference.

New aspects presented to the Conference included information on corrosion cracking of the steel jackets of fuel elements, and the substantial irreversible loss of strength, heat resistance, and ductility in steels and nickel alloys at high temperatures after irradiation at comparatively low temperatures. The accumulation of papers on steels and nickel alloys paints, if not an alarming, at any rate a complex picture regarding the technology of water- and steam-cooled nuclear reactors (water-moderated water-cooled, boiling-water, and other reactors with vessels of stainless steel). In some papers, doubts were expressed regarding the endurance of reactor vessels of ferritic-pearlitic steels at high neutron doses.

A Soviet contribution presented results of a study of the mechanical properties of a number of steels and nickel heat-resistant alloys before and after irradiation, the properties of the irradiated materials being examined over a wide temperature range (339a).[2] Figures 1 and 2 give the results of these tests. We see the considerable fall in the long-term strength of steel 1Kh18N9T and in the ductility of the nickel alloy in the temperature range 500 to 650°C. To this we should add that the residual elongation of commercial nickel irradiated at 150 to 200°C with a dose of $1.7 \cdot 10^{20}$ neutrons/cm^2, as measured in short-term tensile tests, falls to 1 to 3% at 500 to 600°C, instead of rising to 25 to 50% as in nonirradiated nickel.

It was noted in an American contribution, by way of a new and important problem, that embrittlement may be intensified as a result of irradiation at elevated temperatures (242). As generally known, until recently it was considered that the effect of irradiation (for example, of austenitic steels) weakens at high irradiating temperatures. This has proved incorrect. Figure 3 (242) shows the mechanical properties of completely softened austenitic steel 348 (type 18/9 steel stabilized with niobium) at room temperature after irradiation at < 100 and 290°C. We see that the steel irradiated at < 100°C retains residual elongation greater than 30% after a neutron dose of 10^{22} neutrons/cm^2. At the same time steel 348 irradiated at 290°C with a dose of 10^{21} neutrons/cm^2 acquires a yield stress of ~100 kg/mm^2, while the elongation falls to 2 to 5%. Clearly for a slightly larger neutron dose the steel becomes completely brittle. It should be noted, however, that the sharp fall in the elongation values at a neutron dose around 10^{21} neutrons/cm^2 indicates that at a slightly smaller irradiation the steel is still quite ductile.

---

[1] An account of the papers by Soviet scientists was published in "Atomnaya Énergiya 17, No. 3, 235 (1964), and a list of foreign papers in "Atomnaya tekhnika za rubezhom," No. 9, parantheses.

[2] Numbers of contributions shown in 27 (1964).

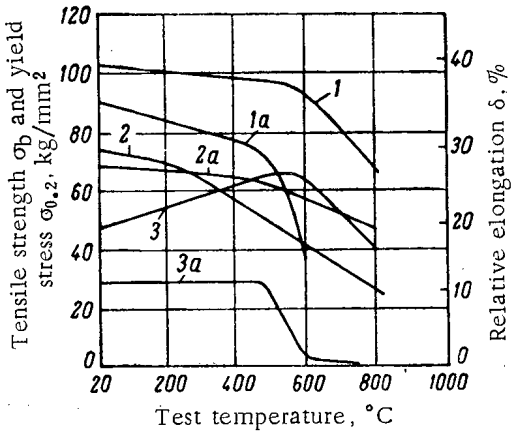

Fig. 1. Mechanical properties of nonirradiated (1, 2, 3) and irradiated (1a, 2a, 3a) heat-resistant nickel alloy KhN77TYuR (20% Cr, 2.5% Ti, 0.8% Al, balance Ni) [radiation dose $(1-3)\cdot 10^{20}$ neutrons/cm^2 at 150-200°C] as functions of test temperature: 1), 1a) tensile strength (σ_b); 2), 2a) yield stress ($\sigma_{0,2}$); 3), 3a) relative elongation (δ).

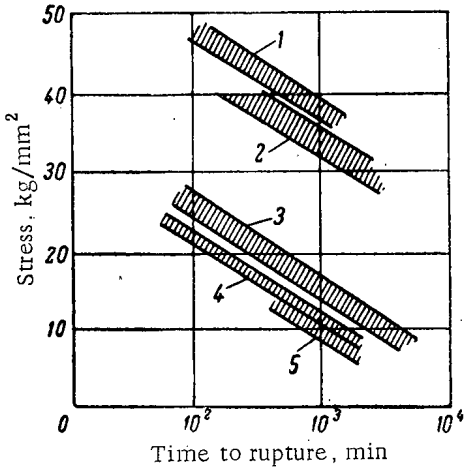

Fig. 2. Long-term strength of 1Kh18N9T steel at temperatures 600 and 700°C: 1) 600°C, nonirradiated; 2) 600°C, irradiated at 450°C by neutron dose $(1-3)\cdot 10^{20}$ neutrons/cm^2; 3) 700°C, nonirradiated; 4) 700°C, irradiated at 450°C by neutron dose $(1-3)\cdot 10^{20}$ neutrons/cm^2; 5) 700°C, irradiated at 550°C by neutron dose $(1-3)\cdot 10^{20}$ neutrons/cm^2.

It is pointed out in the same paper that, in the radiation embrittlement of austentic steels, the role of thermal neutrons is no less, if no more, than that of the fast neutrons. Analysis of the question carried out in Soviet (339a), American (242), and other contributions shows that, apart from the acceleration of diffusion processes caused by the radiation (leading to metal embrittlement by the precipitation of impurities at grain block boundaries of the substructure), the transmutational effect of the irradiation must also be taken into account. Thus (339a) indicates two nuclear reactions leading to the appearance of a gas phase in the steel: $B^{10}(n, \alpha)Li^7 \rightarrow$ helium and $Ni^{58}(n, p)Co^{58} \rightarrow$ hydrogen.

For high burnups, the neutron dose received by the fuel-element jackets may prove sufficiently high for the gases diffusing to grain boundaries to form gas cavities, bubbles, etc., and produce embrittlement. In operating conditions, the fuel-element jackets undergo strain (pressure of fission gases, swelling of fuel under the action of "solid" fission fragments), and are washed on the outside by a heat carrier capable of producing corrosion failure, for instance corrosion cracking under stress. Hence radiation embrittlement is extremely dangerous, and it is the responsibility of the constructor to take careful account of the whole array of operating factors affecting the life of the fuel elements.

An analysis is given of the behavior of fuel elements in power reactors of the water-moderated water-cooled and boiling-water types (255). Out of 700 fuel elements (tablets of uranium dioxide in tubes made of steel 304) irradiated in the Valesitos boiling-water reactor at 320°C on the surface, 22 went out of order as a result of corrosion cracking of the jackets under stress. The causes of these accidents were: high tensile stresses, and residual stresses from the cold work involved in giving the tubes their final dimensions. At the same time, the jackets of the same type of dioxide fuel element in the "Yanki" reactor (water-moderated water-cooled) made of completely softened steel 348 retained their good appearance at the end of the run, and not a single fuel element went out of order. Internal-pressure rupture tests of the jackets of fuel elements so treated showed a residual elongation of 18% with respect to diameter, i.e., the steel was fairly ductile after a burnup of 18,300 (MW·day)/m. Comparison of these results with the curves in Fig. 3 leads to the conclusion that the whole neutron flux in the jackets of the "Yanki" reactor did not exceed $5-6\cdot 10^{20}$ neutrons/cm^2.

Thus we may agree with the authors of many papers in concluding that, for successful use of fuel elements with steel jackets we must as far as possible eliminate stress from the latter, since over practically the whole range of working temperatures for the surfaces of fuel elements in power reactors (i.e., between 300-700°C) the ductility and long-term strength of steel is greatly reduced, the more so, the longer the run.

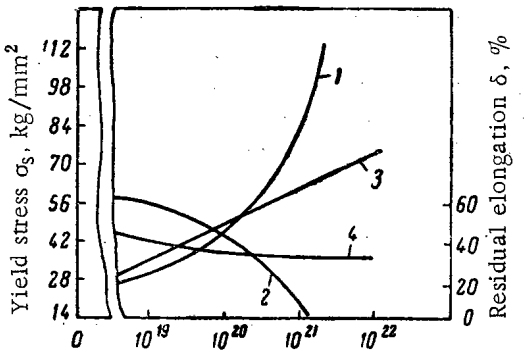

Fig. 3. Effect of irradiating completely softened steel 348 on the mechanical properties at room temperature: 1) yield stress (σ_s), irradiation at 290°C; 2) residual elongation (δ, %), irradiation at 290°C; 3) yield stress (σ_s), irradiation at < 100°C; 4) residual elongation (δ, %), irradiation at < 100°C.

It is not easy, however, to eliminate stress from the jackets, and the development of new materials more stable as fuel-element jackets than stainless steel is called for. It appears from an American contribution (243) that, from the corrosion point of view, high-nickel steels and alloys (Inconel-600, Incoloy-800, etc.) have preference over austenitic steels with 10-20% nickel and 15-20% chromium; high-nickel materials are not subject to corrosion cracking under stress. There has not yet, however, been a serious attempt to use these alloys in reactors.

A Soviet contribution contains results of studying the tendency of ferritic-pearlitic steels intended for the vessels of reactors toward embrittlement under irradiation (339). Detailed information is given on the yield point, residual elongation at rupture, and cold-shortness threshold (for impact strength) as functions of neutron dose and temperature of irradiation. It appears from these data that (in contrast to austenitic steels) the embrittlement is the less, the higher the irradiation temperature, and raising the test temperature to 350-450°C practically removes the embrittlement, i.e., there is a recovery of ductility. Theoretical analysis of the role of thermal and fast neutrons and comparison of calculated and experimental data leads the authors to the conclusion that the neutron spectrum has a considerable influence on the degree of embrittlement.

Some interesting data are given (242) regarding the effect of the annealing time at 315°C on the position of the cold-shortness threshold of low-carbon boiler steel irradiated at 150°C with a dose of $1.3 \cdot 10^{19}$ neutrons/cm^2 (in all, the irradiation shifted the cold-shortness threshold by +110°C). It transpired that annealing for 65 h shifted the threshold almost back to its original value, but an extension of the annealing to 168 h again resulted in embrittlement. This result, together with data on the effect of the method of killing (deoxidizing) steel with aluminum or silicon, the effect of structure, alloying, etc., leads to the conclusion that, after submitting steel samples to a whole cycle of metallurgical and radiation tests, one can with more or less accuracy predict the reliability of a particular steel in operation. Here we must bear in mind that high-grade ferritic-pearlitic steels only receive a dangerous neutron dose after extremely prolonged operation (of the order of 10 years or more).

Soviet (343) and American (244) contributions also present results of systematic studies of the behavior of construction materials in molten metals. The mechanism of the corrosive action of molten metals, the effect of the composition of the constructional metals, and most of all that of the content of oxygen and other harmful impurities in molten metals on corrosion and mass transfer are considered. The high stability of molybdenum at temperatures up to 900°C in molten sodium containing up to 0.01% oxygen is indicated. Steels operating in molten lithium fail as a result of interaction between the lithium and carbides, oxides, sulfides, and other nonmetallic phases.

The accumulation of information contained in these papers enables the reactor constructor to make a correct choice of materials and to effect the necessary purification of the heat carriers so as to ensure reliable operation of the fuel-element jackets.

Zirconium and its Alloys

Back at the time of the Second Geneva Conference, in 1958, scientists of many countries had noted that zirconium and its alloys absorbed hydrogen in the course of the corrosive action of high-temperature water and steam. Precipitating at grain boundaries and inside grains in the form of a hydride phase, the hydrogen causes embrittlement; taken together with radiation embrittlement, this casts doubt on the suitability of zirconium for power reactors with a water heat carrier. This circumstance gave rise to a wide study of the corrosion and hydrogen embrittlement of zirconium and its alloys. At the same time, the economically necessitated tendency toward increased working temperature of the fuel elements and heat carriers presented scientists with the problem of discovering new zirconium alloys of increased heat resistance with satisfactory anticorrosion properties. Almost all the papers on zirconium were devoted to these two problems.

In paper 342, there are some results on the structure and mechanical properties of alloys developed in the USSR and containing 1 and 2.5% Nb, after submitting to hydrogen absorption and subsequent irradiation (342). Special experiments were made to determine the variation in the mechanical properties and structure of these alloys with the tensile stress during 1000 h corrosion tests in 400°C steam. Also studied were jackets made of an alloy of zirconium with 1% Nb taken from fuel elements operated in a reactor to a burnup of 45,000 (MW · day)/m (total flux $5.3 \cdot 10^{20}$ neutrons/cm^2, water temperature 300-350°C). The general conclusions are as follows:

1) the hydride precipitates are oriented in a definite fashion in the structure of the alloys containing 1 and 2.5% Nb, depending on the magnitude and direction of the tensile stresses;

2) the alloys containing 1 and 2.5% Nb have high operational reliability in water-moderated water-cooled power reactors;

3) the frequently-observed unsatisfactory behavior of zirconium alloys is to be explained by insufficient allowance having been made for the part played by stresses in the corrosion and hydrogen-absorption processes. This factor should strictly be allowed for in designing reactor components made of zirconium and its alloys for water-moderated water-cooled, boiling-water, and other reactors with water heat carriers.

In another Soviet contribution the mechanism of zirconium corrosion was studied in connection with the role of carbon, nitrogen, and alloying elements (341). The authors, using the radioisotopes C^{14}, Ni^{63}, and Fe^{59}, established that, during the corrosion process, carbon left the oxide film in the form of gaseous oxides. This problem may be weakened by introducing the alloying elements Sn, Nb, Fe, and Ni into the zirconium. The authors established a connection between the nitrogen content in the zirconium and the form of the hydride distribution in the structure: the lower the nitrogen content, the more favorable the distribution of the hydrides, which disposed themselves in the form of individual zones.

Canadian scientists presented two papers. One was devoted to the behavior of Zircaloy-2 under irradiation (21), and the other to the development of zirconium-niobium alloys (22). It should be noted that not only Canadian contributions, but also others from Great Britain, Sweden, and the Federal German Republic were devoted to studying alloys with 2-2.5% Nb. This undoubtedly bears witness to the great success of Soviet scientists: zirconium-niobium alloys were discovered and studied in the USSR before the Second Geneva Conference, at which R. S. Ambartsumyan et al., presented a circumstantial contribution on zirconium alloys containing 1, 2.5%, and higher amounts of niobium.

The Canadian paper gave detailed data on the behavior of Zircaloy-2 in thick-walled high-pressure pipe-channels and fuel-element jackets in the NPD and CANDU reactors. The authors studied the effect of hydrogen absorption and irradiation on the following properties: creep under irradiation, effect of irradiation on corrosion at temperatures in the range 250-300°C. The pipes proved to be practically unaltered after a year's service: the fuel-element jackets, the hydrogen content of which, after a 10,000 (MW · day)/m burnup, reached 0.04%, also appeared undamaged, and the change in dimensions was insignificant. An acceleration of creep occurred in Zircaloy-2 under irradiation, and the effects of hydrogen absorption and irradiation on impact strength were additive. Noting the importance of the directional precipitation of hydride lamellas in the structure under the influence of stresses, the authors established a connection between the absorption of hydrogen and the oxygen content of the heat carrier. They considered that irradiation could even retard the absorption of hydrogen on account of the formation of an oxidizing agent in the heat carrier, binding the hydrogen of the corrosion reaction.

Another Canadian paper (22) is interesting because it gives results of systematic studies of zirconium alloys containing 2.5% Nb and 2.5% Nb + 0.5% Cu as compared with Zircaloy-2. Study of the conditions of heat treatment of the alloys showed that quenching from 880 and 1000°C with subsequent aging at 400-535°C gave 2.5% Nb and 2.5% Nb + 0.5% Cu alloys with extremely high mechanical properties both before and after radiation doses of 10^{21} neutrons/cm^2; at 300°C the yield point was 75-85 kg/mm^2 with an elongation of 5-10%. At 300°C, the niobium-containing alloys were 50% stronger than Zircaloy-2 for the same ductility. The creep resistance of these alloys was also 50% higher, and they also had a higher impact strength and lower radiation embrittlement than Zircaloy-2. Cold working between quenching and aging improved the anticorrosion properties of the zirconium-niobium alloys in water and carbon dioxide. In order of diminishing corrosion resistance in water and steam at 316-400°C, the three alloys lie in the following sequence: Zr + 2.5% Nb + 0.5% Cu, Zircaloy-2, Zr + 2.5% Nb. At 300°C, however, even this last alloy after 30 years operation (according to calculations) will only corrode 0.1 mm of the wall thickness. At the present time new niobium-containing alloys are being tested in Canada in the CANDU reactor in the form of spacers and high-pressure pipe-channels.

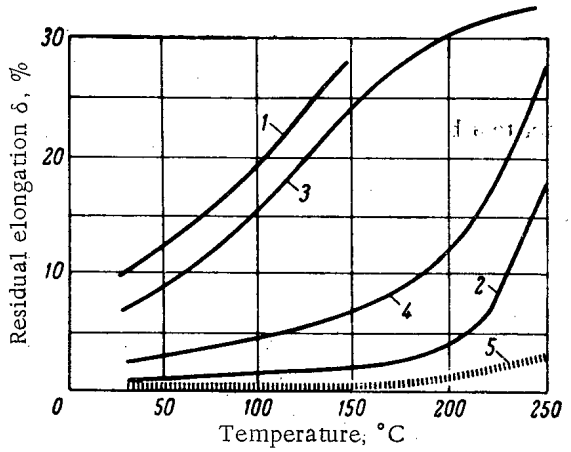

Fig. 4. Residual elongation of beryllium and beryllium-0.4% calcium alloy (extruded from an ingot) at various temperatures. 1) Residual elongation (longitudinal), unalloyed beryllium; 2) residual elongation (tangential), unalloyed beryllium; 3) residual elongation (longitudinal), Be-0.4% Ca alloy; 4) residual elongation (tangential), Be-0.4% Ca alloy; 5) residual elongation for metal-powder electrolytic beryllium.

Zircaloy-2 and an alloy containing 2.5% Nb were also considered and compared in a British contribution (158). The latter alloy has the higher strength and promises to be more reliable in pipe-channels, with a 20-30-year period of service. The corrosion properties of the two alloys are studied, together with their creep and the effect of irradiation on the mechanical properties of samples respectively annealed and cold-worked to a high strength. The British scientists regard the advantages of the stronger alloy containing 2.5% Nb as obvious, but for final selection of a zirconium alloy for pipe-channels and fuel-element jackets further study is required.

A Swedish contribution was devoted mainly to considering the corrosion mechanism of zirconium and the formation of the hydride phase (419). Results of ordinary "rapid" failure tests are compared with those of "slow" tests. For slow tests, the ductility appears to be 30-50% lower, and the sample in question shows a typical brittle fracture. The authors link this feature of zirconium and its alloys with hydrogen embrittlement. By analog with the embrittlement of titanium, the authors consider that the precipitation of the hydride in zirconium is a result of working. Embrittlement will take place when the rate of working is small enough for the hydrogen to be able to diffuse to the precipitation sites, but when the stresses are great enough to produce hydrogen enrichment beyond the solubility limit of the hydride. It is proposed to study and compare an alloy containing 2.5% Nb with Zircaloy-2 for the fuel-element jackets and channels of the R-3 (Agesta) and R-4 (Marviken) reactors. Zircaloy-2 and zirconium-niobium alloys are also compared in a contribution from the Federal German Republic (477). The authors regard a ternary alloy of zirconium with 3% Nb and 1% Sn as most interesting. In the authors' opinion, this alloy has an incontestable advantage over Zircaloy-2 up to 450°C. An interesting aspect of this paper is the improvement of the zirconium-niobium phase diagram and the effect of tin and other alloying elements, and also oxygen, on the solubility boundaries of the β-phases of zirconium and niobium in the α- and β-solutions. In this connection the dependence of the alloy properties on the conditions of heat treatment is also indicated.

A review paper summarizes the uses of Zircaloy-2 fuel-element jackets and concludes (225) that, for operating in water at 300°C, one may count on an accident-free period of service up to 30,000 h fuel-element power 31 W/cm^2, number of fissions $2.2 \cdot 10^{21}$ in 1 cm^3). The anisotropy in the properties of Zircaloy-2 tubes and the role of stresses in the use of fuel-element jackets are discussed. Some new processes in manufacturing zirconium components are of interest: welding spacer wires on to tubes, extruding fin-tubes, joining Zircaloy-2 to steel by simultaneous pressing, etc. It is concluded that zirconium serves equally well with steel as a main constructional material for fuel-element jackets and other components in the active zone of water- and steam-cooled power reactors. One must agree with this conclusion, since it devolves from all the papers presented as well as articles published in journals. A second important outcome is confirmation of the fact that the zirconium alloys containing 2-3% niobium (in some cases further alloyed with copper or tin) developed by Soviet scientists have spread to a number of other countries. Heat treatment of such alloys improves their properties, and this has an important bearing on the duration of service at temperatures up to 400-500°C.

Beryllium

The use of beryllium in nuclear power systems, especially in the form of moderator and reflector components, has become so generally accepted that the only remaining problem in this sphere is the high cost of beryllium. Examples of the use of beryllium are given in a Soviet contribution, which describes the technology of preparing beryllium reflectors for the experimental VVR-M and MR reactors (351). These and similar components are made by hot-pressing beryllium powder, purified by vacuum distillation, in vacuum. For pressing such components (not subject to high-strength requirements), powder with maximum grain size 500 μ is used. The tensile strength of hot-pressed components of this powder at 20°C is 15-17 kg/mm^2. For stronger components, powder with maximum grain size 50 μ is used. In this case the tensile strength reaches 26-27 kg/mm^2.

In the United States there is no great use of beryllium moderators (254). The authors of this paper do not indicate the reasons for the limitations on the use of beryllium.

The question of using beryllium as a material for fuel-element jackets was studied in a French paper (101). The possibility of providing the EL-4 reactor with fuel-element jackets in the form of beryllium tubes 13-15 mm in diameter is discussed. The fuel elements in this reactor are cooled by carbon dioxide, the jacket temperature being 600°C. It was primarily established that at 600°C the creep rate was very high, in view of which beryllium jackets could not operate as rigid components sustaining the pressure of the heat carrier, but could only cover a hard core acting as the bearing part of the whole fuel element. Furthermore, calculation and direct experiments showed that on heating and cooling the fuel elements from 20 to 650°C and back to 20°C a 0.4-mm strain developed in the jacket. Hence a beryllium jacket must ensure (with a margin of 0.4 mm) an elongation $\geq 1\%$ without rupture. In connection with this modest ductility requirement the authors present results on the deformability of beryllium and the ductile properties of extruded tubes. The authors' conclusion are:

1) the use of superhigh-purity beryllium cannot solve the problem, since together with a rise in ductility for slip in the basal plane the over-all anisotropy of the ductility of beryllium crystallites rises sharply;

2) extrusion of tubes with large stretch (up to 100) from metalloceramic billets leads to high ductility in the direction along the tube, but zero transverse ductility. Better results are obtained with a stretch not exceeding 10, and preliminary pressurizing before extrusion further improves the transverse ductility. Even in this case, however, the ductility is too low for safe use of the jackets. It is an important point that the main cause of the low transverse ductility arises from oxide inclusions which stretch out along the axis of the tube in the form of films, preventing transverse tangential strain from taking place without rupture;

3) in view of what has just been said, the authors consider metalloceramic beryllium, which contains a great deal of oxide, as less suitable than cast beryllium. Tubes were made from cast billets in the hot condition by high-pressure extrusion with stretch 90. After recrystallization annealing for fine grain, the tubes had a high longitudinal ductility with a fair transverse (tangential) ductility (around 1-2%), which satisfied operational requirements (see above). The addition of 0.4% calcium further improved the properties of the tubes, also giving a high corrosion resistance to beryllium in damp carbon dioxide up to 700°C. Figure 4 shows the temperature dependence of ductility (elongation at rupture) of beryllium and beryllium-0.4% calcium alloy samples extruded from cast billets and annealed. Thus the authors have set the course for solving the problem of making beryllium jackets for the fuel-elements of the EL-4 reactor, namely, high-pressure extrusion with high stretch and recrystallization annealing for fine grain. For a final solution of the question, however, the durability of beryllium tubes irradiated by the required integral neutron fluxes must be studied.

This latter question is briefly considered in an American review paper (255). It is pointed out that in the United States interest in beryllium fuel-element jackets has fallen off, owing to phenomena arising from the reactions (n, α) and (n, 2n). Swelling due to the accumulation of helium in the beryllium is by itself not large at temperatures below 700°C, but the authors note a sharp fall in ductility as a result of irradiation at 430°C with integral fast-neutron fluxes of 10^{21} neutrons/cm^2. Thus, after irradiation, the relative elongation at 25°C became zero instead of 3%, at 200°C it was 5% instead of 35%, and at 600°C it was 5% instead of 17%. The tensile strength after irradiation almost doubled, this taking place for all test temperatures from 20 to 600°C.

A Japanese paper (799) was also devoted to beryllium. The data presented on the strength and ductility of beryllium hot-pressed from electrolytic-beryllium powder did not differ from earlier-published American, British, and other data. A feature of the work was the manner of preparing the powder: the electrolytic beryllium was melted and converted into powder with spheroidal particles by a pulverizing method. The detailed technology of this method was not given in the paper.

The conference papers confirmed the poor prospects of using beryllium as material for fuel-element jackets in gas-cooled reactors, in view of the very low ductility of beryllium in the original and especially in the irradiated state. This, however, does not relate to beryllium moderators and reflectors working below 700°C, when the radiation swelling is negligible and the mechanical properties not very important.

Aluminum, Magnesium, High-Meling-Point Metals

Intensive investigations into the corrosion resistance of aluminum and its alloys in high-temperature water conducted between the Second and Third Conferences has not led so far to any decisive improvements. From a

Norwegian contribution (591) we see that it is difficult to choose between three alloys: 1% Ni + 12% Si + 1% Mg + 0.3% Fe (IFA-3); 1% Ni + 0.2% Si + 0.3% Fe (X 8001); 1% Ni + 0.02% Si + 0.5% Fe (M-388).

As regards corrosion resistance in superheated water at 230-315°C, the alloys are similar, but IFA-3, hardened by 1% Mg and 12% Si, is clearly preferable as regards mechanical properties. Imminent large-reactor tests should decide the possibility of employing aluminum alloys in power reactors.

Soviet (340) and British (146) papers give some data on the further development and improvement of magnesium alloys for fuel-element jackets cooled by carbon dioxide. The general conclusion from these contributions reduces to the fact that magnesium-alloy fuel-element jackets may be used in carbon-dioxide-cooled reactors for jacket temperatures up to 500-550°C.

On the application of the high-melting metals Mo, W, Nb, and Ta, there were no special contributions to the Conference. It was only indicated that the industrial manufacture of thin-walled vanadium, niobium (and three niobium-base alloy), tantalum, molybdenum, and tungsten tubes for fuel-element jackets and other shapes was introduced in the United States in 1963 (255). Such components are useful in space-research systems. A detailed description is given of vanadium and its alloys, intended for large fast-neutron power reactors.

RESERVES OF NUCLEAR MATERIALS, PROSPECTING, EXTRACTION, AND TREATMENT OF URANIUM ORE

A. A. Zadikyan

Translated from Atomnaya Énergiya, Vol. 18, No. 4, pp. 400-401, April, 1965

The reserves of uranium and thorium, requirements for raw materials, prospecting, and ore treatment were discussed at two sectional meetings at the Conference; eighteen papers were presented.[1]

Almost all the speakers observed that a need had arisen for expanding as rapidly as possible the search for new deposits of nuclear materials. The reserves known today are sufficient to satisfy the needs of all countries of the world only until 1980. By the year 2000 at least three million tons of uranium will be needed to satisfy the requirements of nuclear power stations using converter-reactors. However, if heavy-water reactors or breeder reactors are brought into general use for electrical power generation before that time, the figure may be considerably less.

In recent years the reserves in such countries as Spain, Argentina, India, Portugal, and Yugoslavia have increased considerably. The reserves in Argentina amount today to 7000 tons, and there are good prospects for increasing this figure to 13,000 tons. India will soon be able to increase its reserves to 30,000 tons of uranium. The total uranium reserves of the capitalist countries are estimated today at 500,000 tons. The cost of extracting one pound of uranium is about 8 dollars. The price is expected to remain at this level until 1970, but after that it may increase to 10-30 dollars per pound unless further prospecting operations lead to the discovery of large new deposits.

France seems to be (72)[2] the only country engaged in an intensive search for uranium deposits. The reason for this is that France intends to expand its nuclear-power development program. Three-fourths of the uranium required for the French nuclear program is obtained from mines in metropolitan France, while one-fourth is purchased from Madagascar and Gabon. The Mona deposits in Gabon provide 120 tons of concentrate per month (883).

The ore deposits in Spain (494) amounts to 10,000 tons of U_3O_8. A uranium-ore treatment plant with a capacity of 200 tons per day is now in operation in Spain, and a second plant with a capacity of 1000 tons per day is in the planning stage.

The Indian report gave a survey of the uranium and thorium reserves in the country (752). It is noted that large uranium deposits have been discovered in the Bihar region. Monazite deposits are found in India in greater abundance than perhaps anywhere else in the world.

It was observed that the uranium needs of the United States will be determined in the future not by military requirements but by the scale of development of nuclear power generation (256). It is evident even today that an intensified search for new deposits of uranium will start in the near future, although the total output of the uranium extraction and treatment industry today is in excess of the required level. The United States report expressed confidence that prospecting operations will lead to the discovery of new uranium deposits and that the cost of the uranium obtained from these will be no higher than that of the uranium obtained from currently worked deposits.

The Canadian report stated (24) that the country's present reserves amount to 37% of the total reserves of those countries which have published statistical data on uranium deposits. Until 1958 Canada was the world's leading uranium-producing country. After 1958 the production level declined rapidly with the contraction of uranium markets. By the end of 1963 only seven mines were in operation. It is expected that two mines will be in operation at the end of 1965. The report stated that if there were a good market for thorium at prices comparable to those of

[1] A list of the papers delivered by Soviet scientists was published in Atomnaya Énergiya, Vol. 17, No. 3, 235 (1964), and a list of papers delivered by non-Soviet scientists was published in Atomnaya Tekhnika Za Rubezhom, No. 9, 27 (1964).

[2] The numbers in parentheses are the numbers of the papers.

uranium, the average cost of extraction of U_3O_8 from currently worked deposits would be substantially reduced, and a considerable proportion of the potential U_3O_8 reserves could be classed in the category of more economically workable deposits.

Uranium prospecting and extraction in Argentina were discussed in a special report, which also gave detailed data on uranium deposits in various countries (405).

Brazil presented a report (483) discussing the work done in assessing that country's nuclear-fuel reserves since 1962. It was noted that Brazil expects to discover within the next two or three years deposits sufficient to satisfy the country's needs for the next few years; these deposits will serve as the basis for a promising future development.

A report presented by the Netherlands commented on the need for discovering inexpensive uranium sources and also stated that in the future a large part in nuclear energy production will be played by fast breeder reactors, that the expanded use of present-day reactors is undesirable, and that during the transition period—while the development of fast breeder reactors is being perfected—it will be advisable to utilize reactors with reproduction factors close to those of breeder reactors.

Summarizing the discussion, we may state that such countries as the United States, Canada, the Republic of South Africa, and France expect to double their reserves during the next 20 years. This includes only those reserves from which uranium can be obtained at the cost of 8-10 dollars per pound.

The world's reserves of thorium are fairly large, especially in India, the United States, Brazil, Canada, and Madagascar; however, it would be premature to predict that they could be utilized for present or future nuclear power stations.

A considerable number of the reports were devoted to questions of ore treatment. During the years immediately following the Second Geneva Conference (1958) little was done to develop new treatment methods for uranium ores. However, in recent years a great deal of work has been devoted to more progressive methods of extracting uranium from its ores.

A new method for enriching thorium ores has been developed in Australia (521); this method makes it possible to extract from Australian monazites the thorium required by the power reactors now being developed in that country.

Definite advances have been made in Japan since 1957 in the discovery of new uranium deposits and in ore treatment. Japan has developed new processes suitable for treating low-grade ores with a high clay content, as high as 70% in some ores (884). Extraction using high-pressure water based on the properties of these ores, is now being carried on on an experimental basis.

Yugoslav scientists discussed processes for the treatment of uranium ores and uranium reduction (uranium VI to uranium IV) by means of a catalytic agent (UO_2) which is obtained at the same time from the reaction itself (414). They gave a description of a pilot plant for the continuous precipitation of uranium from carbonate solutions. From the technological and economic point of view, this method can be utilized on an industrial scale.

The latest achievements of the Federal Republic of Germany in the field of uranium-ore prospecting and enrichment were discussed in another paper (478). The Federal Republic of Germany does not have large uranium reserves. An experimental plant for the improvement of uranium-ore treatment processes was put into operation in 1960. Topics of interest mentioned in the paper included the production of uranium of nuclear purity directly from the ore, the development of a pyrochemical method for extracting uranium from the ore, and chlorination with gaseous chlorine at 1100°C.

A report presented by Portugal described scientific research on uranium-ore treatment by semimobile units for small deposits (10-5 tons of uranium). These units make it possible to economize on funds for the construction of a permanent installation or the transporation of ore (503).

The USSR report gave new experimental data on the leaching of uranium out of ores (353). The process consists of the heterogeneous oxidation of UO_2, with subsequent leaching of the uranium in acid solutions.

Another report (450) discussed investigations of certain aspects of the treatment of Hungarian ores.

The report presented by the Republic of South Africa (464) described an experimental plant for producing uranium tetrafluoride by the thermal decomposition of uranium-ammonium tetrafluoride; the plant has a capacity

of 100 tons per year. It was noted that this periodic-operation plant could be used as the basis for setting up a continuous-operation commercial plant.

The reports delivered by scientists of various countries at the section entitled "Uranium and Thorium Reserves" and "Ore Prospecting and Treatment" indicated that the countries which have well-developed nuclear industries did not submit any new material on more progressive trends in the treatment of uranium and thorium ores and that there had been a considerable reduction in the scope of uranium-ore extraction and concentrate production, particularly in the United States and Canada. At the same time, in countries which are now developing their atomic industries—such as France, the Federal Republic of Germany, Italy, among others—the search for new deposits of uranium and thorium is being intensified and industrial ore-treatment plants are being built, in an attempt to satisfy with domestic raw materials the uranium and thorium needs of each country's nuclear power industry.

CONTRIBUTION TO THE THEORY OF LONGITUDINAL FOCUSING OF RADIATION-ACCELERATED CHARGED-PARTICLE BUNCHES

(UDC 621.384.623)

V. V. Yankov

Translated from Atomnaya Énergiya, Vol. 18, No. 4,
pp. 402-403, April, 1965
Original article submitted January 24, 1964; revision submitted July 27, 1964

The present article is devoted to a theoretical consideration of certain problems that arose in the development of the coherent radiation method for accelerating bunches of charged particles, which was proposed by V. I. Veksler [1]. The results of the previous theoretical investigations of this acceleration principle were published earlier [2, 3]. We shall examine the possibility of securing longitudinal bunch stability, which is especially important, since the transverse dimensions of a bunch can be limited by means of constant fields.

Following the approximate approach [4] to the very complicated problem of the behavior of bunches under the influence of radiation, we shall consider the electrodynamic forces of interaction between the electrons in a bunch with a certain given configuration, where the density of particles is assumed to be steady during time intervals of the order of the period of the hf field. This assumption is usually well justified. The solution of this simplified problem, of course, can only indicate the trend of the initial deformation of the bunch.

We shall calculate the spatial distribution of the time-averaged radiation forces that appear in a plasma bunch which scatters the external radiation flux. We shall discuss the simplest model of a bunch of quasineutral transparent plasma, for which the effective number of particle collisions is negligibly small in comparison with the frequency of the oncoming wave.

We are basically interested in the distribution of the electrodynamic wave forces in the direction of propagation of the incident radiation. These forces are caused by the back reaction of bunch radiation, which leads directly to the acceleration of the bunch as a whole.

Our aim was to determine the specific characteristics of the spatial distribution of the wave radiation pressure on a continuous bounded medium, which was in contrast to the previously discussed quasistatic effects, where the wavelength in vacuum was assumed to be large in comparison with the dimensions of the medium (see, for instance, [5-7]). The solution can readily be obtained within the framework of the one-dimensional problem if the plasma bunch is approximated by an infinite plane-parallel layer of a homogeneous medium whose dielectric constant $\varepsilon(\omega)$ depends on the field frequency ω and if the accelerating radiation field is approximated by a plane wave which is normally incident to the layer plane. The configuration of the reflecting flat body is characterized by the layer thickness d, while the incident plane wave is characterized by the wave number $k=\omega/c$, where c is the velocity of light in vacuum.

By using the well-known solution of the corresponding boundary value problem [8] and applying the usual expression for the averaged over the wave period volumetric density of pondermotive forces in a transparent gaseous dispersive medium, $f=(\varepsilon-1)_{\Delta}|E|^2/16\pi$, we find the distribution of radiation forces inside the layer:

$$f(z)=\begin{cases}\dfrac{E_0^2}{4\pi}k\sqrt{\varepsilon}\,\dfrac{(\varepsilon-1)^2\sin 2k\sqrt{\varepsilon}(d-z)}{4\varepsilon+(\varepsilon-1)^2\sin^2 k\sqrt{\varepsilon}\,d} & \text{for } \varepsilon>0,\\ -\dfrac{E_0^2}{4\pi}k\sqrt{|\varepsilon|}\,\dfrac{(\varepsilon-1)^2\operatorname{sh}2k\sqrt{|\varepsilon|}(d-z)}{4\varepsilon-(\varepsilon-1)^2\operatorname{sh}^2 k\sqrt{|\varepsilon|}\,d} & \text{for } \varepsilon<0,\end{cases}$$

where the distance z is measured from the forward boundary of the layer, which faces the incident wave $E_0 e^{-i(\omega t - kz)}$. The above equation reflects the general regularity characteristic for any bounded system of charges, which consists in the fact that the dissipative wave radiation pressure produced by the interaction between particles does not act on the bunch elements adjacent to its back boundary (z = d) and that it continuously increases with an increase in the distance from this boundary toward the bunch interior to a value $s \leq \lambda/8$ for $\varepsilon > 0$ or right to the forward boundary s = d for $\varepsilon \leq 0$ (λ is the wavelength inside the bunch), i.e., it focuses the medium by pinching it. For instance, in the coherent case for a very thin layer ($d \ll \lambda/4\pi$), the radiation forces monotonically decreases in the direction of propagation of the incident wave, $f(z) = E_0^2 R(d-z)/2\pi d^2$, where R is the over-all coefficient of reflection from the layer. Moreover, an analysis of the specific structural characteristics of the interference field immediately in front of the medium layer (z < 0) reflecting the radiation shows that a rather thin layer of radiation-accelerated plasma generates returning forces, which retain individual particles that have left the bunch for any chance reason:

$$F(s') = -\frac{r_e E_0^2}{k} \times \frac{(\varepsilon-1)\sqrt{\varepsilon}\sin 2k\sqrt{\varepsilon}\,d}{4\varepsilon+(\varepsilon-1)^2\sin^2 k\sqrt{\varepsilon}\,d}\cos 2ks' > 0 \qquad (0<\varepsilon<1),$$

where s' is the remoteness of a particle from the layer's forward boundary, F(s') is the returning force acting on an electron, and $r_e = e^2/mc^2$ is the classical electron radius.

It is important that the pinching of the plasma layer by the pressure exerted by reflected radiation is the more effective, the thinner and denser the bunch. This offers possibilities favorable to automatic longitudinal bunch focusing by the reaction of self-radiation.

However, in an actual bunch (with three-dimensional boundaries), incident radiation unavoidably creates, besides the radiation reaction, quasistatic fields, which do not accelerate the bunch as a whole, but cause its deformation. In bunches whose transverse dimensions are small in comparison with the wavelength in vacuum, such fields may play a predominant role.

If the accelerating radiation forces are invariant, i.e., if they always focus a small bunch in the longitudinal direction, the character of the action of internal (quasisteady-state) forces basically depends on the configuration of the incident wave and of the bunch. In particular, in [9], where the regularity of automatic longitudinal phase control of a charge system by radiative dissipative forces was first determined, it was shown that short-lived quasisteady-state radiation forces lead to the mutual repulsion of pairs of closely positioned (one behind the other) electrons in the case of transverse polarization of the electric field by the scattered wave and to their mutual attraction in the case of longitudinal polarization, due to which the longitudinal orientation of the accelerating wave's electric vector may predominate over the transverse orientation.

It is obvious that the tendency to automatic longitudinal focusing of a thin medium layer in the radiation flux of the medium's self-radiation reaction, which favors the stability of accelerated plasma bunches, can be used, in principle, for maintaining and confining a localized steady-state medium (for instance, by utilizing the wave pressure of independent opposing radiation fluxes). The author is deeply grateful to Academician V. I. Veksler and Prof. M. S. Rabinovich for their interest in this project and the useful discussions.

LITERATURE CITED

1. V. I. Veksler, Atomnaya Énergiya, 2, 427 (1957).
2. M. L. Levin, M. S. Rabinovich, and G. A. Askar'yan, Proc. of Inter. Conf. CERN (1959), p. 315.
3. G. A. Askar'yan et al., Nuclear Fusion, Supplement, Part 2 (1962), p. 797.
4. I. E. Tamm, Trudy FIAN SSSR, 18, 3 (1962).
5. V. V. Yankov, ZhÉTF, 32, 926 (1957).
6. L. M. Kovrizhnykh, ZhÉTF, 33, 72 (1957).
7. M. L. Levin, Atomnaya Énergiya, 8, 134 (1960).
8. D. A. Stratton, Theory of Electromagnetism [Russian translation], Moscow, Gostekhteoretizdat (1948).
9. V. V. Yankov, ZhÉTF, 45, 1634 (1963).

CALCULATION OF THE MEAN SQUARE OF THE RECOIL NUCLEUS MOMENTUM IN EVAPORATION

(UDC 539.17.014)

F. P. Denisov and V. P. Milovanov

Translated from Atomnaya Énergiya, Vol. 18, No. 4,
pp. 403-404, April, 1965
Original article submitted April 22, 1964

In investigating nuclear reactions at high energies, it is necessary to take into account the momentum acquired by the recoil nucleus in the evaporation of nuclear particles. In [1, 2], the mean square of the recoil nucleus momentum p_0^2 was calculated in the same manner as the momentum of a Brownian particle:

$$\overline{p_0^2} = \sum_{i=1}^{m} \overline{p_i^2}, \tag{1}$$

where p_i is the momentum of the i-th evaporated particle, and m is the number of evaporated particles. However, such calculation, based on analogies, is approximate by nature and may often lead to considerable errors.

A more rigorous analysis of the problem requires the consideration of the nucleus' motion caused by the evaporation of all the preceding particles from the nucleus.

Consider an immobile nucleus with the mass A, excited to an energy E_0, from which m particles with momentum p_i and masses a_i evaporate. According to the law conservation of momentum, the momentum acquired by the recoil nucleus is equal to

$$p_0 = -\sum_{i=1}^{m} p_i. \tag{2}$$

Let us square this equation in scalar fashion and average it with respect to the directions and absolute values of the vectors p_0:

$$\overline{p_0^2} = \sum_{i=1}^{m} \overline{p_i^2} + \sum_{i \neq j}^{m} \overline{(p_i, p_j)}. \tag{3}$$

It is obvious that the actual expression for p_0^2 differs from expression (1) by the additional term $\delta = \sum_{i \neq j}^{m} \overline{(p_i, p_j)}$.

In order to estimate δ, we shall substitute each momentum p_i in a laboratory coordinate system in the form of its isotropic part p_{i0}, i.e., in the form of the momentum acquired by the i-th nucleon in a moving nucleus system and the momentum p_{i1} connected with the nucleus' motion and caused by the evaporation of all the preceding nucleons from the nucleus.

It is obvious that $p_{i1} = -\sum_{l=1}^{i-1} \alpha_l p_l$, where $\alpha_l = a_l/A_l$ (here, A_l is the nuclear mass after the evaporation of

the l-th particle). Assuming, for the sake of simplicity, that $\alpha_i = \bar{\alpha} = \sum_{l=1}^{m} \frac{\alpha_l}{m}$, and $\overline{p_{i0}^2} = \overline{p_i^2}$ in the expression for δ, and considering that $\overline{(p_{i0}, p_{j0})} = 0$ and neglecting the terms with α^2, we obtain

$$\delta = \sum_{i \neq j}^{m} \overline{(p_i, p_j)} = -2\bar{\alpha} \sum_{i=1}^{m} (m-i)\, \overline{p_i^2}.$$

If we neglect the change in the temperature of the residual nucleus, we can consider that $\overline{p_i^2} = \overline{p_j^2}$ in the correction, where i, j = 1, 2, ..., m. Then

$$\delta = -2\bar{\alpha} \sum_{i=1}^{m} (m-i)\, \overline{p_i^2} = -\bar{\alpha}\,(m-1) \sum_{i=1}^{m} \overline{p_i^2}$$

and

$$\overline{p_0^2} = [1 - \bar{\alpha}\,(m-1)] \sum_{i=1}^{m} \overline{p_i^2}. \qquad (4)$$

Equation (4) for m = 3 was first used in [3, 4]. For $\bar{\alpha} = 0$, Eq. (4) is transformed into relationship (1). However, for $\bar{\alpha} \approx 0.1$ ($A \approx 10$), the error incurred in using relationship (1) may attain 20-30%.

LITERATURE CITED

1. S. Fung and I. Perlman, Phys. Rev., 87, 723 (1952).
2. N. I. Borisova, M. Ya. Kuznetsova, L. N. Kurchatova, V. N. Mekhedov, and L. V. Chistyakov, ZhÉTF, 37, 366 (1959).
3. F. Denisov and P. Cherenkov, Proc. Conf. Nucl. Phys. Dunod, Paris (1959), p. 676.
4. V. A. Balitskii and F. P. Denisov, In the book: Transactions of the Second All-Union Conference on Nuclear Reactions at Low and Medium Energies [in Russian], Moscow, Izd. AN SSSR (1962), p. 450.

All abbreviations of periodicals in the above bibliography are letter-by-letter transliterations of the abbreviations as given in the original Russian journal. *Some or all of this periodical literature may well be available in English translation.* A complete list of the cover-to-cover English translations appears at the back of this issue.

SPECTRA OF FAST NEUTRONS IN HEAVY MEDIA AND WATER

(UDC 621.039.538.7)

D. L. Broder, A. S. Zhilkin, and A. A. Kutuzov

Translated from Atomnaya Énergiya, Vol. 18, No. 4,
pp. 404-408, April, 1965
Original article submitted June 8, 1964

The protective properties of iron, lead, and iron-water and lead-water compositions were investigated earlier experimentally and theoretically [1-3]. The measurements were performed by means of threshold detectors.

The calculations for heavy media were performed in the P_8-approximation of the method of spherical harmonics. The spectra of fast neutrons moderated in iron and lead were calculated in [1, 2]. The accuracy of these calculations was checked by comparing the theoretical and experimental activation values for different threshold detectors. However, it is difficult to determine the neutron spectrum with respect to the results obtained in measurements by means of threshold detectors.

The behavior of the neutron spectrum near the interface between the heavy medium and water is also of interest, since the presently used methods for calculating biological shields are least accurate precisely in the regions near the boundary as a result of abrupt changes in the spectrum and the angular distributions of neutrons.

In our experiments, the spectra of neutrons from monoenergetic sources with E_0 = 3.4 MeV and E_0 = 15 MeV which were moderated in iron, lead, or water behind iron and lead layers were measured by means of a scintillation spectrometer. A stilbene crystal in combination with an FÉU-13 photomultiplier and an AI-100 amplitude analyzer with 100 channels was used as the spectrometer. The γ-background discrimination was effected with respect to the luminescence time [4].

The measurements were performed with iron and lead prisms whose dimensions were 710 × 710 × 600 mm. In the case of measurements in water, the iron and lead layers were placed between the accelerator target and a tank containing water.

Figures 1-6 show the measured spectra of moderated neutrons from sources with E_0 = 3.35 MeV and E_0 = 14.9 MeV. All of the spectra were reduced to the same neutron flux value in the 3.2-3.5 MeV energy range for the source with E_0 = 3.3 MeV and in the 14.45-15.65 MeV range for the source with E_0 = 14.9 MeV. Moreover, for the sake of comparison, Fig. 1 also shows the neutron spectrum measured in [5] with an E_0 = 3 MeV source in a barrier geometry. It is seen that the spectrum measured in our experiments was softer than that in [5]. This can be explained by the difference between the experimental geometries.

Comparisons show a significant discrepancy between the spectrum of neutrons from a source with E_0 = 14.9 MeV in iron that was calculated in [1, 2] and the spectrum measured at a distance of 40.5 cm from the source. Thus, for E values equal to 1.25 and 4 MeV, the spectra differ by factors of 4 and 6, respectively. This can probably be explained by the fact that the calculations in [1, 2] were performed under several simplifying assumptions. In particular, moderation in elastic scattering was neglected, and the neutrons found in the energy interval from 6-14 MeV were not taken into account. Moreover, the inaccuracies in the values and angular dependences of the effective cross sections of interaction between neutrons and iron nuclei may have played a certain role.

Figure 4 provides a compar son between the measured spectrum of neutrons in lead and the spectrum calculated in [2]. It is seen that the agreement is satisfactory. In this case, elastic moderation could play a much lesser role, while the deviation of the spectrum of inelastically scattered neutrons in the 6-14 MeV energy interval from the Maxwellian spectrum was taken into account in calculations.

Figures 5 and 6 show the neutron spectra measured in water behind iron (E_0 = 3.35 MeV) and lead (E_0 = 14.9 MeV) layers. In the case of considerable distances in water behind a lead or iron layer, the spectrum of neutrons

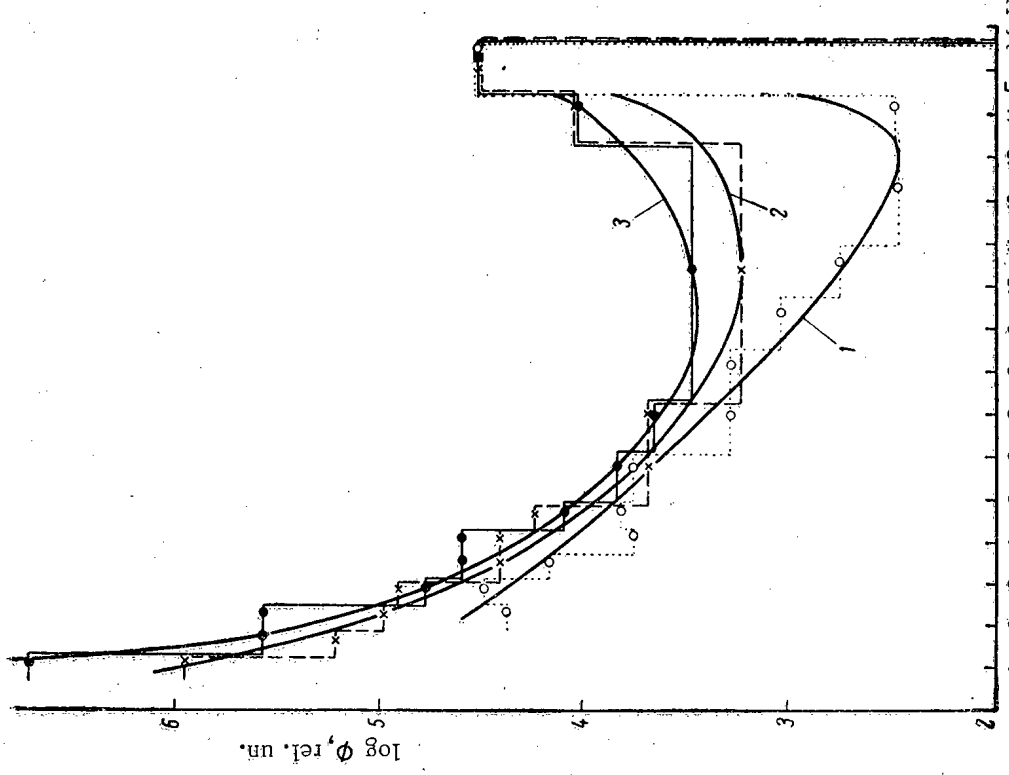

Fig. 2. Spectra of neutrons in iron (source with E_0 = 14.9 MeV) for the following ΔFe values (cm): 1(○) 10.5; 2(×) 25.5; 3(●) 40.5.

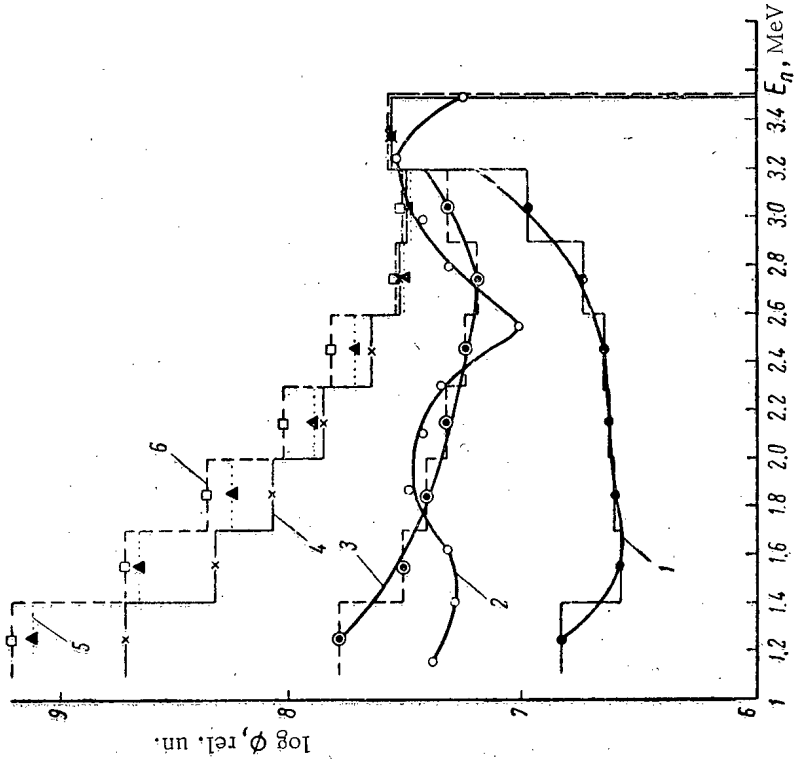

Fig. 1. Spectra of neutrons in iron (source with E_0 = 3.35 MeV) for the following ΔFe values (cm): 1 (●) 0; 2 (○) 15 [5]; 3 (◉) 10.5; 4 (×) 25.5; 5 (▲) 40.5; 6 (□) 47.5.

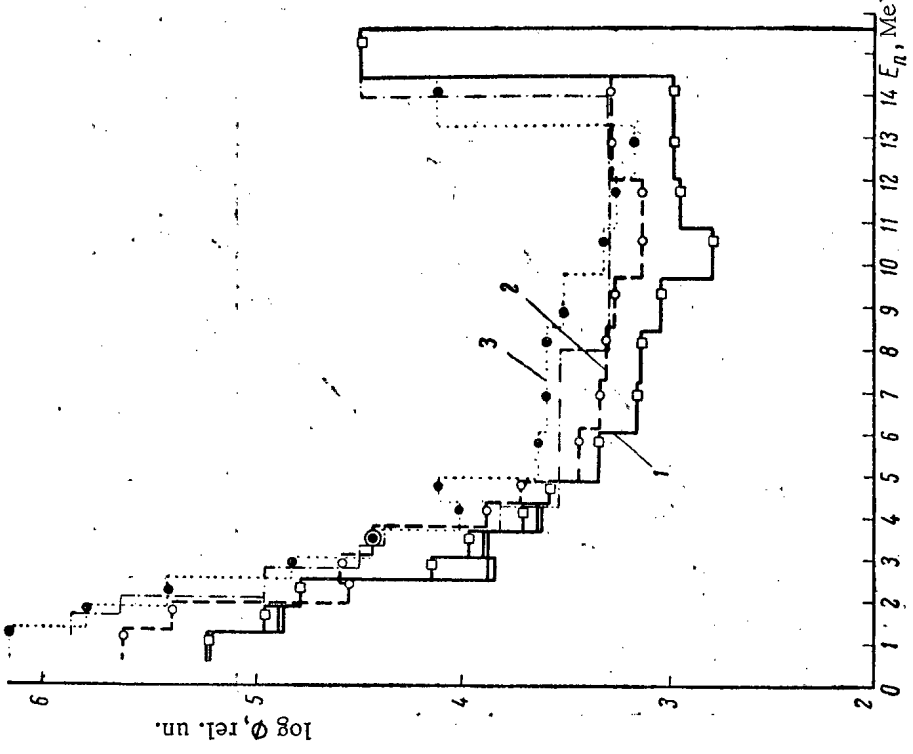

Fig. 4. Spectra of neutrons in lead (source with E_0 = 14.9 MeV) for the following ΔPb values (cm): 1 (□) 19.5; 2 (○) 30.5; 3 (●) 49.5; —·—·—) 49.5 (calculation [1, 2].

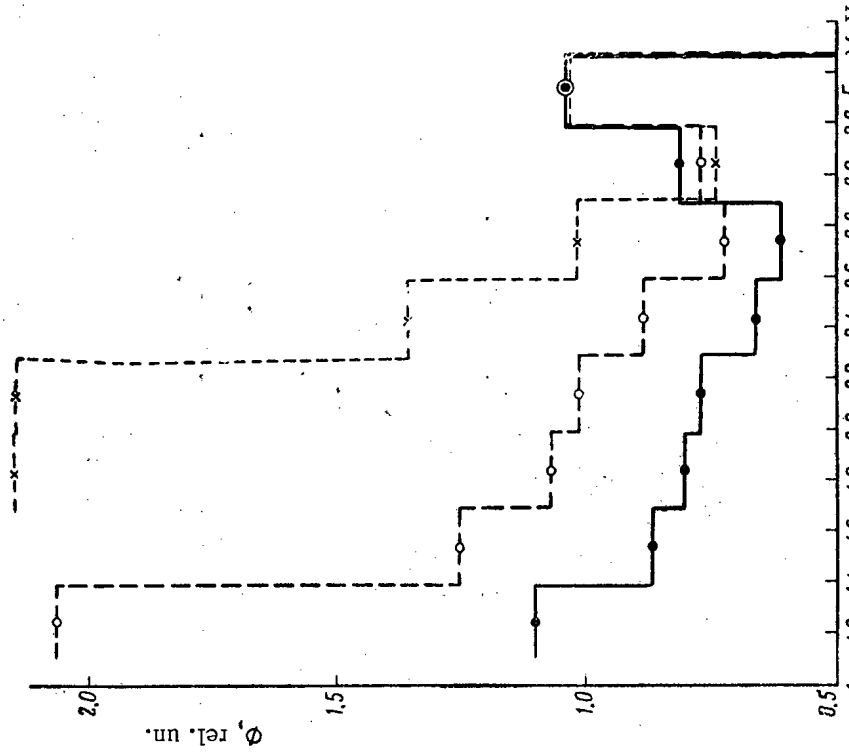

Fig. 3. Spectra of neutrons in lead (source with E_0 = 3.35 MeV) for the following ΔPb values (cm): ●) 19; ○) 30; ×) 49.

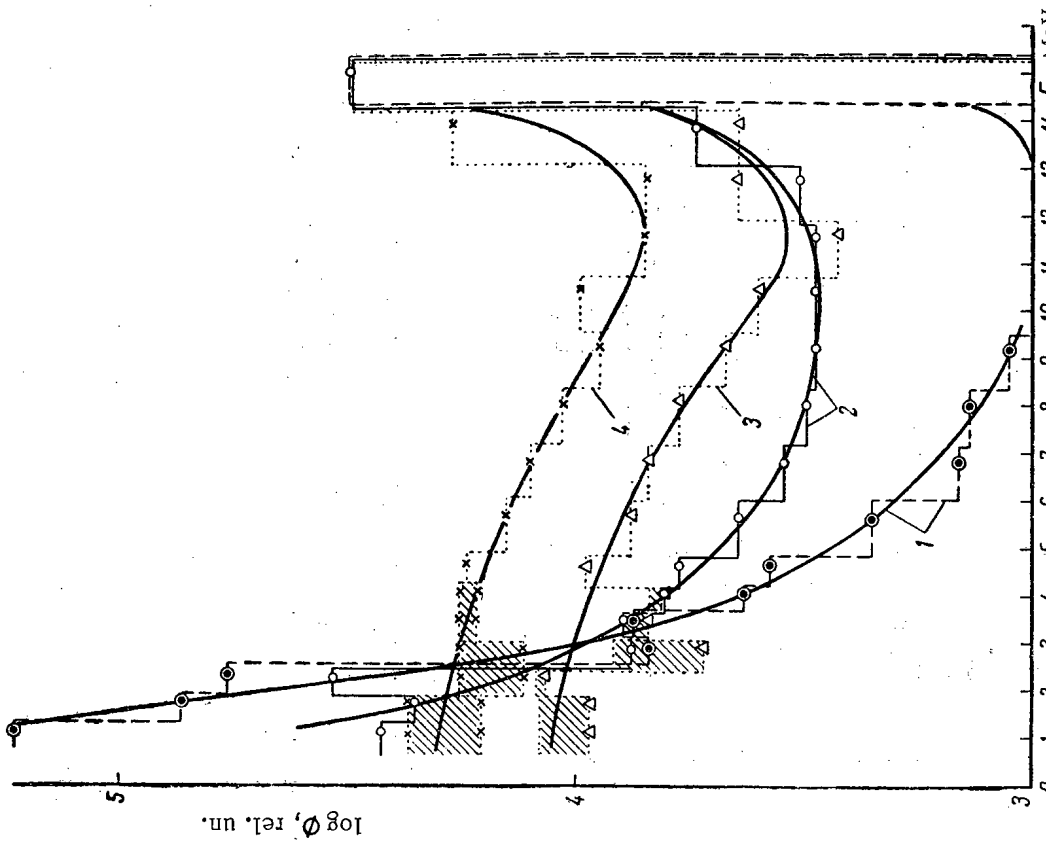

Fig. 6. Spectra of neutrons in lead and water (source with E_0 = 14.9 MeV) for the following ΔPb and ΔH_2O values (cm): 1 (●) ΔPb = 19.5 (lead); 2 (○) ΔPb = 19.5, ΔH_2O = 3.5 (water behind lead); 3 (△) ΔH_2O = 46 (water); 4 (×) ΔPb = 19.5, ΔH_2O = 45 (water behind lead).

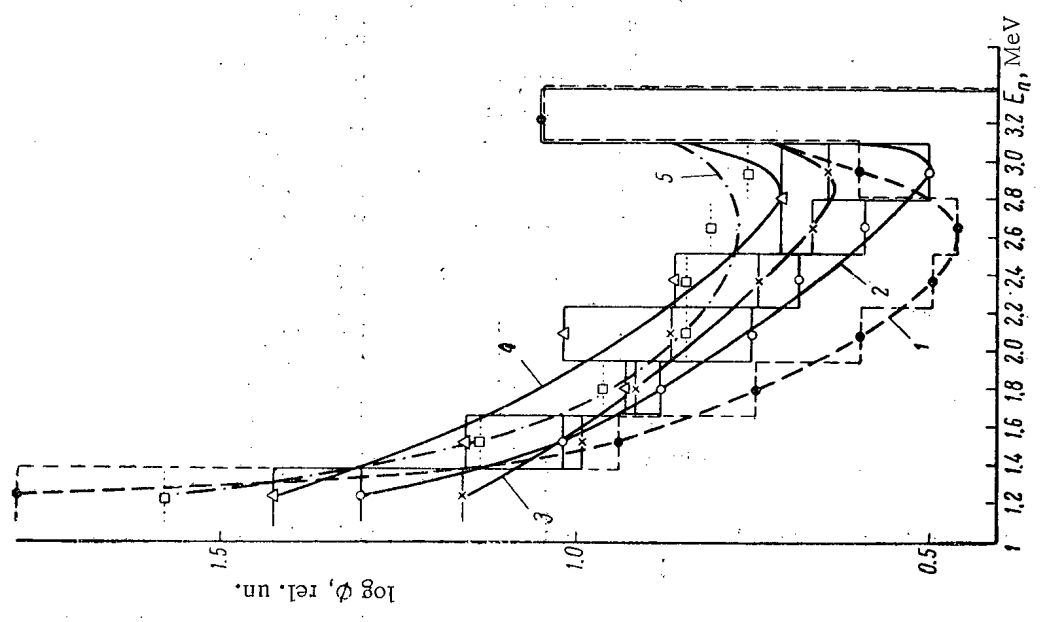

Fig. 5. Spectra of neutrons in iron and water (source with E_0 = 3.35 MeV) for the following ΔFe and ΔH_2O values (cm): 1 (●) ΔFe = 15 (iron); 2 (○) ΔFe = 15, ΔH_2O = 3.5 (water behind iron); 3 (×) ΔFe = 15, ΔH_2O = 13.5 (water behind iron); 4 (△) ΔFe = 15, ΔH_2O = 33.5 (water behind iron); 5 (□) ΔH_2O = 36 (water).

from a source with E_0 = 14.9 MeV differs considerably from the neutron spectrum in pure water at the same distances. The spectrum of neutrons in water behind a lead layer has a much larger number of scattered and moderated neutrons than the spectrum in pure water, while the shape of the scattered neutron spectrum is the same. This is due to the fact that, behind a lead or iron layer, the flux of neutrons with an energy close to the initial energy becomes isotropic, which leads to greater attenuation than in pure water. As can be seen from Figs. 1-4, the neutron spectrum becomes considerably softer with an increase in the thickness of iron or lead, while the softening is much greater in iron. In the moderation of neutrons from a source with an energy of 14.9 MeV in iron or lead, the accumulation of neutrons occurs mainly in the energy range $E_n < 4$ MeV. This agrees well with the evaporation model of inelastic scattering at such neutron energies.

The authors take this opportunity to thank V. G. Zolotukhin, B. A. Kalmykov, V. I. Lobanov, M. P. Tarasko, V. E. Tyrkich, and E. V. Shestopalov for their assistance in the work and also L. A. Trykov for the discussion of the results.

LITERATURE CITED

1. D. L. Broder et al., In the book: Transactions of the Second International Conference on the Peaceful Uses of Atomic Energy. Reports by Soviet scientists [in Russian], 2, Moscow, Atomizdat (1959), p. 674
2. D. L. Broder et al., Atomnaya Énergiya, 7, 313 (1959).
3. V. P. Mashkovich and S. G. Tsypin, Atomnaya Énergiya, 11, 251 (1961).
4. F. Brooks, Nucl. Instrum. and Methods, 4, 151 (1959).
5. G. During, R. Jansson, and N. Starfelt, Neutron Dosimetry, 1, International Atomic Energy Agency, Vienna (1963), p. 359.

THE WEIGHT-EFFECTIVENESS INDEX OF TWO-COMPONENT MATERIALS USED FOR SHIELDING AGAINST NEUTRONS AND γ-RAYS

(UDC 539.121.73)

G. A. Lisochkin and F. A. Predovskii

Translated from Atomnaya Énergiya, Vol. 18, No. 4,
408-409, April, 1965
Original article submitted April 25, 1964

The weight effectiveness of different shielding materials used for protection against neutron and γ-rays can easily be compared by using the value of the mass coefficient of γ-ray attenuation, μ/ρ, and the analogous characteristic of the material with respect to neutrons, $1/\rho L$ where ρ is the density of the material and L is the relaxation length of the neutron flux.

In many cases, one of the materials which interests us is a more effective shielding material against neutrons, while the second material is more effective against γ-rays; in such cases the above coefficients do not permit us to decide which material is preferable.

In order to estimate the weight effectiveness of two-part compositions which differ from each other in both components (for example, iron and water as against lead and boron carbide), we must consider the relationship between the absorption characteristics for neutrons and those for γ-quanta.

Let the total dose rate P be expressed as a function of the weights of components x_1 and x_2 be expressed by the formula

$$P = P_1 e^{-\left(\frac{x_1}{q_{11}}+\frac{x_2}{q_{12}}\right)} + P_2 e^{-\left(\frac{x_1}{q_{21}}+\frac{x_2}{q_{22}}\right)}, \quad (1)$$

where P_1 and P_2 are the neutron and γ-ray dose rates, respectively, behind the shielding in the original variant; q_{kn} is the absorption weight index, equal to that weight of shielding component n which will attenuate the dose rate from source k by a factor of e.

As an index of the effectiveness of a two-component material used for shielding against neutrons and γ-quanta we shall take the total change in the weight of the two components which will change the γ-ray dose rate and the neutron dose rate by the same factor (for example, a factor of e).

The value of the weight-effectiveness index, $K = x_1 + x_2$, which interests us is of the form

$$K = \frac{\frac{1}{q_{11}} - \frac{1}{q_{12}} + \frac{1}{q_{22}} - \frac{1}{q_{21}}}{\frac{1}{q_{11}} \cdot \frac{1}{q_{22}} - \frac{1}{q_{12}} \cdot \frac{1}{q_{21}}}. \quad (2)$$

In the present study we use mass attenuation coefficient values for γ-rays with an energy of 6 MeV and removal cross sections for the hard part of the neutron fission spectrum taken from [1, 2]. In using the removal cross section, we presuppose that the construction of the shield satisfies the conditions required for the use of this quantity.

Table 1 shows the results obtained by comparing the various possible compositions on the basis of formula (2).

The ratio of the index (2) for various two-part compositions may be characterized by the ratio of the weights of the protective shield made of these materials, with an accuracy which depends on the difference between the build-up factors of the scattered γ-radiation. As an example, we may point out that the build-up factor values

TABLE 1. Values of the Weight-Effectiveness Index

First component	Second component	K, g/cm^2
Lithium borohydride	Uranium	23.89
Lithium hydride	Uranium	24.13
Polyethylene	Uranium	24.15
Water	Uranium	24.74
Lithium borohydride	Lead	24.88
Polyethylene	Lead	25.03
Lithium hydride	Lead	25.11
Water	Lead	25.56
Lithium borohydride	Tungsten	25.89
Polyethylene	Tungsten	25.96
Lithium hydride	Tungsten	26.12
Water	Tungsten	26.46
Boron carbide	Lead	27.40
Beryllium	Uranium	27.84
Beryllium	Lead	28.54
Boron carbide	Uranium	28.73
Beryllium	Tungsten	29.49
Boron carbide	Tungsten	29.90
Polyethylene	Zirconium hydride†	30.04
Water	Zirconium hydride†	30.17
Titanium hydride*	Tungsten	31.08
Boron carbide	Zirconium hydride†	31.31
Titanium hydride*	Zirconium hydride†	31.63
Zirconium hydride†	Tungsten	32.46
Polyethylene	Iron	33.05
Concrete	Lead	33.10
Water	Iron	33.10
Zirconium hydride†	Lead	33.20
Lithium borohydride	Iron	33.30
Lithium hydride	Iron	33.36
Titanium hydride*	Iron	33.40
Zirconium hydride†	Uranium	33.52
Boron carbide	Iron	33.84
Beryllium	Iron	34.37
Concrete	Iron	34.97

*$TiH_{1.6}$.
†$ZrH_{1.5}$.

calculated on the basis of the data given in [3] for iron-water, uranium-water, and lead-water multi-layer shields have values of 7.8, 8, and 9.7, respectively (for a total of 10 neutron path lengths and 12 γ-ray path lengths), i.e., are practically identical. It must be borne in mind that the results so obtained refer to plane geometry.

In addition, when three-dimensional sources of capture γ-radiation are distributed in the shielding material, the γ-quantum dose rate in relation to the shielding thickness (weight) [see Eq. (1)] may be characterized by other quantities than the value of the absorption coefficient μ/ρ.

The authors take this opportunity to express their gratitude to E. A. Murinson for his valuable criticism of this work.

LITERATURE CITED

1. Nuclear Reactors [Russian translation], Published by the United States Atomic Energy Commission, 1, Moscow, Izd-vo inostr. lit. (1956).
2. Chapman and Storrs, In "Shielding of Nuclear-Powered Propulsion Plants" [Russian translation], Edited by V. V. Orlov and S. G. Tsypin, Moscow, Izd-vo inostr. lit. (1961), p. 128.
3. D. L. Broder, Yu. P. Kayurin, and A. A. Kutuzov, Atomnaya Énergiya, 12, 30 (1962).

ANGULAR DISTRIBUTION OF FAST NEUTRONS SCATTERED BY MEDIUM AND HEAVY NUCLEI

(UDC 539.125.5:539.121.72)

A. G. Guseinov, M. N. Nikolaev, A. G. Dovbenko,
V. E. Kolesov, and V. N. Morozov

Translated from Atomnaya Énergiya, Vol. 18, No. 4,
pp. 409-415, April, 1965
Original article submitted October 28, 1963; revision submitted October 24, 1964

Reference [1] gives data on $\beta(\mu)$—the macroscopic scattering cross section at an angle θ, where $\theta = \arccos \mu$—for neutrons of the upper fission spectrum group ($E_n \gtrsim 1.5$ MeV), scattered by light nuclei. As stated, $\beta(\mu)$ takes account of all scattering processes, elastic and inelastic, which leave the neutron in the group. As a rule, however, there are no detailed data on the energy dependence of the differential scattering cross sections for medium and heavy nuclei in the energy region of interest; there are also insufficient data on the energy distribution of inelastically-scattered neutrons. It is therefore desirable to measure $\beta(\mu)$ for medium and heavy nuclei, which is the aim of the work described here.

The experiments were performed in a neutron beam of 5 cm, diameter produced by the core of a BR-5 reactor [2]. The neutron spectrum with energy ~ 1.5 MeV in this beam is somewhat softer than the corresponding part of the fission spectrum [5]; this is characteristic of the core spectra of fast reactors.

The neutron detector was a fission chamber with layers of Th^{232} containing ~ 1.0 g thorium. The chamber was positioned 41 cm from the scattering material. The over-all angular resolution was then ±7°.

The scatterers were disks of 45 mm, diameter placed at 45° to the beam. Their thicknesses were chosen to scatter ~ 10% of the incident neutrons. The fraction of particles undergoing repeated scattering was thus negligible.

Angular dependences were measured for neutrons scattered by the following elements:

Ti, V, Cr, Mn, Fe, Co, Ni, Cu, Zn, Br, Zr, Nb, Mo, Ag, Cd, Sb, I, Cs, Ba, W, Ir, Hg, Pb, Bi, Th and U (natural).

The results are given in Fig. 1. The experimental points on the angular distribution curves of the differential cross sections have errors of 3-6 and 8-12% for forward and reverse scattering, respectively.

The greater error for reverse scattering was due to the greater background in this case.

Table 1 gives the integral scattering cross sections β/N and the coefficients of the expansion in Legendre polynomials, obtained by approximating the experimental data in the form

$$\frac{1}{N} \cdot \frac{d\beta}{d\mu} = \frac{\beta}{2N} \left[1 + \sum_{L=1}^{m} (2L+1) f_L P_L(\mu) \right] \text{ barn} \qquad (1)$$

by the method of least squares. The least number of terms, m, required to represent the experimental data within the experimental error was determined by Gauss' criterion. The calculations were made on a fast computer. A similar analysis was made of the previously published data on the angular distribution of fast neutrons scattered by light nuclei [1]. The results and the errors in the expansion coefficients are also given in Table 1.

It is noteworthy that the errors in the coefficients of the corresponding harmonics for various angular distributions, measured with the same number of points according to angle, are almost identical.

To find how far the various harmonics were correlated, we calculated the matrix of correlation coefficients

(Table 2) for magnesium:

$$\varrho_{LL'} = \frac{\langle \delta f_L \delta f_{L'} \rangle}{\sqrt{\langle \delta f_L^2 \rangle \langle \delta f_{L'}^2 \rangle}}. \tag{2}$$

Here $\langle \delta f_L^2 \rangle$ is the mean standard deviation of the L-th harmonic's contribution to the scattering cross section; $\langle \delta f_L \delta f_{L'} \rangle$ is the mean correlation moment between harmonics L and L'.

Since the errors of the expansion coefficients depend only weakly on the atomic weight, it follows that the matrix of the correlation moments cannot be very different for the other elements.

The thin continuous lines in Fig. 1 represent the angular distributions for the above elements, calculated on the optical model of the nucleus ($v_0 = 1.45 \cdot 10^{-13}$ cm). The calculations were made on the assumption that the cross sections of the reactions taking place via a compound nucleus are isotropic. Thus the anisotropy of the calculated angular distributions was caused by anisotropy of the elastic scattering proper, which was calculated by the formula

$$\sigma_{s,l}(E, \mu) = \frac{d\sigma}{d\mu} = \frac{\pi}{2k^2} \left| \sum_l (2l+1)(1-\eta_l) P_l(\mu) \right|^2 \text{ barn} \tag{3}$$

for all energies falling within the upper group, with varying steps of 0.25, 0.5 and 1 MeV. The values of η_l were calculated for the Woods-Saxon potential,

$$V(r) = -\frac{V_0(1+i\xi)}{1+\exp\left(\frac{r-R}{a}\right)}, \tag{4}$$

where $V_0 = 45$ MeV, $a = 0.5 \cdot 10^{-13}$ cm and $\xi = 0.1$. The method of calculating $\sigma_{s,l}(E, \mu)$ was given in [3].

$\sigma_{s,l}(E, \mu)$ was then averaged over the upper group, taking account of the detector efficiency:

$$\bar{\sigma}_{s,l}(\mu) = \frac{\int_{E_1}^{\infty} \sigma_{s,l}(E, \mu)\, \varphi(E)\, \sigma_f^{\mathrm{Th}}(E)\, dE}{\int_{E_1}^{\infty} \varphi(E)\, \sigma_f^{\mathrm{Th}}(E)\, dE}, \tag{5}$$

where $\varphi(E)\sigma_f^{\mathrm{Th}}(E)$ is the weighting function, $\varphi(E)$ being the fission-neutron spectrum above E_1 in MeV and $\sigma_f^{\mathrm{Th}}(E)$ the fission cross section of Th^{232}. The final theoretical cross section for a given element was determined by the formula

$$\left.\frac{d\sigma}{d\mu}\right|_{\text{calc.}} = [\bar{\sigma}_{s,l}(\mu) + K\langle \sigma_c(E) \rangle] \text{ barn}, \tag{6}$$

where $\langle \sigma_c(E) \rangle$ is the cross section for inelastic processes, averaged over the upper group:

$$\langle \sigma_c(E) \rangle = \frac{\int_{E_1}^{\infty} \varphi(E)\, \sigma_c(E)\, dE}{\int_{E_1}^{\infty} \varphi(E)\, dE}; \tag{7}$$

here K is a dimensionless coefficient which takes account of the fraction of inelastic scattering which leaves the neutron in the group. K was calculated from the system of multi-group constants [4]. A comparison of the experimental and theoretical data (see Fig. 1) shows that there is satisfactory agreement for most of the elements. In the cases when there was a clear discrepancy, we calculated a further curve (dotted lines in Fig. 1) for which r_0 was taken as $\sim 1.30 \cdot 10^{-13}$ cm.

The angular distributions $\beta(\mu)$ are shown in Fig. 2 in order of atomic weight.

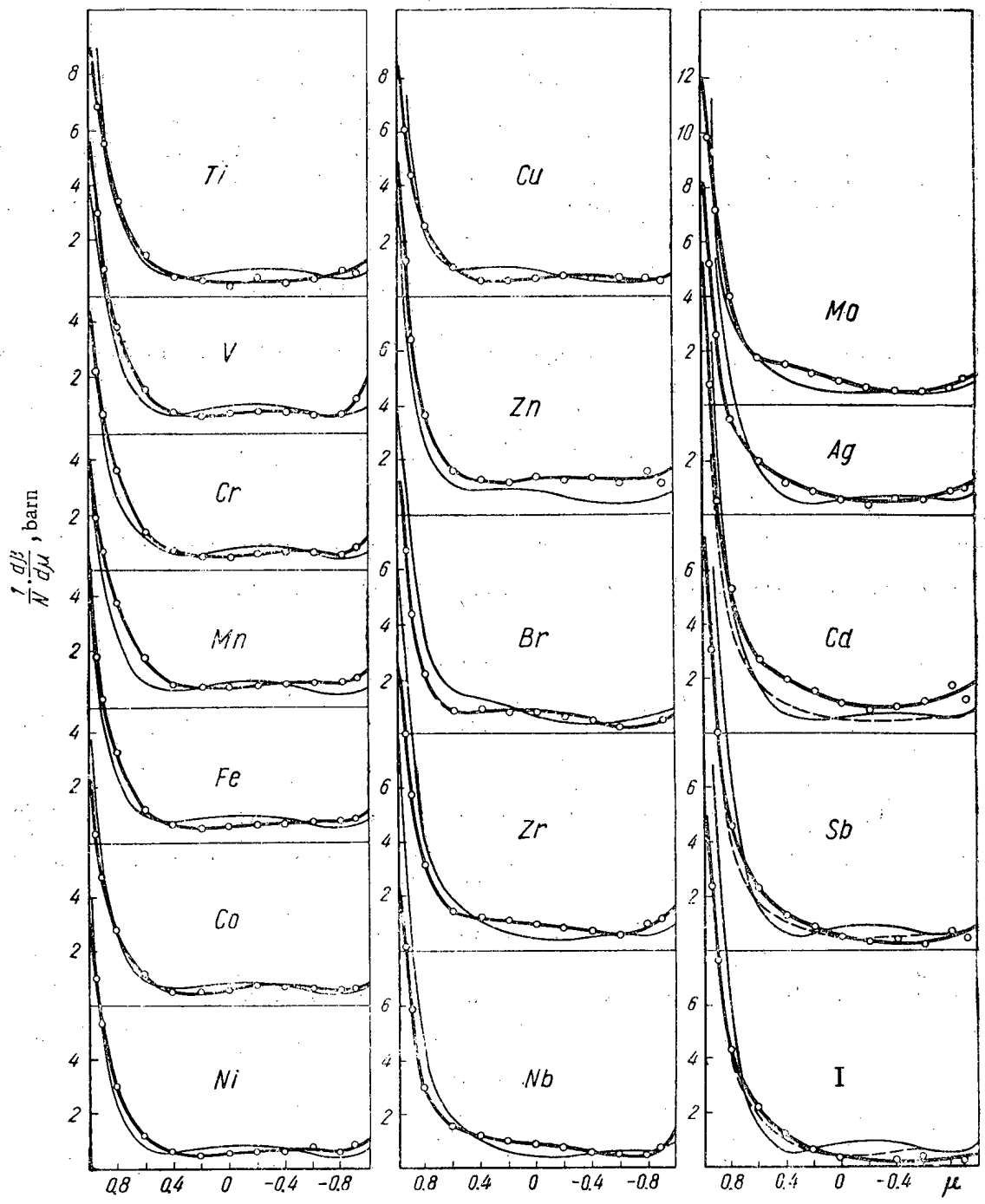

Fig. 1. Angular distributions of fast neutrons scattered by medium and heavy nuclei.

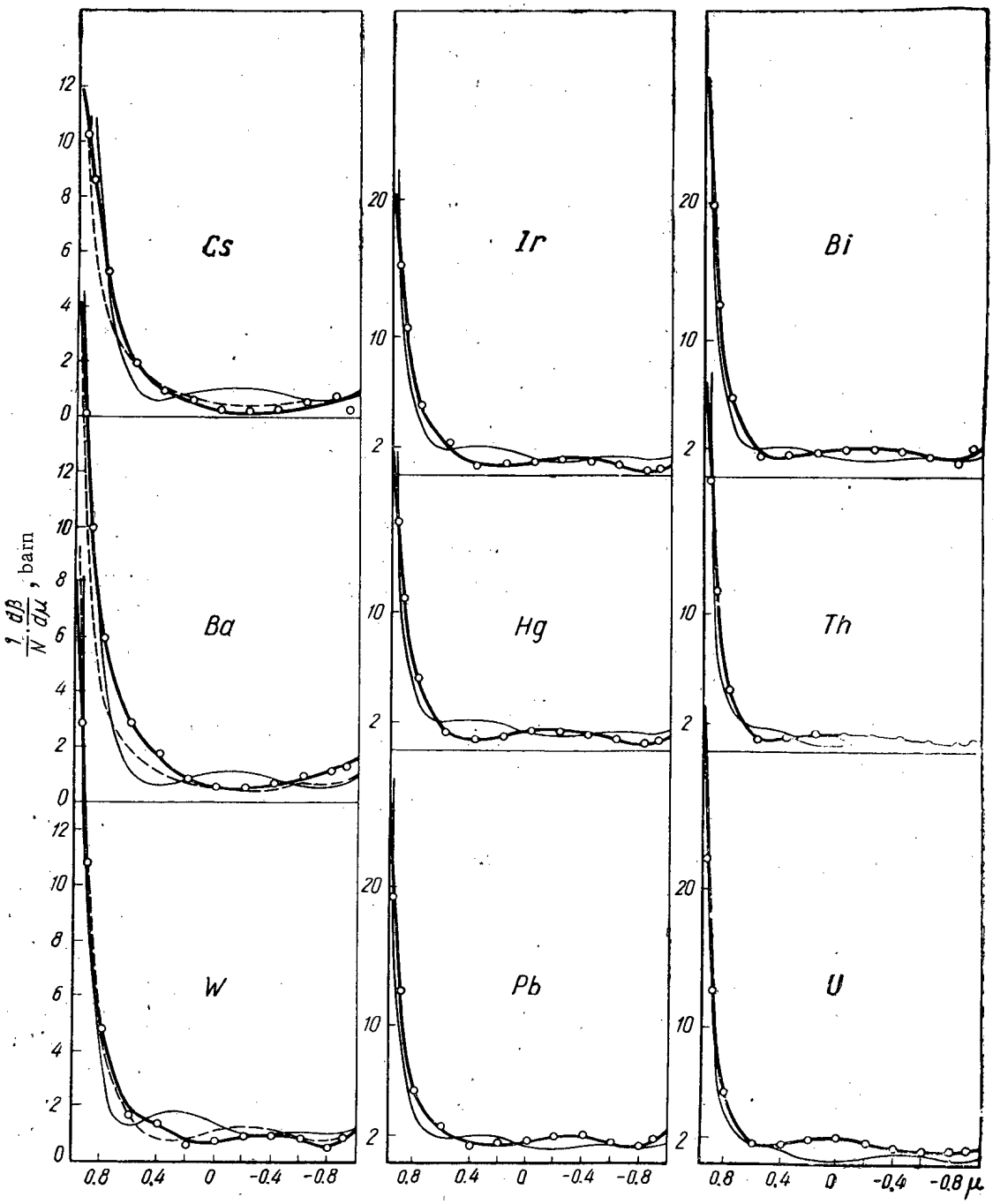

Fig. 1 (cont.)

TABLE 1. Harmonics of the Scattering Cross Section, Approximated by (1)

Elements	β/N	f_1	f_2	f_3	f_4
Li	1.31±0.02	0.389±0.009	0.223±0.009	0.0968±0.0100	0.0439±0.0100
Be	1.75±0.03	0.423±0.009	0.281±0.009	0.123±0.010	0.0343±0.0100
B	1.35±0.02	0.280±0.009	0.184±0.009	0.0730±0.0100	0.0280±0.0100
C	1.54±0.03	0.169±0.009	0.184±0.009	0.0402±0.0100	0.0161±0.0100
N	1.40*	0.204±0.009	0.160±0.009	0.0602±0.0100	0.0206±0.0100
O	1.42±0.03	0.262±0.009	0.173±0.009	0.0752±0.0100	0.0352±0.0100
F	1.93*	0.300±0.009	0.121±0.009	0.0427±0.0100	0.0180±0.0100
Na	1.92±0.04	0.437±0.009	0.186±0.009	0.0850±0.0100	0.0391±0.0100
Mg	1.73±0.04	0.382±0.009	0.234±0.009	0.0912±0.0100	0.0542±0.0100
Al	2.72±0.06	0.399±0.009	0.187±0.009	0.0644±0.0100	0.0251±0.0100
Si	2.02±0.04	0.420±0.009	0.257±0.009	0.0885±0.0100	0.0513±0.0100
P	2.78±0.05	0.448±0.009	0.266±0.009	0.0921±0.0100	0.0436±0.0100
S	2.48±0.05	0.468±0.009	0.283±0.009	0.0879±0.0100	0.0417±0.0100
Cl	2.10±0.05	0.379±0.009	0.265±0.009	0.0751±0.0100	0.0290±0.0100
K	2.86±0.06	0.431±0.009	0.322±0.009	0.111±0.010	0.0629±0.0100
Ti	2.70±0.08	0.423±0.012	0.359±0.013	0.174±0.014	0.0741±0.0140
V	3.18±0.09	0.388±0.012	0.335±0.013	0.154±0.014	0.103±0.014
Cr	2.78±0.09	0.427±0.012	0.357±0.013	0.177±0.014	0.0964±0.0140
Mn	3.12±0.09	0.372±0.012	0.292±0.013	0.149±0.014	0.0619±0.0140
Fe	2.62±0.09	0.407±0.012	0.337±0.013	0.201±0.014	0.0962±0.0140
Co	2.46±0.08	0.385±0.012	0.315±0.013	0.201±0.014	0.103±0.014
Ni	2.62±0.07	0.399±0.009	0.344±0.009	0.195±0.010	0.111±0.010
Cu	2.40±0.07	0.377±0.012	0.290±0.013	0.202±0.014	0.105±0.014
Zn	3.54±0.10	0.322±0.012	0.237±0.013	0.191±0.014	0.0921±0.0140
Br	2.22±0.07	0.465±0.012	0.305±0.013	0.184±0.014	0.190±0.014
Zr	3.26±0.09	0.374±0.012	0.282±0.013	0.145±0.014	0.125±0.014
Nb	3.02±0.09	0.441±0.012	0.311±0.013	0.164±0.014	0.148±0.014
Mo	3.62±0.05	0.463±0.009	0.323±0.009	0.148±0.010	0.130±0.010
Ag	3.26±0.09	0.467±0.012	0.350±0.013	0.164±0.014	0.105±0.014
Cd	4.38±0.10	0.421±0.012	0.284±0.013	0.164±0.014	0.0763±0.0140
Sb	3.50±0.09	0.600±0.012	0.381±0.013	0.205±0.014	0.109±0.014
I	3.14±0.09	0.662±0.012	0.392±0.013	0.241±0.014	0.0802±0.0140
Cs	3.48±0.09	0.569±0.012	0.430±0.013	0.204±0.014	0.0971±0.0140
Ba	4.8±0.10	0.504±0.012	0.387±0.013	0.189±0.014	0.0979±0.0140
W	4.36±0.10	0.532±0.012	0.451±0.013	0.294±0.014	0.202±0.014
Ir	4.24±0.10	0.542±0.012	0.411±0.013	0.257±0.014	0.199±0.014
Hg	4.66±0.10	0.524±0.012	0.382±0.013	0.306±0.014	0.202±0.014
Pb	6.14±0.11	0.472±0.012	0.345±0.013	0.295±0.014	0.168±0.014
Bi	6.34±0.12	0.382±0.012	0.344±0.013	0.228±0.014	0.206±0.014
Th	4.98±0.10	0.518±0.012	0.442±0.013	0.303±0.014	0.276±0.014
U	5.20±0.11	0.481±0.012	0.366±0.013	0.283±0.014	0.227±0.014

*Obtained by normalizing with the data in [6].

Table 1 (cont.)

f_5	f_6	f_7	f_8	f_9	f_{10}
0.0146±0.0100	0.0058±0.0110	—	—	—	—
—	—	—	—	—	—
0.0081±0.0110	0.0850±0.0110	—	—	—	—
0.0061±0.0110	0.0059±0.0110	—	—	—	—
—	—	—	—	—	—
0.0093±0.0110	—	—	—	—	—
0.0004±0.0110	0.0131±0.0100	0.0060±0.0110	0.0142±0.0120	—	—
0.0160±0.0110	—	—	—	—	—
0.0167±0.0110	0.0062±0.0110	0.0067±0.0120	—	—	—
0.0146±0.0100	0.0067±0.0100	0.0048±0.0120	—	—	—
0.0273±0.0110	0.0169±0.0110	0.0090±0.0120	—	—	—
0.0159±0.0110	0.0024±0.0110	0.0040±0.0120	0.0015±0.0120	0.0020±0.0130	—
0.0106±0.0110	—	—	—	—	—
—	—	—	—	—	—
0.0122±0.0110	—	—	—	—	—
0.0305±0.0150	—	—	—	—	—
0.0059±0.0150	0.0140±0.0110	—	—	—	—
0.0104±0.0150	0.0176±0.0160	0.0695±0.0170	—	—	—
0.0108±0.0150	—	—	—	—	—
0.0298±0.0150	0.0111±0.0160	—	—	—	—
0.0256±0.0150	0.0206±0.0160	0.0068±0.0160	0.0098±0.0170	—	—
0.0294±0.0110	0.0226±0.0110	0.0004±0.0120	0.0093±0.0120	0.0051±0.0130	—
0.0412±0.0150	0.0177±0.0150	0.0106±0.0150	0.0049±0.0160	—	—
0.0633±0.0150	0.0102±0.0150	0.0208±0.0150	—	—	—
0.0576±0.0150	0.0574±0.0150	—	—	—	—
0.0610±0.0150	0.0251±0.0150	0.0107±0.0160	—	—	—
0.0554±0.0150	0.0492±0.0150	0.0128±0.0150	0.0115±0.0150	0.0036±0.0160	—
0.0586±0.0110	0.0351±0.0110	0.0015±0.0120	0.0027±0.0120	0.0058±0.0130	—
0.0638±0.0150	0.0356±0.0150	0.0136±0.0160	—	—	—
0..785±0.0150	0.0188±0.0160	0.0155±0.0160	—	—	—
0.0749±0.0150	0.0286±0.0150	0.0197±0.0160	—	—	—
0.104±0.015	0.0192±0.0160	0.0335±0.0170	—	—	—
0.0474±0.0150	0.0151±0.0160	—	—	—	—
0.0637±0.0150	0.0395±0.0160	0.0173±0.0160	0.0082±0.0170	—	—
0.849±0.0150	0.0739±0.0160	0.0238±0.0170	0.0179±0.0170	—	—
0.0731±0.0150	0.0472±0.0160	0.0075±0.0170	0.0074±0.0170	—	—
0.0828±0.0150	0.0418±0.0160	0.0155±0.0170	0.0097±0.0170	0.0027±0.0180	—
0.111±0.015	0.0655±0.0160	0.0638±0.0170	0.0225±0.0170	0.0303±0.0180	—
0.0669±0.0150	0.0609±0.0150	0.0031±0.0160	0.0076±0.0170	—	—
0.120±0.015	0.0984±0.0160	0.0169±0.0160	0.0272±0.0170	0.0032±0.0170	0.0118±0.0180
0.125±0.015	0.0604±0.0160	0.0248±0.0160	0.0166±0.0170	—	—

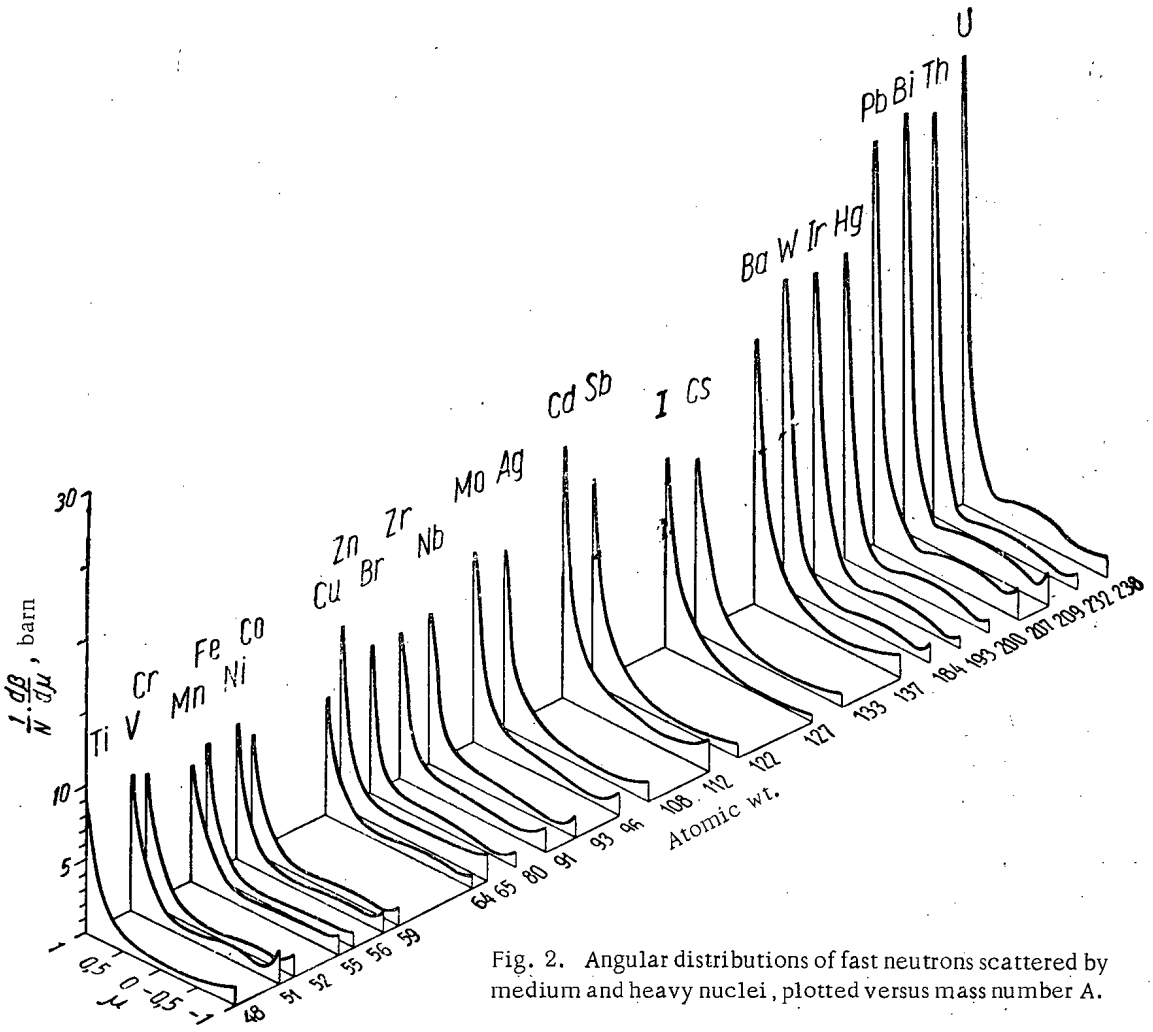

Fig. 2. Angular distributions of fast neutrons scattered by medium and heavy nuclei, plotted versus mass number A.

TABLE 2. Matrix of Correlation Coefficients $\rho_{LL'}$ for Magnesium

L'	L							
	0	1	2	3	4	5	6	7
0	1	0.12	0.35	0.05	0.22	0.06	0.15	—0.05
1	0.12	1	0.08	0.40	0.15	0.22	0.02	—0.32
2	0.35	0.08	1	0.04	0.35	0.05	0.15	—0.05
3	0.05	0.40	0.04	1	0.03	0.21	0.01	—0.25
4	0.22	0.15	0.35	0.03	1	0.06	0.18	—0.03
5	0.06	0.22	0.05	0.21	0.06	1	0.12	—0.13
6	0.15	0.02	0.15	0.01	0.18	0.12	1	0.05
7	—0.05	—0.32	—0.05	—0.25	—0.03	0.13	0.05	1

LITERATURE CITED

1. A. G. Guseinov and M. N. Nikolaev, Atomnaya Énergiya, 12, 243 (1962).
2. A. I. Leipunskii et al., Atomnaya Énergiya, 5, 277 (1958).
3. S. M. Ermakov, V. E. Kolesov, and G. I. Marchuk, In Symposium "Neitronnaya fizika" [Neutron Physics], Moscow, Atomizdat (1961), p. 314.
4. L. P. Abagyan et al., Group Constants for Calculation on Nuclear Reactors [in Russian], Moscow, Atomizdat (1964).
5. A. I. Leipunskii et al., Atomnaya Énergiya, 11, 498 (1961).
6. J. Hughes, Atlas of Effective Neutron Cross Sections of the Elements [in Russian translation], Moscow, Izd-vo AN SSSR (1955).

NUMERICAL CALCULATIONS ON THE PENETRATION OF γ-QUANTA THROUGH MATTER

(UDC 539.121.78:539.166)

V. S. Galishev

Translated from Atomnaya Énergiya, Vol. 18, No. 4, p. 415, April, 1965.
Original article submitted April 30, 1964

An analytical treatment of the transmission and reflection of γ-radiation by a plane parallel layer of finite thickness is given in [1]. In this note the method is used for calculating the energy build-up factor of radiation passing through a layer. The energy of the plane source is taken as 10 MeV. Lead is chosen as absorber. All the calculations were carried out on the "Ural-1" electronic computer.

The energy build-up factor is defined as the ratio of the integral energy flux transported by all the γ-quanta to the integral flux for the primary quanta. The integral energy flux of the γ-quanta in turn is found in terms of the flux-density function of the γ-quanta. The flux density of scattered γ-quanta transmitted and reflected by the plane parallel layer, according to [1], may be presented as an expansion (27) in orders of scattering. The flux densities for singly scattered γ-quanta have simple analytical expressions satisfying Eq. (12) and boundary conditions (13), while those for γ-quanta experiencing two, three, etc., scatterings are found by means of recurrence relations (23) and (24).

The results of our calculations of energy build-up factors are compared with those found by the Monte Carlo method [2] in Table 1. The results agree closely for small layer thicknesses ($\mu_0 a$ = 0.5-1). This confirms the validity of the theory developed in [1]. For large layer thicknesses ($\mu_0 a$ = 2-4), however, our calculations give low values for the build-up factors, indicating the inapplicability of our computing method for comparatively thick absorbers.

The author thanks N. A. Ipatova for help in programing the problem and carrying out the calculations.

TABLE 1. Energy Build-up Factors for the Passage of γ-Radiation at 10 MeV Energy through a Layer of Lead

$\mu_0 a$	Build-up factor	
	our results	data of [2]
0.5	1.04	1.03
1	1.06	1.08
2	1.10	1.17
4	1.14	1.40

LITERATURE CITED

1. V. S. Galishev, "Atomnaya Énergiya," 14, 453 (1963).
2. M. Berger and J. Doggett, J. Res. Nat. Bur. Standards, 56, 89 (1956).

SPATIAL ENERGY DISTRIBUTION AND DOSE RATE OF γ-RADIATION FROM UNIDIRECTIONAL AND ISOTROPIC Co^{60} SOURCES AT THE GROUND – AIR INTERFACE

(UDC 539.121.72 + 539.122)

S. M. Ermakov, B. A. Efimenko, V. G. Zolotukhin,
Yu. A. Kolevatov, and V. I. Kukhtevich

Translated from Atomnaya Énergiya, Vol. 18, No. 4,
pp. 416-418, April, 1965
Original article submitted Agust 13, 1964

The present article provides the results obtained in measuring and calculating, by means of the Monte Carlo method, the spatial and energy distributions of scattered γ-radiation from a unidirectional Co^{60} source (mean energy: 1.25 MeV) for distance R between the source and the detector equal to 15 and 30 m and the same elevation H(2, 10, 30, and 53 m) of the source and the detector above the ground. The measurements and calculations were performed for two orientation angles θ_0(60 and 90°) of the unidirectional source.

The experimental device consisted of the source S, the detector D, and a girder for fixing the distance R between the source and the detector (Fig. 1). The source (a radioactive Co^{60} specimen) had a spherical shape with a diameter of 0.005 m. The source was covered with a shade shield whose total flare angle was 5° in order to reduce the background of unscattered radiation. There was no radiation scattered within the source. A scintillation spectrometer with a NaI(Tl) crystal whose diameter and length were equal to 0.04 m served as the detector of γ-quanta. The spectrometer's energy resolution for E_0 = 0.661 MeV was 11%. The matrix method was used for transforming the amplitude distribution of pulses into the energy distribution [1]. In measurements, the source was enclosed in a uranium container with a collimating opening defining an angle $\Delta\gamma = 31.2°$. The measurements made it possible to determine the absolute flux values in dependence on the energy of γ-quanta. A standard source whose radiation intensity was known with an accuracy to ± 2% was used for calibration. The mean error in determining the energy distributions was 10-15%.

The variant of the Monte Carlo method used for calculating the γ-radiation spectrum at a fixed point in space, produced by a unidirectional source with a certain given energy, is known as the method of local flux calculation[2]. This method is especially efficient in the case where the problem is not characterized by spatial and angular symmetry and also in the presence of considerable flux gradients at small distances. These conditions prevail near the interface between two media whose densities are widely different.

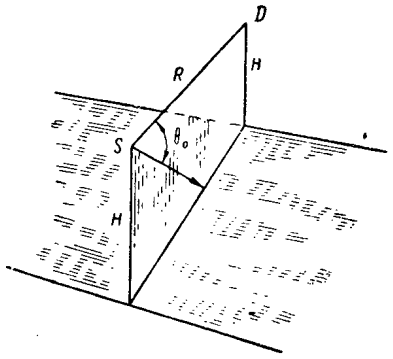

Fig. 1. Experimental and calculation geometry for determining the spatial distribution due to a unidirectional point source.

Since the contribution of singly scattered radiation amounts to a considerable share of the scattered flux, it is advisable to separate the analytical spectrum of singly scattered radiation. This was done by using the systematic sampling technique, which was described in [3]. In the case of a unidirectional source, the random variable determining the fluctuation of the singly scattered flux is the mean free path t. In the n-th γ-quantum history, the mean free path t_n before the first scattering was determined by means of the random number

$$\alpha_n = \frac{N-n+1}{N}$$

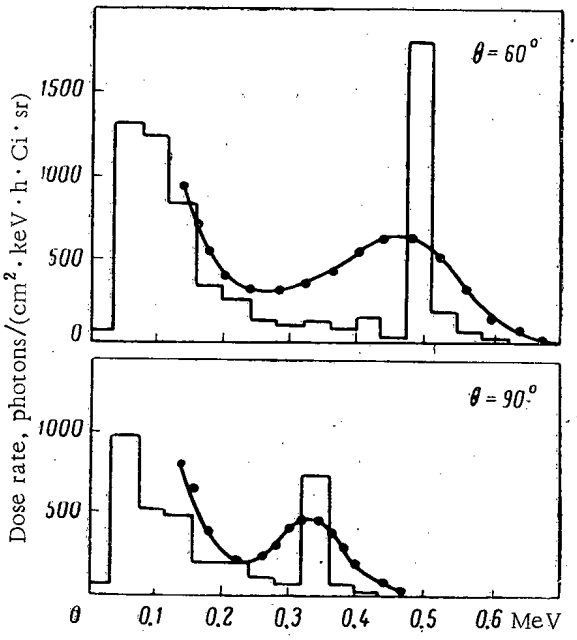

Fig. 2. Spatial and energy distributions of scattered γ-radiation from a unidirectional Co^{60} source. ●) Experimental data; the histograms represent the calculation results.

TABLE 1. Spatial Distribution of the Dose Rate Due to a Unidirectional Source

Orientation angle of the source, degree	Dose rate of scattered γ-radiation mR/(h · Ci · sr)	
	Experiment	Calculation
60	0.047	0.040
90	0.019	0.015

TABLE 2. Spatial Distribution of the Dose Rate Due to an Isotropic Source

H, m	Dose rate, mR/(h · Ci)				
	R = 15 m			R = 30 m	
	Experiment	Calculation	Data from [4]	Experiment	Calculation
2	0.93	0.95	—	0.30	0.31
10	0.49	0.57	0.56	0.27	0.31
∞	0.39	0.40	—	0.20	0.19

by using the ordinary equation

$$1-\alpha_n = \int_0^{t_n} l^{-\tau(t)}\, d\tau\,(t),$$

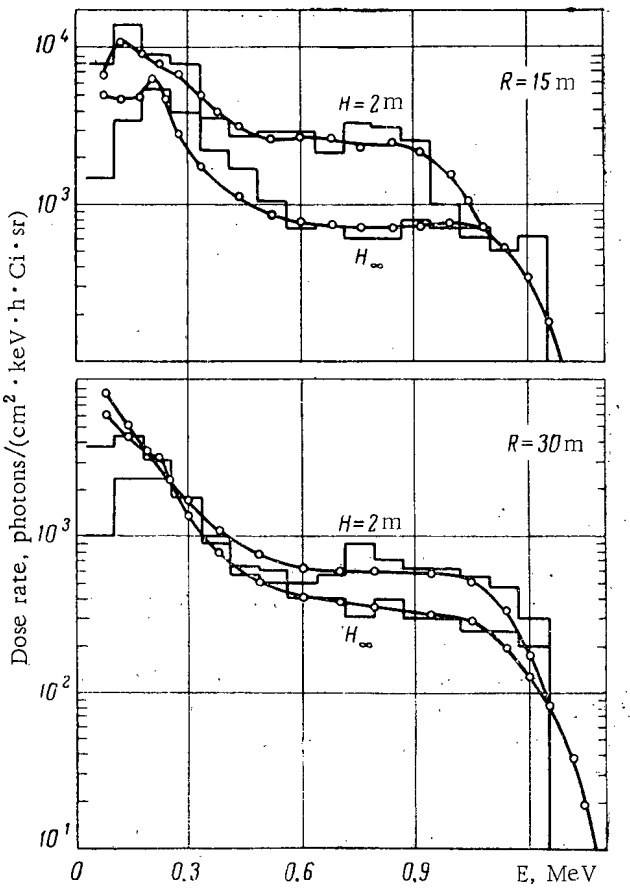

Fig. 3. Spatial and energy distributions of scattered γ-radiation from an isotropic Co^{60} source. ●) Experimental data; the histograms represent the calculation results.

where N is the total number of histories, and $\tau(t)$ is the optical distance. In other respects, the method of local flux calculation was used without changes. A history was interrupted when the γ-quantum energy dropped below 10 keV or when the γ-quantum "weight" was reduced by a factor larger than 10^3. The program provided for the spectral analysis of radiation for determining the distance between the source and the detector in a given history, so that the sampling was correlated.

For calculating a single variant characterized by the direction Ω_0 and the energy E_0 of the source's γ-quanta, it is sufficient to have 2000 histories, which involves a statistical error whithin 5-7% in the dose and an error of the order of 20% in the spectrum.

The density of the earth was $1.8 \cdot 10^3$ kg/m^3 at the location of experiments; this value was also used in calculations. The density of air was assumed to be 1.29 kg/m^3.

Figure 2 shows the calculated and measured spatial and energy distributions of scattered γ-radiation from a unidirectional source for R = 15 m and H = 2 m. The broadening of maximums that can be observed in the experimental data is connected with the finite energy resolution of the spectrometer and the relatively large angular aperture of the source. The ends of spectra in the high energy region correspond to γ-rays singly scattered in air at the angle θ_0. The intensity maximums at energies of 0.33 and 0.45 MeV are due to single scattering from the ground. A much better agreement is observed in comparing the spatial distributions of dose rates produced by a unidirectional source (Table 1).

Figure 3 shows the calculated and measured spatial and energy distributions of scattered γ-radiation from an isotropic source for the two cases H = 2 m and H = ∞ for R values equal to 15 and 30 m. The distributions for the 30- and 53-m elevations virtually coincide with the distribution for H = ∞. The theoretical and experimental spectra agree with each other within the limits of experimental and calculation (statistical) errors.

It is seen from Table 2 that the calculated and experimental dose rates are in good agreement. For the sake of comparison, the table also provides the experimental data borrowed from [4], where the spatial distribution of the dose rate at the interface between the ground and air was measured for R = 3.15-21.4 m and H = 2.7-17.3 m with a Co^{60} isotropic point source.

The authors are grateful to Yu. I. Bublik and K. G. Ivanov for their assitance in performing the experiments.

LITERATURE CITED

1. Yu. A. Kazanskii, Pribory i Tekhnika Éksperimenta, No. 4, 32 (1959).
2. V. G. Zolotukhin and S. M. Ermakov, In the Collection: Problems in the Physics of Reactor Shields, Edited by D. L. Broder et al., [in Russian], Moscow, Gosatomizdat (1963), p. 171.
3. H. Steinberg, Nucl. Sci. Engng., 15, 142 (1963).
4. Reactor Handbook, Vol. 3, Part B, Shielding, Edited by E. Blizard, New York (1962), p. 271.

INDUCED γ-ACTIVITY IN POLYETHYLENE AS A RESULT OF NEUTRON IRRADIATION

(UDC 543.53:678.742)

N. A. Dubinskaya, A. Yu. Lyul', and L. L. Pelekis

Translated from Atomnaya Énergiya, Vol. 18, No. 4,
pp. 418-419, April, 1965
Original article submitted March 30, 1964

One of the problems arising in performing activation analysis is the choice of the material for the specimen's container and packing. It is desirable that this material be free from elements which would produce noticeable induced activity as a result of neutron irradiation, which is especially important in using the instrumental analysis method without repacking the specimen.

At the present time, Kapron, nylon, polyethylene, polypropylene, and Teflon are used as materials for the container and packing in the case of short irradiation exposure times (up to a few hours) [1-4]. From among the above materials, nylon and Kapron are characterized by the least induced activity; however, their radiation resistance is low, which explains the wider use of polyethylene.

We investigated the characteristics of induced γ-activity of high-pressure (HP) and low-pressure (LP) polyethylene, produced by various domestic enterprises. Granulated polyethylene was irradiated in the vertical channel of the IRT reactor in a thermal neutron flux of $9 \cdot 10^{12}$ neutrons/(cm^2 · sec), using two irradiation times t_{irr}: 15 min and 4 h.

The induced γ-activity was estimated with respect to the integral load, measured by means of a scintillation γ-spectrometer with a 40 x 40-mm NaI(Tl) crystal. The distance between the source and the crystal was 4 mm. The measurement results are given in Table 1; besides data for the domestically produced polyethylene, this table also provides data for the British-made polyethylene—Alkathene WJG.

Investigations of γ-spectra and induced activity decay curves have shown that the γ-radiation of neutron-irradiated polyethylene is due to the presence of the Al^{28}, Cl^{38}, Mn^{56}, Na^{24}, and Cu^{64} radioactive isotopes in the case of high-pressure polyethylene and the Al^{28}, Br^{80}, Cl^{38}, Mn^{56}, Na^{24}, and Br^{82} isotopes in the case of low-pressure polyethylene.

TABLE 1. Integral Load Due to 1 g Neutron-Irradiated Polyethylene, Measured by Means of the Scintillation Spectrometer

Specimen No.	Locality of polyethylene production	Polyethylene type	t_{irr} = 15 min, t_{cool} = 5 min		t_{irr} = 4 h, t_{cool} = 1.5 h	
			integral load (per 1 g polyethylene)			
			pulses/sec	rel. units	pulses/sec	rel. units
1	Ufa	HP	6,620	1.5	3,970	2.3
2	Okhta	HP	5,380	1.1	3,980	2.3
3	Great Britain	HP	7,650	1.6	3,580	2.1
4	Groznyi	LP	540,000	120	125,000	73.5
5	Salavat-Yulaev	HP	4,500	1	1,700	1
6	Kuibishev District	LP	330,000	73.4	71,000	41.8

TABLE 2. Cooling-Off Times Necessary for Tenfold and Hundredfold Reductions in the Polyethylene Activity

Specimen No.	Polyethylene type	Attenuation factor	t_{cool}, r: t_{irr} = 15 min	t_{cool}, r: t_{irr} = 4 h
3	HP	10	1.2	20
3	HP	100	10.3	71
4	LP	10	1.5	44.5
4	LP	100	10.0	160

TABLE 3. Content of the Elements Detected in 1 g Polyethylene, %

Element	LP polyethylene	HP polyethylene
Mn	$2.8 \cdot 10^{-5}$	$2.6 \cdot 10^{-6}$
Na+Cu	$3.7 \cdot 10^{-4}$	$3.3 \cdot 10^{-5}$
Br	$5.7 \cdot 10^{-4}$	
Al	$8.9 \cdot 10^{-3}$	$2.0 \cdot 10^{-4}$
Cl	$1.8 \cdot 10^{-2}$	$2.1 \cdot 10^{-4}$

After the termination of irradiation, the total specific activities with respect to the above isotopes were equal to 4 and 8 μCi/g for high-pressure polyethylene and 150 and 400 μCi/g for low-pressure polyethylene (the irradiation times were equal to 15 min and 4 h, respectively).

Table 2 provides the cooling-off times (t_{cool}) necessary for tenfold and hundredfold reductions in the activity.

In order to estimate the percentages of the elements detected (per 1 g polyethylene), we decomposed the decay curves into their components. The average results for low-pressure polyethylene (specimen No. 4) and high-pressure polyethylene (specimen No. 2) are given in Table 3.

In these experiments, we did not seek to determine accurately the percentages of impurities. The experimental error was 30-40%.

A knowledge of the technology of polyethylene production provides a basis for assuming that polyethylene is contaminated with the above elements in using polymerization catalysts and also during the purification of the raw material and the polymerization product.

LITERATURE CITED

1. W. Meinke, Nucleonics, 17, No. 9, 86 (1959).
2. P. Stallowood and W. Mott, D. Fanale, Anal. Chem., 35, 6 (1963).
3. F. C. Acderscheld, Proceedings of a Seminar, Production and Use of Short-Lived Radioisotopes from Reactors, Vienna (1963), p. 31.
4. W. W. Meinke, Ibiden, p. 93.

ASYMPTOTIC SOLUTION OF THE KINETIC EQUATION AND THE DIFFUSION CHARACTERISTICS

(UDC 621.039.51.12)

Ya. I. Granovskii and A. A. Kostritsa

Translated from Atomnaya Énergiya, Vol. 18, No. 4,
pp. 419-422, April, 1965
Original article submitted March 30, 1964; final version submitted July 28, 1964

The diffusion theory is usually identified with the P_1-approximation of the method of spherical harmonics. However, the same properties are also observed in the case of exact solutions of the kinetic equation, which has been investigated only for the simplest scattering functions. We shall attempt to analyze more thoroughly the diffusion properties of the asymptotic part of the kinetic equation's solution for the general case of scattering and source anisotropy. It is found that these properties essentially constitute the intrinsic properties of the kinetic equation's Green function.

The linearity of the kinetic equation of neutron transport makes it possible to write the solution of this equation in the following form:

$$N(\mathbf{r}, t, \mathbf{n}) = \int e^{i(\mathbf{qr} - \omega t)} S(\mathbf{q}, \omega, \mathbf{n}) G(\mathbf{q}, \omega, \mathbf{n}) d\mathbf{q}\, d\omega, \tag{1}$$

where $S(\mathbf{q}, \omega, \mathbf{n})$ is the Fourier transform of the neutron source, and $G(\mathbf{q}, \omega, \mathbf{n})$ is the Green function.

The behavior of the neutron density at large distances (asymptotic behavior) is determined by the position of the singular points $G(\mathbf{q}, \omega, \mathbf{n})$ in the neighborhood of $\mathbf{q} = 0$. If the singularity closest to zero is a pole, the asymptotic density and flux obey the diffusion equations.

The singular points of the Green function coincide with those $\mathbf{q}$ values for which the homogeneous kinetic equation

$$\left(-i\omega + i\mathbf{qv} + \frac{v}{l}\right) N(\mathbf{q}, \omega, \mathbf{n}) = \frac{v}{4\pi l_s} \int N(\mathbf{q}, \omega, \mathbf{n}) \mu(\Phi) d\Omega' \tag{2}$$

has a nontrivial solution. Here, v is the neutron velocity and l, l_s are the mean free path and the scattering length, respectively.

If we expand the scattering function $\mu(\Phi)$ in a series with respect to Legendre polynomials,

$$\mu(\Phi) = \sum_j \mu_j' P_j(\cos\Phi), \tag{3}$$

we can calculate the integral with respect to angles by using the summation theorem; we then obtain

$$N = \frac{1}{4\pi} \sum_j \frac{\mu_j P_j(\cos\theta) N_j}{z - \cos\theta}, \tag{4}$$

where

$$\mu_j = \frac{i\mu_j'}{q l_s}, \tag{5a}$$

$$z = \frac{\omega}{qv} + \frac{i}{ql} \,. \tag{5b}$$

The values

$$N_j = \int N P_j(\cos\theta)\, d\Omega \tag{6}$$

satisfy the system of algebraic equations

$$N_k = \sum_j \mu_j C_{jk} N_j, \tag{7}$$

which is obtained from (4). The C_{jk} coefficients can be expressed in terms of Legendre functions of the second kind:

$$C_{jk} = \frac{1}{4\pi} \int \frac{P_j(\cos\theta)\, P_K(\cos\theta)\, d\Omega}{z - \cos\theta} = P_j(z)\, Q_k(z) \quad (j \leqslant k). \tag{8}$$

Diffusion Length Equation

The homogeneous system (7) has a nontrivial solution if its determinant is equal to zero:

$$\Delta = |\, \delta_{jk} - \mu_j C_{jk} \,| = 0. \tag{9}$$

This condition determines the z value—the only free parameter in Eq. (9)—of the q value if we consider only the steady-state case where $\omega = 0$. The q value is connected with the attenuation distance of the asymptotic part of a neutron flux with the diffusion length L.

In expanded form, Eq. (9) is given by

$$\Delta = \begin{vmatrix} 1-\mu_0 Q_0 & -\mu_1 Q_1 & -\mu_2 Q_2 & -\mu_3 Q_3 \ldots \\ -\mu_0 Q_1 & 1-\mu_1 P_1 Q_1 & -\mu_2 P_1 Q_2 & -\mu_3 P_1 Q_3 \ldots \\ -\mu_0 Q_2 & -\mu_1 P_1 Q_2 & 1-\mu_2 P_2 Q_2 & -\mu_3 P_2 Q_3 \ldots \\ -\mu_0 Q_3 & -\mu_1 P_1 Q_3 & -\mu_2 P_2 Q_3 & 1-\mu_3 P_3 Q_3 \ldots \\ \ldots & \ldots & \ldots & \ldots \end{vmatrix} = 0. \tag{10}$$

This equation can be written in a much simpler manner if we subtract from the n-th row the first row multiplied by P_n:

$$\Delta = \begin{vmatrix} 1-\mu_0 Q_0 & -\mu_1 Q_1 & -\mu_2 Q_2 & -\mu_3 Q_3 \ldots \\ \mu_0 W_{10} - P_1 & 1 & 0 & 0 \ldots \\ \mu_0 W_{20} - P_2 & \mu_1 W_{21} & 1 & 0 \ldots \\ \mu_0 W_{30} - P_3 & \mu_1 W_{31} & \mu_2 W_{32} & 1 \ldots \\ \ldots & \ldots & \ldots & \ldots \end{vmatrix} = 0, \tag{11}$$

where

$$W_{ik} = P_i Q_k Q_i \tag{12}$$

is a polynomial whose degree is $|i - k| - 1$.

By using the relationship

$$Q_k(z) = P_k(z)\, Q_0(z) - W_{k-1}(z), \tag{13}$$

borrowed from [1], all the logarithmic terms contained in Q_0 can be separated from Eq. (11):

$$\mu_0 Q_0(z) = \frac{\Delta(W)}{\Delta(P)} . \tag{14}$$

The determinants in this expression differ from the determinant in Eq. (11) only by the first row, which is given by

$$\text{in } \Delta(W): 1 \quad \mu_1 W_0 \quad \mu_2 W_1 \quad \mu_3 W_2 \ \ldots \quad \text{in } \Delta(P): 1 \ \frac{\mu_1}{\mu_0} P_1 \frac{\mu_2}{\mu_0} P_2 \frac{\mu_3}{\mu_0} P_3 \ \ldots$$

All elements of these determinants and, consequently, the determinants themselves constitute polynomials with respect to z.

Equation (14) constitutes a generalization of the well-known transcendental equations used for determining the diffusion length (see, for instance, equations (32.27) and (32.36) in [2]). Equation (14) assumes a simple form for polynomial scattering laws, since $\mu_{j>n} = 0$ in these cases, and both determinants are cut off at the (n + 1)-th row.

Let us consider two examples for the steady-state case.

1. Linear anisotropy: $\mu_0' = 1$, $\mu_1' = 3c_1$, $\mu_{j\geq 2}' = 0$. Here,

$$\Delta(W) = \begin{vmatrix} 1 & \mu_1 \\ \mu_0 W_{10} - P_1 & 1 \end{vmatrix} = 1 - \mu_1(\mu_0 - P_1); \quad \Delta(P) = \begin{vmatrix} 1 & \frac{\mu_1}{\mu_0} P_1 \\ \mu_0 W_{10} - P_1 & 1 \end{vmatrix} = 1 - \frac{\mu_1}{\mu_0} P_1(\mu_0 - P_1).$$

After introducing the diffusion length by using the equation $i/q = L$, we obtain $P_1(z) = L/l$, $\mu_0 = L/l_s$, $\mu_1 = 3c_1 L/l_s$. Finally,

$$\mu_0 - P_1 = \frac{L}{l_s} - \frac{L}{l} = -\frac{L}{l_a} , \tag{15}$$

where l_a is the absorption length.

By substituting these values in (14), we find

$$\frac{L}{2l_s} \ln \frac{L+l}{L-l} = \frac{1 + \frac{3c_1 L^2}{l_s l_a}}{1 + \frac{3c_1 L^2}{l l_a}} , \tag{16}$$

which coincides with (32.36) in [2]. For $L \gg l$, Eq. (16) leads to the expression for the diffusion length that is obtained in the transport approximation:

$$L_0^2 = \frac{l_a l_s}{3} \left(1 - c_1 \frac{l}{l_s}\right)^{-1} . \tag{17}$$

2. Quadratic anisotropy: $\mu' = 1$, $\mu_1' = 0$, $\mu_2' = \beta$, $\mu_{j\geq 3}' = 0$. Here,

$$\frac{\Delta(W)}{\Delta(P)} = \frac{1 - \mu_2 W_1(\mu_0 W_{20} - P_2)}{1 - \frac{\mu_2}{\mu_0} P_2(\mu_0 W_{20} - P_2)} .$$

Considering that $W_{20} = W_1 = (3/2)z$, we obtain

$$\mu_0 W_{20} - P_2(z) = \frac{1}{2}\left(1 - \frac{3L^2}{ll_a}\right),$$

so that

$$\frac{L}{2l_s}\ln\frac{L+l}{L-l} = \frac{1-\beta\frac{3L^2}{4ll_s}\left(1-\frac{3L^2}{ll_a}\right)}{1+\frac{\beta}{4}\left(1-\frac{3L^2}{l^2}\right)\left(1-\frac{3L^2}{ll_a}\right)}. \tag{18}$$

Rayleigh scattering, for which $\beta = 1/2$, is an important particular case of the example considered above. By solving (18) with respect to L^2 (for $L \gg l$), we find the expression for the diffusion length in the case of Rayleigh scattering:

$$L^2 = \frac{ll_a}{3}\left(1+\frac{8l_s}{9l_a}\right)^{-1}. \tag{19}$$

Fick Law in the Theory of Neutron Transport

The basic law in the elementary diffusion theory is the proportionality of the flux of neutrons to the gradient of their density (Fick law). Since, in the case of asymptotic behavior, all N_k depend exponentially on the distance with the attenuation distance L, the validity of the Fick law is obvious. In the case of plane geometry, the diffusion coefficient is given by

$$D = vL\frac{N_1}{N_0}. \tag{20}$$

In the case of asymptotic behavior, it can be considered that all N_k values satisfy the homogeneous system (7) with the determinant $\Delta = 0$. Due to this relationship, the N_k/N_0 ratios are fixed in a well-defined manner. In order to find N_1/N_0, we shall subtract the first equation of system (7), multiplied by P_1, from the second equation:

$$N_1 - P_1N_0 = \sum_j \mu_j (C_{j1} - P_1C_{j0}) N_j = \mu_0 (Q_1 - P_1Q_0) N_0 = -\mu_0 N_0. \tag{21}$$

Consequently, $N_1/N_0 = P_1 - \mu_0$, and

$$D = vL(P_1 - \mu_0). \tag{22}$$

In the case of steady-state conditions, taking into account Eq. (15), we arrive at the well-known equation

$$D = \frac{vL^2}{l_a}, \tag{23}$$

i. e., the factor of proportionality between the flux and the gradient of neutron density in the case of asymptotic behavior is related to the attenuation distance in the same manner as in the diffusion approximation. The effect of the scattering anisotropy on the diffusion coefficient is limited to the change in the diffusion length L, which is determined from (14). The anisotropy of sources does not affect the L and D values.

In the case of unsteady-state condition this important property of the asymptotic behavior [see (23)] vanishes. For instance, for a uniformly moving source,

$$D = \frac{vL^2}{l_a}\left(1-\frac{ul_a}{vL}\right), \tag{24}$$

where u is the velocity of the source.

Since all the N_j/N_0 values are determined in a well-defined manner by system (7), one readily arrives at the other characteristic of the distribution of neutrons that have experienced a large number of collisions: the angular distribution does not depend on the anisotropy of the source. The dependence of the asymptotic neutron density N_{as} on the intensity and the angular distribution of the source consists in the constant factor N_0, which, or course, cannot be determined on the basis of the homogeneous Eq. (2).

In the presence of sources, the solution of the nonhomogeneous equation leads to the following system of equations instead of (7):

$$N_k = \sum_j \mu_j C_{jk} N_j + F_k \tag{25}$$

for Fourier transforms, where

$$F_k = \frac{S(\mathbf{q}, \omega)}{4\pi} \int \frac{f(\theta) P_k \, d\Omega}{-i\omega + i\mathbf{qv} + v/l} = \frac{i}{qv} S(\mathbf{q}, \omega) \varphi_k, \tag{26}$$

where $f(\theta)$ is the angular distribution of the source neutrons.

The Fourier transform of the function to be determined is given by

$$N = \frac{iS(\mathbf{q}, \omega)}{4\pi qv (z - \cos\theta) \Delta} \sum_j \mu_j \Delta_j P_j (\cos\theta) + \frac{iS(\mathbf{q}, \omega) f(\theta)}{4\pi qv (z - \cos\theta)}, \tag{27}$$

where Δ_j differs from Δ, determined by Eq. (11), by the substitution of the φ_0, φ_1, φ_2, ... values for the j-th column.

Reverting from the Fourier transform (27) to the neutron density, we obtain the solution of the problem of neutron distribution about the source. Let us consider the asymptotic part of the solution, which is determined by the contribution of the pole for $\Delta = 0$ in the particular case of a source defined by the expression

$$S(\mathbf{q}, \omega, \theta) = \frac{s_0}{2\pi} \delta(\omega - uq_x) \delta(q_y) \delta(q_z) f(\theta). \tag{28}$$

From (27), we obtain the asymptotic density of neutrons in front of a moving source:

$$N_{as} = Ae^{-(x-ut)/L} \frac{\sum_j \mu_j \Delta_j P_j (\cos\theta)}{z - \cos\theta}. \tag{29}$$

Here,

$$A = \frac{s_0}{8\pi^2} \cdot \frac{L}{v} \cdot \frac{2\pi i}{\delta}, \tag{30}$$

$$z = \frac{L}{l} + \frac{u}{v}, \tag{31}$$

where $\delta = \Delta'(i/L)$, while $i/q = L$ was used in Δ_j.

From the equation

$$N_k = 4\pi A e^{-\frac{x-ut}{L}} \Delta_k, \tag{32}$$

we find

$$j=vN_1=-vL\frac{\Delta_1}{\Delta_0}\cdot\frac{dN_0}{dx} \tag{33}$$

and, consequently,

$$D=vL\frac{\Delta_1}{\Delta_0}. \tag{34}$$

In order to calculate the ratio of determinants in Eq. (34), we note the following expressions derived from (29):

$$\left.\begin{aligned} N_0(x,t) &= 4\pi Ae^{-(x-ut)/L}\sum_j \mu_j\Delta_jQ_j\ , \\ N_1(x,t) &= 4\pi Ae^{-(x-ut)/L}\left(P_1\sum_j \mu_j\Delta_jQ_j-\mu_0\Delta_0\right)\ , \\ N_2(x,t) &= 4\pi Ae^{-(x-ut)/L}\left(P_2\sum_j \mu_j\Delta_jQ_j-\frac{3}{2}P_1\mu_0\Delta_0-\frac{1}{2}\mu,\Delta_1.\right. \end{aligned}\right\} \tag{35}$$

The relationships between the determinants can readily be obtained from Eqs. (32) and (35):

$$\Delta_1=\Delta_0(P_1-\mu_0), \tag{36}$$

$$\Delta_2=\Delta_0\left[(P_1-\mu_0)\left(\frac{3}{2}P_1-\frac{1}{2}\mu_1\right)-\frac{1}{2}\right]. \tag{37}$$

From (34) and (36), we naturally obtain Eq. (23), while, from (36), (37), and similar equations, we find, after substitution in (29), that the angular distribution N_{as} does not depend on the source.

Finally, it follows from (36)-(37) that, for u = 0,

$$j=-\frac{\frac{vl}{3}}{1-c_1\frac{l}{l_s}}\left(1+2\frac{N_2}{N_0}\right)\frac{dN_0}{dx}. \tag{38}$$

Expression (38) is a consequence of the generalized Fick law [3], which was derived for isotropic sources. This relationship holds for asymptotic behavior and for anisotropic sources. In using the method of spherical harmonic and cutting off the infinite system at the P_1-approximation, it is assumed that

$$2\frac{N_2}{N_0}=2\frac{\Delta_2}{\Delta_0}=\frac{L^2}{L_0^2}-1\ll 1, \tag{39}$$

where L is the exact expression for the diffusion length, which is determined from (14), while L_0 is the attenuation distance of the solution in the P_1-approximation.

LITERATURE CITED

1. I. S. Gradshtein and I. M. Ryzhik, Tables of Integrals, Sums, Series, and Products [in Russian], Moscow, Fizmatgiz (1962).
2. A. D. Galanin, Theory of Nuclear Thermal Reactors [in Russian], Moscow, Atomizdat (1959).
3. S. Glasstone and M. C. Edlund, Elements of Nuclear Reactor Theory, Van Nostrand (1954).

ROD-LIQUID INTERACTION IN CONTROL AND PROTECTION SYSTEMS

(UDC 621.039.515)

R. R. Ionaitis

Translated from Atomnaya Énergiya, Vol. 18, No. 4,
pp. 422-426, April, 1965
Original article submitted January 17, 1964; final revision submitted September 11, 1964

The rods of a reactor control and protection system (CPS), which are smooth or segmented circular cylinders, flat plates, or cruciform rods (Fig. 1), usually move in a liquid. They are therefore subject to a hydrodynamic force [1], and in a CPS this force may change (increase or decrease) the load on the drive system, change the response time, decelerate the rods at the end points of their motion, raise (left) the rods, and increase the time required for preparing the system for operation.

Since the CPS rods move in channels, the liquid flow acting on them is restricted. The available literature on the questions involved in the motion of an elongated solid in such a flow is scanty, although it does contain experimental data [2, 3], as well as some recommendations on calculation [2, 4, 5]. In addition, approximate calculations of the hydrodynamic force are made in engineering practice; the pressure drop in the clearance slot between the channel wall and the moving CPS rod is defined as the pressure drop in a slot with stationary walls.

The calculation method proposed in the present study was developed because of the need for obtaining physically justifiable, simple, and sufficiently accurate formulas for calculating the hydrodynamic force acting on a CPS rod, the liquid flow required for withdrawing the rod from the active zone, the velocity of insertion of the rod into the zone, etc. results so obtained should be applied to calculating the velocity of rod motion in a channel only in those cases in which the operating time of the CPS is fairly long and in which the intervals of transient motion have little effect on the total process.

The diagrams of Fig. 2 illustrate the flow of a liquid past a cylindrical rod. Here p_{fr} is a pressure which varies as a function of radius and acts on the frontal surface of the rod; p_r is an analogous pressure on the rear surface; p_1 and p_2 are the pressures at the inlet and outlet of the clearance slop respectively.

The force acting on the channel wall as a result of liquid friction against the wall may be written in the form

$$P_w = \tau_w \chi_w l = c_{F_w} \varrho \frac{W_{sl}^2}{2} \chi_w l, \tag{1}$$

where τ_w is the tangential stress on the wall; c_F is the frictional-resistance coefficient; ϱ is the density of the liquid; W_{sl} is the velocity in the slot, averaged over the cross-sectional area.

The force P_{rod} acting on the rod may be resolved into a tangential force acting on the lateral surface,

$$P_t = \tau_{rod} \chi_{rod} l = c_{F_{rod}} \varrho \frac{(W_{sl} - W_{rod})^2}{2} \chi_{rod} l, \tag{2}$$

where τ_{rod} is the tangential stress on the rod, and a normal force, acting on the rear or frontal surface [1],

$$P_n = \int_S p\, dS = \int_{f_{surf}} p\, df + 0 = \int_f (p_{fr} - p_r)\, df, \tag{3}$$

where S is the surface area of the rod.

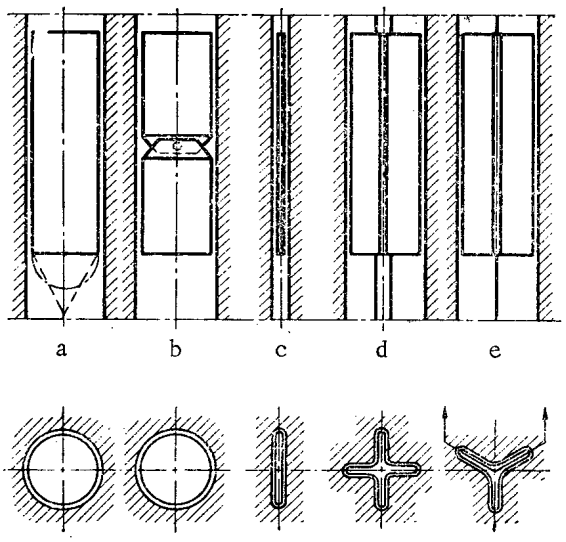

Fig. 1. Rods and channels used in control and protection systems: a) smooth cylinder; b) segmented cylinder; c) flat plate; d, e) cruciform rods.

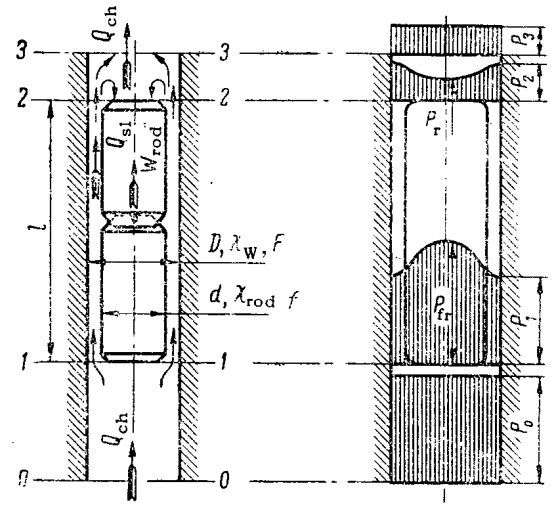

Fig. 2. Liquid flow past a cylindrical rod: p_r) Rear pressure; p_{fr}) frontal pressure; Q_{ch}) liquid flow rate in channel; Q_{sl}) liquid flow rate in clearance slot; d, D) inner and outer diameters of slot; χ_{rod}, χ_W) parameters of rod and wall; l) length of rod; f, F) cross-sectional areas; W_{rod}) velocity of rod.

If the difference between p_{fr} and p_1 and the difference between p_r and p_2 are much less than the difference between p_1 and p_2, the normal force may be regarded as a force acting on the front and rear surfaces of the rod because of the restricted nature of the flow, i. e., because of the change in pressure in the space between the rod and the channel wall:

$$P_n=(p_1-p_2)\,f. \tag{4}$$

The momentum equation for steady-state flow between the cross sections 1-1 and 2-2 (see Fig. 2) yields[1]

$$\Delta p_{sl}(F-f)=P_W+P_{rod}=\tau_W\chi_W l+\tau_{rod}\chi_{rod}\,l, \tag{5}$$

where Δp_{sl} represents the pressure loss in the slot.

Knowing all the geometric characteristics, measuring the pressure drop in the slot, and determining the frictional-resistance coefficient of the wall from the handbooks (taking account of the fact that

$$c_{F_W}=\frac{\lambda_{sl}}{4}, \tag{6}$$

where λ_{sl} is the frictional resistance coefficient in a smooth slot), we can easily determine from Eq. (5) the experimental coefficient of frictional resistance of the rod for each type of segmenting (see Fig. 1b).

For continuous rods (see Figs. 1a, c, d, e), from an analysis of the theoretical and experimental data (see [6] and the associated literature) in the range which is specific for nuclear reactors ($0.5 < f/F < 1$), we find

$$c_{F_{rod}}=c_{F_W}=\frac{\lambda_{sl}}{4}. \tag{7}$$

Taking the above points into consideration, we obtain the following expression for the hydrodynamic force acting on cylindrical rod moving in a restricted flow:

$$P_{hyd}=\Delta p_{sl}f+\tau_{rod}\chi_{rod}l. \tag{8}$$

Evidently, as the length of the slot increases, the effect of the pressure fields on the front and rear surfaces and the inlet and outlet resistances becomes less and less, and at some "critical" length this effect becomes completely negligible. The smoother the head and trail portions of the rod are, of course, the shorter this length will be. Since control and protection systems have long rods [7], the assumptions made are entirely valid for these systems.

The relationships between the flow rates or velocities can be found from the equation of continuity, which in this case has the form [2, 4, 5]

$$Q_{ch}=W_{ch}F=Q_{sl}+W_{rod}f. \tag{9}$$

Hence the velocity in the slot, averaged over the cross section, is

$$W_{sl}=\frac{Q_{sl}}{F-f}=\frac{1}{F-f}(W_{ch}F-W_{rod}f). \tag{10}$$

The expression for the hydrodynamic force now becomes

$$P_{hyd}=\frac{f}{F-f}\left[\frac{c_{F_{rod}}}{2}\varrho(W_{sl}-W_{rod})^2\chi_{rod}\,l+\frac{c_{F_W}}{2}\varrho W_{sl}^2\chi_W l\right]+\frac{c_{F_{rod}}}{2}\varrho(W_{sl}-W_{rod})^2\chi_{rod}\,l$$

$$=\frac{F}{F-f}\cdot\frac{c_{F_{rod}}}{2}\chi_{rod}\,l\varrho(W_{sl}-W_{rod})^2+\frac{f}{F-f}\cdot\frac{c_{F_W}}{2}\chi_W\,l\varrho W_{sl}^2. \tag{11}$$

We utilize the relationship (10) between the velocities. Then

$$P_{hyd}=\frac{c_{F_{rod}}}{2}\chi_{rod}\,l\left(\frac{F}{F-f}\right)^3\left[\varrho(W_{ch}-W_{rod})^2+\frac{c_{F_W}}{c_{F_{rod}}}\cdot\frac{\chi_W}{\chi_{rod}}\cdot\frac{f}{F}\varrho\left(W_{ch}-W_{rod}\frac{f}{F}\right)^2\right]$$

$$=\varrho\frac{c_{F_{rod}}}{2}\chi_{rod}\,l\left(\frac{F}{F-f}\right)^3\left[\left(1+\frac{c_{F_W}}{c_{F_{rod}}}\cdot\frac{\chi_W}{\chi_{rod}}\cdot\frac{f}{F}\right)W_{ch}^2-2\left(1+\frac{c_{F_W}}{c_{F_{rod}}}\cdot\frac{\chi_W}{\chi_{rod}}\cdot\frac{f^2}{F^2}\right)W_{ch}W_{rod}\right.$$

$$\left.+\left(1+\frac{c_{F_W}}{c_{F_{rod}}}\cdot\frac{\chi_W}{\chi_{rod}}\cdot\frac{f^3}{F^3}\right)W_{rod}^2\right]=\varrho\frac{c_{F_{rod}}}{2}\chi_{rod}\,l\left(\frac{F}{F-f}\right)^3(k_{f_1}W_{ch}^2-2k_{f_2}W_{ch}W_{rod}+k_{f_3}W_{rod}^2), \tag{12}$$

where

$$k_{f_n}=1+\frac{c_{F_W}}{c_{F_{rod}}}\frac{\chi_W}{\chi_{rod}}\frac{f^{(n)}}{F^{(n)}},\quad n=1,\ 2,\ 3.$$

Equation (12) is a general equation relating the variables and parameters which apply to the steady-state motion of a rod in a restricted flow. A number of special cases can easily be derived from this equation.

A. The rod is motionless (suspended), i. e., $W_{rod}=0$. Then

$$P_{hyd\ s}=\frac{c_{F_{rod\ s}}}{2}\chi_{rod}\,l\left(\frac{F}{F-f}\right)^3k_{f_1}\varrho W_{ch_0}^2 \tag{13}$$

where W_{ch_0} is the velocity of the liquid in the channel at which the rod is suspended in the restricted flow. From formula (13) it is easy to determine the velocity or flow rate for such suspension, and since CPS rods must be withdrawn from the active zone at the minimum possible velocity, this formula also yields the flow rate of the liquid when the rod is lifted.

B. Steady-state descent of the solid in a stationary liquid, i. e., $W_{ch}=0$. Then

$$P_{hyd\ d}=\frac{c_{F_{rod\ d}}}{2}\chi_{rod}\,l\left(\frac{F}{F-f}\right)^3k_{f_3}\varrho W_{rod_0}^2 \tag{14}$$

where W_{rod_0} is the velocity of descent of the rod in a stationary liquid. It should be noted that the start-up interval for the descent of the rod in a stationary liquid is short [2].

Determining the velocity of descent of the rod in a stationary liquid is necessary not only in order to facilitate the solution of the general case rod motion; it also has a practical significance of its own, since a number of reactors use control and protection systems in which the rod descends in a stationary liquid.

In steady-state motion, which is the case considered here, the force of the liquid acting on the rod is counterbalanced by the sum of a number of forces: the weight of the rod and the net load acting on the control rod through a coupling rod, a cable, or a spring. These forces are independent of the manner in which the control rod moves;

therefore, comparing the right-hand side of formulas (13) and (14) we find

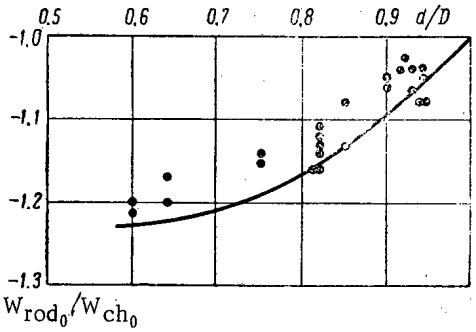

Fig. 3. Variation of the velocity ratio W_{rod_0}/W_{ch_0} as a function of the ratio of diameters, d/D. The dots represents the experimental data, while the solid curve represents the calculated values.

$$\frac{W_{rod_0}}{W_{ch_0}} = -\frac{c_{F_{rod\,s}}}{c_{F_{rod\,d}}}\sqrt{\frac{k_{f_1}}{k_{f_2}}}. \tag{15}$$

We assume that the resistance coefficients for the case of a suspended rod differ little from the coefficients for the case of a rod descending in a stationary liquid (we assume that the CPS rods are so long [7] that the change in the length of the stabilization interval may be neglected). Then formula (15) can be simplified to yield

$$\frac{W_{rod_0}}{W_{ch_0}} = -\sqrt{\frac{k_{f_1}}{k_{f_2}}}. \tag{16}$$

For smooth rods the ratio $c_{F_W}/c_{F_{rod}}$ is equal to unity, and in this case, in order to determine the velocity of descent of the rod in a stationary liquid it is sufficient to know (from experiment or calculation) the liquid velocity at which the rod is suspended:

$$\frac{W_{rod_0}}{W_{ch_0}} = -\sqrt{\frac{1+d/D}{1+d^5/D^5}}. \tag{17}$$

A comparison of the W_{rod_0}/W_{ch_0} values obtained from formula (17) and those obtained experimentally [2] is given in Fig. 3. The experiments in [2] were conducted with smooth cylinders ($c_{F_W} = c_{F_{rod}}$) over a fairly wide range of variation of the parameters: 0.60-0.94 for d/D; 0.12-1.46 m/sec for W_{ch_0}; 1.3-7.2 g/cm^3 for γ_{rod}; 0.13-1.70 m/sec for W_{rod_0}. The mean-square deviation of the experimental points from the calculated curve was 29%. Thus, the assumption that the resistance coefficients for suspension of the rod are close to those for its descent in a stationary liquid was confirmed with an accuracy sufficient for the calculations.

We assume, moreover, that in the other cases of rod motion the resistance coefficients remain close to the values for suspension of the rod. In that case, comparing the right-hand sides of formulas (12)-(14), we find

$$k_{f1}W_{ch}^2 - 2k_{f_2}W_{ch}W_{rod} + k_{f_3}W_{rod}^2 = k_{f_1}W_{ch_0}^2 = -k_{f_3}W_{rod_0}^2$$

Applying a number of transformations, we obtain

$$\left(\frac{W_{rod}}{W_{rod_0}}\right)^2 + 2k\frac{W_{rod}}{W_{rod_0}}\frac{W_{ch}}{W_{ch_0}} + \left(\frac{W_{ch}}{W_{ch_0}}\right)^2 = 1, \tag{18}$$

where

$$k = \frac{k_{f2}}{\sqrt{k_{f_1}k_{f_3}}}. \tag{19}$$

Solving (18) for W_{rod}/W_{rod_0}, we obtain

$$\frac{W_{rod}}{W_{rod_0}} = -k\frac{W_{ch}}{W_{ch_0}} + \sqrt{\left(\frac{W_{ch}}{W_{ch_0}}\right)^2(k^2-1)+1}. \tag{20}$$

The calculations show that as f/F varies from 1 to 0.5, the coefficient k varies from 1 to 0.95; consequently, formula (20) may be written approximately as

$$\frac{W_{rod}}{W_{rod_0}} = 1 - \frac{W_{ch}}{W_{ch_0}} = 1 - \frac{Q_{ch}}{Q_{ch_0}}. \tag{21}$$

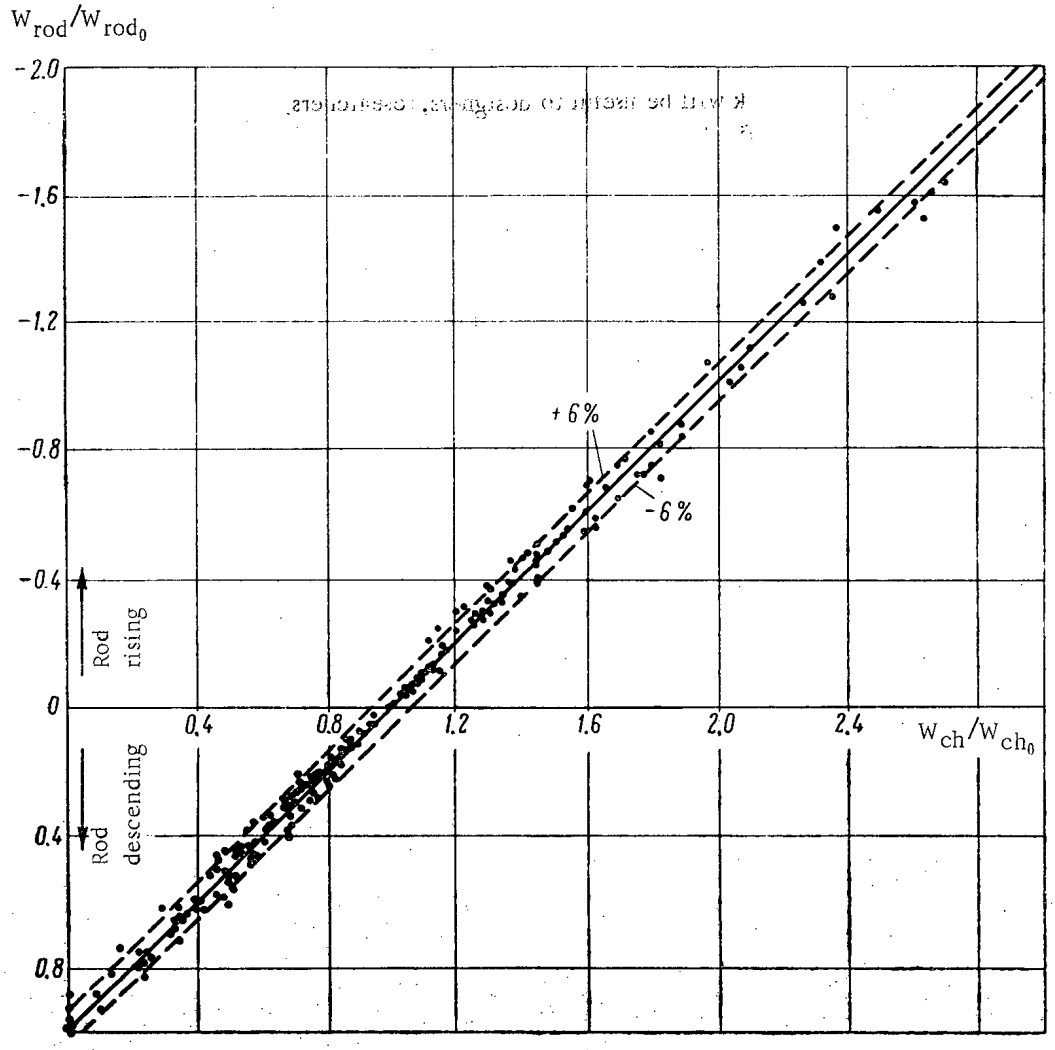

Fig. 4. Relative rod velocity, W_{rod}/W_{rod_0} as a function of W_{ch}/W_{ch_0}, the relative liquid velocity in the channel. The dots represent the experimental data for smooth rods; the solid line represents the calculated values.

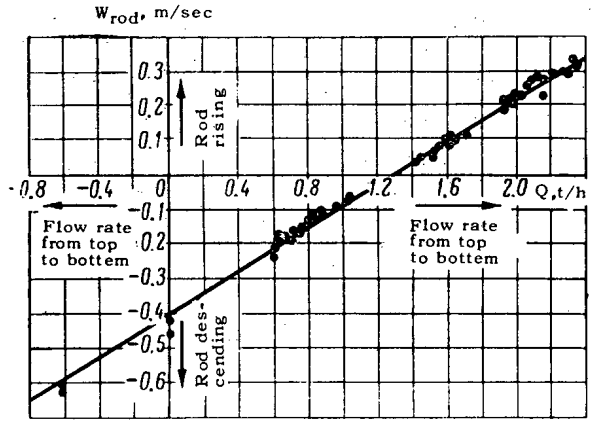

Fig. 5. Velocity of a segmented rod, W_{rod}, as a function of the flow rate Q.

This very simple relationship between W_{ch}/W_{ch_0}, the relative velocity of liquid motion in the channel, and W_{rod}/W_{rod_0}, the relative velocity of rod motion in a restricted flow, is satisfactorily confirmed by experiment. Figure 4 shows the points obtained from the data of experiments conducted on smooth rods [2] over a fairly wide range of values: $d/D = 0.60$-0.94; $W_{ch} = 0$-1.7 m/sec; $W_{rod} = 1.7$-0.6 m/sec. The error value is small. Figure 5 shows the points obtained from the data of experiments conducted with a segmented rod with $d/D = 0.87$ and $c_{F_w}/c_{F_{rod}} = 2.4$. The deviation from linearity is practically negligible, in spite of the fact that the points were obtained with different test stands.

On the basis of the above investigation, we obtained simple and sufficiently accurate calculation formulas which are supported by experimental data and which enable us to calculate the liquid flow rate required for

suspending (or for slowly lifting) a CPS rod, by formula (13), the velocity ofrod descent in a stationary liquid by formula (14) or (16), and the velocity of rod motion in a counter current or its velocity when it is lifted, depending on the liquid flow rate, by formula (20) or (21).

The author hopes that the present work will be useful to designers, researchers, and operators not only in nuclear engineering but also in other related fields.

LITERATURE CITED

1. N. E. Kochin et al., Theoretical Fluid Mechanics [in Russian], Moscow, Fizmatgiz (1963).
2. M. G. Minigazimov, Study of the Descent of Solids of Various Shapes in a Jet of Liquid [in Russian], Dissertation, Moscow, Vses. neftegaz. NII (1960).
3. G. D. Shapoval, Izv. Dnepropetr. gorn. in-ta, No. 40, 283 (1961); Gornyi zhurnal, No. 8, 122 (1962).
4. G. Z. Zakirov and V. S. Yablonskii, Izv. Vyssh. uchebn. zavedenii, Neft' i gaz, No. 3, 75 (1961); No. 7, 91 (1961).
5. Z. D. Karimov and V. I. Chernikin, Neft. kh-vo, No. 4 (1961); No. 3, 49 (1962).
6. R. R. Ionaitis, Atomnaya Énergiya, 15, 166 (1962).
7. T. A. Gruzinova et al., Atomnaya Énergiya, 11, 421 (1962).

IMPROVING THE ACCURACY OF THE RADIOMETRIC ANALYSIS OF MULTICOMPONENT SPECIMENS

(UDC 543.52)

S. I. Bacichenko, L. N. Krylov, V. S. Raikov, and A. P. Utekhin

Translated from Atomnaya Énergiya, Vol. 18, No. 4, pp. 426-428, April, 1965
Original article submitted February 24, 1964; revision submitted July 18, 1964

The method of multicomponent radiometric analysis of weakly-radioactive specimens has been throughly analyzed in [1]. In the present article, the requirements for the stability of γ-spectrometers are estimated on the basis of an analysis of the γ-spectra $N = f(E)$ for uranium, radium, thorium, and potassium. The design principle of a high-stability pulse amplitude analyzer with several differential channels is considered.

Instrumental Measurement Error. The spectrometer stability is usually defined by the stability of the position and width of the energy channel. The absolute values of the above parameters do not determine the final accuracy of radiometric analysis. The character of the spectra $N = f(E)$ of the radioactive elements to be analyzed, i. e., the variation of the counting rate N in the channel in dependence on the radiation energy E or $N = f(U_d)$, where U_d is the discrimination level, also plays an important role.

For acontinuous "white" spectrum, the counting rate variation ΔN in the channels is determined by the drift ΔU_c of the channel width. Changes in the channel position (ΔU_d) are also important on steep sections of the spectrum. Figure 1 shows the differential γ-spectra for balanced uranium, mixed lower and higher uranium oxides (U_3O_8), thorium, and potassium for a channel width of 15 keV and discrimination level variations in the 95 ± 3-keV range. Corresponding spectra were also obtained for other energy ranges [1].

The data characterizing the spectra are given in Table 1. They represent the average values of the counting rate variation in channels in measuring standard specimens of radioactive elements in the case where the discrimination level is raised by 1%.

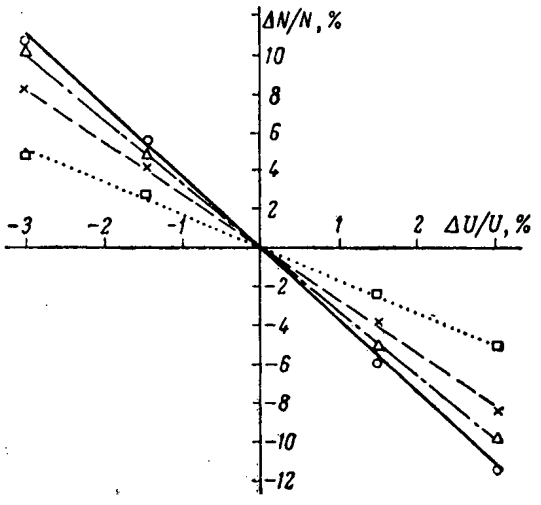

Fig. 1. Variation of the counting rate for radioactive element specimens in dependence on the shift of the first channel (95-110 keV) from its initial position. □) Potassium; x) thorium; Δ) balanced uranium; ○) unbalanced uranium (U_3O_8).

The dependence of the counting rate on the drift of the channel width is approximately linear. The change in the gain corresponds to inversely proportional changes in the discrimination level and the discriminator's channel width. Table 2 provides the values of the counting rate's drift due to a reduction of 1% in the gain, calculated on the basis of the data in Table 1.

By using these data in calculating the uranium equivalents and the working equations from [1], we can calculate the errors in determining the coefficients of the theoretical equations.

When the gain is reduced by 1%, the theoretical expressions for determining the percentages of radioactive elements in analyzing specimens with respect to four γ-measurements assume the following form:

$$U = 1.000a_1A_1 + 1.001b_1A_2 + 1.002c_1A_3 + 0.965d_1A_4,$$
$$Ra = 1.102a_2A_1 + 1.009b_2A_2 + 1.029c_2A_3 + 0.968d_2A_4,$$
$$Th = 0.978a_3A_1 + 1.024b_3A_2 + 1.017c_3A_3 + 1.006d_3A_4,$$
$$K = 0.967a_4A_1 + 1.019b_4A_2 + 0.963c_4A_3 + 1.021d_4A_4.$$

TABLE 1. Dependence of the Averaged Counting Rate Values in the Channels on the Discrimination Level, %

Standard	Channel number				
	1	2	3	4	5
	Channel width				
	95-110 keV	320-380 keV	220-260 keV	1.4-1.5 MeV	β-channel, integral count
U_3O_8	− 3.7	− 4.0	− 8.0	− 1.0	− 1.0
K	− 1.7	− 1.7	− 0.5	− 3.0	− 1.0
Th	− 2.7	− 0.5	− 1.8	− 0.5	− 1.0
U_b	− 3.3	− 1.7	− 0.8	− 1.0	− 1.0

TABLE 2. Dependence of the Counting Rate on the Gain, %

Standard	Channel number				
	1	2	3	4	5
	Channel width				
	95-110 keV	320-360 keV	220-360 keV	1.4-1.5 MeV	β-channel, integral count
U_3O_8	− 2.7	− 3.0	− 7.0	0	− 1.0
K	− 0.7	− 0.9	+ 0.5	− 2.0	− 1.0
Th	− 1.7	− 0.5	− 0.8	+ 1.5	− 1.0
U_b	− 3.3	− 1.7	+ 0.2	0	− 1.0

For analyzing specimens by using γ- and β-measurements, the calculation expressions have the following form:

$$U = 0.996a'_1A_1 + 0.996b_1A_2 + 0.998c'_1A_3 + 0.940d_1A_5,$$
$$Ra = 0.917a'_2A_1 + 1.011b'_2A_2 + 1.025c'_2A_3 + 0.957d'_2A_5,$$
$$Th = 1.132a'_3A_1 + 1.026b'_3A_3 + 1.016c'_3A_3 + 1.033d'_3A_5,$$
$$K = 0.997a'_4A_1 + 1.000b'_4A_4 + 0.998c'_4A_3 + 0.996d'_4A_5.$$

Here, U, Ra, Th, and K are the percentages of the radioactive elements, a_1, a_2, ..., d_3, d_4 are the coefficients in the working expressions, and A_1, ..., A_5 are the activities of specimens in the above channels; the numbers in front of a_1A_1, ..., d'_4A_5 are correction factors.

As can be seen from expressions (1)-(8), the values of the correction factors are mostly equal to 1-3% per 1% of change in the gain. Larger values of the correction factors are observed for small absolute values of the coefficients in the working expression; they do not greatly affect the analysis results. It is also seen that the error in determinining the percentage of radioactive elements in complex specimens that is caused by the instability of the spectrometer's parameters depends on the relative percentages of these elements in the specimen.

On the basis of the calculations performed and the results of an experimental check, it can be considered roughly that time changes of ± 1% in the gain and of ± 1.5-2% in the channel position and width will result in an error of about 5% in determining the percentages of elements (without taking into consideration the statistical error). If the above spectrometer parameters drift simulataneously, the error in determining the percentage may diminish (as a result of mutual compensation) or increase to about 10%.

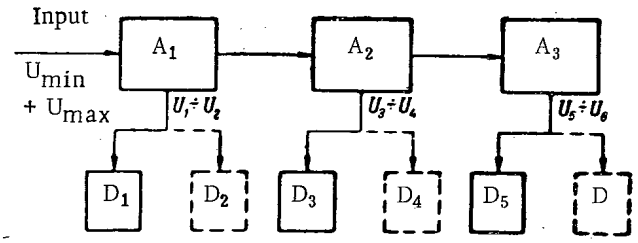

Fig. 2. Block diagram of the analyzer.

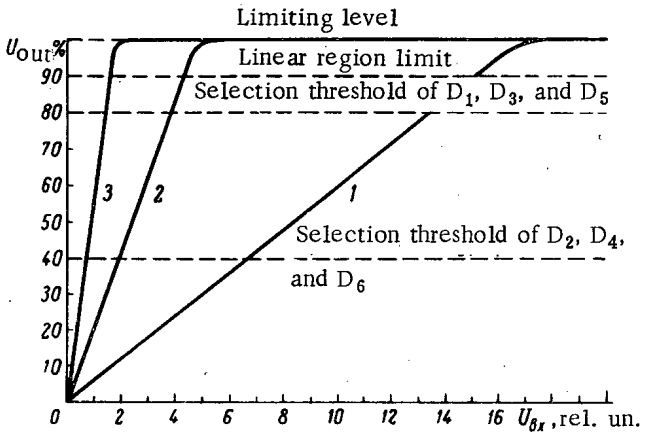

Fig. 3. Amplitude characteristics of the amplifiers. 1) A_3; 2) A_2; 3) A_1.

Automatic Stabilization of the Operating Conditions of the Scintillation γ-Counter. The instrumental error in spectral measurements is basically determined by the drift of the characteristics of the scintillation counter (the photomultiplier and the phosphor crystal).

In using automatic stabilization with respect to the integral radiation of a reference source [2], the resulting instability of the γ-data transmitted can be expressed thus:

$$\Delta = \frac{\Delta ws}{1+K} + \Delta_d.$$

Here, Δ_d is the threshold instability in the discriminator of the stabilization channel, Δ_{ws} is the data transmitter's instability in the absence of stabilization, and K is the stabilization factor,

$$K = GS,$$

where G is a parameter characterizing the operation of the measuring system (discriminator + ratemeter) V/%, and S is a parameter determining the slope of the characteristic of the system's controlled element (in this case, the photomultiplier) (%/V).

In the device (LSU-5k) for separate high-accuracy determinations of radioactive elements, we realized an automatic stabilization system with the parameters G = 5-7 V/% and S = 3%/V for a crystal resolution of 9-10% with respect to the reference α-radiation and an intensity of about 50-60 pulses/sec of the recorded α-radiation (over-all activity: 200 pulses/sec). The relative drift of the discrimination threshold Δ_d due to its higher level was readily reduced to less than 1% by suitably increasing the signal amplitude.

Thus, the instability of the data transmitter's signal was reduced by a factor of 15-20; however, on the average, it was still equal to about 1% due to the Δ_d value.

The basic disadvantage of the described stabilization system, which is due to the finite amplitude resolution of the radiation spectrum of the reference α-source, is the limited energy range in which analysis can be performed, especially in the case of specimens with a low percentage of radioactive components.

Design Principle of a High-Stability Pulse Amplitude Analyzer with Several Differential Channels. The described principle of improving the parameter stability of pulse amplitude analyzers is based on the fact that the selection of pulses in a wide dynamic range is effected at a sufficiently high amplitude level, at which the effect of the drift of the threshold stage's characteristic is considerably reduced.

Figure 2 shows the block diagram of an analyzer with several differential channels, which contains a three-section amplifier (A_1, A_2, and A_3) and differential discriminators (D_1, D_2, etc.). The entire range of input amplitudes from U_{min} to U_{max} is divided into three subranges, which are limited by the levels U_1-U_2, U_3-U_4, and U_5-U_6 with respect to the inputs of the corresponding amplifier sections.

Figure 3 shows the amplitude characteristics of the amplifiers with respect to each of the outputs; the selection thresholds of the corresponding discriminators are also indicated.

The dynamic range of the amplitudes to be analyzed in the described analyzer can generally be represented thus:

$$A_{d\Sigma} = A_{di}^{n},$$

where $A_d\Sigma$ and A_{di} are the dynamic ranges of the amplitudes to be analyzed with respect to the analyzer and the discriminator inputs, respectively, and n is the number of series-connected amplifier sections. It is considered that $A_{d1} = A_{d2} = \ldots = A_{dk}$, where k is the number of channels (discriminators).

The described principle of amplitude analyzer design can be recommended in cases where not more than eight to ten channels are used.

LITERATURE CITED

1. A. L. Yakubovich et al., Atomnaya Énergiya, 15, 224 (1963).
2. S. I. Babichenko et al., Radiometric Equipment for Control and Measurement [in Russian], Moscow, Gosatomizdat (1963).

HEAT GENERATION IN HIGHLY RADIOACTIVE SOLID PREPARATIONS IN CONNECTION WITH THE PROBLEM OF THEIR BURIAL AND UTILIZATION

P. V. Zimakov, B. S. Kolychev, V. V. Kulichenko, and Yu. P. Martynov

Translated from Atomnaya Énergiya, Vol. 18, No. 4, pp. 428-431, April, 1965
Original article submitted March 20, 1964; revision submitted July 27, 1964

In any product containing radioactive isotopes there will inevitably be spontaneous heating caused by the heat generated during radioactive decay. In the radioactive wastes of nuclear industrial plants the heat generation continues for a number of years, owing to the presence of long-lived fission-product isotopes [1].

Problems of heat generation are of special importance in the conversion of liquid radioactive wastes into solid fused preparations, and more particularly in the burial of the latter [2, 3].

In the treatment of radioactive wastes it is natural to try to concentrate the fission-product isotopes into the smallest possible volume; this leads to the formation of fused preparations with a high specific activity and a correspondingly high level of heat generation (Table 1). As a result, there is a considerably amount of spontaneous heating in preparations which are to be permanently buried. The amount of spontaneous heating depends on the quantity of heat generated and on the conditions of heat ransfer to the surrounding medium. The calculated data listed in Table 2 show that the temperature of an individual block may be controlled by limiting its volume (in the case of a cylindrical block, limiting the radius of the cylinder). However, even if the dimensions of each block are limited, the large number of such blocks accumulated at the burial site necessitates special methods of heat removal.

Table 3 shows some of the characteristics of burial sites for fused radioactive preparations when various heat-removal systems are used to keep the temperature of the burial site from rising above a prescribed level.

The total activity of the blocks accumulated in the burial site runs to millions of curies, and the heat generated over the storage period runs to terajoules (Table 4). This suggests that the heat so generated may be put to practical use, while at the same time research should be conducted to determine the conditions for maintaining a fixed temperature in the burial site.

One of the possible ways to regulate the temperature in the burial site is to conduct an endothermic process at the site. Smelting is one such process.

TABLE 1. Specific Heat Generation of a Fused Preparation of Fission-Product Isotopes (Due to β- and γ-Radiation), W/dm^3

Age of fission products	Initial specific activity of preparation, Ci/dm^3		
	3000	15,000	30,000
120 days	11.6	58.00	116.0
1 year	2.56	12.80	25.6
2 years	0.91	4.55	9.1
5 years	0.16	0.81	1.6

In order to determine the theoretical conditions for utilizing the melting of a vitreous charge to maintain at a predetermined level the temperature of the highly radioactive blocks in the burial site, electrical-simulation experiments were conducted; the purpose of these experiments was to determine how the temperature in the burial site varied as a function of the amount and specific activity of the material in the blocks, the amount and required drying rate of the vitreous charge, and a number of other factors. These experiments were expected to provide the necessary initial values for designing and equipping burial sites for highly radioactive blocks.

The apparatus set up for conducting the experiments (Fig. 1) consisted of a cavity about 1 m^3 in volume, lined

TABLE 2. Stationary Temperature of Highly Radioactive Blocks as a Function of Specific Activity and Dimensions (Under conditions of national convection)

Specific activity, Ci/dm^3	Temperature at center of preparation (°K) for cylinders with diameters of			
	100 cm	50 cm	8 cm	4 cm
125,000	42,270*	14,270*	1520*	860
25,000	8,670*	3,070*	530	390
10,000	3,670*	1,370	380	320

*In view of the fact that the thermal stability of fused preparations does not exceed 1470°K, the construction of such blocks is impossible in practice.

TABLE 3. Characteristics of Some Burial Sites for Solid Radioactive Preparations

Type of burial site	Methods for regulating the temperature in the burial site	Disadvantages
Vertical boreholes in the ground with diameters equal to block diameters	Heat removal into the ground; distance between boreholes about 3 m	Complicated work involved in depositing the blocks; large area required for burial site
"Bulk" loading of blocks in pit without cooling	Gradual filling of burial site over period of 5-10 years; layer depth no greater than one or two blocks per year	Large areq required for burial site
"Bulk" loading of blocks in pit with forced air cooling	Blowing of large quantities of air through the pile of blocks	Need for filtering equipment at the air outlet; cost of electric power for operating the air blowers
Vertical metal tubes or compartments with surface air cooling	The required air flow rate is achieved by installing an exhaust pipe of specified dimensions (diameter and height)	"Aiming" system of depositing the blocks in the burial site

with chamotte bricks surrounded by a layer of insulation with external dimensions of 2.75 x 2.75 x 2 m. The insulation used was ul'tralegkoves, whose coefficient of thermal conductivity in the 300-900°K range is expressed by the formula [4]:

$$\lambda = 3 \cdot 10^{-4} T_{av} \ W/m \cdot deg$$

(where T_{av} is the average temperature of the Ul'tralegkoves in °C).

TABLE 4. Accumulation of Heat Generated During the Storage of 1 m^3 of Fused Fission-Product Concentrate with an Initial Specific Activity of 30,000 Ci/dm^3 (for a Fission-Product Age of 120 Days)

Duration of storage	Average heat generation rate at end of period, joules/month	Total heat generated over the storage period, joules
2 months	$2.3 \cdot 10^{11}$	$4.6 \cdot 10^{11}$
8 months	$7.6 \cdot 10^{10}$	$1.2 \cdot 10^{12}$
2 years	$2.1 \cdot 10^{10}$	$1.7 \cdot 10^{12}$
3 years	$6.3 \cdot 10^{9}$	$1.9 \cdot 10^{12}$
5 years	$3.3 \cdot 10^{9}$	$2.1 \cdot 10^{12}$

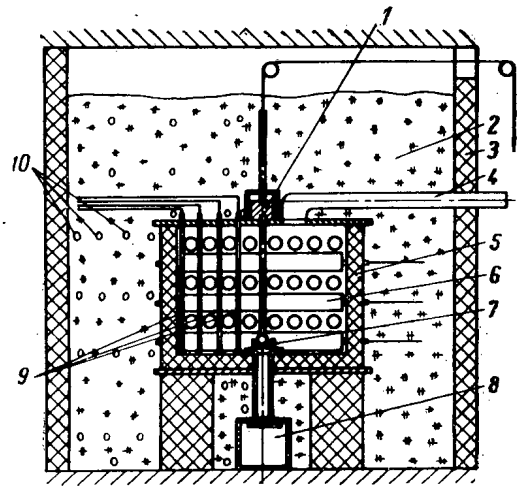

Fig. 1. Diagram of apparatus for electrical simulation of heat generation in fused highly radioactive preparations: 1) melt discharge-rate control; 2) Ul'tralegkoves; 3) thermal insulation vessel; 4) opening for input of the charge; 5) operating vessel; 6) heating blocks; 7) discharge opening; 8) compartment for receiving the melted charge; 9) thermocouples in operating vessel; 10) thermocouples in Ul'tralegkoves.

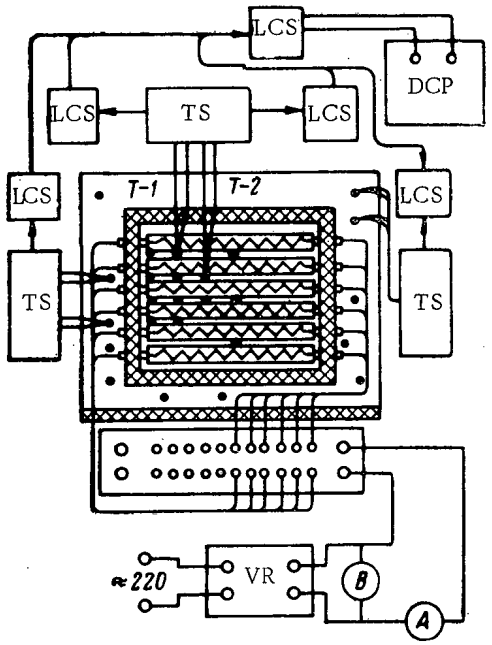

Fig. 2. Measuring system of the electrical-simulation apparatus: TS) thermostat; LCS) low-current switch; DCP) d-c potentiometer; VR) voltage regulator; T) thermocouple.

The electrical-simulation blocks (representing the highly radioactive blocks) were placed in the inner vessel; these were steel pipes with an outer diameter of 80 mm and a length of 1 m. Electrical heaters were installed inside the pipes. The vessel contained 48 pipes distributed in six rows. Chromel-alumel thermocouples were used for monitoring the temperatures: 12 thermocouples were placed in the blocks, 20 at various points of the inner vessel, and 35 in the surrounding insulating vessel. The measuring system of the apparatus is shown in Fig. 2. The power supplied to the blocks varied from 2.5 to 10 kW, simulating a specific activity of 2500 to 10,000 Ci/dm^3. In order to regulate the temperature in the vessel, a vitreous charge with a melting point of about 1100°K was periodically fed into the vessel. After some time, the charge was melted, and the melt was discharged through an opening at the bottom of the vessel.

The burial-site simulation experiments showed that the average output of vitreous melt was 2 kg/h per kW of power beyond the amount required to keep the temperature at the melting point of the charge. Table 5 shows how the amount of melted charge, calculated or determined from the experiments, varies as a function of the specific activities of the blocks.

TABLE 5. Amount of Melted Charge in a 1 m^3 Burial-Site Simulator Containing a 240 dm^3 of Preparation, Simulating a Highly Radioactive Melt with Various Specific-Activity Values

Specific activity, Ci/dm^3	Amount of melted charge		
	kg/h	kg/day	x 10^3 kg/month
6,600*	4.4	105	3.1
7,500*	6.0	144	4.3
15,000†	18.7	450	13.5
30,000†	44	1050	31.5

* Simulated by supplying the appropriate amount of electrical power.
† Calculated data.

TABLE 6. Heat Generation of Fission-Product Concentrates as a Function of the Activity and Age of the Radioactive Isotopes

Age of fission-product isotopes	Specific activity, x 10^4 Ci/dm^3	Heat generation, W/dm^3	
		taking account of complete absorption of β- and γ-radiation	neglecting the absorption of γ-rays
120 days	8.1	290	264
180 days	5.3	190	180
2 years	1.3	43	40
5 years	0.3	8	7.4

The burial-site simulation experiments were conducted over a long period of time (40 days), with various simulated specific-activity values of the "buried" blocks (2.5-10 Ci/dm^3), by periodically feeding a vitreous charge into the burial site; it was found possible to keep the temperature in the burial site between 1070 and 1170°K. The temperature level within these limits could be controlled by varying the amount of charge.

The above-described system for regulating the temperature in burial sites for highly radioactive blocks by using them to melt a vitreous charge necessitates an increase in the total volume of the burial site. However, it should be taken into consideration that the operation of nuclear plants produces not only highly active wastes but also low-activity liquid wastes whose volume is much greater than that of the high-activity wastes. The mixture obtained by combining the dry residue from the calcination of the less active wastes with the appropriate fluxes may be used as the vitreous charge. The melting point of such a charge should be kept no higher than 1170°K, in order to avoid melting the high-activity blocks.

Figure 3 shows the amount of charge that can be melted in a burial site containing 1 m^3 of fused preparation with an initial activity of 30,000 Ci/dm^3. This method makes it possible not only to maintain the temperature in the high-activity block burial site at a predetermined level but also to convert large quantities of low-activity calcined wastes into a melt and to avoid the need for melting equipment fo liquefy these wastes.

However, the utilization of high-activity concentrates should not be limited to these purposes. On the basis of the properties of the fused fission-product concentrates to be buried (high specific activity, high degree of localization of radioactive isotopes, radiation stability, and thermal stability), it has been recommended that this concentrate be used as a high-power source of ionizing radiation [5, 6].

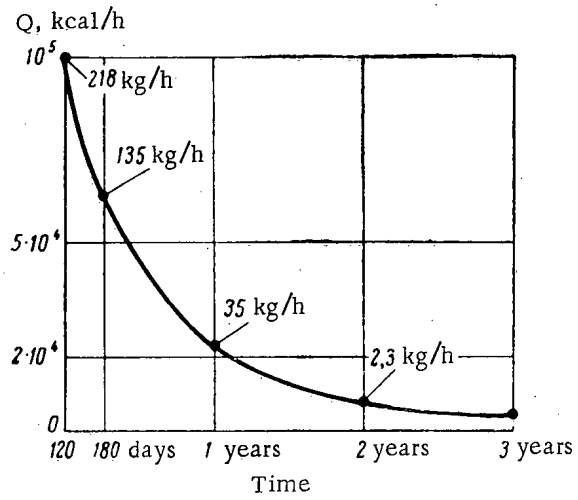

Fig. 3. Amount of charge that can be melted in a burial site in storing 1 m^3 of fused preparation (initial activity of 30,000 Ci/dm^3), as a function of time.

The high energy output of these preparations also makes possible their use as heat sources for various purposes. In particular, the fused preparations obtained from the treatment of highly radioactive wastes have been used as isotopic sources of electrical energy. A great deal of attention is now being devoted to such sources of current [7, 8]. On the basis of the data shown in Table 6, it should be possible to utilize such preparations in cases in which the limitations on the weight and volume of the generator are not too severe.

The most convenient preparation to use for relatively high-power short-term (3-5 months) sources is one in which the age of the isotopes is 120-180 days, while a preparation with an age of 2 years is more suitable for low-power sources intended for long-term operation.

Thus, the above discussion indicates that the heat generated by the fused fission-product preparations obtained in the solidification of the radioactive products of nuclear plants creates difficulties in setting up the burial sites. However, if the sites are efficiently designed, the heat so generated can be utilized for melting charges of low-activity wastes. In addition, fused highly radioactive preparations may be used before burial as sources of heat and electrical energy.

LITERATURE CITED

1. E. Coppinger and R. Tomlinson, Chem. Engng. Progr., 52, 417 (1956).
2. P. V. Zimakov and V. V. Kulichenko, Disposal of Radioactive Wastes, Vienna, IAEA (1960), p. 432.
3. C. Amphlett, Progress in Nuclear Energy, Ser. 3, Process Chemistry, Vol. 2, Pergamon Press (1958).
4. V. L. Shevel'kov, Thermophysical Characteristics of Insulating Materials [in Russian], Moscow, Gosénergoizdat (1958).
5. A. G. Bykov, P. V. Zimakov, and V. V. Kulichenko, Atomnaya Énergiya, 10, 362 (1961).
6. P. V. Zimakov et al., In "Proceedings of the Second International Conference on the Peaceful Uses of Atomic Energy" [in Russian], Reports of Soviet Scientists, Vol. 4, Moscow, Atomizdat (1959), p. 247.
7. W. Corliss, Nucleonics, 18, 58 (1960).
8. Nucleonics, 19, 27 (1961).

CONFERENCE ON EXPERIMENTAL RESEARCH REACTOR TECHNIQUES

A. M. Demidov

Translated from Atomnaya Énergiya, Vol. 18, No. 4,
pp. 432-434, April, 1965

At the October 1962 IAEA symposium on uses of research reactors, a decision was adopted to convene regional workshop conferences on special topics concerning the use of reactors. In line with this decision, a conference was held in Bucharest in late October 1964 gathering together research scientists working at nuclear research centers in Europe and in the Mediterranean area, to discuss the latest achievements in the field of experimental techniques in research reactor work, the new spheres of applications of research reactors, and experience in the operation of sophisticated experimental equipment.

The conference was held under the auspices of IAEA in collaboration with the Committee on Atomic Energy of the Council of Ministers of the Rumanian Peoples Republic.

Topics discussed at the conference included research reactor physics, reactor kinetics, in-pile dosimetry, tests of fissionable and miscellaneous reactor structural materials, cryogenic experimental pile channels for radiation physics research, irradiation techniques employed in research on isotope chemistry and isotope production, aspects of safety in in-pile irradiation experiments, the irradiation of channels for work on the dynamics of the condensed state, channel equipment for nuclear physics research, and the use of pulsed reactors.

Just by the listing of topics, we readily see that the scope of the conference was quite extensive. This to some extent influenced the nature of the papers presented, most of them being of a tutorial survey nature.

Research reactor physics topics were discussed in reports presented by delegates of Great Britain (B. Wade), Italy (F. Cassali), Yugoslavia (F. Zerdin et al., P. Struhar et al.), and the USSR (A. N. Isaev et al.). The report by P. Struhar et al., evoked considerable interest. This paper described a concept by which the Belgrade heavy-water reactor could be redesigned and modernized. Since the core of this reactor consists of separate units, it could be divided into two parts such that a horizontally placed reflector could be set up at the center. Then a buildup of thermal flux should be observed in this reflector and consequently in beams initiated in this reflector. The epithermal flux and γ-ray flux in these beams must be reduced. Experiments conducted on a critical assembly demonstrated an increased thermal flux in this central reflector.

The paper presented by B. Wade dealt with reactor physics problems which took shape in the course of operating the DIDO and PLUTO reactors at Harwell. Special attention was centered on the potentialities of the DAPHNE zero-power reactor whose core is quite similar to those of the other two reactors mentioned.

Reactor kinetics was discussed in papers submitted by IAEA (D. Magnuson), Yugoslavia (M. Petrovic), Rumania (I. Purica), and the USSR (A. N. Isaev et al.). These reports placed the brunt of their attention on experimental techniques for determining the time behavior of neutron flux in a pile using pulsed neutron sources. D. Magnuson's survey paper gave a detailed description of measurements performed at the Oak Ridge zero-power reactor with the aid of the small Cockroft-Walton 150-200 keV pulsed accelerator boasting an output of up to 10^{11} neutrons/sec. The critical aseembly was built around the horizontal channel beam at the reactor in Rumania; the beam was chopper-modulated.

Tutorial survey papers on in-pile dosimetry were presented by the Yugoslav delegation (N. Rajzic and B. Radak). It was noted in the discussion that one of the major problems in present-day dosimetry is how to improve the accuracy of the data acquired. The determination of absolute dose values requires that several nuclear parameters (neutron interaction cross sections, γ-radiation yields, etc.) be known to higher orders of accuracy. The IAEA representative R. Skildebrand reported that intensive research is planned on standardization of dosimetric techniques.

Topics associated with in-pile testing of fissionable materials and miscellaneous reactor structural materials were the subject of discussion in papers submitted by Japan (R. Hara), Sweden (B. Svenson), USSR (B. V. Samsonov),

and Great Britain (D. Merrett, R. Atkinson). Samsonov's paper on loop tests run on the SM-2 reactor, which has the highest neutron flux of any pile in the world, was heared with rapt interest.

Loop tests were described in depth and in great detail in the British papers. Mention was made of the use of large special test loops with complicated process equipment, operations which were poorly justified because of the high costs and exorbitant time required to fabricate the associated loop equipment. The loops could be feasibly used generally only for testing fuel elements under natural conditions. Fuel assembly pods or ampules are now coming into widespread use in Great Britain for the solution of various problems in the behavior of fuel element compositions or of structural materials. Ampules contain two or three fuel element jackets, as a rule. The state of the ampules is monitored by the activity yield from the space between jackets, and also by x-raying the ampules from time to time.

R. Atkinson's report noted that a steady trend toward rising operation temperatures in fuel elements and rising specific heat loadings is underway. Research programs have been developed at Dounreay, therefore, to test reactor materials at elevated temperatures (as high as 2000°C) and under high heat loadings (up to 900 W/g). The specimens are heated via absorption of γ-radiation, and in some cases additional heating is resorted to aid in stabilizing the temperature. The temperature within the ampules may also be controlled by varying the helium pressure in the space intervening between two jackets. The heat is carried off from the ampule outer wall by a coolant undergoing nucleate boiling.

In Great Britain, attention continues to be focused, as earlier, on research using loops with water at critical temperature and pressure. Severe difficulties have been encountered in work with test loops when fuel elements rupture and fission fragments get into the loop circuits. To cope with this problem, new and, what is particularly important, small-size loops are being designed to fit entirely inside the pile (pump and ancillary equipment included). Provisions must also be made to ensure ease of withdrawal of the loop from the pile and scramming instrumentation must be installed.

Reports on cryogenic channels (using liquid nitrogen, liquid hydrogen, liquid helium) were contained in papers submitted by Japan (R. Hara), West Germany (W. Mart), France (L. Bochirolle), Great Britain (D. Merrett), USA (R. Coltman), and the USSR (A. M. Demidov). In discussing the design of these cryogenic channels, authors laid special stress on measures to render them explosionproof. The usual coolant is helium or high-purity nitrogen, which is circulated in a closed loop between the specimen placed in the radiation field and the cryogenic heat exchanger which may contain either technical-grade nitrogen or helium.

Since the radiation effects produced by γ-radiation, thermal, intermediate-spectrum, and fast neutrons is different in each case, irradiation limited to a relative "clean" flux of one single mode of radiation acquires added interest. Research on low-temperature radiation physics with thermal neutrons is being carried on the Oak Ridge, in the USA. A bed of moderator, 45 cm thick with heavy water, is employed to produce a thermal flux of $8 \cdot 10^{11}$ neutrons/($cm^2 \cdot sec$). This bed abuts against the core of a 1 MW rating water-cooled water-moderated reactor. The bulk of the research on radiation physics is being carried out with fast neutrons obtained from a uranium converter. A soon as liquid helium temperatures are reached, we are confronted with the very acute problem of heating of the channel and the specimen by γ-radiation. In any work with fast neutrons, one way out is to use tungsten to minimize to heating, since the tungsten will simultaneously absorb both γ-rays and thermal neutrons.

Mention was made in a report by U. Farinelli (Italy) of research on radiation physics and radiation biology where fast flux is required, and where there is added point to the use of fast reactors in which the γ-ray background will be low. The TAPIRO reactor, 1 kW, constructed at Casaccia, fits these needs.

For the first time, a discussion was held at an international conference on safety in conducting pile irradiation experiments. Even though only one survey paper, submitted by D. Merrett (Great Britain), was heard on this topic, a whole session was reserved for discussion on this one topic. In the course of the discussion, delegates mentioned that experiments on in-pile irradiation of specimens are being performed in increasingly more complex and exacting facilities, at higher temperatures and pressures, with the use of liquid metals, liquefied gases, etc. As a result, the potential danger of a large-scale accident capable of putting a reactor our of commission and leading to consequences of the most serious nature has been greatly increased. At Harwell, a practice has already been initiated of estimating the danger inherent in any experiment being undertaken and of inspecting the pile irradiation equipment. The head of the reactor staff is responsible for the safe operation of the reaction when any experiments are carried out. A consultative team of experimental engineers has been organized to assist the reactor staff

head in considering all aspects of an experiment and in estimating the potential hazards. The discussion of the pile experiment covers three stages: 1) discussion of the ideas and concepts embodied and to be tested in the experiment; 2) a detailed perusal of the experimental method after the design of the experiment has been frozen; 3) given a go-ahead to plans to carry out the experiment after experimental devices have been fabricated and tested.

Much time was spent at the conference on discussion of channel equipment for work on the physics of the condensed state. It is of the utmost importance to have available high fluxes of "cold" neutrons such that $\lambda > 4$ A to carry out these experiments. Increases may be achieved in the number of cold neutrons extracted from reactor channels by using a small volume of cooled hydrogen-containing moderator placed around the core. Sources of cold neutrons of this type have already been in use for several years at Harwell and Saclay. Use of these sources has made it possible to increase the neutron flux at $\lambda > 4$ A by 5-10 times. Papers presented by Britain (D. Merrett), West Germany (W. Mart), Finland (E. Tunkelo), and the USSR (A. M. Demidov) showed that work on the design of cold-neutron sources is well underway in other nuclear research centers as well. Liquid hydrogen is the moderator of choice in these programs. Best results are provided by solid methane; but this substance decomposes when bombarded by radiation and its usefulness is limited to a very short period of time. A bismuth shield has been proposed in order to decrease the amount of heat generated in the source by absorption of γ-rays, and shields of this type are in use. The papers devoted close attention to the safety problems attendant upon the operation of cryogenic facilities. These sources are placed, as a rule, in a zirconium cylinder capable of sustaining the pressure encountered in case the source explodes. Another cryogenic course of cold neutrons has been built at the pulsed reactor in Finland.

In addition to the work on designing cold-neutron sources, an intensive program of research and development is underway to improve various other components of research facilities (filters, monochromators, spectrometers, neutron detectors), and on the use of electronic computers to process the results of measurements.

Results of a systematic study of filters for thermal and cold neutrons were submitted in a paper presented by the Belgian delegation (V. Van Dingenen and S. Hauteclaire). Their findings were that the best filter for thermal neutrons is the magnolite single crystal MgO, and that the best filter for cold neutrons is polycrystalline beryllium. Addition of a bismuth single crystal to decrease γ-ray flux is recommended.

F. Carvalho et al., (Karlsruhe, West Germany) reported on a multipurpose neutron spectrometer with rotating crystal. Several neutron structural and neutrons dynamical investigations can be carried on simultaneously using this rotating-crystal spectrometer. In this case, beams of monochromatic neutrons aimed in various directions by a rotating aluminum single crystal were employed. This is a major improvement, specially suited to the situation where the problem is to make use of a single reactor channel, e. g., with a source of cold neutrons.

The possibility of increasing the flux of epithermal neutrons ($\lambda < 1$ A) by additional shaping of the spectrum in locally heated regions of moderator was discussed in papers presented by Britain (D. Saunderson) and the USSR (A. N. Isaev). The heating was carried out at temperatures up to 1000-1500°C.

Papers submitted by A. M. Demidov (USSR) and O. Schult (West Germany) reported on the successful design of channels whose function is to measure γ-ray spectra and internal-conversion electron spectra resulting from the capture of thermal neutrons. The principal problem here is to reduce the background emerging from the reactor channel by appropriate design of filters and collimators. This is particularly necessitated whenever separated isotopes present in small quantities have to be measured, or when a substance with a very low thermal neutron capture cross section is to be dealt with.

During their stay in Bucharest, the conference delegates were extended the opportunity to visit the Institute of Atomic Physics, where they inspected the VVR-S reactor, the U-120 cyclotron, the 25 MeV betatron built at that institute, and an electronic computer.

ALL-UNION SEMINAR ON INDUSTRIAL γ-RAY FLAW DETECTION

Translated from Atomnaya Énergiya, Vol. 18, No. 4,
pp. 434-435, April, 1965

An All-Union seminar on industrial γ-ray nondestructive testing was held in November 1964 at the Exhibit Hall of the Achievements of the National Economy of the USSR. Participating in the deliberations of this seminar were 230 representatives of industrial firms, to discuss 34 papers and communications.

A. S. Shtan' (of VNIIRT – the All-Union Research Institute for Radiation Engineering) dwelt in detailed fashion on the potential use of various industrial radiography techniques, including radiometric and neutron inspection techniques, for nondestructive monitoring and testing. The report told of greater detail obtained in flaw-detection work, tighter specifications on photographic materials and screens, new attention being given to the special aspects of the use of bremsstrahlung x-radiation from both β-ray sources and betatrons, and touched on the status and future outlook of development of stereoscopic radiography, and on the use of the xerographic method to record detected flaws. The report mentioned that the principal technique in γ-ray nondestructive testing at present is the radiographic method with detected flaws recorded in film.

A. M. Yakobson reported on work in progress to develop visual techniques of γ-ray flaw detection, by making use of scintillation and semiconductor detector techniques of γ-ray optical image conversion, as well as observations in quality control of weldments with the aid of the x-ray television introscope.

V. S. Tokmakov (Ferrous metallurgy research institute – TsNIIchermet) cited data on the basic characteristics of Soviet and foreign electronic image converters. He further discussed the influence of a variety of factors on the sensitivity and productivity of the visual method of x-ray and γ-ray inspection, and reported some data drawn from calculations of quality control costs in inspection of weldments in mass production when various techniques of radiography are employed.

I. S. Ivakhnenko (Heavy machinery research institute – TsNIItyazhmash) discussed ionization techniques for recording radiations, presented a comparative analysis of rival techniques for recording detected flaws based in attaining the limiting theoretically possible sensitivity to changes in thickness under optimum conditions. Designs of scintillation sensor equipment for quality control of manufactured parts were presented and data on their use were appended.

A paper submitted by V. G. Firstov (VNIIRT) was devoted to the radiography of steel, concrete, reinforced concrete, and miscellaneous structures by employing high-level Cs^{137} sources. Radiographic techniques employing miniaturized sources of radiation were reported on by E. N. Neelov.

Radiation flaw detection using the bremsstrahlung from betatrons for inspecting parts made of either nomogeneous or unlike materials was the topic of a report by V. A. Vorob'ev (Tomsk Polytechnic Institute). The paper focused particularly on the fact that radioactive isotopes and x-ray equipment has virtually exhausted their possibilities as sources of penetrating radiation for inspection of steel parts of more than 200-250 mm thickness. Fineness of detail in the detection of flaws is impaired at such large thicknesses by the increased intensity of scattered radiation. The use of a betatron as the source of bremsstrahlung, with peak energies to 30 MeV, makes it possible to radiograph steel of up to 500-600 mm thickness, and aluminum or concrete as thick as 1500-2000 mm. The sensitivity obtained at these thicknesses amounts to 1-2% of the thickness radiographed through, and the exposure time is 160-200 mm when lead intensifying screens are utilized. A further increase in output of betatron radiography of materials may be achieved by the use of scintillation counters or ionization chambers to record the intensity of the radiation passed. Portions of the inspected object for which the radiation intensity deviates from the average contain some flaw whose shape and type may be ascertained by a radiographic method. This combination of scintillation and radiographic techniques in betatron nondestructive testing provides a possibility of continuous high-speed quality control under production conditions.

A. I. Kaminaskas (Electrography research institute) reported on the outlook for adoption of the electroradiographic (xerographic) method in industry. The reporter gave a detailed account of the essence of the method, and of the ERGA-S electroradiographer. Excellent quality is currently obtained in xerographic reproductions, it was noted, in radiography of plastic parts of up to 150 mm thickness, aluminum parts of up to 50 mm thickness, and steel parts of up to 25 mm thickness, but this method is applied only in some industrial plants; to date no mass production of ERGA-S equipment or xerographic materials is in progress.

A description of γ-ray flaw detection scopes was provided in a report by A. G. Sul'kin, E. A. Zhukovskii, A. N. Maiorov (VNIIRT), E. S. Baran (of the Moscow x-ray plant "Mosrentgen") and L. M. Anan'ev (of Tomsk Polytechnic Institute). A normal series of γ-ray flaw detection scopes and the design and engineering specifications of the RID-35 and RID-22 γ-ray nondestructive testing equipments were reported on by E. A. Zhukovskii. New portable γ-ray nondestructive testing gear were reported by A. N. Maiorov; a detailed description of the design and the engineering specifications of a hose type general purpose γ-ray nondestructive testing outfit provided with a magazine of containers for a set of different radiation sources (Cs^{137}, Ir^{192}, Se^{75}, Tm^{170}) were presented. γ-ray nondestructive testing outfits now being produced in a regular line by the Mosrentgen works were the subject of a paper by E. S. Baran. L. M. Anan'ev reported on portable betatrons.

Accessories and auxiliary materials for use in radioisotope flaw detection were the subject of reports by E. E. Kulish (State Committee on Uses of Atomic Energy, USSR), L. K. Yakovlev (V/O Izotop), G. G. Orlova, V. S. Gostishchev (Heavy machinery research institute), I. Ya. Serebryakov (VNIIRT), and N. S. Nikitin. These papers shed light on the radioactive radiation sources employed in γ-ray nondestructive testing, ways in which to improve their quality, scheduling of delivery and reloading of isotope containers for the NDT equipment, organization of maintenance and repair operations, automation of various processes in γ-ray and x-ray flaw detection work; a list is presented of dosimetric monitoring instrumentation and the basic characteristics of the instruments, to aid personnel in achieving radiation safety in their γ-radiography work.

N. I. Leshchinskii (VNIIRT) acquainted the delegates at the Seminar with the safety conditions to be observed in work with both stationary and portable γ-radiography equipment.

Experience in the use of radioisotope NDT equipment in industry was reflected in papers by A. V. Dzhabadari, E. V. Sharapenko (Azovstal' steel works), V. S. Gostishchev (Heavy machinery research institute), S. P. Chaus (Luga machine repair and adjustment center), A. P. Sergeenko (Bryansk machine tool plant), A. P. Dmitriev (Makeevka S. M. Kirov metallurgical works), E. D. Spitsyn (Ukrzapadugol' repair and maintenance center for western Ukraine mining), A. N. Timofeev (MADI – Moscow highway institute). The reporters gave a detailed account of the use of γ-ray nondestructive testing work in metallurgy, boiler making operations, machine tool manufacture, and in the coal mining industry. They cited some concrete examples and data on engineering costs savings.

While the seminar was in progress, an exhibit of γ-ray nondestructive testing equipment now being produced on a regular basis by industry, plus some new items and designs in the experimental stage, was opened up in the pavilion "Atomic Energy" of the Exhibit of the Achievements of the National Economy. Consultations were also arranged with specialists on various aspects of the most fruitful exploitation of the potentialities of γ-ray nondestructive testing work.

NEW PUBLIC HEALTH REGULATIONS GOVERNING THE DESIGN AND OPERATION OF HIGH-LEVEL ISOTOPE FACILITIES

V. I. Sinitsyn

Translated from Atomnaya Énergiya, Vol. 18, No. 4,
pp. 435-436, April, 1965

The chief public health and epidemiological control board of the Ministry of Public Health of the USSR has elaborated and adopted for 1964 some new "Public health regulations governing the design and operation of high-level isotope facilities," No. 482-64, constituting an extension and further development of the "Public health regulations governing the handling of radioactive materials and ionizing radiation sources," No. 333-60 [cf., Atomnya énergiya, 9, 525 (1960)].

These instruction sheets and materials are being dispatched to all facilities using high-level isotope γ-ray equipment of an industrial, semi-industrial, or research nature intended for the various radiation processes in use, and are obligatory for all institutions and enterprises engaged in the design, construction, and operation of high-level isotope γ-ray facilities of source activity superior to 500 gram-equivalents of Ra. The rules do not extent to radiation facilities in which spent fuel elements are the sources of the γ-radiation, nor to radiation loops and cores of nuclear reactors, accelerators of several types employed in medical γ-radiation facilities (GUT type), nor to various portable facilities and "γ-field" facilities.

These new regulations take into account the experience acquired in the operation of radiation facilities throughout the Soviet Union in recent years, and are based on the need to guarantee safety in work on isotope γ-ray facilities with proper attention to the critical tolerance levels of external radiation as stipulated in the Public Health Regulations No. 333-60.

Depending on the activity of the irradiator used, facilities may be divided up into three categories:

a) the 1st category includes facilities with an irradiator of activity greater than 10^6 gram-equivalents of radium;

b) the 2nd category includes facilities with an irradiator of activity in the 10^4 to 10^6 range of gram-equivalents of radium;

c) the 3rd category includes facilities with an irradiator of activity in the 500 to 10^4 range of gram-equivalents of radium.

Radiation facilities of the industrial, semi-industrial, and research types are further subdivided into two groups depending on whether the subjects irradiated present an explosion hazard (1st group if yes, 2nd group if no).

High-level γ-ray facilities belonging to the 1st group of any of these three categories, or to the 2nd group of the 1st category, must be housed in buildings apart from the rest of the research or work center. But γ-radiation facilities of this type need not necessarily be housed separately if the requirements of continuity in the technological process aided by the radiation dictate otherwise. High-level γ-radiation facilities of the 2nd group in either the second or third categories may be housed in adjoining wings, in the basements of the main process building, etc. But the rooms housing the facilities must nevertheless be separate and apart from other rooms in these buildings, and must be separated by flooring, ceiling, and main partition walls, must have their own separate entrance and an independent ventilation system. The distance between the building housing the radiation facility and other nearby structures is stipulated in the "Public health rules governing the design of industrial plants," SN-245-63.

Rules are provided for shielded and personnel exclusion zones: a) rules SN-245-63 to apply to facilities in the 1st group (Appendix 1, chemical production); b) 50 meters clearance around facilities in the 2nd group of the first category. No such exclusion zones are needed for facilities in the 2nd group of the second or third categories.

Requirements on siting and housing of facilities are mandatory for all radiation facilities now being designed and planned. The extent of coverage of these requirements in application to radiation facilities already in operation or now being built will have to be decided in each specific case by consultation with agencies of the public health and epidemiological service.

The regulations specify concrete requirements to be imposed on shielding for radiation facilities. The dose rate for γ-radiation on the outer surfaces of the buildings housing the facilities, with the exception of such openings as windows, doors, etc., is not to exceed 0.28 mR/h, and must not exceed 2.8 mR/h on any point of the outer surface of the shielding projecting into rooms where personnel are to be working. Because of certain imprecisions in shielding calculations, not to mention possible flaws in shielding (such as small blowpipes in concrete, etc.) provisions are made for a margin of error to amount to 5% of the shielding thickness.

Considerable attention is given to the inspection of radiation facilities both after completion of building, installation, and assembly operations and in reloading.

A special section of the regulates deals with specifications for interlocking and alarm annuciation systems designed to eliminate any possibility of the irradiator being raised to operating position while the door leading to the irradiation room remains open. A visual and auditory alarm annunciation system is envisaged which will give warning of the need to leave the irradiation room. Scheduling of inspection operations on the irradiation room and sequencing of operations to turn the irradiator on are specified. Also envisaged are a system for interlocking of assembly and repair openings, manways, etc., as well as an entrance door to the irradiation room to allow access during the exclusion time with the added safeguard that ventilation will reduce to a tolerable level whatever concentration of toxic substances in the irradiation room.

Specifications for intake and exhaust ventilation designed to lower the concentration of toxic substances gaining access to the personnel working room from irradiated objects, and also to remove ozone and nitrogen oxides formed as a result of ionization of the air, are listed. The throughput of the ventilation system is set to match the categories of radiation facilities; e. g., 20-fold air turnover per hour is required in the irradiation room where facilities of the first category are used; 10 to 15-fold air turnovers per hour for the second category, and 5 to 10-fold air turnovers per hour for radiation facilities belonging to the third category.

In order to avert any possible contamination in the rooms housing the radiation facilities, specifications are provided for coating the walls and ceilings of the irradiation rooms with low-sorption and readily deactivated materials, and for covering the floors with linoleum or PVC laminates.

Water storage ponds designed for the storage of γ-radiation sources must be stainless-steel-lined and reliably waterproofed. The water in the ponds is to be deactivated as soon as the concentration of radioactive substances in it goes over 10 times the critical tolerance level stipulated for water in open reservoirs.

Special attention is reserved for the loading and reloading of facilities using γ-radiation sources. Design organizations responsible for working out the original design of the facilities must provide measures to assure radiation safety during the loading operations, and must elaborate suitable loading and reloading technology.

A special section in the rules deals with the organization of dosimetric and radiometric monitoring operations, as well as inspection routines to check compliance with all effective radiation safety requirements. A scheduling sequence is established for recording the results of dosimetric measurements, and recommendations are given on the frequency with which dosimetric and radiometric measurements should be carried out. For instance, personnel dosimetric monitoring and check-outs of the functioning of interlocking and alarm annunciation systems are called for once each day, measurements of radioactive contaimination by the smear method and γ-radiation intensity on metal sheets must be performed no less frequently than once a month, and so forth.

Aside from periodic measurements, dosimetric and radiometric monitoring must be carried out in all cases where there may be change in the nature of the objects being monitored periodically (such as rechecks on the effectiveness of shielding whenever visible cracks appear, or new measurements when radiation process channels are redesigned or modified).

Among the measures taken to prevent accidents, the rules specify requirements on instruments for forced remote-control return of the irradiator to a storage position in any case where the irradiator conveyer system malfunctions; the need for calculating thermal conditions of sources both in storage position and in working position must be attended to in the design stage of the facility.

The basic concepts, definition, and terminology applicable to the rules are appended to aid the reader or user in consulting the book. Formulas and tables, as well as illustrative examples of radiation shielding calculations are provided in addition to miscellaneous useful information.

The introduction of these new regulations will eliminate some persisting uncertainties in the design and operation of high-level isotope γ-radiation facilities, and lays down clear requirements adapted to modern concepts on the effects of γ-radiation on the organism, so that this publication will indubitably contribute to a more widespread and safer use of radiation facilities.

NEW BOOKS

Translated from Atomnaya Énergiya, Vol. 18, No. 4,
pp. 437-439, April, 1965

La Diffraction et la Diffusion des Neutrons [Neutron diffraction and diffusion – in French]. Paris, Center National de la Recherche Scientifique, 1964, 236 pages. Reviewed by Yu. Abov.

This book assembles under one cover the papers presented at the international conference on diffraction and inelastic scattering of slow neutrons (September 3-5, 1963, Grenoble, France). The papers are divided under the following headings: a) neutronography of nonmagnetic structures (19 papers); b) research on magnetic structures (23 papers); c) anomalous dispersion of slow neutrons in crystals (1 paper); d) diffusion of magnons (3 papers); e) diffusion of phonons (3 papers).

The level of neutron structural research has undergone a significant growth. The research efforts of the Oak Ridge National Laboratory team (USA) in this area are particularly noteworthy; these scientists have at their disposal an automatic programmed diffractometer for thier work. Single crystal specimens are placed on a goniometer capable of rotation in three directions (three-circle goniometer). All of the motions are programmed ahead of time and carried out automatically from commands punched on tape. The results of the measurements are also punched out on tape and fed to an electronic computer for processing. Neutron diffraction studies are accompanied by painstaking x-ray structural analysis measurements. Reports were presented on studies of XeF_2, XeF_4, $BaCl_2 \cdot 2H_2O$, K_2NbF_7 structures (J. Browne, H. Levy). Single crystal specimens of different thicknesses were used in order to eliminate the effect of extinction on strong reflections.

A team of Japanese physicists (N. Kunitomi et al.) have made a study of the structure of UF_4, using improved neutron diffraction equipment (a powder specimen was used, and the position of the lines was compared to the results of x-ray structural analyses). The lattice parameters and the sites of the fluorine atoms were determined. These scientists also made a study of the magnetic structure of Mn–Cr alloys, the energy dependence of neutron transmission by titanium hydride (the position of the minimum in the effective cross section of this crystal is due to optical lattice vibrations). An investigation of the reflectivity of mosaic crystals was presented, with account taken of the effects introduced by collimating devices.

B. Lupstra (Netherlands) reported on an investigation of the structure of U_3O_8 (spatial group: Amm2). The spacings between uranium and oxygen atoms were ascertained. B. Willis (Harwell, Great Britain) studied the structures of UO_2, UO_{2+x}, U_4O_9. He utilized single crystal specimens, and took measurements in the temperature range from 20° to 1100°C. Some interesting data were obtained on the position of intermediary oxygen atoms in UO_{2+x} compositions.

A group of scientists at the nuclear center in Puerto Rico (I. Almodovar et al.) studied $CaWO_4$ single crystals (values of the oxygen atom site coordinates were refined), $CuSO_2$ single crystals (establishing the type of antiferromagnetic structure involved), and the structures of $BaNiO_2$ and Fe_2SiO_4.

R. A. Alikhanov (USSR Academy of Sciences) presented data on a neutron diffraction study of solid oxygen. Magnetic moment changes due to antiferromagnetic ordering were observed in the reflection planes (111) and (110) of the rhombohedral β-phase. Neutron diffraction patterns of the α-phase were obtained for temperatures 20.4° and 4.2°K.

Positions of the hydrogen and deuterium atoms in several crystal structures, notably $NiZrH_3$, $NiZrD_3$ (S. Peterson et al., Washington State University), HoD_3 (M. Mansmann and W. Wallace, Pittsburgh University), nickel hydride (J. Cabe et al., ORNL), the ReH_9^{2-} ion (S. Abrahams and K. Nox, Bell Telephone Company, USA), were studied in an array of papers.

A paper by S. Pickart et al., (Brookhaven National Laboratory) deserves to be singled out among the neutron diffraction studies reported on. This work was done with polarized neutrons to study the distribution of electrons

corresponding to weak ferromagnetism in hematite. The presence of a ferromagnetic moment in hematite (at temperatures above 250°K) must lead to the appearance of an impurity in magnetic scattering of neutrons to purely nuclear reflections. In view of the low value of this ferromagnetic moment, the magnetic moment addition to the intensity of scattered neutrons is insignificant, so that it was very difficult to perform suitable measurements. Moreover, the contribution due to covalent spin density could be contained in "forbidden" magnetic increments. The magnetic scattering of neutrons due to the weak ferromagnetism of hematite was successfully isolated. The authors drew the conclusion that the spatial distribution of the ferromagnetic spin density differs from the distribution of antiferromagnetic spin density in hematite.

Some very interesting research has been completed by a group of Italian physicists (B. Antonini et al., nuclear research center at Casaccia). In using polarized neutrons to probe the structure of the alloy $MnNi_3$ at various degrees of atomic ordering, they arrived at the conclusion that the curve of the temperature dependence of the magnetization in the partially ordered states of this alloy consists of two distinct parts, one of which is associated with short ordering, the other associated with long-range atomic order. Superstructural reflections are due to regions of long-range order, while contributions to the principal reflections are given by regions of both long-range order and short-range order. An investigation of the ordered alloy Fe_3Si was also reported on. The magnetic moments of the iron atoms in two types of this alloy were determined. The results were compared to the findings of an investigation of the alloy Fe_3Al. The results of measurements of the temperature dependence of magnetic neutron scattering by cubic cobalt were of special interest. In an earlier paper, F. Meisinger and B. Paoletti had discovered a temperature dependence of magnetic scattering of neutrons by cubic cobalt which is not associated with any variation in the magnetization of the specimen. This effect could be accounted for either by a temperature dependence of magnetic form factor, or by the difference in the amplitudes of vibration of the nuclei and outer unpaired electrons in the single crystal of cubic cobalt (alloy $Co_{0.92}Fe_{0.08}$; 8% iron was introduced in order to record the cubic phase), or by the two effects simultaneously.

In a paper published in a recent symposium, the authors reported on some additional research which could possibly eliminate any inference of a difference in the vibration amplitudes of the nuclei and unpaired electrons in the crystal. The authors arrived at the conclusion that the spatial distribution of unpaired cobalt electrons varies as the temperature is increased (to 873°K). This fundamental conclusion calls for both a theoretical explanation and for additional experimental confirmation.

L. Corliss and J. Hastings (Brookhaven National Laboratory) presented a review of magnetic structural research. It was shown that the intermetallic compounds Ni_5Er is a uniaxial ferromagnetic material. It turned out that the nickel atoms possess no magnetic moment. Neutron diffraction studies of $MnSn_2$ revealed that there exists an abrupt transition in this compound from the usual antiferromagnetic structure of a sinusoidal antiferromagnetic structure. In addition, a study was made of the magnetic structure of Cr_2O_3, of the temperature dependence of antiferromagnetic reflections of $MnSe_2$, and the results of these researches were correlated with theoretical predictions.

Structures known as spiral magnetic structures were investigated in some research programs reported on: $CoCr_2O_4$ (N. Menuc et al., MIT), $FeCr_2O_4$ (G. Bacquel, Saclay, France); magnetic properties of spinels were investigated (W. Roth, General Electric labs), and miscellanesous other magnetic structures were probed. H. Smith and S. Peterson (ORNL) investigated diffraction of neutrons on CdI_2 single crystals. They obtained values of the real and imaginary parts of the complex scattering amplitude of the nuclide Cd^{113}. The possibility of exploiting the anomalous dispersion of neutrons in crystals for structure determinations was demonstrated.

A theoretical treatment of critical magnetic scattering of neutrons was reported in a paper by J. Villin (Saclay, France), where a comparison with experimental data was also carried out. A. Wanik (Krakow, Poland) investigated inelastic magnetic scattering of neutrons by a pyrrhotite single crystal (FeS). The research was performed in Yugoslavia at the heavy water reactor, where a triaxial neutron crystal spectrometer of the Krakow Institute of Nuclear Physics had been set up. The dispersion relation of the acoustic magnon branch was obtained. An optical branch was also discovered. In a jointly authored paper, Polish and Yugoslav physicists (S. Krasnitskii et al.) employed the same instrument to study the temperature variation of inelastic magnetic scattering of monochromatic neutrons in pyrrhotite.

V. Ardent (Ispra, Italy) presented a theoretical paper discussing scattering of slow neutrons by organic molecules, with the object of securing information on the dynamics of the molecules.

V. Van Dingenen and S. Hauteclaire (Mol, Belgium) studied the energy dependence of scattering of cold neutrons (beryllium filter, mechanical neutron chopper) in orthoxylene, paraxylene, and metaxylene. These authors also presented a paper on inelastic scattering of neutrons in nickel.

Physics and Material Problems of Reactor Control Rods. Proceedings of Vienna November 11-15, 1963, IAEA symposium. Vienna, IAEA, 1964, 796 pages, in English. Reviewed by Yu. Mityaev.

This book is a collection of papers delivered at the IAEA Vienna symposium of November 1963 on this topic. It consists of six sections: 1) control rod theory; 2) theoretical and experimental research on control rods; 3) nuclear and engineering characteristics of control rod materials; 4) design, production, and characteristics of control rods; 5) control rod engineering problems; 6) reactivity control techniques.

The three papers in the first section discuss two-group control rod theory in a multizoned reactor, single-group and two-group techniques for calculating absorbing slabs, homogeneous and heterogeneous methods for control rod calculations in heavy-water lattices.

The next section offers three papers by Soviet scientists. One paper develops the three-group theory of control rod calculations for rods placed in a reflector; the second paper cites theoretical and experimental data on the effectiveness of absorber rods in VVER reactor assemblies. The third report presents calculations of the effective fraction of delayed neutrons in the VVR-M reactor, knowledge of which is required to make experimental determinations of absorbing power of the rods over the time the reactor is run up to full power. Several papers in this section deal with various experimental techniques for measuring the effectiveness of control rods, and calibrating them, in critical and exponential assemblies and in the LATINA, AGR, and ZENITH reactors. A Japanese paper presents a variational method for calculating the worth of absorber rods and plates, a British paper presents a procedure for experimental determination of the service life of cadmium plates for the PLUTO reactor and the results of determinations, while a paper submitted by Italian specialists discusses problems coming up in the design of control rods for the PRO reactor.

The third section is highly interesting for two Soviet reports discussing variations in the mechanical and heat transfer properties of control rod materials as functions of the content of various poisons. Two USA papers cite characteristics of control rod materials where a variety of rare earths are used as poisons.

Most of the papers appearing in the fourth section deal with the production technology and characteristics of control rods in the reactors HTP (Japan), BR-2 (Belgium), HFR (Netherlands), SILOE (France), EGCR (USA), and several cruciform rods made of boron carbide tubes. A West German paper discusses the possibilities in using indium tantalate and cadmium tantalate as absorbing materials in high-temperature reactors, while the problems involved in the development of absorbing materials for graphite-moderated reactors are taken up in a USA paper.

Four reports in the next section are devoted to control rod drives. Papers presented by Britain and West Germany describe the design and tests results of scram rod drives in the DIDO and SNEAK reactors, while a Norwegian paper cites experience acquired in the design, production technology, and operational characteristics of control rod drives and scram rod drives for the reactor powering the atomic ship Redieri-atom. An American paper presents a brief description of the design of pneumatically controlled scram rod drives and hydraulic drives for "chain type" rods, as well as combined scram-control rods.

The concluding section in this symposium is started off with a tutorial review paper (USA) discussing special aspects of control and techniques for fast reactor calculations and control system design, then proceeding to a discussion of reactivity effects and the effect of homogeneous and heterogeneous poisons on the characteristics of large reactors burning metal and oxide fuel. A second USA paper describes an original reactivity compensation system incorporating a system of tubes through which a stream of fluid flows to move a set of small cylinders or spheres of absorber material. A Franch paper discusses the advantages and inherent possibilities of reactivity control by means of absorber dissolved in the moderator. Two other reports describe reactivity compensation systems using absorbing particulates suspended in a stream (USA) or using a variable-pressure gas capable of absorbing neutrons (France).

The 34 papers included in this symposium will be of high interest to specialists in these fields.

C. A. Junge. Air Chemistry and Radioactivity. International Geophysics Series, Vol. 4, in English. New York and London, Academic Press, 1963, 382 pages.

This book, written by a renowned specialist is a complete critical review of the literature on all aspects of the chemical composition of the atmosphere. Special attention is centered on the relationship between concentrations of gaseous substances and aerosols (both radioactive and stable aerosols) on the time and place above the earth's surface, and cyclic variations in the height of the atmosphere or the geographic latitude are laid bare.

The book is made up of five chapters, the first three comprising the great bulk. Chapter 1 presents information on compounds of stable isotopes present as gases in the atmosphere (water vapor, CO_2, ozone, SO_2, H_2S, H_2, He, nitrogen compounds, halides, methane, CO, and formaldehyde). The list of literature surveyed in this chapter runs to well over 10 pages. Chapter 2 takes up aerosols of stable isotopes, their physicsl characteristics and properties, the chemical composition and distribution in the troposphere and stratosphere. In this case the list of literature surveyed runs to 9 pages.

Chapter 3 is given over to a description of radioactive substances present in the atmosphere. A short introduction is followed by a detailed analysis of the behavior of radon, thoron, and their daughters. Data on radioactive isotopes formed by cosmic radiation are presented later on; special attention is given to the concentration of Be^7 and the dependence of that concentration on several meteorological parameters. This chapter closes with a long section (stretching about 50 pages) on artificially produced radioactive materials, most of the information concerning nuclear fallout products. The list of pertinent literature takes up 6 pages.

The book ends with two short chapters devoted to the chemistry of fallout (in particular to a description of washout of fallout from the atmosphere and dry fallout), as well as atmospheric pollution in the neighborhood of large-scale industrial centers. The monograph ends with a detailed author and subject index.

SOVIET JOURNALS AVAILABLE IN COVER-TO-COVER TRANSLATION

This list includes all Russian journals which—to the publisher's knowledge—were available in cover-to-cover translation on June 30, 1965, or for which definite and immediate plans for cover-to-cover translation had been announced by that date. The list reflects only *current* publication arrangements, but the date and issue listed for first publication refer to translations available from any source. Thus, earlier volumes of a translation journal may have been published by an organization other than that listed as the current publisher, and possibly under a different title (and, for *Doklady Akademii Nauk SSSR*, in a different arrangement of sections).

Five bits of information are furnished, separated by bullets:

1. The abbreviation(s) by which the journals are most frequently referred to in Russian bibliographies (if the name of the journal is customarily spelled out, no abbreviation is given).
2. The transliterated full name of the journal.
3. The full name of the translation journal (in bold type).
4. The year, volume (in parentheses), and issue of first publication of the translation (parentheses are empty if the Russian journal does not use volume numbers).
5. The current publisher of the translation [AGI—American Geological Institute, AGU—American Geophysical Union, AIP—American Institute of Physics, CB—Consultants Bureau, CH—Clearing House for Federal Scientific and Technical Information, CS—The Chemical Society (London), FP—Faraday Press, IEEE— Institute of Electrical and Electronic Engineers, ISA—Instrument Society of America, PP—Pergamon Press].

For convenience in locating bibliographic references the journals are listed in alphabetical order of the *abbreviated* titles.

AÉ • Atomnaya énergiya • **Soviet Journal of Atomic Energy** • 1956(1)1 • CB

Akust. zh. • Akusticheskii zhurnal • **Soviet Physics—Acoustics** • 1955(1)1 • AIP

Astrofiz. • Astrofizika • **Astrophysics** • 1965(1)1 • FP

Astr(on). zh(urn). • Astronomicheskii zhurnal • **Soviet Astronomy—AJ** • 1957(34)1 • AIP

Avtomat. i telemekh. • Avtomatika i telemekhanika • **Automation and Remote Control** • 1956(27)1 • ISA

Avto(mat). svarka • Avtomaticheskaya svarka • **Automatic Welding** • 1959(12)1 • British Welding Research Association

Avtometriya • **Autometry** • 1965(1)1 • CB

Biokhim. • Biokhimiya • **Biochemistry** • 1956(21)1 • CB

Byul. éksp(erim). biol. (i med.) • Byulleten' éksperimental'noi biologii i meditsiny • **Bulletin of Experimental Biology and Medicine** • 1959(41)1 • CB

DAN (SSSR) • *see* Doklady AN SSSR

Defektoskopiya • **Soviet Defectoscopy** • 1965(1)1 • CB

Diff. urav. • Differentsial'nye uravneniya • **Differential Equations** • 1965(1)1 • FP

Dokl(ady) AN SSSR; DAN (SSSR) • Doklady Akademii Nauk SSSR • The translation of Doklady is published in various journals, according to subject matter. The sections of Doklady contained in each of the translation journals are listed in parentheses.

Doklady Biochemistry (biochemistry) • 1957(112)1 • CB

Doklady Biological Sciences Sections (anatomy, cytology, ecology, embryology, endocrinology, evolutionary morphology, parasitology, physiology, zoology) • 1957(112)1 • CB

Doklady Biophysics (biophysics) • 1957(112)1 • CB

Doklady Botany (botany, phytopathology, plant anatomy, plant ecology, plant embryology, plant physiology, plant morphology) • 1957(112)1 • CB

Doklady Chemical Technology (chemical technology) • 1956(106)1 • CB

Doklady Chemistry (chemistry) • 1956(106)1 • CB

Doklady Earth Sciences Sections (geochemistry, geology, geophysics, hydrogeology, lithology, mineralogy, paleontology, permafrost, petrography) • 1959(124)1 • AGI

Doklady Physical Chemistry (physical chemistry) • 1957(112)1 • CB

Doklady Soil Science (soil science) • 1964(154)1 • Soil Science Society of America

Soviet Mathematics—Doklady (mathematics) • 1960(130)1 • American Mathematical Society

Soviet Oceanography (oceanology) • 1959(124)1 • AGU

Soviet Physics—Doklady (aerodynamics, astronomy, crystallography, cybernetics and control theory, electrical engineering, energetics, fluid mechanics, heat engineering, hydraulics, mathematical physics, mechanics, physics, technical physics, theory of elasticity • 1956(106)1 • AIP

Élektrokhimiya • **Soviet Electrochemistry** • 1965(1)1 • CB

Élektrosvyaz' • combined with Radiotekhnika in **Telecommunications and Radio Engineering** • 1957(16)1 • IEEE

Élektrotekh. • Élektrotekhnika • **Soviet Electrical Engineering** • 1965(36)1 • FP

Éntom(ol). oboz(r). • Éntomologicheskoe obozrenie • **Entomological Review** • 1958(37)1 • Entomological Society of America

Fiz. goreniya i vzryva • Fizika goreniya i vzryva • **Combustion, Explosion, and Shock Waves** • 1965(1) • FP

Fiziol(ogiya) rast. • Fiziologiya rastenii • **Soviet Plant Physiology** • 1957(4)1 • CB

Fiz.-khim. mekh(anika) mater(ialov); FKhMM • Fizikokhimicheskaya mekhanika materialov • **Soviet Materials Science** • 1965(1)1 • FP

Fiz. met. i metallov.; FMM • Fizika metallov i metallovedenie • **Physics of Metals and Metallography** • 1957(5)1 • Acta Metallurgica

Fiz.-tekhn. probl. razr. polezn. iskopaem. • Fizikotekhnicheskie problemy razrabotki poleznykh iskopaemykh • **Soviet Mining Science** • 1965(1)1 • CB

Fiz. tv(erd). tela; FTT • Fizika tverdogo tela • **Soviet Physics—Solid State** • 1959(1)1 • AIP

FKhMM • *see* Fiz.-khim. mekhanika materialov

FMM • *see* Fiz. met. i metallov.

FTT • *see* Fiz. tverd. tela

Geliotekh. • Geliotekhnika • **Applied Solar Energy** • 1965(1)1 • FP

Geol. nefti i gaza • Geologiya nefti i gaza • **Petroleum Geology** • 1958(2)1 • Petroleum Geology, Box 171, McLean, Va.

Geomagnet. i aéronom. • Geomagnetizm i aéronomiya • **Geomagnetism and Aeronomy** • 1961(1)1 • AGU

Inzh.-fiz. zh. • Inzhenerno-fizicheskii zhurnal • **Journal of Engineering Physics** • 1965(8)1 • FP

Inzh. zh. • Inzhenernyi zhurnal • **Soviet Engineering Journal** • 1965(5)1 • FP

Iskusstv. sputniki Zemli • Iskusstvennye sputniki Zemli • **Artificial Earth Satellites** • 1958(1)1 • CB [superseded by Kosmich. issled.]

Izmerit. tekhn(ika) • Izmeritel'naya tekhnika • **Measurement Techniques** • 1958(7)1 • ISA

Izv. AN SSSR, o(td.) kh(im.) n(auk) (*or* ser. khim.) • Izvestiya Akademii Nauk SSSR: Otdelenie khimicheskikh nauk (*or* Seriya khimicheskaya) • **Bulletin of the Academy of Sciences of the USSR: Division of Chemical Science** • 1952(16)1 • CB

Izv. AN SSSR, ser. fiz(ich). • Izvestiya Akademii Nauk SSSR: Seriya fizicheskaya • **Bulletin of the Academy of Sciences of the USSR: Physical Series** • 1954(18)3 • Columbia Technical Translations

Izv. AN SSSR, ser. fiz. atm. i okeana • Izvestiya Akademii Nauk SSSR: Seriya fiziki atmosfery i okeana • **Izvestiya, Atmospheric and Oceanic Physics** • 1965( )1 • AGU

Izv. AN SSSR, ser. fiz. zemli • Izvestiya Akademii Nauk SSSR: Seriya fiziki zemli • **Izvestiya, Physics of the Solid Earth** • 1965( )1 • AGU

Izv. AN SSSR, ser. geofiz. • Izvestiya Akademii Nauk SSSR: Seriya geofizicheskaya • **Bulletin of the Academy of Sciences of the USSR: Geophysics Series** • 1957(7)1 • AGU [superseded by Izv. AN SSSR, ser. fiz. atm. i okeana and Izv. AN SSSR, ser. fiz. zemli]

Izv. AN SSSR, ser. geol. • Izvestiya Akademii Nauk SSSR: Seriya geologicheskaya • **Bulletin of the Academy of Sciences of the USSR: Geologic Series** • 1958(23)1 • AGI

Izv. AN SSSR, ser. neorgan. mat(er). • Izvestiya Akademii Nauk SSSR: Seriya neorganicheskie materialy • **Inorganic Materials** • 1965(1)1 • CB

Izv. AN SSSR, tekhn. kiber(netika) • Izvestiya Akademii Nauk SSSR: Tekhnicheskaya kibernetika • **Engineering Cybernetics** • 1963(1)1 • IEEE

Izv. v(yssh.) u(ch.) z(av.) aviats. tekh. • Izvestiya vysshikh uchebnykh zavedenii. Aviatsionnaya tekhnika • **Aviation Engineering** • 1963(6)1 • CH

Izv. v(yssh.) u(ch.) z(av.) fiz. • Izvestiya vysshikh uchebnykh zavedenii. Fizika • **Soviet Physics Journal** • 1965(8)1 • FP

Izv. v(yssh.) u(ch.) z(av.) geodez. i aérofot. • Izvestiya vysshikh uchebnykh zavedenii. Geodeziya i aérofotos"emka • **Geodesy and Aerophotography** • 1959(4)1 • AGU

Izv. v(yssh.) u(ch.) z(av.) priborostr. • Izvestiya vysshikh uchebnykh zavedenii. Priborostroenie • **Izvestiya VUZOV. Instrument Building** • 1962(5)1 • CH

Izv. v(yssh.) u(ch.) z(av.) radiofiz. • Izvestiya vysshikh uchebnykh zavedenii. Radiofizika • **Izvestiya VUZOV. Radiophysics** • 1958(1)1 • CH

Izv. v(yssh.) u(ch.) z(av.) radiotekhn(ika) • Izvestiya vysshikh uchebnykh zavedenii. Radiotekhnika • **Izvestiya VUZOV. Radio Engineering** • 1959(2)1 • CH

Izv. v(yssh.) u(ch). z(av.) tekh. teks. prom. • Izvestiya vysshikh uchebnykh zavedenii. Tekhnologiya tekstilnoi promyshlennosti • **Technology of the Textile Industry, USSR** • 1960(4)1 • The Textile Institute (Manchester)

Kauch. i rez. • Kauchuk i rezina • **Soviet Rubber Technology** • 1959 (18)3 • Maclaren and Sons Ltd.

Khim. getero(tsik). soed. • Khimiya geterotsiklicheskikh soedinenii • **Chemistry of Heterocyclic Compounds** • 1965(1)1 • FP

Khim. i neft. mash(inostr). • Khimicheskoe i neftyanoe mashinostroenie • **Chemical and Petroleum Engineering** • 1965( )1 • CB

Khim. i tekhnol. topliv i masel • Khimiya i tekhnologiya topliv i masel • **Chemistry and Technology of Fuels and Oils** • 1965( )1 • CB

Khim. prirod. soed. • Khimiya prirodnykh soedinenii • **Chemistry of Natural Compounds** • 1965(1)1 • FP

Kib. • Kibernetika • **Cybernetics** • 1965(1)1 • FP

Kinet. i katal. • Kinetika i kataliz • **Kinetics and Catalysis** • 1960(1)1 • CB

Koks i khim. • Koks i khimiya • **Coke and Chemistry, USSR** • 1959( )8 • Coal Tar Research Assn. (Leeds, England)

Kolloidn. zh(urn). • Kolloidnyi zhurnal • **Colloid Journal** • 1952(14)1 • CB

Kosmich. issled. • Kosmicheskie issledovaniya • **Cosmic Research** • 1963(1)1 • CB

Kristallog. • Kristallografiya • **Soviet Physics—Crystallography** • 1957 (2)1 • AIP

Liteinoe proiz(-vo). • Liteinoe proizvodstvo • **Russian Castings Production** • 1961(12)1 • British Cast Iron Research Association

Mag. gidrodin. • Magnitnaya gidrodinamika • **Magnetohydrodynamics** • 1965(1)1 • FP

Mekh. polim. • Mekhnika polimerov • **Polymer Mechanics** • 1965(1)1 • FP

Metalloved. i term. obrabotka metal.; MiTOM • Metallovedenie i termicheskaya obrabotka metallov • **Metal Science and Heat Treatment** • 1958(6)1 • CB

Metallurg • **Metallurgist** • 1957( )1 • CB

Mikrobiol. • Mikrobiologiya • **Microbiology** • 1957(26)1 • CB

MiTOM • *see* Metalloved. i term. obrabotka metal.

Ogneupory • **Refractories** • 1960(25)1 • CB

Opt. i spektr.; OS • Optika i spektroskopiya • **Optics and Spectroscopy** • 1959(6)1 • AIP

Osnovan. fund. i mekh. gruntov • Osnovaniya fundamenty i mekhanika gruntov • **Soil Mechanics and Foundation Engineering** • 1964 ( )1 • CB

Paleon. zh(urn). • Paleontologicheskii zhurnal • **Journal of Paleontology** • 1962( )1 • AGI

Plast. massy • Plasticheskie massy • **Soviet Plastics** • 1960(8)7 • Rubber and Technical Press, Ltd.

PMM • *see* Prikl. matem. i mekhan.

PMTF • *see* Zhur. prikl. mekhan. i tekhn. fiz.

Pochvovedenie • **Soviet Soil Science** • 1958(53)1 • Soil Science Society of America

Poroshk. met. • Poroshkovaya metallurgiya • **Soviet Powder Metallurgy and Metal Ceramics** • 1962(2)1 • CB

Priborostroenie • **Instrument Construction** • 1959(4)1 • Taylor and Francis, Ltd.

Pribory i tekhn. éksp(erimenta); PTÉ • Pribory i tekhnika éksperimenta • **Instruments and Experimental Techniques** • 1958(3)1 • ISA

Prikl. biokhim. i mikrobiol. • Prikladnaya biokhimiya i mikrobiologiya • **Applied Biochemistry and Microbiology** • 1965(1)1 • FP

Prikl. matem. i mekh(an).; PMM • Prikladnaya matematika i mekhanika • **Applied Mathematics and Mechanics** • 1958(22)1 • PP

Probl. pered. inform. • Problemy peredachi informatsii • **Problems of Information Transmission** • 1965(1)1 • FP

Probl. severa • Problemy severa • **Problems of the North** • 1958( )1 • National Research Council of Canada

PTÉ • *see* Pribory i tekhn. éksperimenta

Radiokhim. • Radiokhimiya • **Soviet Radiochemistry** • 1962(4)1 • CB

Radiotekh. • Radiotekhnika • combined with Élektrosvyaz' in **Telecommunications and Radio Engineering** • 1961(16)1 • IEEE

Radiotekhn. i élektron(ika) • Radiotekhnika i élektronika • **Radio Engineering and Electronic Physics** • 1961(6)1 • IEEE

Stal' • **Stal' in English** • 1959(19)1 • The Iron and Steel Institute

Stanki i instr. • Stanki i instrument • **Machines and Tooling** • 1959 (30)1 • Production Engineering Research Association

Stek. i keram. • Steklo i keramika • **Glass and Ceramics** • 1956(13)1 • CB

Svaroch. proiz(-vo). • Svarochnoe proizvodstvo • **Welding Production** • 1959(5)4 • British Welding Research Association (London)

Teor. i éksperim. khim. • Teoreticheskaya i éksperimental'naya khimiya • **Theoretical and Experimental Chemistry** • 1965(1)1 • FP

Teor. veroyat. i prim. • Teoriya veroyatnostei i ee primenenie • **Theory of Probability and Its Application** • 1956(1)1 • Society for Industrial and Applied Mathematics

Teploénergetika • **Thermal Engineering** • 1964(11)1 • PP

Teplofiz. vys(ok). temp. • Teplofizika vysokikh temperatur • **High Temperature** • 1963(1)1 • CB

Tsvet. metally • Tsvetnye metally • **The Soviet Journal of Nonferrous Metals** • 1960(33)1 • Primary Sources

Usp. fiz. nauk; UFN • Uspekhi fizicheskikh nauk • **Soviet Physics—Uspekhi** • 1958(66)1 • AIP

Usp. khim.; UKh • Uspekhi khimii • **Russian Chemical Reviews** • 1960(29)1 • CS

Usp. mat. nauk; UMN • Uspekhi matematicheskaya nauk • **Russian Mathematical Surveys** • 1960(15)1 • Cleaver-Hume Press, Ltd.

Vest. Akad. med. nauk SSSR • Vestnik Akademii meditsinskikh nauk SSSR • **Vestnik of USSR Academy of Medical Sciences** • 1962(17)1 • CH

Vest. mashinostroeniya • Vestnik mashinostroeniya • **Russian Engineering Journal** • 1959(39)4 • Production Engineering Research Association

Vest. svyazi • Vestnik svyazi • **Herald of Communications** • 1954(14)1 • CH

Vysoko(molek). soed(ineniya) • Vysokomolekulyarnye soedineniya (SSSR) • **Polymer Science (USSR)** • 1959(1)1 • PP

Yadernaya fizika • **Soviet Journal of Nuclear Physics** • 1965(1)1 • AIP

Zashch(ita) met(allov) • Zashchita metallov • **Protection of Metals** • 1965(1)1 • CB

Zav(odsk). lab(oratoriya); ZL • Zavodskaya laboratoriya • **Industrial Laboratory** • 1958(24)1 • ISA

ZhÉTF pis'ma redaktsiyu • **JETP Letters** • 1965(1)1 • AIP

Zh(ur). anal(it). khim(ii); ZhAKh • Zhurnal analiticheskoi khimii • **Journal of Analytical Chemistry** • 1952(7)1 • CB

Zh(ur). éks(perim). i teor. fiz.; ZhÉTF • Zhurnal éksperimental'noi i teoreticheskoi fiziki • **Soviet Physics—JETP** • 1955(28)1 • AIP

Zh(ur). fiz. khimii; ZhFKh • Zhurnal fizicheskoi khimii • **Russian Journal of Physical Chemistry** • 1959(33)7 • CS

Zh(ur). neorg(an). khim.; ZhNKh • Zhurnal neorganicheskoi khimii • **Russian Journal of Inorganic Chemistry** • 1959(4)1 • CS

Zh(ur). obshch. khim.; ZhOKh • Zhurnal obshchei khimii • **Journal of General Chemistry of the USSR** • 1949(19)1 • CB

Zh(ur). org. khim.; ZhOrKh(im) • Zhurnal organicheskoi khimii • **Journal of Organic Chemistry of the USSR** • 1965(1)1 • CB

Zh(ur). prikl. khim.; ZhPKh • Zhurnal prikladnoi khimii • **Journal of Applied Chemistry of the USSR** • 1950(23)1 • CB

Zh(ur). prikl. mekhan. i tekhn. fiz. • Zhurnal prikladnoi mekhaniki i tekhnicheskoi fiziki • **Journal of Applied Mechanics and Technical Physics** • 1965( )1 • FP

Zh(ur). prikl. spektr. • Zhurnal prikladnoi spektroskopii • **Journal of Applied Spectroscopy** • 1965(2)1 • FP

Zh(ur). strukt(urnoi) khim.; ZhSKh • Zhurnal strukturnoi khimii • **Journal of Structural Chemistry** • 1960(1)1 • CB

Zh(ur). tekhn. fiz.; ZhTF • Zhurnal tekhnicheskoi fiziki • **Soviet Physics—Technical Physics** • 1956(26)1 • AIP

Zh(ur). vses. khim. ob-va im. Mendeleeva • Zhurnal vsesoyuznogo khimicheskogo obshchestva im. Mendeleeva • **Mendeleev Chemistry Journal** • 1965(10)1 • FP

Zh(ur). vychis. mat. i mat. fiz. • Zhurnal vychislitel'noi matematika i matematicheskoi fiziki • **USSR Computational Mathematics and Mathematical Physics** • 1962(1)1 • PP

ZL • *see* Zavodsk. laboratoriya

Declassified and Approved For Release 2013/09/24 : CIA-RDP10-02196R000700010004-3